AD-A061 134 MASSACHUSETTS INST OF TECH CAMBRIDGE AEROELASTIC AND--ETC F/G 1/3
GUST RESPONSE AND ITS ALLEVIATION FOR A HINGELESS HELICOPTER RO--ETC(U)
SEP 78 M YASUE N00019-76-C-0278
UNCLASSIFIED ASRL-TR-189-1 NL

1 OF 2
AD
A061134

34

AD A061134

ASRL TR 189-1

LEVEL II

GUST RESPONSE AND ITS ALLEV
HINGELESS HELICOPTER ROTOR IN

Masahiro Yasue

Aeroelastic and Structures Resea
Department of Aeronautics and
Massachusetts Institute of Te
Cambridge, Massachusett

September 1978

Distribution of this report is

Prepared for the
DEPARTMENT OF THE NAV
NAVAL AIR SYSTEMS COMMA
AIRFRAMES DIVISION
WASHINGTON, D.C. 2036

CONTRACT NOS. N00019-76-C-0278 AND

DDC FILE COPY

78 11

UNCLASSIFIED

SECURITY CLASSIFICATION OF THIS PAGE *(When Data Entered)*

REPORT DOCUMENTATION PAGE

READ INSTRUCTIONS BEFORE COMPLETING FORM

1. REPORT NUMBER (14) ASRL-TR-189-1	2. GOVT ACCESSION NO.
3. RECIPIENT'S CATALOG NUMBER	
4. TITLE *(and Subtitle)* (4) Gust Response and Its Alleviation for a Hingeless Helicopter Rotor in Cruising Flight	5. TYPE OF REPORT & PERIOD COVERED (9) FINAL rept.
6. PERFORMING ORG. REPORT NUMBER	
7. AUTHOR(s) (10) Masahiro Yasue	8. CONTRACT OR GRANT NUMBER(s) (15) N00019-76-C-0278, N00019-77-C-0535
9. PERFORMING ORGANIZATION NAME AND ADDRESS Massachusetts Institute of Technology Department of Aeronautics and Astronautics Cambridge, Massachusetts 02139	10. PROGRAM ELEMENT, PROJECT, TASK AREA & WORK UNIT NUMBERS
11. CONTROLLING OFFICE NAME AND ADDRESS (12) 182 p.	12. REPORT DATE (11) September 1978 13. NUMBER OF PAGES 181
14. MONITORING AGENCY NAME & ADDRESS *(if different from Controlling Office)* Department of the Navy Naval Air Systems Command Airframes Division Washington, D.C. 20361	15. SECURITY CLASS. *(of this report)* 15a. DECLASSIFICATION/DOWNGRADING SCHEDULE

16. DISTRIBUTION STATEMENT *(of this Report)*

Distribution of this report is unlimited.

17. DISTRIBUTION STATEMENT *(of the abstract entered in Block 20, if different from Report)*

18. SUPPLEMENTARY NOTES

19. KEY WORDS *(Continue on reverse side if necessary and identify by block number)*

Helicopter
Rotor
Gust Response
Gust Alleviation
Vibration

20. ABSTRACT *(Continue on reverse side if necessary and identify by block number)*

The vertical gust response and its alleviation for hingeless helicopter rotor blades in cruising flight is studied theoretically and experimentally. An evaluation is performed of the effectiveness of torsional stiffness variation in conjunction with chordwise center-of-gravity shift in alleviating the blade flapping response to decrease the root bending moment.

The theoretical analysis utilizes the equations of motion of hingeless rotor blades exposed to vertical gusts in forward flight for the flapping.

next page

DD FORM 1 JAN 73 1473 EDITION OF 1 NOV 65 IS OBSOLETE

UNCLASSIFIED

SECURITY CLASSIFICATION OF THIS PAGE *(When Data Entered)*

006 850 8 11 09 061

20. lagging, and elastic and rigid pitch degrees of freedom. The equations include the effect of steady-state deflections in the trim conditions and various hingeless rotor configurations such as precone, droop and torque offset as well as chordwise center-of-gravity shift and aerodynamic center offset.

The experimental program involves the wind tunnel tests of a five-foot diameter rotor subject to a sinusoidal waveform gust. Testing involves variation of the blade chordwise center-of-gravity location, the blade torsional stiffness, rotor advance ratio, and vertical gust frequency.

SUMMARY

The vertical gust response and its alleviation for hingeless helicopter rotor blades in cruising flight is studied theoretically and experimentally. An evaluation is performed of the effectiveness of torsional stiffness variation in conjunction with chordwise center-of-gravity shift in alleviating the blade flapping response to decrease the root bending moment.

The theoretical analysis utilizes the equations of motion of hingeless rotor blades exposed to vertical gusts in forward flight for the flapping, lagging, and elastic and rigid pitch degrees of freedom. The equations include the effect of steady-state deflections in the trim conditions and various hingeless rotor configurations such as precone, droop and torque offset as well as chordwise center-of-gravity shift and aerodynamic center offset.

The experimental program involves the wind tunnel tests of a five-foot diameter rotor subject to a sinusoidal waveform gust. Testing involves variation of the blade chordwise center-of-gravity location, the blade torsional stiffness, rotor advance ratio, and vertical gust frequency.

ACCESSION for
NTIS [illegible] Section
DDC Buff Section
[illegible]
JUSTIFICATION
BY
DISTRIBUTION/AVAILABILITY CODES
[illegible] SPECIAL
A

FOREWORD

This research was conducted by the Aeroelastic and Structures Research Laboratory, Department of Aeronautics and Astronautics, Massachusetts Institute of Technology, Cambridge, Massachusetts under Contract Nos. N00019-76-C-0278 and N00019-77-C-0535, supervised by Mr. Raymond Malatino of the Airframes Division, Naval Air Systems Command, Department of the Navy.

The author wishes to express his appreciation to Mr. Malatino for his useful comments and suggestions.

The author is deeply indebted to Professor N.D. Ham, and Major C.A. Vehlow for their assistance in the course of this study.

The digital computations were carried out at the MIT Information Processing Center.

CONTENTS

Section		Page
1	INTRODUCTION	1
	1.1 General	1
	1.2 Brief Survey of Past Work	2
	1.3 The Purpose and Scope of the Research	5
2	THEORETICAL ANALYSIS	7
	2.1 The Equations of Motion for the Rotating Blade	7
	2.1.1 Rotor Configuration	7
	2.1.2 Coordinate Systems and Inertia Loadings	7
	2.1.3 Equilibrium Equations of the Beam	20
	2.1.4 Moment and Displacement Relation	22
	2.1.5 Partial Differential Equations of Motion	24
	2.2 Natural Frequencies and Associated Mode Shapes	30
	2.2.1 Introduction	30
	2.2.2 Variational Functional	31
	2.2.3 Finite Element Formulation	33
	2.2.4 Boundary Conditions	39
	2.2.5 Subspace Iteration Method	39
	2.3 Aerodynamic Loading	41
	2.3.1 Introduction	41
	2.3.2 Relative Velocity of the Blade	41
	2.3.3 Section Aerodynamic Forces	46
	2.3.4 Aerodynamic Moments	50
	2.3.5 Gust Velocity Gradient Due to the One-Dimensional Gust	52
	2.4 Rotor Trim and Steady State Deflections	54
	2.4.1 Introduction	54
	2.4.2 Equations of Motion for the Steady Equilibrium Condition	54
	2.4.3 Thrust Coefficient	59
	2.4.4 Procedure for the Trim Condition	60

CONTENTS (Continued)

Section		Page
	2.5 Modal Equations of Motion	62
	2.5.1 The Perturbation Equations of Motion	62
	2.5.2 Modal Equations in Rotating Coordinate Systems	67
	2.5.3 Modal Equations in Nonrotating Coordinate Systems	69
	2.5.4 Mathematical Methods for Determining System Characteristics	74
3	EXPERIMENTAL PROGRAM	77
	3.1 General Description of Model	77
	3.2 Rotor Blades	77
	3.3 Model Hub and Support	78
	3.4 Instrumentation	78
	3.5 Rotor Blade with Chordwise Center-of-Gravity Shift Configuration	79
	3.6 Experimental Procedure	80
4	RESULTS AND DISCUSSION	83
	4.1 Introduction	83
	4.2 Natural Frequencies and Mode Shapes	83
	4.3 Trim Conditions and Steady-State Deflections	84
	4.4 Frequency Response to the Vertical Gust	85
	4.4.1 Experimental Data Reduction	85
	4.4.2 Three-Bladed Rotor Gust Response	88
	4.4.3 Single-Bladed Rotor Gust Response with Chordwise Center-of-Gravity Shift	89
	4.4.3.1 30 MPH (μ = 0.192) Configuration	89
	4.4.3.2 60 MPH (μ = 0.384) Configuration	91
	4.4.4 Summary of the Vertical Gust Response Analysis	92
5	CONCLUSIONS AND COMMENTS	94
	5.1 Conclusions	94
	5.2 Suggestions for Future Research	95

CONTENTS (Concluded)

Section		Page
REFERENCES		97
TABLE		102
FIGURES		103
APPENDICES		136
A	EXPRESSIONS ASSOCIATED WITH STEADY-STATE EQUATIONS	136
B	EXPRESSIONS ASSOCIATED WITH MODAL EQUATIONS	139
C	OUTLINE OF EQUATIONS OF MOTION WHEN CYCLIC PITCH CONTROL IS APPLIED	149
D	GUST RESPONSE OF THE FULL-SIZE ROTOR	151
E	ADEQUACY OF HARMONIC BALANCE METHOD	154
F	CORRELATION OF HUB SHEARS WITH BLADE FLAPPING RESPONSE	161

LIST OF ILLUSTRATIONS

Figure		Page
1	Rotor Blade Configuration	103
2	Coordinate Systems	104
3	Blade Displacement	105
4	Position Vectors	106
5	Equilibrium of Forces and Moments	106
6	Directions of Positive Displacements and Rotations at Nodes of the Beam Element in the Finite Element Method	107
7	Orientation of Cruising Velocity, Inflow, and Gust Velocity	108
8	Rotor Blade Section Aerodynamics	109
9	Gust Velocity Gradient Due to Gust Nonuniformity over the Rotor Disc	110
10	Three-Bladed Rotor	111
11	Structural Characteristics of Wind Tunnel Model Blade	112
12	Rotor Blade Flexure, Strain Gages and Lead-Lag Damper	114
13	Single Blade Rotor with Tip Weight	115
14	Mode Shapes of the Wind Tunnel Model Blade	116
15	Steady-State Conditions in No-Trim Operation for the Wind Tunnel Three-Bladed Rotor Model	117
16	Rotor Hub Details	118
17	Typical Time History of the Vertical Gust Responses of Flap and Torsion Motions	119
18	Typical Frequency Spectrum of the Vertical Gust Responses of Flap and Torsion Motions	120
19	Vertical Gust Amplitude at the Center of the Rotor Disc	121
20	Three-Bladed Rotor Vertical Gust Response	122
21	Effect of the Gust Velocity Gradient on the Flap Response	124
22	Single-Bladed Rotor Vertical Gust Response in Advance Ratio [illegible]02 with Chordwise Center-of-Gravity Shift	125
23	[illegible]-Bladed Rotor Vertical Gust Responses in Advance Ratio 0.[illegible] with Chordwise Center-of-Gravity Shift	130
24	Von Karman Gust Power Spectral Density Scaled to the Wind Tunnel Model Blade	135

LIST OF SYMBOLS

a	Blade sectional lift curve slope
$\vec{a}$	Acceleration vector in the hub coordinate systems (x,y,z) defined in Eq. 12
$\vec{a}_{EA}$	Acceleration vector in the undeformed elastic coordinate systems (x",y",z") defined in Eq. 13
$\vec{a}$	Acceleration vector in the feathering axis coordinate systems (x',y',z') defined in Eq. 21
A	Blade cross-section area
A_M	Defined in Eq. 88
$[A]$	Matrix defined in Eq. 119
B_M	Defined in Eq. 119
$[B]$	Matrix defined in Eq. 119
C_T	Thrust coefficient defined as $\frac{T}{\rho(\pi R^2)(\Omega R)^2}$
$[C]$	Matrix defined in Eq. 119
c	Blade chord length
c_{d_o}	Blade sectional drag coefficient
c_{m_o}	Blade sectional pitching moment coefficient
c_{m_α}	Blade sectional pitching moment curve slope
c_m	Blade sectional pitching moment coefficient
D	Blade sectional drag
e_o	Torque offset
e_N	Tension center in the blade cross-section
EI_F	Blade flapwise stiffness
EI_c	Blade chordwise stiffness

$[f]$	Matrix defined in Eq. 44
$[f_i]$	Matrix defined in Eq. 117d
$[F]$	Matrix defined in Eq. 116
GJ	Blade torsional rigidity
$H_{o1}^{(1)}$, $H_{o2}^{(1)}$, $H_{11}^{(1)}$, $H_{12}^{(1)}$	Hermitian interpolation functions defined in Eq. 45
$[H]$	Matrix defined in Eq. 112
I_B	Blade flapping moment of inertia
I_i	Generalized mass defined in Eq. B.1 in Appendix B
I_o	Blade cross-sectional moment of inertia per unit length
I_{qi}	ith generalized mass defined in Eq. A.1 in Appendix A
I_{xp}, I_{zp}	Defined in Eq. 17
$[J]$	Transformation matrix in Eq. 59
k_A^2	Defined in Eq. 29
$[k_n]$	nth element stiffness matrix defined in Eq. 51
$[k_n^c]$	Matrix defined in Eq. 56
$[k_n^s]$	Matrix defined in Eq. 52
K_θ	Stiffness spring constant for the rigid pitch motion
$[k]$	Stiffness matrix defined in Eq. 59
$[K]$	Stiffness matrix defined in Eq. 114
ℓ	Element size
L	Blade section lift
m	Blade mass per unit length

$[m_n]$	nth element mass matrix
M_A	Blade section aerodynamic pitching moment defined in Eq. 84
M_{A_θ}	Blade aerodynamic pitching moment defined in Eq. 90
M_{FA}	Blade aerodynamic feathering moment defined in Eq. 90
M_ϕ	Aerodynamic pitching moment for the elastic torsion motion
M_θ	Aerodynamic pitching moment for the rigid pitch motion
[M]	Mass matrix defined in Eq. 59
[M]	Mass matrix defined in Eq. 114
M_x, M_y, M_z	Resultant moments in x, y, z coordinate systems
$M_{x"}$, $M_{y"}$, $M_{z"}$	Resultant moments in x", y", z" coordinate systems
M_{x_p}, M_{y_p}, M_{z_p}	Resultant moments in x_p, y_p, z_p coordinate systems
N	Number of blades
N	Number of mode shapes employed in the modal equations
p_x, p_y, p_z	Blade distributed forces
$\vec{P}^I_{EA}$	Inertial loadings defined in Eq. 14
P_v, P_w	Aerodynamic forces defined in Eq. 78
P_x, P_z	Aerodynamic forces defined in Eq. 77
$\bar{q}_k$	Generalized coordinates for the steady-state motion (k = 1, 2)
q_j	Generalized coordinates for the perturbation equations

q_x, q_y, q_z	Blade distributed moments
$q_j^o, q_j^{lc}, q_j^{ls}$	jth generalized coordinates for the collective and cyclic motion in the perturbation equations
$\{q_n\}$	Generalized coordinates defined in Eq. 43
q_{FA}^I	Inertial moment about the feathering axis defined in Eq. 23
$\vec{q}_{FA}^I$	Inertial moment vector in the feathering axis coordinate systems (x', y', z') defined in Eq. 22
$\vec{q}^I$	Inertial moment vector in the elastic axis coordinate systems (x, y, z) defined in Eq. 16
r	Radial coordinate from the pitch change bearing
r_o	Rigid shank length
$\vec{r}_B$	Position vector from the origin to the arbitrary point of the blade cross-section defined in Eq. 11
$\vec{r}_D$	Position vector defined in Eq. 4
$\vec{r}_{FA}$	Position vector defined in Eq. 18
$\vec{r}_e$	Position vector for the torque offset defined in Eq. 11
$\vec{r}_o$	Position vector for the rigid shank defined in Eq. 8
$\vec{r}_p$	Position vector defined in Eq. 15
$\vec{r}_x$	Position vector defined in Eq. 1
R	Blade radius
t	Time
T	Tension force defined in Eq. 36

T_o	Tension force defined in Eq. 110
$[T]$	Transformation matrix defined in Eq. 2
$[T_\beta]$, $[T_\theta]$, $[T_\delta]$	Transformation matrices defined in Eq. 6 and 9
u	Radial displacement defined in Eq. 5
u_T, u_R, u_p	Blade relative velocities in the trim condition in the tangential, radial, and perpendicular directions, respectively
$\{u\}$	Matrix defined in Eq. 43
$\vec{u}$	Velocity vector for the blade relative velocities
$\vec{U}$	Resultant velocity defined in Eq. 71
U_T, U_R, U_P	Resultant velocity components in the tangential, radial, and perpendicular directions, respectively defined in Eq. 72
v	Blade chordwise deflection (positive opposite to the rotational direction)
v_o	Blade steady-state chordwise deflection (positive opposite to the rotational direction)
v_i	Induced velocity (positive downward)
$\vec{v}_B$	Velocity vector defined in Eq. 66
$\vec{v}_{EA}$	Velocity vector defined in Eq. 68
V	Vehicle cruising velocity
V_k	kth blade steady-state chordwise deflection mode shape
V_j	jth blade chordwise deflection mode shape
V_x, V_z	Shear forces defined in Eq. 25
$\vec{V}$	Cruising velocity vector defined in Eq. 69

w_G	Vertical gust velocity (positive upward)
$\bar{w}_G$	Normalized gust velocity $w_G/(\Omega R)$
W_k	kth blade steady-state out-of-plane deflection mode shape (positive upward)
W_j	jth blade out-of-plane deflection mode shape (positive upward)
x	Nondimensional radial coordinate $(r_o+r)/R$
x, y, z	Rotor hub coordinate systems defined in Section 2.1.2
x', y', z'	Blade feathering axis coordinate systems defined in Section 2.1.2
x", y", z"	Blade elastic axis coordinate systems defined in Section 2.1.2
x_p, y_p, z_p	Blade cross-section coordinate systems
x_A	Blade cross-sectional aerodynamic center location from the elastic axis (positive aft of the elastic axis) normalized by the blade chord
x_I	Blade cross-sectional center-of-gravity location from the elastic axis (positive aft of the elastic axis)
{X}	Matrix defined in Eq. 119
{Y}	Matrix defined in Eq. 116
α	Angle defined in Eq. 79
α_s	Shaft tilt angle (positive forward tilt)
β_p	Rotor precone angle (positive up)
$\bar{\beta}_o$, $\bar{\beta}_{1c}$, $\bar{\beta}_{1s}$	Rotor steady-state flapping deflections; collective and cyclic motions, respectively

γ	Lock number $\frac{\rho a c R^4}{I_B}$
δ	Perturbation operator
δ_{ij}	Kronecker delta
δ_D	Rotor droop angle (positive up)
ε	Accuracy defined in Eq. 64
$\bar{\zeta}_o$, $\bar{\zeta}_{1c}$, $\bar{\zeta}_{1s}$	Rotor steady-state lagging deflections; collective and cyclic motions, respectively
θ	Blade pitch angle defined in Eq. 3
θ_c	Blade pitch angle due to the control input
θ_m	Blade ptich angle defined in Eq. 7
θ_o	Blade collective pitch angle
$\bar{\theta}_o$, $\bar{\theta}_{1c}$, $\bar{\theta}_{1s}$	Blade trim pitch angles; collective and cylic pitches, respectively
θ_R	Blade rigid pitch motion
θ_s	Blade pitch angle defined in Eq. 83
θ_{TW}	Blade built-in angle of twist
Θ_j	jth blade rigid pitch mode shape
λ	Inflow ratio defined in Eq. 70
μ	Advance ratio defined in Eq. 70
π	Variational functional defined in Eq. 40
π_n	nth element variational functional
ρ	Air density
ρ_B	Blade density
ϕ	Blade elastic torsion motion (positive nose up)
ϕ_I	Induced angle defined in Eq. 76

Φ_j	jth blade elastic torsion mode shape
ψ	Blade azimuth angle
Ω	Blade rotational speed
ω_j	jth blade natural frequency
ω_β	Blade flapping frequency
ω_ζ	Blade lagging frequency
ω_ϕ	Blade torsion frequency
$(\dot{\ })$, $(\ddot{\ })$	Time derivatives $\frac{\partial}{\partial t}$, $\frac{\partial}{\partial t^2}$
$(^{o})$, $(^{oo})$	Nondimensional time derivatives, $\frac{\partial}{\partial(\Omega t)}$, $\frac{\partial^2}{\partial^2(\Omega t)^2}$
$(\ )'$, $(\ )''$	Derivatives, $\frac{\partial}{\partial r}$, $\frac{\partial^2}{\partial r^2}$
$[\ ]^T$	Transposed matrix

SECTION 1

INTRODUCTION

1.1 General

Over the last decade the hingeless rotor has attained acceptance as an attractive concept for rotorcraft, and considerable research, development, and testing has been conducted. The main advantages of this system are improved flying qualities, and design simplicity of the rotor and rotor hub. The improved flight characteristics are achieved by transmission of the large blade moments to the aircraft because of the cantilevered boundary condition at the blade root of the hingeless rotor, while the conventional articulated rotor has reduced control power and damping due to the flapping hinge pin which eliminated the large bending moment. Higher control power and angular motion damping are thus obtained in the hingeless rotor flying qualities and the maneuverability are greatly improved. Another advantage is the simplicity of the rotor and the hub, which leads to lower manufacturing cost, greater weight and space savings, and simplified maintenance.

However, rotor blade aeroelastic stability and response become more sensitive to the various hingeless rotor configurations because of structural coupling between bending (flapwise and chordwise) and torsion of the long slender cantilever blade. Also, hingeless-rotor helicopters without feedback systems or without large horizontal tails have weak longitudinal dynamic stability with respect to attitude in the upper speed range and are sensitive to atmospheric turbulence.

Therefore, the study of the response of the hingeless rotor to atmospheric turbulence is necessary in evaluating the blade fatigue characteristics and the riding comfort of the vehicle, and in the development of gust alleviation systems. This study will aid in attaining better hingeless rotor flying qualities. However, like the fixed-wing aircraft for which extensive literature on analysis and testing of turbulence response exists, very little information is available on the response of rotorcraft to turbulence.

In view of such deficiencies mentioned above, it is necessary to perform

further theoretical analysis to establish an analytical method for determining hingeless rotor blade response to atmospheric turbulence in forward flight and to develop a gust-alleviation system. In this report, blade chordwise mass balance will be chosen as a principal ingredient to the gust alleviation system because this will provide a very simple blade-integrated feedback system equivalent to controlling blade pitch.

1.2 Brief Survey of Past Work

A good review and physical descriptions of the various dynamic and aeroelastic problems associated with hingeless rotorcraft have been given by Hohenemser in Ref. 1. Therefore, references pertinent only to the present problem will be cited below.

It may be said that the linear equations developed by Houbolt and Brooks in Ref. 2 were the first comprehensive equations applicable to rotating elastic cantilevered beams with twist. These free-vibration equations have been further developed by Hodges and Dowell in Ref. 3 to include nonlinear terms expressing large steady-state deflections.

In the early analyses of hingeless rotor instability, Young (Ref. 4) investigated the role of nonlinear coupling terms in flap-lag instability. Subsequent investigation was done by Hohenemser and Heaton (Ref. 5), using a numerical integration scheme to analyze flap-lag instability in hover and forward flight. A linear stability analysis of the hingeless blade in hover was conducted by Ormiston and Hodges (Ref. 6). They introduced structural flap-lag coupling to supplement the spring-restrained, centrally-hinged, rigid blade model which most predecessors used. The perturbation method in multiple time scales was applied to the nonlinear flap-lag instability problem of the spring-restrained, centrally-hinged, rigid blade by Tong (Refs. 7 and 8). The next logical step was to study the flap-lag instability of elastic cantilever blades. Friedmann and Tong (Refs. 9 and 10) studied flap-lag instability in hover and forward flight using the perturbation method in multiple time scales and a numerical integration method. Friedmann extended his work in Refs. 11 and 12. Peters (Ref. 13) studied the flap-lag instability in forward flight and showed the validity of the linearized perturbation equations for $\mu < 0.5$.

Concurrent with these flap-lag instability analyses, flap-lag-torsion equations of the hingeless rotor blade were developed and investigated. Miller and Ellis (Ref. 14) developed the flap-lag-pitch equations and showed the results of the effect of distributed torsion and finite steady-state deflections.

Friedmann and Tong (Ref. 10) investigated the elastic flap-lag-pitch equations. For the torsion degree of freedom, the rigid pitch due to control link flexibility was chosen. Friedmann extended the analysis to incorporate elastic torsion motion (Ref. 15).

Hodge and Ormiston applied their flap-lag-torsion equations to the uniform cantilever beam in hover; they extended their work in Ref. 16. In Ref. 17 they incorporated rigid pitch motion due to control link flexibility.

Extensive investigations were conducted on the hingeless helicopter BO-105 using the rigid offset-hinged blade mathematical model (Refs.18 through 24). They described various important design considerations for the hingeless rotor and showed analytical results in good agreement with experimental data. They also showed the significance of structural coupling such as pitch-lag coupling. Hansford and Simons (Ref. 25) also mentioned the important role of bending-torsion coupling.

Unfortunately, very little literature is available on the response of the helicopter to atmospheric turbulence as mentioned before. Among those, Refs. 26, 27, 28, and 29 analyzed the random blades response to random inputs, using various methods of computing the random response of a time-varying linear system. Gaonker and Hohenemser (Ref. 30) also showed the adequacy of the assumption that the turbulence velocity is uniform over the entire rotor disk if the ratio of the turbulence scale length to the rotor radius is larger than 4.0.

Arcidiacono et al. (Ref. 31) conducted an analytical study of articulated helicopter response to various gust profiles such as sine-squared and ramp gusts. They confirmed that the current gust alleviation factors specified in MIL-S-8698(ARG) are too conservative. However, they pointed out that the gust loadings can be an important consideration from a ride-comfort standpoint.

For the tilt-rotor aircraft, extensive analyses of the gust response in cruising flight were conducted by Johnson (Ref. 32) and Yasue (Ref. 33). In Ref. 32, Johnson summarized the comparison of theory with the results of full-scale tests of two proprotors in terms of critical damping ratios and frequencies of modes. The agreement between the theory and the experiment was good. He extended his theory (Ref. 34) to include various rotor configurations such as precone and droop as well as the transition flight regime between hovering and cruising flight. Concurrent with the extension of the theory, Frick and Johnson (Ref. 35) applied modern control theory to develop a gust alleviation system for the tilt-rotor. Wind tunnel experiments were conducted at M.I.T., using a one-ninth-scale tilt-rotor model subjected to vertical and longitudinal sinusoidal gusts as well as collective and cyclic pitch control inputs (Ref. 36). The experimental results showed good agreement with the theoretical analysis of Ref. 33. Further investigations were performed to develop a gust alleviation device for the gimballed tilt-rotor (Ref. 37), and subsequently, wind tunnel testing was conducted to verify the theory predictions (Ref. 38).

Finally, the chordwise blade mass balance system is briefly reviewed. Miller (Ref. 39) suggested chordwise blade mass balance to improve the helicopter flying quality. Hirsh et al. (Ref. 39) applied chordwise mass balance to the articulated rotor helicopter XH-17 and reduced the vibration stresses from 35 to 45 percent. Miller and Ellis (Ref. 14) analyzed the effectiveness of chordwise mass balance to reduce the vibratory root shear of the articulated helicopter. According to Refs. 19 and 23, a 2.5% forward shift of the center-of-gravity of the BO-105 blade reduced the rotor angle-of-attach instability time-to-double amplitude from 7 to 22 seconds. In conjunction with the improvement of the stability characteristics, a favorable gust response reduction was also obtained, as shown in Refs. 23 and 24. A 5% center-of-gravity forward shift reduced the flapping response by about 40% in trimmed flight at 100 knots, compared with no chordwise mass balance. Thus, blade center-of-gravity forward of the aerodynamic center will reduce both the angle-of-attack instability and the gust sensitivity.

1.3 The Purpose and Scope of the Research

The purpose of this work is to investigate the effectiveness of chordwise center-of-gravity shift in conjunction of blade torsional stiffness variation in alleviating the blade flapping response of the hingeless rotor blade theoretically and experimentally.

As the first step of the theoretical analysis, free vibration equations for the flap-lag-torsion-rigid pitch motion of the rotating nonuniform beam will be developed including precone, droop, torque offset, offsets between the elastic axis and cross-sectional center of gravity, built-in twist, and collective pitch. The rigid-pitch motion is due to control linkage flexibility. Based on these equations, the natural frequencies and corresponding normal coupled mode shapes of a rotating nonuniform rotor blade will be obtained using the subspace iteration method of the finite-element method. By the use of Galerkin's Method, the equations of motion for the blade with aerodynamic forces will be converted to modal equations. The equations will include the effect of steady-state deflections and the quasi-steady assumption will be employed for the aerodynamic forces. The coefficients of the equations are periodic in time in forward flight, so the harmonic balance approximation method (Ref. 40) will be used to avoid the complexity of periodic coefficients. These modal equations with constant coefficients will be the basis for a study of the hingeless rotor response to the vertical gust in cruising flight.

Eigenvalue analysis will be used to examine the rotor system stability with the blade mass balance, because the hingeless rotor system stability is very sensitive to the rotor configuration. To measure the effectiveness of blade chordwise mass balance to reduce blade gust response, the frequency response of the blade motion to vertical gusts will be analyzed.

The experimental program involves the design, construction, and testing of a five-foot diameter rotor. The rotor design is such that the torsional stiffness of the blade as well as the blade chordwise center-of-gravity location can be varied during the various phases of the test. The rotor is exposed to a sinusoidal waveform vertical gust and the flap, lag and torsion response of the rotor is measured. The construction and validation tests are

performed first on a three-bladed rotor employing "stiff torsion" blade. The tests continue on a rotor utilizing two counterweights and a single blade. In this configuration, a chordwise center-of-gravity shift is applied to the single blade in conjunction with variable blade torsional stiffness.

The experimental results are compared with the theoretical predictions.

SECTION 2

THEORETICAL ANALYSIS

2.1 The Equations of Motion for the Rotating Blade

2.1.1 Rotor Configuration

The hingeless rotor configuration considered in this report is described here. A cantilever rotor blade is attached to a rigid hub which incorporates built-in precone, the inclination of the pitch change bearing with respect to the plane of rotation (Fig. 1). Torque offset between the blade pitch axis and the center of rotation to minimize the steady-state blade stresses is included. Another angular offset considered here is droop, the inclination of the blade outboard of the pitch change bearing. Although built-in sweep is not treated here, the blade coning motion about the blade pitch bearing produces sweep at certain collective pitch settings.

The blade outboard of the pitch change bearing can be rotated about the feathering axis by moving the control linkage. Therefore, the control linkage flexibility will allow rigid-body pitching motion of the blade (called rigid pitch in this report). Blade flexibility will permit flap bending, lead-lag bending, and elastic torsion motions. The present analysis treats these deflections of a twisted blade with nonuniformities of mass, bending stiffness, and torsional rigidity distribution. Furthermore, the blade cross-sectional center of gravity, tension axis, and aerodynamic center offsets from the elastic axis are considered because these are important factors for the study of the mass-balanced-blade gust response.

The above configurations may differ for certain hingeless rotor designs. For example, the Westland WG-13 rotor design (Ref. 25), positioned the pitch change bearing outboard of the hub. In addition, a flapwise flexible element inboard and a matched stiffness element outboard of the pitch change bearing are incorporated to eliminate blade bending-torsion coupling. For this configuration, certain modifications are necessary in the present analysis.

2.1.2 Coordinate Systems and Inertia Loadings

The coordinate system x, y, and z (Fig. 2) is rotating with a constant

rotor angular velocity Ω about the z axis which is the axis of rotation. The x, y plane is a hub plane with the projection of the undeformed blade elastic axis with zero collective pitch lying on the y axis. The second coordinate system x', y', and z' is defined with the y' axis lying on the blade feathering axis and the x' axis parallel to the x axis. The third coordinate system, x", y", and z" is fixed to the blade root and as such locates the origin at the intersection of the blade elastic axis and blade root chordline. The y" axis coincides with the undeformed blade axis, the x" axis with the chordline, and the z" axis perpendicular to the x", y" plane.

The transformation between these three coordinate systems is described as follows: the x, y, z coordinate system is translated to the negative x direction at the torque offset distance e_o (positive forward). Then this transformed system is rotated about the x axis at the precone angle β_p (positive upward). Thus, the y' axis is determined, which coincides with the feathering axis. The x' axis is parallel to the x axis and the z' axis is also inclined at the angle of the precone from the z axis. The origin of the system is next translated along the new y axis at the distance of the rigid shank r_o (a portion of the hub). The system is rotated about the new x' axis at the droop angle δ_D (positive upward), then the y' axis lies on the y" axis. This intermediate system is again rotated about the y" axis at the pitch angle θ_m (positive nose-up), which includes the collective pitch θ_o, perturbation control pitch input θ_c, and the rigid pitch θ_R. This scheme makes the x', y', z' axes lie on the x",y",z" axes (Fig. 2).

The deformations described by the displacements of the elastic axis parallel to the x" and z" axes are v and w, respectively (Fig. 3). The radial displacement u parallel to the y" axis is included in this report. The in-plane displacement v is positive backward with respect to rotation. The out-of-plane displacement w is positive upward. It should be noted that v and w are displacements, respectively, parallel and perpendicular to the blade root chordline which is inclined at the collective pitch angle.

The x_p and z_p axes are the principal axes of the blade cross section for the shear center and y_p is the tangent to the deformed elastic axis. The

inclindation between the x", z" axes and the x_p, z_p axes defines the built-in angle of twist θ_{TW} and elastic torsion ϕ, which are both positive nose up (Fig. 3). The relation between the x", y" and z" axes and x_p, y_p, and z_p axes are defined by the rotation about x", z" axes at the deflection slope angles v' and w', and rotated about the y" axis at the angle of twist and torsion angle.

Next, the position vector to the arbitrary point of the blade cross section is defined. This point on the cross section expressed in the principal coordinates is as follows:

$$\vec{r}_x = \begin{bmatrix} x_p \\ 0 \\ z_p \end{bmatrix} \tag{1}$$

This vector is transformed by the transformation matrix [T] to the undeformed elastic axis system.

$$[T] = \begin{bmatrix} 1 & 0 & 0 \\ 0 & 1 & -w' \\ 0 & w & 1 \end{bmatrix} \begin{bmatrix} 1 & v' & 0 \\ -v' & 1 & 0 \\ 0 & 0 & 1 \end{bmatrix} \begin{bmatrix} \cos\theta & 0 & \sin\theta \\ 0 & 1 & 0 \\ -\sin\theta & 0 & \cos\theta \end{bmatrix} \tag{2}$$

$$\begin{bmatrix} \cos\theta & v' & \sin\theta \\ -v'\cos\theta + w'\sin\theta & 1 & -v'\sin\theta - w'\cos\theta \\ -\sin\theta & w' & \cos\theta \end{bmatrix}$$

where

$$\theta = \theta_{TW} + \phi$$

$$w' = \frac{\partial w}{\partial r} \quad , \quad v' = \frac{\partial v}{\partial r} \tag{3}$$

The built-in angle of twist is expressed by θ_{TW}; ϕ is the elastic torsion deflection; and v and w are chordwise and vertical deflections, respectively. The radial coordinate from the pitch change bearing along the undeformed elastic axis is taken as r.

The distance from the origin of the x", y", z" coordinate system to the origin of the principal axes of the blade cross section is defined by

$$\vec{r_D} = \begin{bmatrix} v \\ r+u \\ w \end{bmatrix} \tag{4}$$

where u is the radial displacement given by:

$$u = -\frac{1}{2} \int_0^r \left\{ (w')^2 + (v')^2 \right\} dr \tag{5}$$

It should be noted that the radial displacement includes only the geometrical shortening effect due to bending deflections. The displacement due to the tensile forces is neglected in this analysis.

The x", y" and z" systems are transformed by the transformation matrices $[T_\theta]$ and $[T_\delta]$ which are related to the collective pitch θ_m and the droop δ_D, respectively:

$$[T_\theta] = \begin{bmatrix} \cos\theta_m & 0 & \sin\theta_m \\ 0 & 1 & 0 \\ -\sin\theta_m & 0 & \cos\theta_m \end{bmatrix}, \quad [T_\delta] = \begin{bmatrix} 1 & 0 & 0 \\ 0 & 1 & -\delta_D \\ 0 & \delta_D & 0 \end{bmatrix} \tag{6}$$

where

$$\theta_m = \theta_o + \theta_R + \theta_c \tag{7}$$

The rigid shank position which will be added to the radial position is written as

$$\vec{r_o} = \begin{bmatrix} 0 \\ r_o \\ 0 \end{bmatrix} \tag{8}$$

The entire system will be rotated at the precone angle, for which the transformation matrix $[T_\beta]$ is

$$[T_\beta] = \begin{bmatrix} 1 & 0 & 0 \\ 0 & 1 & -\beta_p \\ 0 & \beta_p & 1 \end{bmatrix} \tag{9}$$

Finally, the translation due to the torque offset e_o is expressed by

$$\vec{r_e} = \begin{bmatrix} 0 \\ -e_o \\ 0 \end{bmatrix} \tag{10}$$

The position vector, $\vec{r}_B$, taken from the origin of the x,y,z system to the point on the blade cross section may be written

$$\vec{r_B} = \vec{r_e} + [T_\beta]\left\{\vec{r_o} + [T_\theta][T_\delta]\left(\vec{r_D} + [T]\,\vec{r_x}\right)\right\}$$

$$\begin{bmatrix} -e_o + r\delta_D \sin\theta_m + v\cos\theta_m + w\sin\theta_m \\ \quad + x_p\cos(\theta_m+\theta) + z_p\sin(\theta_m+\theta) \\ \text{----------} \end{bmatrix}$$

$$= \begin{bmatrix} r_o + r + u - r\beta_p\delta_D \cos\theta_m + \beta_p v \sin\theta_m \\ -(\delta_D + \beta_p \cos\theta_m) w + x_p\{\delta_D \sin\theta + \\ \beta_p \sin(\theta_m+\theta) - v'\cos\theta + w'\sin\theta\} \\ + z_p\{-\delta_D\cos\theta - \beta_p\cos(\theta_m+\theta) + v'\sin\theta \\ + w'\cos\theta\} \\ \hline r\delta_D\cos\theta_m + \beta_p(r_o+r) - v\sin\theta_m \\ + w\cos\theta_m - x_p\sin(\theta_m+\theta) \\ + z_p\cos(\theta_m+\theta) \end{bmatrix}$$

(11)

The acceleration $\vec{a}$ of the fixed coordinate system when the blade is rotating at angular velocity Ω about the z axis is:

$$\vec{a} = \ddot{\vec{r}}_B + 2\vec{\Omega}\times\dot{\vec{r}}_B + \vec{\Omega}\times(\vec{\Omega}\times\vec{r}_B)$$

$$\begin{bmatrix} \ddot{v}\cos\theta_m + \ddot{w}\sin\theta_m + r\delta_D\ddot{\theta}_R\cos\theta_m \\ + (\ddot{\theta}_R + \ddot{\phi})\{-x_p\sin(\theta_m+\theta) + z_p\cos(\theta_m+\theta)\} \\ - 2\Omega\{\beta_p(\dot{v}\sin\theta_m - \dot{w}\cos\theta_m) - \delta_D\dot{w} \\ + x_p(-\dot{v}'\cos\theta + \dot{w}'\sin\theta) \\ + z_p(-\dot{v}'\sin\theta - \dot{w}'\cos\theta)\} \end{bmatrix}$$

$$
\begin{bmatrix}
-\Omega^2\{-e_o + r\delta_D \sin\theta_m + v\cos\theta_m + w\sin\theta_m \\
+ x_p\cos(\theta_m+\theta) + z_p\sin(\theta_m+\theta)\} \\
+ \ddot{\theta}_R w\cos\theta_m - \ddot{\theta}_R v\sin\theta_m - 2\Omega\dot{u} \\
+ 2\dot{\theta}_R\dot{w}\cos\theta_m - 2\dot{\theta}_R\dot{v}\sin\theta_m \\
\hline
\ddot{u} + \beta_p(\ddot{v}\sin\theta_m - \ddot{w}\cos\theta_m) - \delta_D\ddot{w} \\
+ x_p(-\ddot{v}'\cos\theta + \ddot{w}'\sin\theta) + z_p(-\ddot{v}'\sin\theta - \ddot{w}'\cos\theta) \\
+ 2\Omega\left[\dot{v}\cos\theta_m + \dot{w}\sin\theta_m + (\dot{\theta}_R+\dot{\phi})\{-x_p\sin(\theta_m+\theta)\right. \\
\left. + z_p\cos(\theta_m+\theta)\} + r\delta_D\dot{\theta}_R\cos\theta_m\right] \\
= \quad -\Omega^2\left[r_o + r - r\beta_p\delta_D\cos\theta_m + \beta_p v\sin\theta_m\right. \\
-(\delta_D+\beta_p\cos\theta_m)w + x_p\{-v'\cos\theta + w'\sin\theta \\
+ \delta_D\sin\theta + \beta_p\sin(\theta_m+\theta)\} - z_p\{v'\sin\theta \\
\left. + w'\cos\theta + \delta_D\cos\theta + \beta_p\cos(\theta_m+\theta)\}\right] \\
+ 2\Omega\dot{\theta}_R w\cos\theta_m \\
\hline
-\ddot{v}\sin\theta_m + \ddot{w}\cos\theta_m - r\delta_D\ddot{\theta}_R\sin\theta_m \\
- x_p(\ddot{\theta}_R+\ddot{\phi})\cos(\theta_m+\theta) \\
- z_p(\ddot{\theta}_R+\ddot{\phi})\sin(\theta_m+\theta) \\
- \ddot{\theta}_R w\sin\theta_m - \ddot{\theta}_R v\cos\theta_m \\
- 2\dot{v}\dot{\theta}_R\cos\theta_m - 2\dot{w}\dot{\theta}_R\sin\theta_m
\end{bmatrix}
\tag{12}
$$

Although double underlined terms are nonlinear terms, they are retained to describe steady-state deflection effects on the blade pitch motion.

The acceleration $\vec{a}_{EA}$ in the undeformed elastic axis coordinate (x", y", z" coordinate system) is obtained by the transformation.

$$\vec{a}_{EA} = [T_\delta]^T [T_\theta]^T [T_\beta]^T \vec{a}$$

$$= \begin{bmatrix} \ddot{v} + r\delta_D \ddot{\theta}_R + \ddot{\theta}_R w - 2\Omega \dot{u} + 2\dot{\theta}_R \dot{w} \\ + 2\Omega (\beta_p + \delta_D \cos\theta_m) \dot{w} \\ - \Omega^2 [(r_0 + r)\beta_p \sin\theta_m + \cos\theta_m \{-e_0 \\ + r\delta_D \sin\theta_m + v\cos\theta_m + w \sin\theta_m\}] \\ + x_p [-(\ddot{\theta}_R + \ddot{\phi}) \sin\theta + 2\Omega \cos\theta_m (\dot{v}' \cos\theta \\ - \dot{w}' \sin\theta) - \Omega^2 \cos\theta_m \cos(\theta_m + \theta)] \\ + z_p [(\ddot{\theta}_R + \ddot{\phi}) \cos\theta + 2\Omega \cos\theta_m (\dot{v}' \sin\theta \\ + \dot{w}' \cos\theta) - \Omega^2 \cos\theta_m \sin(\theta_m + \theta)] \\ \hline \ddot{u} + 2\Omega (\dot{v} \cos\theta_m + \dot{w} \sin\theta_m \\ + r\delta_D \dot{\theta}_R \cos\theta_m) + 2\Omega\theta_R \dot{w} \cos\theta_m \\ - \Omega^2 [(r_0 + r) + \delta_D \sin\theta_m (-e_0 + r\delta_D \sin\theta_m) \\ + (v \sin\theta_m - w\cos\theta_m)(\beta_p + \delta_D \cos\theta_m)] \\ + x_p [-\ddot{v}' \cos\theta + \ddot{w}' \sin\theta - 2\Omega(\dot{\theta}_R + \dot{\phi}) \sin(\theta_m + \theta) \\ - \Omega^2 \{\delta_D \sin\theta + \delta_D \sin\theta_m \cos(\theta_m + \theta) \\ + \beta_p \sin(\theta_m + \theta) - v' \cos\theta + w' \sin\theta\}] \\ + z_p [-\ddot{v}' \sin\theta - \ddot{w}' \cos\theta + 2\Omega(\dot{\theta}_R + \dot{\phi}) \cos(\theta_m + \theta) \end{bmatrix}$$

$$
\begin{bmatrix}
 & -\Omega^2\{-\delta_D\cos\theta + \delta_D \sin\theta_m \sin(\theta_m+\theta) \\
 & -\beta_p \cos(\theta_m+\theta) - v'\sin\theta - w'\cos\theta\}\big] \\
\hline
 & \ddot{w} - \ddot{\theta}_R v - 2\Omega(\beta_p + \delta_D\cos\theta_m)\dot{v} - 2\dot{v}\dot{\theta}_R \\
 & -\Omega^2\big[-(r_o+r)(\delta_D+\beta_p\cos\theta_m) + (-e_o + \\
 & r\delta_D\sin\theta_m)\sin\theta_m + v\sin\theta_m\cos\theta_m + w\sin^2\theta_m\big] \\
 & + x_p\big[-(\ddot{\theta}_R+\ddot{\phi})\cos\theta - 2\Omega(-\dot{v}'\sin\theta_m\cos\theta \\
 & + \dot{w}'\sin\theta_m\sin\theta) - \Omega^2\sin\theta_m\cos(\theta_m+\theta)\big] \\
 & + z_p\big[-(\ddot{\theta}_R+\ddot{\phi})\sin\theta + 2\Omega(\dot{v}'\sin\theta_m\sin\theta \\
 & + \dot{w}'\sin\theta_m\cos\theta) - \Omega^2\sin\theta_m\sin(\theta_m+\theta)\big]
\end{bmatrix} \tag{13}
$$

The distributed inertia forces $\vec{P}^I_{EA}$ due to the acceleration in the x", y", z" coordinate system are

$$
\vec{P}^I_{EA} = -\int_A \rho_B \vec{a}_{EA}\, dx_p\, dz_p
$$

$$
\begin{bmatrix}
 & m\ddot{v} + m r\delta_D\ddot{\theta}_R + m w\ddot{\theta}_R - 2m\Omega\dot{u} \\
 & + 2m\dot{\theta}_R\dot{w} + 2m\Omega(\beta_p+\delta_D\cos\theta_m)\dot{w} \\
 & - m\Omega^2\{(r_o+r)\beta_p\sin\theta_m + \cos\theta_m(-e_o \\
 & + r\delta_D\sin\theta_m + v\cos\theta_m + w\sin\theta_m)\} \\
 & + m x_I\{-(\ddot{\theta}_R+\ddot{\phi})\sin\theta + 2\Omega\cos\theta_m(\dot{v}'\cos\theta
\end{bmatrix}
$$

$$
= -\left[\begin{array}{l}
\quad -\ddot{v}'\sin\theta - \Omega^2 \cos\theta_m \cos(\theta_m+\theta)\Big\} \\
\hline
m\ddot{u} + 2m\Omega(\dot{v}\cos\theta_m + \dot{w}\sin\theta_m \\
+ r\delta_D \dot{\theta}_R \cos\theta_m + \dot{\theta}_R w \cos\theta_m) \\
- m\Omega^2\{(r_0+r) + \delta_D \sin\theta_m(-e_0 + r\delta_D \sin\theta_m) \\
\quad +(v\sin\theta_m - w\cos\theta_m)(\beta_p + \delta_D\cos\theta_m)\Big\} \\
+ m x_I\big[-\ddot{v}'\cos\theta + \ddot{w}'\sin\theta \\
-2\Omega(\dot{\theta}_R+\dot{\phi})\sin(\theta_m+\theta) - \Omega^2\{\delta_D\sin\theta \\
+\delta_D\sin\theta_m\cos(\theta_m+\theta) + \beta_p\sin(\theta_m+\theta) \\
-v'\cos + w'\sin\theta\}\big] \\
\hline
m\ddot{w} - 2m\Omega(\beta_p + \delta_D\cos\theta_m)\dot{v} \\
- m\Omega^2\{-(r_0+r)(\delta_D+\beta_p\cos\theta_m) + (-e_0 \\
+ r\delta_D\sin\theta_m + v\cos\theta_m + w\sin\theta_m)\sin\theta_m\Big\} \\
+ m x_I\big[-(\ddot{\theta}_R+\ddot{\phi})\cos\theta - v\ddot{\theta}_R \\
-2\Omega\{-\dot{v}'\sin\theta_m\cos\theta + \dot{w}'\sin\theta_m\sin\theta\} \\
-2\dot{v}\dot{\theta}_R - \Omega^2\sin\theta_m\cos(\theta_m+\theta)\big]
\end{array}\right] \qquad (14)
$$

where m is the mass per unit length, x_I is the center of gravity of the cross section (positive aft of the elastic axis), ρ_B is the mass density of the blade, and A is the cross-sectional area of the blade. It is assumed that the cross section is symmetrical about the x_p axis when the sectional integrals are carried out. The position vector $\vec{r}_p$, the distance from the deformed elastic axis to the point on the blade cross section, may be written in the x", y", z" coordinate system as

$$\vec{r}_p = \left[T\right] \vec{r}_x$$

$$= \begin{bmatrix} x_p \cos\theta + z_p \sin\theta \\ x_p(-v'\cos\theta + w'\sin\theta) - z_p(v'\sin\theta + w'\cos\theta) \\ -x_p \sin\theta + z_p \cos\theta \end{bmatrix} \tag{15}$$

The inertial moments $\vec{q}^I$ per unit length in the x", y", z" coordinate system are given by

$$\vec{q}^I = -\int_A \rho_B (\vec{r}_p \times \vec{a}_{EA})\, dx_p\, dz_p$$

$$= -\begin{bmatrix} 2m x_I \Omega \sin\theta(\dot{v}\cos\theta_m + \dot{w}\sin\theta_m) \\ -m x_I \Omega^2 (r_o + r)\sin\theta \\ \hline -m x_I(\ddot{v}\sin\theta + \ddot{w}\cos\theta) - m x_I r \delta_D \sin\theta\, \ddot{\theta}_R \\ + m x_I \Omega^2 \left[-(r_o+r)\left\{\beta_p \cos(\theta_m+\theta) + \delta_D \cos\theta\right\}\right. \\ + (-e_o + r\delta_D \sin\theta_m + v\cos\theta_m \\ \left. + w\sin\theta_m)\sin(\theta_m+\theta)\right] + I_o(\ddot{\theta}_R + \ddot{\phi}) \\ + (I_{zp} - I_{xp})\Omega^2 \cos(\theta_m+\theta)\sin(\theta_m+\theta) \\ \hline 2m x_I \Omega \cos\theta\,(\dot{v}\cos\theta_m + \dot{w}\sin\theta_m) \\ -m x_I \Omega^2 (r_o + r)\cos\theta \end{bmatrix} \tag{16}$$

where I_o is the moment of inertia of the cross section per unit length and I_{zp}, I_{xp} are also defined as

$$I_o \equiv \int_A \rho_B (x_p^2 + z_p^2)\, dx_p\, dz_p$$

$$I_{zp} \equiv \int_A \rho_B\, x_p^2\, dx_p\, dz_p \tag{17}$$

$$I_{xp} \equiv \int_A \rho_B\, z_p^2\, dx_p\, dz_p$$

Thus far, inertial loadings are derived about the undeformed elastic axis. Next, the inertial loading about the feathering axis will be obtained.

The position vector $\vec{r}_{FA}$, the distance from the feathering axis to the point on the blade cross section, is given in the x',y',z' coordinate systems by

$$\vec{r}_{FA} = [T_\beta]^T \left[\vec{r}_B - \left\{ \vec{r}_e + [T_\beta]\left(\vec{r}_o + [T_\theta][T_\delta]\, \vec{r}_R \right) \right\} \right]$$

$$= [T_\theta][T_\delta] \left(\vec{r}_D - \vec{r}_R + [T]\, \vec{r}_x \right) \tag{18}$$

where

$$\vec{r}_R = \begin{Bmatrix} 0 \\ r \\ 0 \end{Bmatrix} \tag{19}$$

Hence,

$$\vec{r}_{FA} = \begin{bmatrix} v\cos\theta_m + w\sin\theta_m + x_p\cos(\theta_m+\theta) + z_p\sin(\theta_m+\theta) \\ +r\delta_D\sin\theta_m \\ \hline x_p(-v'\cos\theta + w'\sin\theta) - z_p(v'\sin\theta + w'\cos\theta) \\ -\delta_D(w - x_p\sin\theta + z_p\cos\theta) \\ \hline -v\sin\theta_m + w\cos\theta_m - x_p\sin(\theta_m+\theta) \\ + z_p\cos(\theta_m+\theta) + r\delta_D\cos\theta_m \end{bmatrix} \tag{20}$$

The accelerations $\vec{a}_{FA}$ in the x',y',z' coordinate systems may be written from Eq. 12 as

$$\vec{a}_{FA} = \left[T_\beta\right]^T \vec{a} \tag{21}$$

The inertial moment $\vec{q}^I$ about the x',y' and z' axes is defined by

$$\vec{q}^I_{FA} = -\int_A (\vec{r}_{FA} \times \vec{a}_{FA})\, dx_p dz_p \tag{22}$$

Only the component of $\vec{q}^I_{FA}$ about the feathering axis is needed, as given by

$$\begin{aligned} q^I_{FA} = &-I_o(\ddot{\phi} + \ddot{\theta}_R) - mr^2\delta^2\ddot{\theta}_R - mr\delta_D\ddot{v} \\ &+ mx_I\ddot{v}\sin\theta + mx_I\ddot{w}\cos\theta + 2mx_I r\delta_D\ddot{\theta}_R\sin\theta \\ &+ mx_I r\delta_D\ddot{\phi}\sin\theta \\ &+ m\Omega^2\beta_p(r_o+r)\left\{x_I\cos(\theta_m+\theta) + r\delta_D\sin\theta_m\right\} \\ &- m\Omega^2 e_o r\delta_D\cos\theta_m + m\Omega^2 r\delta_D x_I\cos(2\theta_m+\theta) \end{aligned}$$

$$
\begin{aligned}
&+ m\Omega^2 v \left\{ \beta_p (r_o + r) \cos\theta_m + e_o \sin\theta_m + r\delta_D \cos 2\theta_m \right. \\
&\left. - x_I \sin(2\theta_m + \theta) \right\} \\
&+ m\Omega^2 w \left\{ \beta_p (r_o + r) \sin\theta_m - e_o \cos\theta_m + r\delta_D \sin 2\theta_m \right. \\
&\left. + x_I \cos(2\theta_m + \theta) \right\} \\
&+ \Omega^2 (I_{xp} - I_{zp}) \cos(\theta_m + \theta) \sin(\theta_m + \theta) \\
&- m\ddot{v} w + m\ddot{w} v + m\Omega^2 w v \cos(2\theta_m) \\
&- \tfrac{1}{2} m\Omega^2 v^2 \sin(2\theta_m) + \tfrac{1}{2} m\Omega^2 w^2 \sin(2\theta_m)
\end{aligned}
\tag{23}
$$

2.1.3 Equilibrium Equations of the Beam

Considering a differential length dx of the deformed beam (Fig. 5), the equilibrium equations will be established in the x',y' and z' coordinate systems (undeformed elastic axis).

The moment equations are

$$
\begin{aligned}
&\frac{\partial M_{y''}}{\partial r} + V_x \frac{\partial w}{\partial r} - V_z \frac{\partial v}{\partial r} + q_y = 0 \\
&\frac{\partial M_{x''}}{\partial r} - T \frac{\partial w}{\partial r} + V_z + q_x = 0 \\
&\frac{\partial M_{z''}}{\partial r} + T \frac{\partial v}{\partial r} - V_x + q_z = 0
\end{aligned}
\tag{24}
$$

Similarly, the force equations are

$$
\begin{aligned}
&\frac{\partial T}{\partial r} + P_y = 0 \\
&\frac{\partial V_x}{\partial r} + P_x = 0 \\
&\frac{\partial V_z}{\partial r} + P_z = 0
\end{aligned}
\tag{25}
$$

where $M_{x"}$ and $M_{z"}$ are structural bending moments and $M_{y"}$ the torsional moment. V_x and V_z are shear forces and T is the tension force. External forces and moments of inertial and aerodynamic origin are described by p_x, p_y, p_z, q_x, q_y, and q_z. Substituting Eq. 25 into Eq. 24 after differentiation of Eq. 25 by r yields

$$\frac{\partial^2 M_{x"}}{\partial r^2} + \frac{\partial q_x}{\partial r} - \frac{\partial}{\partial r}\left(T\frac{\partial w}{\partial r}\right) - p_z = 0$$

$$\frac{\partial M_{z"}}{\partial r^2} + \frac{\partial q_z}{\partial r} + \frac{\partial}{\partial r}\left(T\frac{\partial v}{\partial r}\right) + p_x = 0$$

$$\frac{\partial^2 M_{y"}}{\partial r} + \left(\frac{\partial M_z}{\partial r}\frac{\partial w}{\partial r} + \frac{\partial M_x}{\partial r}\frac{\partial v}{\partial r}\right) + q_z\frac{\partial w}{\partial r} + q_x\frac{\partial v}{\partial r} + q_y = 0 \qquad (26)$$

$$T = \int_r^R p_y\, dr$$

Moments in Eq. 26 will be transformed to moments M_x, M_y, and M_z in the deformed elastic axis coordinate system with the transformation matrix [T'] obtained from Eq. 2 with θ equalling zero:

$$\begin{Bmatrix} M_{x"} \\ M_{y"} \\ M_{z"} \end{Bmatrix} = [T'] \begin{Bmatrix} M_x \\ M_y \\ M_z \end{Bmatrix} \quad ; \quad [T'] = \begin{bmatrix} 1 & v' & 0 \\ -v' & 1 & -w' \\ 0 & w' & 1 \end{bmatrix} \qquad (27)$$

For the force components T, p_x, etc., the same transformation law holds; therefore, an identical transformation may be used with sufficient accuracy. Applying the transformation law in Eq. 27 to Eq. 26 yields

$$\frac{\partial^2 M_x}{\partial r^2} + \frac{\partial q_{bx}}{\partial r} - \frac{\partial}{\partial r}\left(T \frac{\partial w}{\partial r}\right) - P_z = 0$$

$$\frac{\partial^2 M_z}{\partial r^2} + \frac{\partial q_{bz}}{\partial r} + \frac{\partial}{\partial r}\left(T \frac{\partial v}{\partial r}\right) + P_x = 0$$

$$\frac{\partial M_y}{\partial r} + \underline{M_z \frac{\partial^2 w}{\partial r^2} + M_x \frac{\partial^2 v}{\partial r^2}} + q_{bz} \frac{\partial w}{\partial r} + q_{bx} \frac{\partial v}{\partial r} + q_{by} = 0$$

$$T = \int_r^R P_y \, dr \qquad (28)$$

These are the usual simple beam theory equations. It should be noted that the underlined terms in Eq. 28 are elastic torsion-bending structural coupling terms introduced by Mil' et al. (Ref. 41). Similar terms when the motions are rigid pitch-flap were identified by Miller and Ellis in Ref. 14.

2.1.4 Moment and Displacement Relations

Based on the work in Ref. 2, the moment-displacement relation is given in the principal axes coordinate system (x_p, y_p, and z_p axes) by

$$M_{xp} = EI_F (v'' \sin\theta + w'' \cos\theta)$$

$$M_{yp} = (GJ + k_A^2 T)\phi' + k_A^2 T \theta'_{TW} \qquad (29)$$

$$M_{zp} = EI_C (-v'' \cos\theta + w'' \sin\theta) + e_N T$$

where M_{xp} and M_{zp} are bending moments and M_{yp} is the torsional moment. Flapwise and lagwise bending stiffnesses are EI_F and EI_C, torsional rigidity is GJ, tension force is T, e_N is the neutral axis location, positive aft of the

elastic axis of the blade, respectively, and k_A^2 is defined as follows:

$$k_A^2 = \frac{1}{A} \iint_A (x_p^2 + z_p^2)\, dx_p\, dz_p \tag{30}$$

The blade cross-sectional area is expressed as A.

These moments are transformed to the undeformed elastic axis coordinate system (x", y", and z" coordinates) by the transformation matrix [T]:

$$\begin{Bmatrix} M_x \\ M_y \\ M_z \end{Bmatrix} = [T] \begin{Bmatrix} M_{xp} \\ M_{yp} \\ M_{zp} \end{Bmatrix}$$

$$= \begin{bmatrix} (EI_F \cos^2\theta + EI_c \sin^2\theta)\, w'' \\ + \{(EI_F - EI_c)\cos\theta \sin\theta\}\, v'' \\ + (k_A^2 T \theta'_{TW}) v' + e_N T \sin\theta \\ \hline (GJ + k_A^2 T)\, \phi' + k_A^2 T \theta'_{TW} \\ - e_N T (v' \sin\theta + w' \cos\theta) \\ \hline -(EI_F \sin^2\theta + EI_c \cos^2\theta)\, v'' \\ -\{(EI_F - EI_c)\cos\theta \sin\theta\}\, w'' \\ + (k_A^2 T \theta'_{TW})\, w' + e_N T \cos\theta \end{bmatrix} \tag{31}$$

2.1.5 Partial Differential Equations of Motion

By substituting Eqs. 14, 16 and 31 into Eq. 26, the partial differential equations of motion can be obtained in terms of v, w, ϕ, and θ_R. An additional equation for the rigid pitch will be derived later in this subsection. It should be noted that in the bending equations, only first-order terms are retained while in the torsion and rigid-pitch equations up to second-order terms are retained. Generally, the third-order terms are discarded except when these third-order terms have direct effect upon the torsion and rigid-pitch motions. In other words, these are diagonal terms of the coefficients of the torsion and rigid-pitch equations if these equations were expressed in matrix form. Small angle assumptions should also be used as follows:

$$\begin{aligned} \cos\theta_m &= \cos\theta_o - (\theta_R + \theta_c)\sin\theta_o \\ \sin\theta_m &= \sin\theta_o + (\theta_R + \theta_c)\cos\theta_o \end{aligned} \tag{32}$$

and

$$\begin{aligned} \cos\theta &= \cos\theta_{TW} - \phi\sin\theta_{TW} \\ \sin\theta &= \sin\theta_{TW} + \phi\cos\theta_{TW} \end{aligned} \tag{33}$$

where θ_o, θ_R, and θ_c are the collective pitch, the rigid-pitch motion and the control pitch input, respectively. The built-in angle of twist θ_{TW} and the collective pitch angles can be large. Thus, the equations may be written as follows:

w equation:

$$
\begin{aligned}
&\Big[(EI_F \cos^2\theta_{TW} + EI_C \sin^2\theta_{TW})\, w'' \\
&+ \{(EI_F - EI_C)\cos\theta_{TW}\sin\theta_{TW}\}\, v'' + (e_N T \cos\theta_{TW})\,\phi \Big]'' \\
&- \Big[2m x_I \Omega \sin\theta_{TW} (\dot{v}\cos\theta_o + \dot{w}\sin\theta_o) \\
&\quad - m x_I \Omega^2 (r_o + r)(\cos\theta_{TW})\,\phi \Big]' - (T w')' \\
&+ m\ddot{w} - 2m\Omega(\beta_p + \delta_D \cos\theta_o)\,\dot{v} \\
&- m\Omega^2 \{\beta_p (r_o + r)\,\theta_R \sin\theta_o + r\delta_D \theta_R \sin(2\theta_o) \\
&+ v \sin\theta_o \cos\theta_o + w \sin^2\theta_o - e_o \theta_R \cos\theta_o\} \\
&- m x_I (\ddot{\theta}_R + \ddot{\phi})\cos\theta_{TW} - m v \ddot{\theta}_R - 2m\dot{v}\dot{\theta}_R - m\Omega^2 v \theta_R \\
&- 2m\Omega x_I \sin\theta_o (-\dot{v}\cos\theta_{TW} + \dot{w}'\sin\theta_{TW}) \\
&- m x_I \Omega^2 \{\theta_R \cos(2\theta_o + \theta_{TW}) - \phi \sin(\theta_o + \theta_{TW})\sin\theta_o\} \\
&= P_w - m\Omega^2 (r_o + r)(\delta_D + \beta_p \cos\theta_o) \\
&\quad + m\Omega^2 \sin\theta_o (-e_o + r\delta_D \sin\theta_o) \\
&\quad + m\Omega^2 x_I \sin\theta_o \cos(\theta_o + \theta_{TW}) \\
&\quad - \{m x_I \Omega^2 \sin\theta_{TW} (r_o + r)\}' - (e_N T \sin\theta_{TW})''
\end{aligned}
$$

(34)

v equation:

$$
\begin{aligned}
&\Big[(EI_F \sin^2\theta_{TW} + EI_C \cos^2\theta_{TW})\, v'' \\
&\quad \{(EI_F - EI_C)\cos\theta_{TW}\sin\theta_{TW}\}\, w'' + (e_N T \sin\theta_{TW})\phi\Big]'' \\
&+ \Big[2m x_I \Omega \cos\theta_{TW}(\dot v \cos\theta_0 + \dot w \sin\theta_0) \\
&\quad + m x_I \Omega^2 (r_0 + r)(\sin\theta_{TW})\phi\Big]' - (T v')' \\
&+ m\ddot v + m r \delta_D \ddot\theta_R + 2m\Omega(\beta_p + \delta_D \cos\theta_0)\dot w \\
&- 2m\Omega \dot u + m w \ddot\theta_R + 2m \dot w \dot\theta_R - m\Omega^2 w \theta_R \cos\theta_0 \\
&- m\Omega^2 \{\beta_p (r_0 + r)\theta_R \sin\theta_0 + r\delta_D \theta_R \cos(2\theta_0) \\
&+ v\cos^2\theta_0 + w \sin\theta_0 \cos\theta_0 + e_0 \theta_R \sin\theta_0\} \\
&- m x_I (\ddot\theta_R + \ddot\phi)\sin\theta_{TW} \\
&+ 2m x_I \Omega \cos\theta_0 (\dot v' \cos\theta_{TW} - \dot w' \sin\theta_{TW}) \\
&+ m x_I \Omega^2 \{\theta_R \sin(2\theta_0 + \theta_{TW}) + \phi \sin(\theta_0 + \theta_{TW})\cos\theta_0\} \\
&= P_v + m\Omega^2 (r_0 + r)\beta_p \sin\theta_0 \\
&+ m\Omega^2 \cos\theta_0 (-e_0 + r\delta_D \sin\theta_0) \\
&+ m\Omega^2 x_I \cos(\theta_0 + \theta_{TW})\cos\theta_0 \\
&+ \{m x_I \Omega^2 \cos\theta_{TW}(r_0 + r)\}' - (e_N T \sin\theta_{TW})''
\end{aligned}
\tag{35}
$$

ϕ equation:

$$\left\{(GJ + k_A^2 T)\phi'\right\}' - (e_N T \sin\theta_{TW})v'' - (e_N T \cos\theta_{TW})w''$$

$$+ (EI_F - EI_C)\left[\left\{(v'')^2 - (w'')^2\right\}\sin\theta_o\cos\theta_o + w''v''\cos(2\theta_o)\right]$$

$$+ m x_I \Omega^2 (r_o + r)(w'\cos\theta_{TW} + v'\sin\theta_{TW})$$

$$+ m x_I (\ddot{v}\sin\theta_{TW} + \ddot{w}\cos\theta_{TW}) + m x_I r \delta_D \sin\theta_{TW}\ddot{\theta}_R$$

$$+ m x_I \Omega^2 (r_o + r)\beta_p(\theta_R + \phi)\sin(\theta_o + \theta_{TW})$$

$$- m x_I \Omega^2 (r_o + r)\delta_D \phi \sin\theta_{TW}$$

$$- m x_I \Omega^2 r \delta_D \theta_R \cos\theta_o \sin(\theta_o + \theta_{TW})$$

$$- m x_I \Omega^2 \sin(\theta_o + \theta_{TW})(v\cos\theta_o + w\sin\theta_o)$$

$$- m x_I \Omega^2 (-e_o + r\delta_D \sin\theta_o)(\theta_R + \phi)\cos(\theta_o + \theta_{TW})$$

$$- I_o(\ddot{\theta}_R + \ddot{\phi}) - (I_{zp} - I_{xp})\Omega^2(\theta_R + \phi)\cos(2\theta_o + 2\theta_{TW})$$

$$= -M_\phi - m x_I \Omega^2 (r_o + r)\beta_p\left\{\delta_D\cos\theta_{TW} + \cos(\theta_o + \theta_{TW})\right\}$$

$$+ m x_I \Omega^2 \sin(\theta_o + \theta_{TW})(-e_o + r\delta_D \sin\theta_o)$$

$$+ \frac{1}{2}(I_{zp} - I_{xp})\Omega^2 \sin(2\theta_o + 2\theta_{TW}) - (T k_A^2 \theta'_{TW})' \qquad (36)$$

where P_w and P_v are aerodynamic forces corresponding to deflections w and v (positive the same directions as deflections) and M_ϕ is an aerodynamic moment about the elastic axis (positive nose up).

The quantity T in Eqs. 34, 35, and 36 is obtained from Eq. 28 and may be expressed as

$$T = \int_r^R \left[m\Omega^2 (r_o + r) - 2m\Omega (\dot{v}\cos\theta_o + \dot{w}\sin\theta_o) \right] dr \qquad (37)$$

In rigid-pitch motion, the structural stiffness is given by the control linkage flexibility, represented by a spring element K_θ. The aerodynamic moment for the rigid pitch motion is expressed by M_θ (positive nose up). The equation may be expressed as

$$-\int_o^R \left(\xi^I_{\tau A} \right) dr + K_\theta \theta_R = M_\theta \qquad (38)$$

Substituting Eq. 24 into Eq. 37 yields

$$K_\theta \theta_R + \int_o^R \Big[I_o (\ddot{\theta}_R + \ddot{\phi}) + m r^2 \delta_D^2 \ddot{\theta}_R - m\ddot{v} w + m\ddot{w} v$$
$$+ m r \delta_D \ddot{v} - m x_I \ddot{v} \sin\theta_{TW} - m x_I \ddot{w} \cos\theta_{TW}$$
$$- 2m x_I r \delta_D \ddot{\theta}_R \sin\theta_{TW} - m x_I r \delta_D \ddot{\phi} \sin\theta_{TW}$$
$$- (I_{xp} - I_{zp}) \Omega^2 (\theta_R + \phi) \cos(2\theta_o + 2\theta_{TW})$$
$$+ m x_I \Omega^2 \beta_p (r_o + r)(\theta_R + \phi) \sin(\theta_o + \theta_{TW})$$
$$- m\Omega^2 \beta_p r (r_o + r) \delta_D \theta_R \cos\theta_o$$
$$- m\Omega^2 e_o r \delta_D \theta_R \sin\theta_o - m\Omega^2 r^2 \delta_D^2 \theta_R \cos(2\theta_o)$$
$$- m\Omega^2 e_o x_I (\theta_R + \phi) \cos(\theta_o + \theta_{TW})$$
$$+ m\Omega^2 r \delta_D x_I (2\theta_R + \phi) \sin(2\theta_o + \theta_{TW})$$
$$- m\Omega^2 v \{ \beta_p (r_o + r) \cos\theta_o + e_o \sin\theta_o$$

$$
\begin{aligned}
&+ r\delta_D \cos(2\theta_o) - \chi_I \sin(2\theta_o + \theta_{TW})\Big\} \\
&- m\Omega^2 w\Big\{\beta_p(r_o+r)\sin\theta_o - e_o\cos\theta_o \\
&+ r\delta_D \sin(2\theta_o) + \chi_I \cos(2\theta_o + \theta_{TW})\Big\} \\
&+ m\Omega^2 w v \cos(2\theta_o) - \tfrac{1}{2} m\Omega^2 v^2 \sin(2\theta_o) + \tfrac{1}{2} m\Omega^2 w^2 \sin(2\theta_o)\Big] dr \\
= M_\theta + &\int_o^R \Big[\tfrac{1}{2}(I_{xp} - I_{zp})\Omega^2 \sin(2\theta_o + 2\theta_{TW}) \\
&+ m\Omega^2 \beta_p (r_o+r)\chi_I \cos(\theta_o + \theta_{TW}) \\
&+ m\Omega^2 \beta_p r(r_o+r)\delta_D \sin\theta_o - m\Omega^2 e_o r\delta_D \cos\theta_o \\
&+ m\Omega^2 e_o \chi_I \sin(\theta_o + \theta_{TW}) \\
&+ m\Omega^2 r\delta_D \chi_I \cos(2\theta_o + \theta_{TW})\Big] dr
\end{aligned}
\tag{39}
$$

The final equations (Eqs. 34, 35, 36, 37, and 39) are the basic equations of the nonuniform rotating beam and are nonlinear partial differential equations with nonconservative (aerodynamic and mechanical damping) forces.

2.2 Natural Frequencies and Associated Mode Shapes

2.2.1 Introduction

In this section the finite-element-method formulation to obtain the natural frequencies and associated mode shapes is described briefly. The formulation itself is rather straightforward: the coupled motions can be expressed in terms of the natural frequencies and associated mode shapes. It is expected that coupled natural frequencies and mode shapes will give much faster convergence than uncoupled standard mode shapes for a nonrotating uniform cantilever beam will do. The faster convergence will be pronounced when the motion becomes strongly coupled between flapping and torsion due to blade chordwise mass balance or between rigid-pitch motion and elastic torsion due to control linkage flexibility.

Although it has been recognized that the finite-element method is a generalized Ritz method (Ref. 42), the finite-element method is much more versatile because in the Ritz method the assumed displacement modes are extended to the entire structure; thus, for the structure with several different boundary geometries, it will be difficult to choose appropriate admissible displacement modes. In addition to this, when an accurate solution is required, a large number of assumed modes must be used and considerable algebraic manipulation must be performed in the Ritz method. In the case of the finite-element method, the same assumed displacement function,which is usually simple,can be used for each individual element, and boundary conditions of several different types can be applied simultaneously without difficulty.

To obtain the natural frequencies, the second-order differential equations without aerodynamic forces are solved which consist of the symmetric mass and stiffness matrices and the antisymmetric gyroscopic matrix due to coriolis forces. This problem is an eigenvalue problem; however, mode shapes must be expressed by complex numbers expressing the phase lag between motions. This creates further complexities in the complex number algebraic manipulation for a Galerkin method application. Also, since the coriolis force effect is

not strong enough to make a difference in convergence between cases, it is included in the natural frequency and mode-shape calculation, excluded in the natural frequency calculation, and then included later in the Galerkin method application step. Therefore, in the present analysis the natural frequencies and mode shapes are obtained from the eigenvalue problem with only the mass and stiffness matrices, which will produce real mode shapes and natural frequencies.

2.2.2 Variational Functional

For the first step, the variational functional π will be derived from Eqs. 34, 35, 36, 37, and 39. Nonlinear terms and steady-state loading terms are excluded as well as velocity-dependent terms resulting from Coriolis forces. The potential energy and kinetic energy expressions related to the linear terms are retained:

$$
\begin{aligned}
\pi = \int_0^R \Big[& \tfrac{1}{2} m \dot{w}^2 + \tfrac{1}{2} m \dot{v}^2 + \tfrac{1}{2} I_0 \dot{\phi}^2 + \tfrac{1}{2} (I_0 + m r^2 \delta_D^2 \\
& - 2 m x_I r \delta_D \sin\theta_{TW}) \dot{\theta}_R^2 + (m r \delta_D - m x_I \sin\theta_{TW}) \dot{v} \dot{\theta}_R \\
& - (m x_I \cos\theta_{TW}) \dot{w} \dot{\theta}_R - (m x_I \sin\theta_{TW}) \dot{v} \dot{\phi} \\
& - (m x_I \cos\theta_{TW}) \dot{w} \dot{\phi} + (I_0 - m x_I r \delta_D \sin\theta_{TW}) \dot{\phi} \dot{\theta}_R \Big] dr \\
& - \int_0^R \Big[\tfrac{1}{2} (EI_F \cos^2\theta_{TW} + EI_C \sin^2\theta_{TW}) (w'')^2 \\
& + \tfrac{1}{2} (EI_F \sin^2\theta_{TW} + EI_C \cos^2\theta_{TW}) (v'')^2 \\
& + (EI_F - EI_C) \sin\theta_{TW} \cos\theta_{TW} (w'' v'') + \tfrac{1}{2} T (w')^2 + \tfrac{1}{2} T (v')^2 \\
& - \tfrac{1}{2} (m \Omega^2 \sin^2\theta_0) w^2 - \tfrac{1}{2} (m \Omega^2 \cos^2\theta_0) v^2 \\
& - m \Omega^2 (\sin\theta_0 \cos\theta_0) w v + \tfrac{1}{2} (GJ + T k_A^2) (\phi')^2 \\
& + \Big\{ \tfrac{1}{2} (I_{zp} - I_{zp}) \Omega^2 \cos(2\theta_0 + 2\theta_{TW}) \\
& + \tfrac{1}{2} m x_I \Omega^2 \cos(\theta_0 + \theta_{TW}) (-e_0 + r \delta_D \sin\theta_0) \\
& - \tfrac{1}{2} m x_I \Omega^2 (r_0 + r) \beta_p \sin(\theta_0 + \theta_{TW})
\end{aligned}
$$

$$+\tfrac{1}{2} m x_I \Omega^2 (r_o + r) \delta_D \sin\theta_{TW} \Big\} \phi^2$$

$$+\Big\{ \tfrac{1}{2}(I_{zp} - I_{xp}) \Omega^2 \cos(2\theta_o + 2\theta_{TW})$$

$$-\tfrac{1}{2} m \Omega^2 < \beta_p r (r_o + r) \delta_D \cos\theta_o + e_o r \delta_D \sin\theta_o$$

$$+ r^2 \delta_D^2 \cos(2\theta_o) + e_o x_I \cos(\theta_o + \theta_{TW})$$

$$- 2 r \delta_D x_I \sin(2\theta_o + \theta_{TW}) > \Big\} \theta_R^2$$

$$+ m x_I \Omega^2 \sin(\theta_o + \theta_{TW}) \cos\theta_o \; (v\phi)$$

$$+ m x_I \Omega^2 \sin(\theta_o + \theta_{TW}) \sin\theta_o \; (w\phi)$$

$$- m \Omega^2 \Big\{ \beta_p (r_o + r) \sin\theta_o + r \delta_D \sin(2\theta_o)$$

$$- e_o \cos\theta_o + x_I \cos(2\theta_o + \theta_{TW}) \Big\} w\theta_R$$

$$- m \Omega^2 \Big\{ \beta_p (r_o + r) \cos\theta_o + r \delta_D \cos(2\theta_o)$$

$$+ e_o \sin\theta_o - x_I \sin(2\theta_o + \theta_{TW}) \Big\} v\theta_R$$

$$+ \Big\{ m x_I \Omega^2 r \delta_D \sin(2\theta_o + \theta_{TW})$$

$$- m x_I \Omega^2 e_o \cos(\theta_o + \theta_{TW})$$

$$+ (I_{zp} - I_{xp}) \Omega^2 \cos(2\theta_o + 2\theta_{TW})$$

$$- m x_I \Omega^2 (r_o + r) \beta_p \sin(\theta_o + \theta_{TW}) \Big\} \phi\theta_R \Big] dr$$

$$- \tfrac{1}{2} K_\theta \theta_R^2 \qquad (40)$$

2.2.3 Finite-Element Formulation

In the finite-element formulation, the variational functional may be expressed as the summation of the functionals of the subdivided finite number of discrete elements.

$$\pi = \sum_{n=1}^{N} \pi_n \tag{41}$$

where n means the nth element and N is the total number of elements. The displacements $\{u\}$ are represented over the nth element by interpolation functions [f] and by generalized nodal displacements $\{q_n\}$ which are displacements and sometimes derivatives of the displacements of the nth element. Thus, in the matrix form

$$\{u\} = [f]\{q_n\} \tag{42}$$

where

$$\begin{aligned} \lfloor u \rfloor &= \lfloor w \;\; v \;\; \phi \;\; \theta_R \rfloor \\ \lfloor q_n \rfloor &= \lfloor w_n \;\; w_n' \;\; w_{n+1} \;\; w_{n+1}' \;\; v_n \;\; v_n' \;\; v_{n+1} \;\; v_{n+1}' \\ &\qquad \phi_n \;\; \phi_n' \;\; \phi_{n+1} \;\; \phi_{n+1}' \;\; \theta_R \rfloor \end{aligned} \tag{43}$$

In the present analysis the beam element is used, and w_n and w'_n are the vertical displacement and its derivative at the node between (n - 1)th element and nth element. The quantities, w_{n+1} and w'_{n+1} are those between the nth and (n+1)th elements (Fig. 6). The matrix f is written as

$$[f] = \begin{bmatrix} H_{01}^{(1)} & H_{11}^{(1)} & H_{02}^{(1)} & H_{12}^{(1)} & 0 & 0 & 0 & 0 & 0 & 0 & 0 & 0 & 0 \\ 0 & 0 & 0 & 0 & H_{01}^{(1)} & H_{11}^{(0)} & H_{02}^{(1)} & H_{12}^{(1)} & 0 & 0 & 0 & 0 & 0 \\ 0 & 0 & 0 & 0 & 0 & 0 & 0 & 0 & H_{01}^{(1)} & H_{11}^{(1)} & H_{02}^{(1)} & H_{12}^{(1)} & 0 \\ 0 & 0 & 0 & 0 & 0 & 0 & 0 & 0 & 0 & 0 & 0 & 0 & 1 \end{bmatrix} \tag{44}$$

where the Hermitian interpolation functions are defined as

$$\begin{aligned} H_{01}^{(1)} &= 2\left(\frac{x}{\ell}\right)^3 - 3\left(\frac{x}{\ell}\right)^2 + 1 \\ H_{02}^{(1)} &= -2\left(\frac{x}{\ell}\right)^3 + 3\left(\frac{x}{\ell}\right)^2 \\ H_{11}^{(1)} &= \ell\left\{\left(\frac{x}{\ell}\right)^3 - 2\left(\frac{x}{\ell}\right)^2 + \left(\frac{x}{\ell}\right)\right\} \\ H_{12}^{(1)} &= \ell\left\{\left(\frac{x}{\ell}\right)^3 - \left(\frac{x}{\ell}\right)^2\right\} \end{aligned} \tag{45}$$

The element size is expressed by ℓ, and x is the coordinate within the element. Two nodes of the element are located at x = 0 and x = ℓ.

The derivatives can be obtained from Eq. 42. For example,

$$\frac{\partial w}{\partial x} = \frac{dH_{01}^{(1)}}{dx} w_n + \frac{dH_{02}^{(1)}}{dx} w_{n+1} + \frac{dH_{11}^{(1)}}{dx} w'_n + \frac{dH_{12}^{(1)}}{dx} w'_{n+1} \tag{46}$$

Thus, various derivatives can be obtained by differentiating interpolation functions. These displacements and derivatives (Eqs. 42 and 44) may be substituted into the functional in Eq. 40 and the integration should be carried out elementwise.

$$\pi_n = \frac{1}{2}\{\dot{q}_n\}^T [m_n]\{\dot{q}_n\} - \frac{1}{2}\{q_n\}^T [k_n]\{q_n\} \tag{47}$$

where $[m_n]$ and $[k_n]$ are element mass and stiffness matrices.

The element mass matrix is a consistent mass matrix and may be written as

$$[m_n]_{13\times 13} = \begin{bmatrix} d_{11}[m'] & [0] & d_{13}[m'] & d_{14}[m''] \\ & d_{22}[m'] & d_{23}[m'] & d_{24}[m''] \\ & & d_{33}[m'] & d_{34}[m''] \\ & \text{symmetrical} & & d_{44}\,\ell \end{bmatrix} \tag{48}$$

and

$$[m'] = \frac{\ell}{420}\begin{bmatrix} 156 & 22\ell & 54 & -13\ell \\ & 4\ell^2 & 13\ell & -3\ell^2 \\ & & 156 & -22\ell \\ & \text{symmetrical} & & 4\ell^2 \end{bmatrix}\ ;\ [m''] = \frac{\ell}{12}\begin{bmatrix} 6 \\ \ell \\ 6 \\ -\ell \end{bmatrix} \tag{49}$$

The coefficients are

$$\begin{aligned} d_{11} &= m\ ,\ d_{13} = -m x_I \cos\theta_{TW}\ ,\ d_{14} = -m x_I \cos\theta_{TW} \\ d_{22} &= m\ ,\ d_{23} = -m x_I \sin\theta_{TW},\ d_{24} = -m x_I \sin\theta_{TW} \\ d_{33} &= I_o\ ,\ d_{34} = I_o - m x_I r_n \delta_D \sin\theta_{TW} \\ d_{44} &= I_o + m r_n^2 \delta_D^2 - 2 m x_I r_n \delta_D \sin\theta_{TW} \end{aligned} \tag{50}$$

r_n: radial distance from the pitch bearing to the midpoint of the element.

The element stiffness matrix is divided into three portions as

$$[k_n] = [k_n^S] + [k_n^T] + [k_n^C] \tag{51}$$

The stiffness related to the curvature is

$$[k_n^S]_{13\times13} = \begin{bmatrix} s_{11}[k_s'] & s_{12}[k_s'] & [0] & [0] \\ & s_{22}[k_s'] & [0] & [0] \\ & & [0] & [0] \\ \text{symmetrical} & & & 0 \end{bmatrix} \tag{52}$$

and

$$[k_s'] = \frac{1}{\ell^3}\begin{bmatrix} 12 & 6\ell & -12 & 6\ell \\ & 4\ell^2 & -6\ell & 2\ell^2 \\ & & 12 & -6\ell \\ \text{symmetrical} & & & 4\ell^2 \end{bmatrix}$$

$$s_{11} = EI_F\cos^2\theta_{TW} + EI_C\sin^2\theta_{TW}$$

$$s_{12} = (EI_F - EI_C)\cos\theta_{TW}\sin\theta_{TW}$$

$$s_{22} = EI_F\sin^2\theta_{TW} + EI_C\cos^2\theta_{TW} \tag{53}$$

The stiffness due to centrifugal forces and torsional rigidity is

$$[k_n^T] = \begin{bmatrix} t_{11}[k_t'] & [0] & [0] & [0] \\ & t_{22}[k_t'] & [0] & [0] \\ & & t_{33}[k_t'] & [0] \\ \text{symmetrical} & & & 0 \end{bmatrix} \tag{54}$$

and

$$[k_t'] = \frac{1}{30\ell}\begin{bmatrix} 36 & 3\ell & -36 & 3\ell \\ & 4\ell^2 & -3\ell & -\ell^2 \\ & & 36 & -3\ell \\ \text{symmetrical} & & & 4\ell^2 \end{bmatrix} \quad ; \quad \begin{aligned} t_{11} &= T \\ &= \int_{r_n}^{R} m(r_o+r')\Omega^2 dr \\ t_{22} &= T \\ t_{33} &= GJ + Tk_A^2 \end{aligned} \tag{55}$$

The stiffness due to centrifugal forces and mass unbalance is

$$[k_n^c] = \begin{bmatrix} a_{11}[m'] & a_{12}[m'] & a_{13}[m'] & a_{14}[m''] \\ & a_{22}[m'] & a_{23}[m'] & a_{24}[m''] \\ & & a_{33}[m'] & a_{34}[m''] \\ \text{symmetrical} & & & a_{44}\ell \end{bmatrix} \tag{56}$$

and

$$a_{11} = -m\Omega^2 \sin^2\theta_o \quad , \quad a_{12} = -m\Omega^2 \sin\theta_o \cos\theta_o$$

$$a_{13} = m x_I \Omega^2 \sin(\theta_o + \theta_{TW}) \sin\theta_o$$

$$a_{14} = -m\Omega^2 \{ \beta_p (r_o + r_n) \sin\theta_o + r_n \delta_D \sin(2\theta_o) - e_o \cos\theta_o + x_I \cos(2\theta_o + \theta_{TW}) \}$$

$$a_{22} = m\Omega^2 \cos^2\theta_o \quad , \quad a_{23} = m x_I \Omega^2 \sin(\theta_o + \theta_{TW}) \cos\theta_o$$

$$a_{24} = -m\Omega^2 \{ \beta_p (r_o + r_n) \sin\theta_o + r_n \delta_D \cos(2\theta_o) + e_o \sin\theta_o - x_I \sin(2\theta_o + \theta_{TW}) \}$$

$$a_{33} = (I_{zp} - I_{xp})\Omega^2 \cos(2\theta_o + 2\theta_{TW}) + m x_I \Omega^2 \cos(\theta_o + \theta_{TW})(-e_o + r_n \delta_D \sin\theta_o)$$

$$- m x_I \Omega^2 (r_o + r) \beta_p \sin(\theta_o + \theta_{TW}) + m x_I \Omega^2 (r_o + r_n) \delta_D \sin\theta_{TW}$$

$$a_{34} = (I_{zp} - I_{zp}) \Omega^2 \cos(2\theta_o + 2\theta_{TW}) + m x_I \Omega^2 r_n \delta_D \sin(2\theta_o + \theta_{TW})$$
$$- m x_I \Omega^2 e_o \cos(\theta_o + \theta_{TW}) - m x_I \Omega^2 (r_o + r_n) \beta_p \sin(\theta_o + \theta_{TW})$$

$$a_{44} = (I_{zp} - I_{zp}) \Omega^2 \cos(2\theta_o + 2\theta_{TW})$$
$$- m \Omega^2 \{ \beta_p (r_o + r_n) r_n \delta_D \cos\theta_o + 2 e_o r_n \delta_D \sin\theta_o$$
$$+ 2 r_n^2 \delta_D^2 \cos(2\theta_o) + 2 e_o x_I \cos(\theta_o + \theta_{TW})$$
$$- 4 r_n \delta_D x_I \sin(2\theta_o + \theta_{TW}) \} \qquad (57)$$

Substituting Eq. 47 into Eq. 41 and assembling the element mass and stiffness matrices appropriately for compatibility of the interelement nodal displacements, the global mass and stiffness matrices are obtained and the expression for π can be written as

$$\pi = \frac{1}{2} \{\dot{q}\}^T [M] \{\dot{q}\} - \frac{1}{2} \{q\}^T [K] \{q\} \qquad (58)$$

where {q} is the global nodal displacements, and [M] and [K] are, respectively, global mass and stiffness matrices. These may be written as

$$[\{q_1\} \{q_2\} \cdots\cdots \{q_N\}] = [J] \{q\}$$

$$[M] = [J]^T [[m_1] [m_2] \cdots\cdots [m_N]] [J] \qquad (59)$$

$$[K] = [J]^T [[k_1] [k_2] \cdots\cdots [k_N]] [J]$$

Matrix J is a transformation matrix to relate the element nodal displacements $\{q_n\}$ of the element to a column of global displacements {q}.

The application of Hamilton's principle to Eq. 58 will yield the equations of motion,

$$[M]\{\ddot{q}\} + [K]\{q\} = \{0\} \tag{60}$$

2.2.4 Boundary Conditions

Various boundary conditions can be chosen depending upon the rotor configuration and can be applied easily in the finite-element method to specify conditions of the displacements of the first node.

Hingeless Rotor:

$$w_1 = w_1' = v_1 = v_1' = \phi_1 = 0 \tag{61}$$

Gimballed Rotor (Teetering Rotor):

$$w_1 = v_1 = v_1' = \phi_1 = 0 \tag{62}$$

Articulated Rotor:

$$w_1 = v_1 = \phi_1 = 0 \tag{63}$$

If control linkage flexibility exists, the spring and constant K_θ should be included in the element stiffness matrix of the first element. If the control linkage is rigid enough, the rigid pitch degree of freedom should be removed before the eigenvalue calculation.

2.2.5 Subspace Iteration Method

The eigenvalue problem expressed in Eq. 60 can be solved by any eigenvalue technique. In the present analysis, the subspace iteration method (Refs. 43 and 44) is selected to achieve a fast rate of convergence of a large degree-of-freedom system (if ten elements are used to describe the rotor blade, the total degrees-of-freedom will be 67).

The subspace iteration method will be described briefly. Assuming s modes are needed, the total degrees-of-freedom as t ($\{q\}$ in Eq. 60 is a

t x 1 matrix), and denoting [u] as the t x s matrix containing the s vectors, the following procedure will be applied:

a. Assume an arbitrary $[u_o]$ as a starting matrix

b. Calculate the reduced mass and stiffness matrices as

$$[M_R]_{s\times s} = [u_o]^T_{s\times t} [M]_{t\times t} [u_o]_{t\times s}$$

and

$$[K_R]_{s\times s} = [u_o]^T_{s\times t} [K]_{t\times t} [u_o]_{t\times s}$$

c. Solve the small eigenvalue problem

$$[K_R][A] - [D][M_R][A] = \{0\}$$

where [A] is a sxs eigenvector matrix and [D] is a diagonal matrix which includes eigenvalues. This small eigenvalue problem can be achieved by using the Jacobi Method.

d. Calculate $[\bar{u}_o]$ as $[\bar{u}_o]_{t\times s} = [u_o]_{t\times s} [A]_{s\times s}$

e. Calculate $[u_1]$ as $[u_1] = [K]^{-1} [M] [\bar{u}_o]$

f. Replace $[u_o]$ with $[u_1]$ and go to step b.

The criteria of terminating the iteration is set to achieve the specified accuracy as

$$\left| \frac{(\lambda)_{i+1} - (\lambda)_i}{(\lambda)_i} \right| < \varepsilon \qquad (64)$$

where $(\lambda)_i$, $(\lambda)_{i+1}$ are ith and (i+1)th iteration eigenvalue and ε is a specified accuracy.

2.3 Aerodynamic Loading

2.3.1 Introduction

The aerodynamic forces and moments of the rotor blade are derived based on the two-dimensional quasi-steady aerodynamics in Ref. 45. The major assumptions in the present aerodynamic analysis are:

(1) the inflow is uniform over the rotor disc plane, and

(2) the vertical gust is assumed to be one-dimensional in cruising direction,

(3) reverse flow and blade stall are neglected: thus, the analysis is good to an advance ratio of about 0.4.

Also, the rotor unsteady wake effects are neglected. The virtual mass aerodynamic forces and moments are neglected; the terms of order c/R in the aerodynamic lift expressions are neglected; the firstorder velocity terms in the aerodynamic loading are retained; terms of order $(c/R)^3$ in the aerodynamic feathering moments are also neglected; the collective pitch θ_o and the built-in angle of twist θ_{TW} are, hereafter, restricted to small angles which enable the use of the small angle assumptions of helicopter aerodynamics.

2.3.2 Relative Velocity of the Blade

The position vector r_B to the point on the blade elastic axis in the x,y, z coordinate systems after applying the small angle assumption as $\theta_m << 1$ and $\theta << 1$ to Eq. 11 is expressed as

$$\vec{r_B} = \begin{bmatrix} -e_o + v \\ r_o + r \\ w + r\delta_o + (r_o + r)\beta_p \end{bmatrix} \tag{65}$$

The velocity due to deformations may be written in the x,y,z coordinate systems as

$$\vec{v}_B = \dot{\vec{r}}_B + \vec{\Omega} \times \vec{r}_B$$

$$= \begin{bmatrix} \dot{v} - \Omega(r_o + r) + \dot{\theta}(w + r\delta_D) \\ \Omega(-e_o + v) + \beta_p \dot{\theta}(-e_o + v) \\ \dot{w} - \dot{\theta}(-e_o + v) \end{bmatrix} \tag{66}$$

where

$$\vec{\Omega} = \begin{bmatrix} 0 \\ \dot{\theta} \\ \Omega + \beta_p \dot{\theta} \end{bmatrix} \tag{67}$$

and $\dot{\theta}$ includes the angular velocity due to the rigid pitch motion and the cyclic pitch control, while the blade elastic torsion has no effect on the velocity at the blade elastic axis because it is assumed that the elastic torsion deformation occurs after the vertical and chordwise bending deformation shown in Fig. 3.

The velocity seen on the projection of the blade elastic axis to the x-y plane is

$$\vec{v}_{EA} = \vec{v}_B - \vec{\Omega} \times \vec{r}_e$$

$$= \begin{bmatrix} \dot{v} - \Omega(r_o + r) + \dot{\theta}(w + r\delta_D) \\ (\Omega + \beta_p \dot{\theta}) v \\ \dot{w} - \dot{\theta} v \end{bmatrix} \tag{68}$$

The trim velocity may be expressed in the x,y,z coordinate system (the hub plane) as

$$\vec{V} = \begin{bmatrix} \mu \Omega R \sin\psi \\ \mu \Omega R \cos\psi \\ -\lambda \Omega R \end{bmatrix} \tag{69}$$

where μ, λ, and α_s are the rotor advance ratio, inflow ratio and the rotor shaft tilt angle (positive rotor disc tilt forward), respectively, and defined as follows:

$$\mu = \frac{V \cos\alpha_s}{\Omega R}$$

$$\lambda = \frac{V \sin\alpha_s + v_i}{\Omega R} \tag{70}$$

The cruising velocity is V, and the induced flow velocity is v_i. The resultant velocity $\vec{U}$ may be written as

$$\vec{U} = \vec{V} - \vec{v}_{EA}$$

$$= \begin{bmatrix} \mu \Omega R \sin\psi + \Omega(r_0 + r) - \dot{v} - \dot{\theta}(w + z_p + r\delta_0) \\ \mu \Omega R \cos\psi - \Omega(v + x_p) \\ -\lambda \Omega R - \dot{w} - \dot{\theta}(v + x_p) \end{bmatrix} \tag{71}$$

This resultant velocity $\vec{U}$ is resolved to obtain the relative velocity components of the deformed elastic axis coordinate systems (x''', y''', z''' coordinate systems shown in Fig. 3) as

$$\vec{U}_{EA} = \begin{bmatrix} U_T \\ U_R \\ -U_P \end{bmatrix}$$

$$= [T]^T [T_\delta]^T [T_\beta]^T \vec{U}$$

$$= \begin{bmatrix} \Omega(r_o+r) + \mu\Omega R \sin\psi - \dot{v} \\ \qquad -\mu\Omega R\, v' \cos\psi - \dot{\theta}(w + z_p + r\delta_D) \\ \hline \mu\Omega R \cos\psi - \Omega(v+x_p) - \lambda\Omega R(w' + \beta_p + \delta_D) \\ \qquad +\mu\Omega R\, v' \sin\psi + \Omega(r_o+r)v' \\ \hline -\lambda\Omega R - \dot{w} - \mu\Omega R(w' + \beta_p + \delta_D)\cos\psi \\ \qquad +\dot{\theta}(v + x_p) \end{bmatrix}$$

(72)

where U_T, U_R, and U_p are blade tangential, radial, and perpendicular velocities with respect to the deformed elastic axis.

The bending motions are expressed in terms of steady equilibrium quantities and small unsteady perturbation quantities

$$v = v_o + v$$

$$w = w_o + w$$

The same symbols are used for the total bending motions and perturbation motions; however, there will be no confusion.

Equilibrium velocities related to the trim condition are obtained as follows:

$$\vec{u} = \begin{Bmatrix} u_T \\ u_R \\ -u_P \end{Bmatrix}$$

$$= \begin{bmatrix} \Omega(r_0+r) + \mu\Omega R\sin\psi - \dot{v}_0 - \mu\Omega R v_0'\cos\psi \\ \hline \mu\Omega R\cos\psi - \Omega(v_0+x_P) - \lambda\Omega R(w_0'+\beta_P+\delta_0) \\ \quad + \mu\Omega R v_0'\sin\psi + \Omega(r_0+r)v_0' \\ \hline -\lambda\Omega R - \dot{w}_0 - \mu\Omega R(w_0'+\beta_P+\delta_0)\cos\psi \end{bmatrix} \tag{73}$$

where v_o and w_o are bending deflections at the equilibrium condition shown previously, and time derivatives $\dot{v}_o$ and $\dot{w}_o$ are not necessarily zero because in the present analysis no trim operation is considered which involves time-dependent equilibrium position-related harmonic terms; i.e., $\sin\psi$ and $\cos\psi$.

The perturbations of the velocity components including the vertical gust are:

$$\delta\vec{u} = \begin{Bmatrix} \delta u_T \\ \delta u_R \\ -\delta u_P \end{Bmatrix}$$

$$= \begin{bmatrix} -\dot{v} - \mu\Omega R v'\cos\psi - \dot{\theta}(w + r\delta_0) \\ \quad + w_G\sin\alpha_s\sin\psi \\ \hline -\Omega v - \lambda\Omega R w' + \mu\Omega R v'\sin\psi \\ \quad + \Omega(r_0+r)v' + w_G\sin\alpha_s\cos\psi \\ \hline -\dot{w} - \mu\Omega R w'\cos\psi + \dot{\theta}v + w_G\cos\alpha_s \end{bmatrix} \tag{74}$$

where w_G is the vertical gust at a given location, positive upward.

2.3.3 Section Aerodynamic Forces

The section lift and drag are (Fig. 8)

$$L = \frac{1}{2}\rho U^2 c\, a\alpha$$
$$D = \frac{1}{2}\rho U^2 c\, C_{d_o} \tag{75}$$

where

$$U^2 = U_T^2 + U_P^2$$
$$\alpha = \theta - \phi_I \tag{76}$$
$$\phi_I = \tan^{-1}\frac{U_P}{U_T} \approx \frac{U_P}{U_T}$$

and a is the lift curve slope and C_{d_o} the profile drag coefficient. The force components P_z, parallel to U_p, and P_x, parallel to U_T are

$$P_z = L\cos\phi_I - D\sin\phi_I + \frac{1}{2}\rho a\left(\frac{c}{2}\right)^2 U_T(3+4x_A)(\delta\dot{\alpha})$$
$$= \frac{1}{2}\rho ac\, U U_T\alpha - \frac{1}{2}\rho c\, C_{d_o} U U_P + \frac{1}{2}\rho a\left(\frac{c}{2}\right)^2 U_T(3+4x_A)(\delta\dot{\alpha})$$
$$P_x = L\sin\phi_I + D\cos\phi_I + \frac{1}{2}\rho a\left(\frac{c}{2}\right)^2 U_P(3+4x_A)(\delta\dot{\alpha})$$
$$= \frac{1}{2}\rho ac\, U U_P\alpha + \frac{1}{2}\rho c\, C_{d_o} U U_T + \frac{1}{2}\rho a\left(\frac{c}{2}\right)^2 U_P(3+4x_A)(\delta\dot{\alpha}) \tag{77}$$

where x_A is the nondimensionalized distance of the blade chord between the elastic axis and the aerodynamic center (positive aft of the elastic axis). It should be noted that the aerodynamic force in the blade radial direction is neglected and the lift due to the blade pitching angular velocity is included to retain the damping terms of the torsion and rigid pitch motion shown in a later section.

The transformation $[T_\theta]$ in Eq. 6 may be used to resolve the blade forces P_z and P_x into P_W and P_V parallel to the z" and x" axes (the directions of the bending) of the undeformed blade coordinate system.

$$P_W = P_z + P_x \theta_m$$
$$P_V = -P_z \theta_m + P_x \tag{78}$$

The blade section velocities and angle of attack are expanded into equilibrium terms and perturbation terms as follows:

$$U_T = u_T + \delta u_T$$
$$U_P = u_P + \delta u_P$$
$$U = u + \frac{u_T}{u}\delta u_T + \frac{u_P}{u}\delta u_P$$
$$\alpha = (\theta_0 + \theta_{Tw}) + \delta\theta + \delta\phi - \frac{u_T}{u^2}\delta u_P + \frac{u_P}{u^2}\delta u_T \tag{79}$$

where u_T, u_P, δu_T, and δu_P are defined in Eq. 73 and 74, and

$$u = \sqrt{u_P^2 + u_T^2}$$
$$\delta\theta = \theta_K + \theta_C \quad ; \quad \delta\phi = \phi \tag{80}$$

Then, the aerodynamic forces are resolved into equilibrium terms related to trim operation, and perturbation terms due to perturbed motions of the system. Substituting Eq. 79 into Eq. 78 with Eq. 77 yields

$$P_W = (P_W)_0 + \left(\frac{\partial P_W}{\partial u_T}\right)_0 \delta u_T + \left(\frac{\partial P_W}{\partial u_P}\right)_0 \delta u_P + \left(\frac{\partial P_W}{\partial \theta}\right)_0 (\delta\theta + \delta\phi) - \left(\frac{\partial P_W}{\partial \dot{\theta}}\right)_0 (\delta\dot{\theta} + \delta\dot{\phi})$$
$$P_V = (P_V)_0 + \left(\frac{\partial P_V}{\partial u_T}\right)_0 \delta u_T + \left(\frac{\partial P_V}{\partial u_P}\right)_0 \delta u_P + \left(\frac{\partial P_V}{\partial \theta}\right)_0 \delta\theta + \left(\frac{\partial P_V}{\partial \phi}\right)_0 \delta\phi + \left(\frac{\partial P_V}{\partial \dot{\theta}}\right)_0 (\delta\dot{\theta} + \delta\dot{\phi}) \tag{81}$$

where

$$(P_w)_o = \frac{1}{2}\rho a c (\Omega R)^2 \left[x^2\theta_s + 2\mu x\theta_s \sin\psi + \mu^2\theta_s \sin^2\psi - \lambda\mu\sin\psi - (1+\frac{c_{d_o}}{a})x(\lambda + \underline{\underline{\mathring{w}_o}}) \right]$$

$$\left(\frac{\partial P_w}{\partial u_T}\right)_o = \frac{1}{2}\rho a c (\Omega R)\left[2x\theta_s + 2\mu\theta_s \sin\psi - \mu(\underline{\underline{w_o'}} + \beta_p + \delta_D)\cos\psi - (1+\frac{c_{d_o}}{a})(\lambda + \underline{\underline{\mathring{w}_o}}) \right]$$

$$\left(\frac{\partial P_w}{\partial u_p}\right)_o = -\frac{1}{2}\rho a c (\Omega R)\left[(1+\frac{c_{d_o}}{a})(x + \mu\sin\psi - \underline{\underline{\mathring{v}}} - \mu\underline{\underline{v_o'}}\cos\psi) \right]$$

$$\left(\frac{\partial P_w}{\partial\theta}\right)_o = \frac{1}{2}\rho a c (\Omega R)^2 \left[x^2 + \frac{1}{2}\mu^2 + 2\mu x\sin\psi - \frac{1}{2}\mu^2\cos(2\psi) - \underline{\underline{2x\mathring{v}_o}} + \underline{\underline{2\mu x v_o'\cos\psi}} - \underline{\underline{2\mu\mathring{v}_o\sin\psi}} \right]$$

$$\left(\frac{\partial P_w}{\partial\dot{\theta}}\right)_o = \frac{1}{2}\rho a c \left(\frac{c}{R}\right)\left(\frac{3}{4} + x_A\right)(\Omega R)\left[x + \mu\sin\psi - \underline{\underline{\mathring{v}_o}} - \mu\underline{\underline{v_o'}}\cos\psi \right]$$

$$(P_v)_o = \frac{1}{2}\rho a c (\Omega R)^2 \left[x\theta_s(\lambda + \underline{\underline{\mathring{w}_o}}) + \frac{c_{d_o}}{a}x^2 - \lambda^2 - \underline{\underline{2\lambda\mathring{w}_o}} - \theta_o\left\{ x^2\theta_s + 2\mu x\theta_s\sin\psi + \mu^2\theta_s\sin^2\psi - \lambda\mu\sin\psi - (\lambda + \underline{\underline{\mathring{w}_o}}) \right\} \right]$$

$$\left(\frac{\partial P_v}{\partial u_T}\right)_o = \frac{1}{2}\rho a c (\Omega R)\left[\theta_s\left\{ \lambda + \underline{\underline{\mathring{w}_o}} + \mu(\underline{\underline{w_o'}} + \beta_p + \delta_D)\cos\psi \right\} + 2\frac{c_{d_o}}{a}x - \theta_o\left\{ 2x\theta_s + 2\mu\theta_s\sin\psi - (\lambda + \underline{\underline{\mathring{w}_o}}) \right\} \right]$$

$$\left(\frac{\partial P_v}{\partial u_p}\right)_o = \frac{1}{2}\rho a c (\Omega R)\Big[x\theta_s + \mu\theta_s \sin\psi - 2\{\lambda + \underline{\underline{\mathring{w}_o}} + \mu(\underline{\underline{w_o'}} + \beta_p + \delta_D)\cos\psi\} + \theta_o(x + \mu\sin\psi - \underline{\underline{\mathring{v}}} - \underline{\underline{\mu v_o'\cos\psi}})\Big]$$

$$\left(\frac{\partial P_v}{\partial \theta}\right)_o = \frac{1}{2}\rho a c (\Omega R)^2\Big[\lambda x + \underline{\underline{x\mathring{w}_o}} + \lambda\mu\sin\psi + \underline{\underline{\mu\mathring{w}\sin\psi}} + \mu x(\underline{\underline{w_o'}} + \beta_p + \delta_D)\cos\psi + \tfrac{1}{2}\mu^2(\underline{\underline{w_o'}} + \beta_p + \delta_D)\sin(2\psi) - \{x^2\theta_s + 2\mu x\theta_s\sin\psi - x(\lambda + \underline{\underline{\mathring{w}_o}}) + \mu^2\theta_s\sin^2\psi - \lambda\mu\sin\psi\} - \theta_o\{x^2 + \tfrac{1}{2}\mu^2 + 2\mu x\sin\psi - \tfrac{1}{2}\mu^2\cos(2\psi) - \underline{\underline{2x\mathring{v}_o}} + \underline{\underline{2\mu x v_o'\cos\psi}} - \underline{\underline{2\mu\mathring{v}_o\sin\psi}}\}\Big]$$

$$\left(\frac{\partial P_v}{\partial \phi}\right)_o = \frac{1}{2}\rho a c (\Omega R)^2\Big[\lambda x + \underline{\underline{x\mathring{w}_o}} + \lambda\mu\sin\psi + \underline{\underline{\mu\mathring{w}\sin\psi}} + \mu x(\underline{\underline{w_o'}} + \beta_p + \delta_D)\cos\psi + \tfrac{1}{2}\mu^2(\underline{\underline{w_o'}} + \beta_p + \delta_D)\sin(2\psi) - \theta_o\{x^2 + \tfrac{1}{2}\mu^2 + 2\mu x\sin\psi - \tfrac{1}{2}\mu^2\cos(2\psi) - \underline{\underline{2x\mathring{v}_o}} + \underline{\underline{2\mu x v_o'\cos\psi}} - \underline{\underline{2\mu\mathring{v}_o\sin\psi}}\}\Big]$$

$$\left(\frac{\partial P_v}{\partial \dot{\theta}}\right)_o = \frac{1}{2}\rho a c \left(\frac{c}{R}\right)\left(\frac{3}{4} + x_A\right)(\Omega R)\Big[\lambda + \underline{\underline{\mathring{w}}} + \mu(\underline{\underline{w_o'}} + \beta_p + \delta_D)\cos\psi\Big]$$

(82)

It should be noted that the double underlined terms are due to deformations at the equilibrium condition. The nondimensional radial coordinate x

and angle θ_s are given by

$$x = (r_0 + r)/R$$
$$\theta_s = \theta_0 + \theta_{TW} \tag{83}$$

2.3.4 Aerodynamic Moments

The section aerodynamic moment (positive nose up) may be written as

$$M_A = -\frac{1}{2}\rho a U^2 c^2 x_A \alpha + \frac{1}{2}\rho U^2 c^2 (C_{m_0} + C_{m_\alpha}\alpha)$$
$$-\frac{1}{2}\rho a U c^3 C_M \dot{\alpha} \tag{84}$$

where C_{m_o} and C_{m_α} are section aerodynamic moment coefficient and section aerodynamic moment slope, respectively. C_M is a function of x_A:

$$C_M = \frac{1}{8} + \frac{3}{4}x_A + x_A^2 \tag{85}$$

Expanding as before in equilibrium and perturbation terms yields

$$M_A = (M_A)_0 + \left(\frac{\partial M_A}{\partial u_T}\right)\delta u_T + \left(\frac{\partial M_A}{\partial u_P}\right)\delta u_P$$
$$+ \left(\frac{\partial M_A}{\partial \theta}\right)(\delta\theta + \delta\phi) + \left(\frac{\partial M_A}{\partial \dot{\theta}}\right)(\delta\dot{\theta} + \delta\dot{\phi}) \tag{86}$$

where

$$(M_A)_0 = \frac{1}{2}\rho a c^2 (\Omega R)^2 \left[\frac{1}{2}A_M\left(x^2 + \frac{1}{2}\mu^2 + 2\mu x \sin\psi - \frac{1}{2}\mu^2 \cos(2\psi) - 2\mathring{v}_0\right) + B_M x (\lambda + \mathring{w}_0)\right]$$

$$\left(\frac{\partial M_A}{\partial u_T}\right)_0 = \frac{1}{2}\rho a c^2 (\Omega R)\left[A_M(x + \mu\sin\psi - \mathring{v}_0) - B_M(\lambda + \mathring{w}_0)\right]$$

$$\left(\frac{\partial M_A}{\partial u_P}\right)_0 = \frac{1}{2}\rho a c^2 (\Omega R)\left[A_M(\lambda + \mathring{w}_0) + B_M(x + \mu\sin\psi - \mathring{v}_0)\right]$$

$$\left(\frac{\partial M_A}{\partial \theta}\right)_0 = \frac{1}{2}\rho a c^2 (\Omega R)^2 \left[B_M \left\{ x^2 + \frac{1}{2}\mu^2 + 2\mu x \sin\psi - \frac{1}{2}\mu^2 \cos(2\psi) - 2\dot{v}_0 \right\} \right]$$

$$\left(\frac{\partial M_A}{\partial \dot{\theta}}\right)_0 = -\frac{1}{2}\rho a c^3 (\Omega R) \left[C_M (x + \mu \sin\psi - \dot{v}_0) \right]$$

(87)

and

$$A_M = 2 \left(\frac{C_{M_0}}{a} + \frac{C_{M_\alpha}}{a} \theta_s - x_A \theta_s \right)$$

$$B_M = x_A - \frac{C_{M_\alpha}}{a} \tag{88}$$

Aerodynamic moments M_{θ_R} for the rigid-pitch motion consist of two portions: one due to the section aerodynamic moment derived previously and the other due to lift and drag which make moments about the blade feathering axis:

$$M_\theta = M_{A_\theta} + M_{FA} \tag{89}$$

where

$$M_{A_\theta} = \int_0^R M_A \, dr$$

$$M_{FA} = \int_0^R (P_v r_z - P_w r_x) dr \tag{90}$$

and from Eq. 20 r_x and r_z are obtained in the x', y' and z' coordinate systems.

$$\vec{r}_{FA} = \begin{Bmatrix} r_x \\ r_y \\ r_z \end{Bmatrix}$$

$$= \begin{bmatrix} v \\ 0 \\ w + r\delta_D \end{bmatrix} \tag{91}$$

Expanding M_{FA} to equilibrium quantities and small unsteady perturbation quantities yields

$$\begin{aligned} M_{FA} = & \int_0^R \left[(P_v)_0 (w_0 + r\delta_D) - (P_w)_0 v_0 \right] dr \\ & + \int_0^R \Big[(P_v)_0 w - (P_w)_0 v \\ & + v_0 \left\{ \left(\frac{\partial P_w}{\partial u_T}\right)_0 \delta u_T + \left(\frac{\partial P_w}{\partial u_p}\right)_0 \delta u_p + \left(\frac{\partial P_w}{\partial \theta}\right)_0 (\delta\theta + \delta\phi) \right. \\ & \left. + \left(\frac{\partial P_w}{\partial \dot{\theta}}\right) (\delta\dot{\theta} + \delta\dot{\phi}) \right\} \\ & + (w_0 + r\delta_D) \left\{ \left(\frac{\partial P_v}{\partial u_T}\right)_0 \delta u_T + \left(\frac{\partial P_v}{\partial u_p}\right) \delta u_p + \left(\frac{\partial P_v}{\partial \theta}\right)_0 \delta\theta \right. \\ & \left. + \left(\frac{\partial P_v}{\partial \phi}\right)_0 \delta\phi + \left(\frac{\partial P_v}{\partial \dot{\theta}}\right)_0 (\delta\dot{\theta} + \delta\dot{\phi}) \right\} \Big] dr \end{aligned} \tag{92}$$

Steady equilibrium terms and perturbation terms are already defined in Eqs. 82 and 74.

2.3.5 Gust Velocity Gradient Due to the One-Dimensional Gust

As shown in Fig. 9, the one-dimensional sinusoidal gust in the cruising direction has a velocity gradient. The gust magnitude at the nondimensional spanwise location x of the blade of azimuth angle $\psi = \Omega t$ is expressed as:

$$w_G = \bar{w}_{GT} \sin(\omega t - \phi_G) \tag{93}$$

where w_{GT} is a gust amplitude and ω the gust frequency, ϕ_G phase lag of the gust between that location and the center of the rotor. The phase lag ϕ_G is described by the gust wave length λ_G and the location of the given point as:

$$\phi_G = 2\pi \left[\frac{R x \cos(\Omega t)}{\lambda_G} \right] \tag{94}$$

$$= \frac{1}{\mu} \left(\frac{\omega}{\Omega} \right) x \cos(\Omega t)$$

Substituting Eq. 94 into Eq. 93 and expanding the trigonometric function yields:

$$w_G = \bar{w}_{GT} \sin \omega t - \bar{w}_{GT} \left\{ \frac{x}{\mu} \left(\frac{\omega}{\Omega} \right) \right\} \cos \omega t \cos \Omega t$$

$$+ \text{Higher Order Terms} \tag{95}$$

In order to obtain the analytical excitation function, the approximate Eq. 95 is used instead of Eq. 93. The first term shows the uniform part of the gust and the second the gust velocity gradient due to the one-dimensional sinusoidal vertical gust.

2.4 Rotor Trim and Steady-State Deflections

2.4.1 Introduction

In this subsection, an approximate method to obtain the rotor trim condition and steady-state blade deflections will be described. These are required to evaluate the aerodynamic coefficients and structural couplings of the perturbation equations. There are two rotor trim conditions: one is powered trim. This simulates the actual helicopter trim and requires force equilibrium in vertical and horizontal directions as well as moment equilibrium in pitch and roll. The other is moment trim. This simulates wind tunnel testing of the rotor where moment equilibrium in pitch and roll is required and the thrust and drag are reacted by the wind tunnel model support.

In the present analysis, both moment trim and out-of-trim operation are considered with respect to the wind tunnel experiments. In out-of-trim operation, the blade motion is periodic. In this case, the blade torsion and rigid pitch motions are neglected when the steady-state trim condition is obtained.

2.4.2 Equations of Motion for the Steady Equilibrium Condition

Discarding terms related to the elastic torsion ϕ and rigid pitch motion θ_R, and second-order terms, two sets of equations are obtained from Eqs. 3 and 4 as follows:

w_o Equation

$$m\ddot{w}_o - 2m\Omega(\beta_p+\delta_0)\dot{v}_o - (T\frac{\partial w_o}{\partial r})' - m\Omega^2(\sin\theta_0)v_o$$
$$+\left[(EI_F\cos^2\theta_{TW}+EI_C\sin^2\theta_{TW})w_o'' + \{(EI_F-EI_C)\cos\theta_{TW}\sin\theta_{TW}\}v_o''\right]''$$
$$= P_w - m\Omega^2(r_o+r)(\delta_0+\beta_p) \qquad (96)$$

v_o Equation

$$
\begin{aligned}
&m\ddot{v}_o + 2m\Omega(\beta_p+\delta_D)\dot{w}_o + 4m\Omega x_I \dot{v}_o' \\
&-(T\tfrac{\partial v_o}{\partial r})' - m\Omega^2 v_o - m\Omega^2(\sin\theta_o)\, w_o \\
&+\left[(EI_F\sin^2\theta_{TW} + EI_C\cos^2\theta_{TW})\, v_o'' + \{(EI_F - EI_C)\cos\theta_{TW}\sin\theta_{TW}\}\, w_o''\right]'' \\
&= P_v + m\Omega^2(r_o+r)\beta_p\theta_o + m\Omega^2(-e_o + r\delta_D\theta_o) \\
&+ 2m x_I\Omega^2 - m\Omega^2 e_N
\end{aligned}
\tag{97}
$$

Galerkin's Method is applied to Eqs. 96 and 97 to obtain the modal equations of motion for the steady-equilibrium condition, using the two coupled rotating bending mode shapes obtained in Subsection 2.2. The dimensional bending is expressed in terms of a series of generalized coordinates and dimensionless mode shapes which have unit displacement at the blade tip:

$$
\begin{Bmatrix} w_o \\ v_o \end{Bmatrix} = R\sum_{k=1}^{2} \begin{Bmatrix} \overline{W}_k(x) \\ V_k(x) \end{Bmatrix} \overline{\xi}_k(t) \tag{98}
$$

After substituting Eq. 98 into Eqs. 96 and 97, the application of Galerkin's method with coupled mode shapes is as follows:

$$
\int_0^R \{W_k \; V_k\} \left[\begin{array}{l} \text{Left-hand side of Eq. 96 in terms of} \\ \text{generalized coordinates and mode shapes} \\ \hline \text{Left-hand side of Eq. 97 in terms of} \\ \text{generalized coordinates and mode shapes} \end{array}\right] dr
$$

$$
= \int_0^R \{W_k \; V_k\} \left[\begin{array}{l} \text{Right-hand side of Eq. 96 in terms of} \\ \text{generalized coordinates and mode shapes} \\ \hline \text{Right-hand side of Eq. 97 in terms of} \\ \text{generalized coordinates and mode shapes} \end{array}\right] dr \tag{99}
$$

It should be noted that aerodynamic forces P_W and P_V in Eqs. 96 and 97 are evaluated from Eqs. 74 and 82 discarding terms related to torsion ϕ and rigid-pitch motion θ_R and double underlined terms which express the steady-state equilibrium deflection effect on aerodynamic forces; they will be included in the perturbation equations later.

After some algebraic manipulation, the equations of motion for the steady-state equilibrium will be obtained in terms of generalized coordinates as follows:

$$I_{q_1}\ddot{\bar{q}}_1 + (2S_{q_1\dot{q}_1} + M_{q_1\dot{q}_1})\dot{\bar{q}}_1 + (2S_{q_1\dot{q}_2} + M_{q_1\dot{q}_2})\dot{\bar{q}}_2 + I_{q_1}\left(\frac{\omega_1}{\Omega}\right)^2 \bar{q}_1 = M_{C.F.q_1} + M_{q_1} + M_{q_1\theta}\cdot\bar{\theta}$$

$$I_{q_2}\ddot{\bar{q}}_2 + (2S_{q_2\dot{q}_1} + M_{q_2\dot{q}_1})\dot{\bar{q}}_1 + (2S_{q_2\dot{q}_2} + M_{q_2\dot{q}_2})\dot{\bar{q}}_2 + I_{q_2}\left(\frac{\omega_2}{\Omega}\right)^2 \bar{q}_2 = M_{C.F.q_2} + M_{q_2} + M_{q_2\theta}\cdot\bar{\theta}$$

(100)

where $\bar{q}_1$ and $\bar{q}_2$ are generalized coordinates corresponding to the lowest frequency flapping and lagging motion, and $(^{oo})$ and $(^{o})$ are nondimensional time derivatives $d^2/d(\Omega t)^2$ and $d/d(\Omega t)$. Iq_1 and Iq_2 are generalized masses and $Sq_1\dot{q}_1$, $Sq_1\dot{q}_2$, $Sq_2\dot{q}_1$ and $Sq_2\dot{q}_2$ are related to Coriolis forces. Rotating-blade natural frequencies are expressed by ω_1/Ω and ω_2/Ω. $Mq_1\dot{q}_1$, $Mq_1\dot{q}_2$, $Mq_2\dot{q}_1$ and $Mq_2\dot{q}_2$ are aerodynamic dampings, and $M_{C.F.q_1}$ and $M_{C.F.q_2}$ are loading due to centrifugal forces. Mq_1 and Mq_2 are aerodynamic loading, and $M_{q_1\theta}$ and $M_{q_2\theta}$ are coefficients of blade pitch control. These coefficients are defined in Appendix A.

Generalized coordinates $\bar{q}_1$ and $\bar{q}_2$ may be written as

$$\bar{q}_1(t) = \bar{\beta}_o + \bar{\beta}_{1c}\cos\psi + \bar{\beta}_{1s}\sin\psi$$
$$\bar{q}_2(t) = \bar{\zeta}_o + \bar{\zeta}_{1c}\cos\psi + \bar{\zeta}_{1s}\sin\psi \qquad (101)$$

where it is assumed that the flap motion is predominant in $\bar{q}_1(t)$ motion and the lag motion is predominant in $\bar{q}_2(t)$ motion. $\bar{\beta}_o$, $\bar{\beta}_{1c}$, $\bar{\beta}_{1s}$, $\bar{\zeta}_o$ $\bar{\zeta}_{1c}$, and $\bar{\zeta}_{1s}$ are constant and express the amplitudes of the collective and cyclic motions in the steady equilibrium condition. Trim pitch is

$$\bar{\theta} = \bar{\theta}_o + \bar{\theta}_{1c}\cos\psi + \bar{\theta}_{1s}\sin\psi \qquad (102)$$

where $\bar{\theta}_o$, $\bar{\theta}_{1c}$, and $\bar{\theta}_{1s}$ are constant.

Substituting Eq. 101 and the time derivatives of Eq. 101 and also Eq. 102 into Eq. 100 and applying the harmonic balance method yields the following linear simultaneous equations for the out-of-trim operation.

FOR NO TRIM OPERATION

$$
\begin{bmatrix}
I_{\beta_1}\left(\frac{\omega_1}{\Omega}\right)^2 & -\frac{1}{2}M^S_{\beta_1\dot{\beta}_1} + \frac{1}{2}M^C_{\beta_1\beta_1} & 0 & 0 & -\frac{1}{2}M^S_{\beta_1\dot{\beta}_2} + \frac{1}{2}M^C_{\beta_1\beta_2} & 0 \\
M^C_{\beta_1\beta_1} & I_{\beta_1}\left\{\left(\frac{\omega_1}{\Omega}\right)^2 - 1\right\} & 2S_{\beta_1\dot{\beta}_1} + M^o_{\beta_1\dot{\beta}_1} & M^C_{\beta_1\beta_2} & 0 & 2S_{\beta_1\dot{\beta}_2} + M^o_{\beta_1\dot{\beta}_2} \\
0 & -(2S_{\beta_1\dot{\beta}_1} + M^o_{\beta_1\dot{\beta}_1}) & I_{\beta_1}\left\{\left(\frac{\omega_1}{\Omega}\right)^2 - 1\right\} & 0 & -(2S_{\beta_1\dot{\beta}_2} + M^o_{\beta_1\dot{\beta}_2}) & 0 \\
0 & -\frac{1}{2}M^S_{\beta_2\dot{\beta}_1} + \frac{1}{2}M^C_{\beta_2\beta_1} & 0 & I_{\beta_2}\left(\frac{\omega_2}{\Omega}\right)^2 & -\frac{1}{2}M^S_{\beta_2\dot{\beta}_2} + \frac{1}{2}M^C_{\beta_2\beta_2} & 0 \\
M^C_{\beta_2\beta_1} & 0 & 2S_{\beta_2\dot{\beta}_1} + M^o_{\beta_2\dot{\beta}_1} & M^C_{\beta_2\beta_2} & I_{\beta_2}\left\{\left(\frac{\omega_2}{\Omega}\right)^2 - 1\right\} & 2S_{\beta_2\dot{\beta}_2} + M^o_{\beta_2\dot{\beta}_2} \\
0 & -(2S_{\beta_2\dot{\beta}_1} + M^o_{\beta_2\dot{\beta}_1}) & 0 & 0 & -(2S_{\beta_2\dot{\beta}_2} + M^o_{\beta_2\dot{\beta}_2}) & I_{\beta_2}\left\{\left(\frac{\omega_2}{\Omega}\right)^2 - 1\right\}
\end{bmatrix}
\begin{Bmatrix}
\bar{\beta}_0 \\ \bar{\beta}_{1c} \\ \bar{\beta}_{1s} \\ \bar{\zeta}_0 \\ \bar{\zeta}_{1c} \\ \bar{\zeta}_{1s}
\end{Bmatrix}
=
\begin{bmatrix}
M_{c.f.\beta_1} + M^o_{\beta_1} + \frac{1}{2}M^S_{\beta_1\theta}\cdot\bar{\theta}_{1s} \\
(M^o_{\beta_1\theta} + \frac{1}{2}M^{2c}_{\beta_1\theta})\bar{\theta}_{1c} \\
M^S_{\beta_1} + (M^o_{\beta_1\theta} - \frac{1}{2}M^{2c}_{\beta_1\theta})\bar{\theta}_{1s} \\
M_{c.f.\beta_2} + M^o_{\beta_2} + \frac{1}{2}M^S_{\beta_2\theta}\cdot\bar{\theta}_{1s} \\
(M^o_{\beta_2\theta} + \frac{1}{2}M^{2c}_{\beta_2\theta})\bar{\theta}_{1c} \\
M^S_{\beta_2} + (M^o_{\beta_2\theta} - \frac{1}{2}M^{2c}_{\beta_2\theta})\bar{\theta}_{1s}
\end{bmatrix}
\tag{103}
$$

where coefficients used above are defined in Appendix A.

For the moment trim operation, to achieve the state of zero pitching and rolling moments, the following condition is necessary:

$$\bar{\beta}_{1C} = \bar{\beta}_{1S} = 0 \tag{104}$$

which requires trim cyclic pitch. Therefore, the equations for the moment trim operation are

$$\begin{bmatrix}
I_{\zeta_1}\left(\frac{\omega_1}{\Omega}\right)^2 & 0 & -\frac{1}{2}M^{s}_{\zeta_1\theta} & 0 & -\frac{1}{2}M^{s}_{\zeta_1\zeta_2}+\frac{1}{2}M^{c}_{\zeta_1\zeta_2} & 0 \\
M^{c}_{\zeta_1\zeta_1} & -M^{o}_{\zeta_1\theta}-\frac{1}{2}M^{2c}_{\zeta_1\theta} & 0 & M^{c}_{\zeta_1\zeta_2} & 0 & 2S_{\zeta_1\zeta_2}+M^{o}_{\zeta_1\dot{\zeta}_2} \\
0 & 0 & -M^{o}_{\zeta_1\theta}+\frac{1}{2}M^{2c}_{\zeta_1\theta} & 0 & -(2S_{\zeta_1\zeta_2}+M^{o}_{\zeta_1\dot{\zeta}_2}) & 0 \\
0 & 0 & -\frac{1}{2}M^{s}_{\zeta_2\theta} & I_{\zeta_2}\left(\frac{\omega_2}{\Omega}\right)^2 & -\frac{1}{2}M^{s}_{\zeta_2\zeta_2}+\frac{1}{2}M^{c}_{\zeta_2\zeta_2} & 0 \\
M^{c}_{\zeta_2\zeta_1} & -M^{o}_{\zeta_2\theta}-\frac{1}{2}M^{2c}_{\zeta_2\theta} & 0 & M^{c}_{\zeta_2\zeta_2} & I_{\zeta_2}\left\{\left(\frac{\omega_2}{\Omega}\right)^2-1\right\} & 2S_{\zeta_2\dot{\zeta}_2}+M^{o}_{\zeta_2\dot{\zeta}_2} \\
0 & 0 & -M^{o}_{\zeta_2\theta}+\frac{1}{2}M^{2c}_{\zeta_2\theta} & 0 & -2S_{\zeta_2\dot{\zeta}_2}-M^{o}_{\zeta_2\dot{\zeta}_2} & I_{\zeta_2}\left\{\left(\frac{\omega_2}{\Omega}\right)^2-1\right\}
\end{bmatrix}
\begin{Bmatrix}
\bar{\beta}_0 \\ \bar{\theta}_{1C} \\ \bar{\theta}_{1S} \\ \bar{\zeta}_0 \\ \bar{\zeta}_{1C} \\ \bar{\zeta}_{1S}
\end{Bmatrix}
=
\begin{bmatrix}
M_{C.F.\zeta_1}+M^{\bullet}_{\zeta_1} \\ 0 \\ M^{s}_{\zeta_1} \\ M_{C.F.\zeta_2}+M^{\bullet}_{\zeta_2} \\ 0 \\ M_{\zeta_2}
\end{bmatrix} \tag{105}$$

where the coefficients used above are defined in Appendix A.

2.4.3 Thrust Coefficient

The thrust coefficient C_T is defined as

$$C_T = \frac{T}{\rho(\pi R^2)(\Omega R)^2} = \frac{N}{2\pi\rho(\pi R^2)(\Omega R)^2}\int_0^{2\pi}\int_0^{R} P_z(r,\psi)\,dr\,d\psi \tag{106}$$

where T is thrust and N is the number of blades. Assuming $P_z \approx P_w$ and substituting Eqs. 74 and 82 into Eq. 96 yields

$$C_T = \frac{\sigma a}{4}\left[2X_\theta^{(II)} - \left(1+\frac{C_{d_0}}{a}\right)\lambda + \mu^2 X_\theta^{(0)} + \left\{2\mu V_{1\theta}^{(0)} + \mu\left(1+\frac{C_{d_0}}{a}\right)W_1^{(0)}\right\}\bar{\beta}_{1c} + \left\{2\mu V_{2\theta}^{(0)} + \mu\left(1+\frac{C_{d_0}}{a}\right)W_2^{(0)}\right\}\bar{\zeta}_{1c} + \mu\bar{\theta}_{1s}\right] \tag{107}$$

where

$$\sigma = \frac{Nc}{\pi R}$$

$$X_\theta^{(II)} = \int_0^1 (\theta_s x^2)\,dx \quad ; \quad X_\theta^{(0)} = \int_0^1 \theta_s\,dx$$

$$V_{i\theta}^{(0)} = \int_0^1 (\theta_s V_i)\,dx \quad ; \quad W_i^{(0)} = \int_0^1 W_i\,dx$$

and V_i and W_i are mode shapes, and i takes the values 1 or 2.

2.4.4 Procedure for the Trim Condition

The trim condition is obtained using the iteration method. The procedure is described as follows:

(1) Advance ratio μ and shaft tilt angle α_s are given for the wind tunnel experiment condition.

(2) Set an arbitrary value for the thrust coefficient C_T as an initial value.

(3) Evaluate the inflow ratio λ from Eq. 106 below with given μ, α_s and C_T.

$$\lambda = \mu \tan\alpha_s + \frac{C_T}{2\sqrt{\mu^2 + \lambda^2}} \tag{108}$$

This is a fourth-order polynominal in λ. An appropriate root should be chosen from the resulting real and complex roots.

(4) Using the inflow ratio λ obtained in the previous step, aerodynamic coefficients in Appendix A are evaluated and the equilibrium equation of Eq. 103 for the no-trim operation or of Eq. 105 for the moment trim operation are solved.

(5) Substituting the amplitudes of $\overline{\beta}_{1c}$ and $\overline{\zeta}_{1c}$, zero $\overline{\theta}_{1s}$ into Eq. 107 in the case of out-of-trim operation ($\overline{\zeta}_{1c}$, $\overline{\theta}_{1s}$ and zero $\overline{\beta}_{1c}$ should be substituted for the moment trim operation) yields a new thrust coefficient.

(6) Check the accuracy of the new thrust coefficient, compared to the old thrust coefficient. If it is not within the accuracy specified, proceed to the next step.

(7) Replace the old thrust coefficient with the new one and go to step (3) for the iteration.

2.5 Modal Equations of Motion

In this section the nonlinear periodic-coefficient equations of motion, Eqs. 34, 35, 36, and 39 with aerodynamic loadings Eqs. 81, 86, and 89 are linearized for small perturbation motions about the steady-state equilibrium operating condition. Galerkin's method is applied to these equations and modal equations are obtained in terms of generalized coordinates. The equations thus obtained are periodic-coefficient equations. To avoid difficulties in solving the periodic-coefficient equations, the equations are transformed into the nonrotating coordinate frame using the Fourier series expansion, where most of the periodic coefficients are transformed into constant coefficients. Stability calculations and frequency response analysis for vertical gusts are performed, based upon the constant-coefficient equations.

2.5.1 The Perturbation Equations of Motion

Bending motions in terms of steady equilibrium quantities and perturbation motions in Eq. 73 are substituted into Eqs. 34, 35, 36, and 39, and the equilibrium equations are subtracted. Discarding all nonlinear products of perturbation quantities yields

w Equation

$$
\begin{aligned}
&m\ddot{w} - m x_I \ddot{\phi} - m(x_I + \underline{\underline{v_0}})\ddot{\theta}_R - \underline{4 m x_I \Omega \theta_0 \theta_{TW} \dot{w}'} \\
&+ \underline{2 m x_I \Omega (\theta_0 - \theta_{TW}) \dot{v}'} - 2 m \Omega (\underline{\underline{w_0'}} + \underline{\beta_p + \delta_D})\dot{v} \\
&- \underline{\underline{2 m \Omega w_0''}} \int_r^R \dot{v}\, dr - \underline{\underline{(2 m \dot{v}_0)}}\dot{\theta}_R + \left[(EI_F + EI_C \cdot \theta_{TW}^2) w'' \right. \\
&\left. + (EI_F - EI_C)\theta_{TW} v''\right]'' - (T_0 w')' + \underline{\underline{2 m \Omega \left(w' \int_r^R \dot{v}_0 dr\right)'}} - (m\Omega^2 \theta_0) v \\
&+ \underline{(e_N T_0 \phi)''} + \{\underline{m x_I \Omega^2 (r_0 + r)\phi}\}' + m x_I \Omega^2 (\theta_0 + \theta_{TW})\theta_0 \phi \\
&+ m\Omega^2 \{e_0 - x_I - (r_0 + r)\beta_p \theta_0 - r\delta_0 (2\theta_0) - \underline{\underline{v_0}}\}\theta_R \\
&= \left(\frac{\partial P_w}{\partial u_T}\right)_0 \delta u_T + \left(\frac{\partial P_w}{\partial u_P}\right)_0 \delta u_P + \left(\frac{\partial P_w}{\partial \theta}\right)_0 (\delta\theta + \delta\phi)
\end{aligned}
\tag{109a}
$$

v Equation

$$
\begin{aligned}
&m\ddot{v} - (m x_I \theta_{Tw})\ddot{\phi} + \{m(w_0 + r\delta_D - x_I\theta_{Tw})\}\ddot{\theta}_R \\
&+ 2m\Omega(\beta_p + \delta_D)\dot{w} - 2m x_I \Omega(\theta_0 - \theta_{Tw})\dot{w}' \\
&+ 2m\Omega\int_0^r (w_0'\dot{w}')dr - 2m\Omega v_0'\dot{v} - 2m\Omega\dot{v}_0''\int_r^R \dot{v}\,dr \\
&+ 4m x_I \Omega\dot{v}' + 2m\Omega\int_0^r (v_0'\dot{v}')dr + (2m\dot{w}_0)\dot{\theta}_R \\
&+ \left[(EI_F\theta_{Tw}^2 + EI_C)v'' + \{(EI_F - EI_C)\theta_{Tw}\}w''\right]'' \\
&- (m\Omega^2\theta_0)w + 2m\Omega\int_0^r (\dot{w}_0' w')dr - (T_0 v')' - m\Omega^2 v \\
&+ 2m\Omega\left(v'\int_r^R \dot{v}_0\,dr\right)' + 2m\Omega\int_0^r (\dot{v}_0' v')dr \\
&+ (e_N T_0 \theta_{Tw}\phi)'' - \{m x_I \theta_{Tw}\Omega^2(r_0 + r)\phi\}' + (m x_I \Omega^2\theta_s)\phi \\
&- m\Omega^2\{e_0\theta_0 + (r_0 + r)\beta_p + r\delta_D - x_I(\theta_s + \theta_0) + w_0\}\theta_R \\
&= \left(\frac{\partial R_v}{\partial u_T}\right)_0 \delta u_T + \left(\frac{\partial R_v}{\partial u_P}\right)_0 \delta u_P + \left(\frac{\partial R_v}{\partial \theta}\right)_0 \delta\theta + \left(\frac{\partial R_v}{\partial \phi}\right)_0 \delta\phi
\end{aligned}
$$

(109b)

ϕ Equation

$$
\begin{aligned}
&- m x_I \ddot{w} - m x_I \theta_{TW} \ddot{v} + I_o \ddot{\phi} + (I_o - m x_I r \delta_D \theta_{TW}) \ddot{\theta}_R \\
&+ e_N T_o w'' - \underline{m x_I \Omega^2 (r_o + r) w'} + m x_I \Omega^2 \theta_s \theta_o w \\
&- \underline{\underline{(EI_F - EI_C)(w_o'' \theta_{TW} - v_o'') w''}} + \underline{e_N T_o \theta_{TW} v''} \\
&- \underline{m x_I \Omega^2 (r_o + r) \theta_{TW} v'} + m x_I \Omega^2 \theta_s v \\
&+ \underline{\underline{(EI_F - EI_C)(v_o'' \theta_{TW} + w_o'') v''}} - \{(GJ + T_o k_{z_A}^2) \phi'\}' \\
&- m x_I \Omega^2 (r_o + r) \beta_p \theta_o \phi + m x_I \Omega^2 (r_o + r) \delta_D \theta_{TW} \phi \\
&+ m x_I \Omega^2 (-e_o + r \delta_D \theta_o) \phi + (I_{zp} - I_{xp}) \Omega^2 \phi \\
&- m x_I \Omega^2 \{(r_o + r) \beta_p \theta_s - r \delta_D (\theta_s + \theta_o) + e_o\} \theta_R \\
&+ (I_{zp} - I_{xp}) \Omega^2 \theta_R \\
&= \left(\frac{\partial M_A}{\partial u_T}\right)_o \delta u_T + \left(\frac{\partial M_A}{\partial u_p}\right)_o \delta u_p + \left(\frac{\partial M_A}{\partial \theta}\right)_- (\delta\theta + \delta\phi) \\
&\quad + \left(\frac{\partial M_A}{\partial \dot{\theta}}\right)(\delta\dot{\theta} + \delta\dot{\phi})
\end{aligned}
$$

(109c)

θ_R Equation

$$\int_0^R \Big[-m x_I \ddot{w} - \underline{\underline{m v_0 \ddot{w}}} + (m r \delta_D - m x_I \theta_{TW}) \ddot{v} + \underline{\underline{m w_0 \ddot{v}}}$$

$$+ (I_0 - m r \delta_D x_I \theta_{TW}) \ddot{\phi} + (I_0 + m r^2 \delta_D^2 - 2 m x_I r \delta_D \theta_{TW}) \ddot{\theta}_R$$

$$+ m \Omega^2 \{ e_0 - x_I - (r_0 + r) \beta_p \theta_0 - r \delta_D (2\theta_0) - \underline{\underline{v_0}} \} w$$

$$+ \underline{\underline{m \ddot{v}_0 w}}$$

$$- m \Omega^2 \{ e_0 \theta_0 + \beta_p (r_0 + r) + r \delta_D - x_I (\theta_s + \theta_0) + \underline{\underline{w_0}} \} v$$

$$- \underline{\underline{m \ddot{w}_0 v}}$$

$$- m x_I \Omega^2 \{ (r_0 + r) \beta_p \theta_s - r \delta_D x_I (\theta_s + \theta_0) + e_0 \} \phi$$

$$+ (I_{zp} - I_{xp}) \Omega^2 \phi + (I_{zp} - I_{xp}) \Omega^2 \theta_R$$

$$- m \Omega^2 \{ \beta_p \delta_D r (r_0 + r) - e_0 r \delta_D \theta_0 - r^2 \delta_D^2 - e_0 x_I$$

$$- 2 r \delta_D x_I (\theta_s + \theta_0) \} \theta_R \Big] dr + K_\theta \theta_R$$

$$= \int_0^R \Big[\left(\frac{\partial M_A}{\partial u_T}\right)_0 \delta u_T + \left(\frac{\partial M_A}{\partial u_p}\right)_0 \delta u_p + \left(\frac{\partial M_A}{\partial \theta}\right)_0 (\delta\theta + \delta\phi)$$

$$+ \left(\frac{\partial M_A}{\partial \dot{\theta}}\right)_0 (\delta\dot{\theta} + \delta\dot{\phi}) \Big] dr + \int_0^R \Big[(P_v)_0 w - (P_w)_0 v$$

$$+ v_0 \left\{ \left(\frac{\partial P_w}{\partial u_T}\right)_0 \delta u_T + \left(\frac{\partial P_w}{\partial u_p}\right)_0 \delta u_p + \left(\frac{\partial P_w}{\partial \theta}\right)_0 (\delta\theta + \delta\phi) \right.$$

$$\left. + \left(\frac{\partial P_w}{\partial \dot{\theta}}\right)_0 (\delta\dot{\theta} + \delta\dot{\phi}) \right\} + (w_0 + r\delta_D) \left\{ \left(\frac{\partial P_v}{\partial u_T}\right)_0 \delta u_T + \left(\frac{\partial P_v}{\partial u_p}\right)_0 \delta u_p \right.$$

$$\left. + \left(\frac{\partial P_v}{\partial \theta}\right)_0 \delta\theta + \left(\frac{\partial P_v}{\partial \phi}\right)_0 \delta\phi + \left(\frac{\partial P_v}{\partial \dot{\theta}}\right)_0 (\delta\dot{\theta} + \delta\dot{\phi}) \right\} \Big] dr \qquad (109d)$$

where

$$T_0 = \int_r^R m (r_0 + r) \Omega^2 dr \qquad (110)$$

It should be noted that the single underlined terms are terms which are not included in Eq. 40, used to derive the natural frequencies and mode shapes, even though the omitted terms are linear. However, they are retained in the modal analysis. Most of these terms are velocity dependent terms resulting from Coriolis forces. Other terms, for example $(e_N T_o \phi)''$ and $\{mx_I \Omega^2 (r_o + r)\phi\}'$ in Eq. 109a where the former expresses the centrifugal force effect, due to the cross-section neutral axis offset, and the latter is the centrifugal force effect, due to the cross-section center-of-gravity offset, are excluded in Eq. 40 because these terms make the stiffness matrix nonsymmetrical as do the Coriolis force terms.

The double underlined terms are attributed to nonlinear terms in Eqs. 34, 35, 36, and 39, and include steady-state equilibrium deflection effects producing structural couplings. The roles of these terms are described briefly. The term $-mv_o\ddot{\theta}_R$ in Eq. 109a for the w-equation is due to an additional center-of-gravity offset resulting from the steady-state chordwise deflection. The term $-2m\Omega w_o'\dot{v}$ is the Coriolis force effect from the additional precone due to steady-state flapping. The rotation about the feathering axis, due to the rigid pitch, yields the Coriolis force $-2m\dot{v}_o\dot{\theta}_R$. The terms $-2m\Omega(w'\int_r^R \dot{v}_o dr)$ and $-2m\Omega(w_o''\int_r^R \dot{v}\, dr)$ are supplemental to the constant tension force expression in Eq. 110, while the original expression is Eq. 37. The term $(-m\Omega^2 v_o\theta_R)$ expresses the centrifugal force effect due to the center-of-gravity offset from the steady-state chordwise deflection. For the rest of the equations, short explanations will be given if they are different from above.

In Eq. 109b (the v equation) the term $2m\Omega\int_o^r (v_o'\dot{v}' + \dot{v}_o'v' + w_o'\dot{w}' + \dot{w}_o'w')dr$ results from the Coriolis force effect due to $-2m\Omega\dot{u}$ in Eq. 35, which includes the geometrical radial shortening effect from vertical and chordwise bending deflections.

In Eq. 109c (the ϕ equation), the terms $(EI_F - EI_C)[-\{w_o''\theta_{TW} - v_o''\}w'' + \{v_o''\theta_{TW} + w_o''\}v'']$ shows the bending-torsion coupling identified by Mil' et al. (Ref. 41). The bending moment expressions are used to describe the inertia and aerodynamic loadings which cause torsional moments about the deformed elastic axis. It should be noted that there is no structural bending-

torsion coupling in the matched-stiffness rotor blade where EI_F equals EI_C. For the rigid-pitch equation of Eq. 109d, this coupling is directly described in terms of the inertia and aerodynamic loadings and the steady-state blade deflections.

2.5.2 Modal Equations in Rotating Coordinate Systems

The steady-state equilibrium deflections and perturbation deflections may be written

$$\begin{Bmatrix} w_o \\ v_o \end{Bmatrix} = \sum_{k=1}^{2} \begin{Bmatrix} W_k \\ V_k \end{Bmatrix} \bar{q}_k(t) \quad ; \quad \begin{Bmatrix} w \\ v \\ \phi \\ \theta_R \end{Bmatrix} = \sum_{j=1}^{\infty} \begin{Bmatrix} W_j \\ V_j \\ \Phi_j \\ \Theta_j \end{Bmatrix} q_j(t) \qquad (111)$$

Galerkin's method may be applied to Eq. 109 as described in Subsection 2.4.2 using the natural frequencies and coupled mode shapes in Eq. 111 as obtained in Subsection 2.2. Terms without underlines in the left-hand side of Eq. 109 are converted into generalized masses and natural frequencies, and terms with underlines describe cross-couplings between modes.

The modal equation for the ith mode, using N modes, is given by

$$\begin{aligned}
&I_i \overset{\circ\circ}{q}_i + 2\zeta_i \left(\frac{\omega_i}{\Omega}\right) \overset{\circ}{q}_i + \sum_{j=1}^{N} S_{ij\ell} \overset{\circ}{q}_j + I_i \left(\frac{\omega_i}{\Omega}\right)^2 q_i \\
&+ \sum_{j=1}^{N} C_{ij\ell} q_j + \sum_{k=1}^{2} \sum_{j=1}^{N} \Big\{ E_{kij\bar{\ell}\bar{\ell}} \bar{q}_k \overset{\circ\circ}{q}_j + E_{kij\bar{\ell}\dot{\ell}} \overset{\circ}{\bar{q}}_k \overset{\circ}{q}_j \\
&+ E_{kij\bar{\ell}\dot{\ell}} \bar{q}_k \overset{\circ}{q}_j + E_{kij\ddot{\bar{\ell}}\ell} \overset{\circ\circ}{\bar{q}}_k q_j + E_{kij\dot{\bar{\ell}}\ell} \overset{\circ}{\bar{q}}_k q_j + E_{kij\dot{\bar{\ell}}\ell} \overset{\circ}{\bar{q}}_k q_j \\
&+ E_{kij\bar{\ell}\ell} \bar{q}_k q_j \Big\} - \sum_{j=1}^{N} \Big\{ A_{ij\dot{\ell}} \overset{\circ}{q}_j + A^{1s}_{ij\dot{\ell}} \overset{\circ}{q}_j \sin\psi + A_{ij\ell} q_j \\
&+ A^{1s}_{ij\ell} q_j \sin\psi + A^{2c}_{ij\ell} q_j \cos(2\psi) \Big\}
\end{aligned}$$

$$
\begin{aligned}
&- \sum_{k=1}^{2} \sum_{j=1}^{N} \Big\{ A_{kij}\, \dot{\bar{\zeta}}_i \ddot{\bar{\zeta}}_i \overset{\circ}{\bar{\zeta}}_k \overset{\circ}{\zeta}_j + A_{kij}\, \bar{\zeta}_i \dot{\bar{\zeta}}_i \bar{\zeta}_k \overset{\circ}{\zeta}_j \\
&+ A^{1S}_{kij}\, \dot{\bar{\zeta}}_i \bar{\zeta}_k \overset{\circ}{\zeta}_j \sin\psi + A_{kij}\, \dot{\bar{\zeta}}_i \overset{\circ}{\bar{\zeta}}_k \zeta_j + A_{kij}\, \bar{\zeta}_i \bar{\zeta}_k \zeta_j \\
&+ A^{1S}_{kij}\, \bar{\zeta}_i \overset{\circ}{\bar{\zeta}}_k \zeta_j \sin\psi + A^{1S}_{kij}\, \bar{\zeta}_i \bar{\zeta}_k \zeta_j \sin\psi \\
&+ A^{2S}_{kij}\, \bar{\zeta}_i \bar{\zeta}_k \zeta_j \sin(2\psi) + A^{1C}_{kij}\, \bar{\zeta}_i \bar{\zeta}_k \zeta_j \cos\psi \\
&+ A^{2C}_{kij}\, \bar{\zeta}_i \bar{\zeta}_k \zeta_j \cos(2\psi) \Big\}
\end{aligned}
$$

$$
\begin{aligned}
= {} & G_i \bar{\omega}_G + G_i^{2C} \bar{\omega}_G - G_i^{2C} \bar{\omega}_G \cos(2\psi) \\
&+ \sum_{k=1}^{2} \Big\{ G_{ki} \overset{\circ}{\bar{\zeta}}_k \bar{\omega}_G + G^{2C}_{ki} \bar{\zeta}_k \bar{\omega}_G \\
&+ G^{1S}_{ki} \overset{\circ}{\bar{\zeta}}_k \bar{\omega}_G \sin\psi - G^{2C}_{ki} \bar{\zeta}_k \bar{\omega}_G \cos(2\psi) \\
&+ G^{1S}_{ki} \bar{\zeta}_k \bar{\omega}_G \sin\psi + G_{ki} \bar{\zeta}_k \bar{\omega}_G \Big\} \\
&+ \overset{\circ}{\sigma} \Big[\Big\{ G^{C}_{i\mu} \bar{\omega}_G \cos\psi + G^{C^2}_{i\mu} \bar{\omega}_G \cos^2\psi + G^{2SC}_{i\mu} \bar{\omega}_G \sin(2\psi)\cos\psi \\
&+ G^{S^2C}_{i\mu} \bar{\omega}_G \sin^2\psi \cos\psi \Big\} + \sum_{k=1}^{2} \Big\{ G^{C}_{ki\bar{\zeta}\mu} \overset{\circ}{\bar{\zeta}}_k \bar{\omega}_G \cos\psi + G^{C^2}_{ki\bar{\zeta}\mu} \bar{\zeta}_k \bar{\omega}_G \cos^2\psi \\
&+ G^{SC}_{ki\bar{\zeta}\mu} \bar{\zeta}_k \bar{\omega}_G \sin\psi\cos\psi + G^{S^2C}_{ki\bar{\zeta}\mu} \bar{\zeta}_k \bar{\omega}_G \sin^2\psi\cos\psi \\
&+ G^{2SC}_{ki\bar{\zeta}\mu} \bar{\zeta}_k \bar{\omega}_G \sin(2\psi)\cos\psi + G^{3C}_{ki\bar{\zeta}\mu} \overset{\circ}{\bar{\zeta}}_k \bar{\omega}_G \sin\psi\cos\psi \Big\} \Big]
\end{aligned}
\tag{112}
$$

where $i = 1, 2, \cdots N$ and $\overset{\circ}{\sigma} = \sqrt{-1}$.

This is the modal equation of the individual blade where the observer is sitting on the blade and rotating about the rotor shaft with the rotating angular velocity Ω. Therefore, the coefficients of equations are periodic in terms of the blade azimuth angle in cruising flight.

It should be noted that Eq. 112 is applicable to the out-of-trim condition in which rotor shaft tilt is prescribed. However, no cyclic pitch is applied to suppress the first harmonic cyclic flapping motion and eliminate rotor hub moments. Only the vertical gust is considered as a forcing function

in the right-hand side of Eq. 112. Steady-state cyclic pitch effect on the moment trim condition and pitch control as a forcing function are considered in Appendix C because they require a different treatment.

The various coefficients in the present equations are shown in detail in Appendix B. However, they will now be briefly described. The generalized coordinates for the steady-state equilibrium deflections and the perturbation deflections are expressed by $\bar{q}_k$ and q_j, respectively. The generalized mass corresponding to the ith mode shape is I_i. ζ_i is the structural damping of the ith mode in terms of the critical damping ratio. Coriolis force effects are expressed by $S_{ijq}^{\cdot}$, and (ω_i/Ω) is the nondimensionalized rotating blade natural frequency at rotational speed Ω. C_{ijq} coefficients include single underlined terms in Eq. 109, and $E_{kijqq}^{\dddot{\bar{}}}$, $E_{kijqq}^{\ddot{\bar{}}}$, $E_{kijqq}^{\dot{\bar{}}}$, $E_{kijqq}^{\ddot{}}$, $E_{kijqq}^{\bar{}}$, and $E_{kijqq}^{\bar{}}$ consist of double underlined terms in Eq. 109 which describe the steady-state equilibrium deflection effects due to the perturbation blade motion. $A_{ijq}^{\cdot}$ and $A_{ijq}^{1S\cdot}$ are aerodynamic damping terms, and A_{ijq}, A_{ijq}^{1S}, and A_{ijq}^{2C}, are aerodynamic stiffness terms. Superscripts 1S and 2C of coefficients show that these coefficients are coefficients of $\sin\Omega t$ and $\cos 2\Omega t$, respectively. The quantities $A_{kijqq}^{\dot{\bar{}}}$, $A_{kijqq}^{\bar{\cdot}}$, $A_{kijqq}^{1S\bar{\cdot}}$, $A_{kijqq}^{\dot{\bar{}}}$, $A_{kijqq}^{\bar{}}$, $A_{kijqq}^{1S\dot{\bar{}}}$, $A_{kijqq}^{1S\bar{}}$, $A_{kijqq}^{2S\bar{}}$, $A_{kijqq}^{1C\bar{}}$, and $A_{kijqq}^{2C\bar{}}$ are aerodynamic coefficients related to steady-state equilibrium deflections. The quantities G_i and G_i^{2C} are aerodynamic coefficients due to the vertical gust where $\bar{w}_G$ is the nondimensionalized gust velocity, $w_G/(\Omega R)$ at the center of the rotor. The quantities $G_{kijq}^{\dot{\bar{}}}$, $G_{kiq}^{2C\bar{}}$, $G_{kiq}^{1S\dot{\bar{}}}$, $G_{kiq}^{1S\bar{}}$, $G_{kiq}^{\bar{}}$ are aerodynamic coefficients due to the vertical gust and steady-state equilibrium deflections.

2.5.3 Modal Equations in Nonrotating Coordinate Systems

Equation 112 can be solved in closed form only when the flight condition is hovering, in which all periodic coefficients vanish. In cruising flight, it is difficult to obtain closed form solutions because of the periodic coefficients. Therefore, numerical integration techniques are usually employed. However, it is inconvenient to evaluate the characteristics of such systems.

In the present analysis, the harmonic balance approximation method (the nonrotating coordinate transformation) is chosen to evaluate the systems because this method has been shown to be reasonably accurate at advance ratios up to 0.5 (Ref. 40). This range is sufficient for the present purpose, since Eq. 111 holds good to an advance ratio of about 0.4 or 0.5 based on the assumption that the reverse flow is neglected in Subsection 2.4.

In the three-bladed rotor which is chosen as the rotor model in this analysis, the perturbation blade motion $q_j(t)$ of the jth mode in the rotating coordinate system may be written in terms of nonrotating coordinates by a coordinate transformation of the Fourier type.

$$q_j(t) = q_j^0(t) + q_j^{1C}(t)\cos(\Omega t) + q_j^{1S}(t)\sin(\Omega t) \tag{113}$$

For the steady-state equilibrium deflections, the transformation of Eq. 101 is used. If the jth mode corresponds to the flapping mode, $q_j^0(t)$, $q_j^{1C}(t)$, and $q_j^{1S}(t)$ represent blade coning motion, longitudinal flapping motion β_{1c} and lateral flapping motion β_{1s}, respectively. It should be noted that in Eq. 101 $\bar{\beta}_o$, $\bar{\beta}_{1c}$, $\bar{\beta}_{1s}$, $\bar{\zeta}_o$, $\bar{\zeta}_{1c}$, and $\bar{\zeta}_{1s}$ are constant. However, in Eq. 113 q_j^0, q_j^{1C}, and q_j^{1S} are functions of time.

Substituting Eqs. 101 and 113 into Eq. 112 and using a harmonic balance method results in a set of ordinary differential equations with constant coefficients that can be expressed as

$$[M]\{\ddot{Y}\} + [C]\{\dot{Y}\} + [K]\{Y\} = [F]\bar{w}_G \tag{114}$$

where if N mode shapes are used $\{Y\}$ will be

$$\{Y\}^T = \lfloor q_1^0\ q_1^{1C}\ q_1^{1S}\ q_2^0\ q_2^{1C}\ q_2^{1S}\ \cdots\cdots\ q_N^0\ q_N^{1C}\ q_N^{1S} \rfloor \tag{115}$$

and [M], [C], and [K] are generalized mass, generalized damping and generalized stiffness matrices with (3N) by (3N) dimensions, respectively. [F] is a generalized force row matrix with (3N) dimensions. [M], [C] force row matrix with (3N) dimensions. [M], [C] and [K] consist of submatrices $[m_{ij}]$, $[C_{ij}]$ and $[k_{ij}]$, respectively,which are the 3x3 matrices, and [F] of the 3x1 $[f_i]$ matrix.

The composition of the matrices are

$$[M] = \begin{bmatrix} [m_{11}] & [m_{12}] & \cdots & [m_{1N}] \\ [m_{21}] & & & \\ \vdots & & [m_{ij}] & \\ [m_{N1}] & \cdots & & [m_{NN}] \end{bmatrix} ; [F] = \begin{bmatrix} [f_1] \\ [f_2] \\ \vdots \\ [f_i] \\ \vdots \\ [f_N] \end{bmatrix} \quad (116)$$

and similarly [C] and [K] matrices are composed as [M] matrix.

$[m_{ij}]$, $[C_{ij}]$, $[k_{ij}]$ and $[f_i]$ may be written

$$[m_{ij}] = \delta_{ij} \begin{bmatrix} I_i & 0 & 0 \\ 0 & I_i & 0 \\ 0 & 0 & I_i \end{bmatrix} + \sum_{k=1}^{2} \left[\begin{array}{c|c|c} E_{\alpha ij} \ddot{\bar{\zeta}}^{0}_{\beta k} & \frac{1}{2} E_{\alpha ij} \ddot{\bar{\zeta}}^{1c}_{\beta k} & \frac{1}{2} E_{\alpha ij} \ddot{\bar{\zeta}}^{1s}_{\beta k} \\ \hline E_{\alpha ij} \ddot{\bar{\zeta}}^{1c}_{\beta k} & E_{\alpha ij} \ddot{\bar{\zeta}}^{0}_{\beta k} & 0 \\ \hline E_{\alpha ij} \ddot{\bar{\zeta}}^{1s}_{\beta k} & 0 & E_{\alpha ij} \ddot{\bar{\zeta}}^{0}_{\beta k} \end{array}\right] \quad (117a)$$

$$[C_{ij}] = \delta_{ij} \left[\begin{array}{c|c|c} 2 I_i \zeta_i \left(\frac{\omega_i}{\Omega}\right) & 0 & 0 \\ \hline 0 & 2 I_i \zeta_i \left(\frac{\omega_i}{\Omega}\right) & 2 I_i \\ \hline 0 & -2 I_i & 2 I_i \zeta_i \left(\frac{\omega_i}{\Omega}\right) \end{array}\right]$$

$$+ \begin{bmatrix} S_{ij} \dot{\zeta}_\beta & 0 & 0 \\ 0 & S_{ij} \dot{\zeta}_\beta & 0 \\ 0 & 0 & S_{ij} \dot{\zeta}_\beta \end{bmatrix} + \left[\begin{array}{c|c|c} -A_{ij} \dot{\zeta}_\beta & -\frac{1}{2} A^{1c}_{ij} \dot{\zeta}_\beta & -\frac{1}{2} A^{1s}_{ij} \dot{\zeta}_\beta \\ \hline -A^{1c}_{ij} \dot{\zeta}_\beta & -A_{ij} \dot{\zeta}_\beta & 0 \\ \hline -A^{1s}_{ij} \dot{\zeta}_\beta & 0 & -A_{ij} \dot{\zeta}_\beta \end{array}\right]$$

$$
+\sum_{k=1}^{2}
\left[\begin{array}{c|c|c}
\left(E_{kij}\bar{\xi}_i^{\circ}-A_{kij}\bar{\xi}_i^{\circ}\right)\bar{q}_k^{\circ} & -\frac{1}{2}A_{kij}^{1c}\bar{\xi}_i^{\circ}\,\bar{q}_k^{\circ} & -\frac{1}{2}A_{kij}\bar{\xi}_i^{\circ}\,\bar{q}_k^{\circ} \\
-\frac{1}{2}A_{kij}^{1s}\bar{\xi}_i^{1s}\,\bar{q}_k^{1s} & -E_{kij}\bar{\xi}_i^{1s}\,\bar{q}_k^{1s} & +E_{kij}\bar{\xi}_i^{1c}\,\bar{q}_k^{1c} \\
-\frac{1}{2}A_{kij}^{1c}\bar{\xi}_i^{1c}\,\bar{q}_k^{1c} & +\frac{1}{2}\left(E_{kij}\dot{\bar{\xi}}_i^{1s}-A_{kij}\bar{\xi}_i^{1s}\right)\bar{q}_k^{1s} & -\frac{1}{2}\left(E_{kij}\dot{\bar{\xi}}_i^{1c}-A_{kij}\bar{\xi}_i^{1c}\right)\bar{q}_k^{1c} \\
 & +\frac{1}{2}\left(E_{kij}\bar{\xi}_i^{1c}-A_{kij}\dot{\bar{\xi}}_i^{1c}\right)\bar{q}_k^{1c} & +\frac{1}{2}\left(E_{kij}\bar{\xi}_i^{1s}-A_{kij}\dot{\bar{\xi}}_i^{1s}\right)\bar{q}_k^{1s} \\
\hline
-A_{kij}^{1c}\bar{\xi}_i^{\circ}\,\bar{q}_k^{\circ} & -\frac{3}{4}A_{kij}^{1c}\bar{\xi}_i^{1c}\,\bar{q}_k^{1c} & 2E_{kij}\bar{\xi}_i^{\circ}\,\bar{q}_k^{\circ} \\
+\left(E_{kij}\dot{\bar{\xi}}_i^{1s}-A_{kij}\bar{\xi}_i^{1s}\right)\bar{q}_k^{1s} & -\frac{1}{4}A_{kij}^{1s}\bar{\xi}_i^{1s}\,\bar{q}_k^{1s} & -\frac{1}{4}A_{kij}^{1s}\bar{\xi}_i^{1c}\,\bar{q}_k^{1c} \\
+\left(E_{kij}\bar{\xi}_i^{1c}-A_{kij}\dot{\bar{\xi}}_i^{1c}\right)\bar{q}_k^{1c} & +\left(E_{kij}\bar{\xi}_i^{1s}-A_{kij}\dot{\bar{\xi}}_i^{1s}\right)\bar{q}_k^{\circ} & -\frac{1}{4}A_{kij}^{1c}\bar{\xi}_i^{1s}\,\bar{q}_k^{1s} \\
\hline
-A_{kij}^{1s}\bar{\xi}_i^{\circ}\,\bar{q}_k^{\circ} & -2E_{kij}\bar{\xi}_i^{\circ}\,\bar{q}_k^{\circ} & \left(E_{kij}\bar{\xi}_i^{\circ}-A_{kij}\dot{\bar{\xi}}_i^{\circ}\right)\bar{q}_k^{\circ} \\
-\left(E_{kij}\dot{\bar{\xi}}_i^{1c}-A_{kij}\bar{\xi}_i^{1c}\right)\bar{q}_k^{1c} & -\frac{1}{4}A_{kij}^{1s}\bar{\xi}_i^{1s}\,\bar{q}_k^{1c} & -\frac{1}{4}A_{kij}^{1c}\bar{\xi}_i^{1c}\,\bar{q}_k^{1c} \\
+\left(E_{kij}\bar{\xi}_i^{1s}-A_{kij}\dot{\bar{\xi}}_i^{1s}\right)\bar{q}_k^{1s} & -\frac{1}{4}A_{kij}^{1c}\bar{\xi}_i^{1c}\,\bar{q}_k^{1s} & +\frac{3}{4}A_{kij}^{1s}\bar{\xi}_i^{1s}\,\bar{q}_k^{1s}
\end{array}\right]
$$

(117b)

$$
[k_{ij}]=\delta_{ij}\left[\begin{array}{c|c|c}
I_i\left(\frac{\omega_i}{\Omega}\right)^2 & 0 & 0 \\
\hline
0 & I_i\left\{\left(\frac{\omega_i}{\Omega}\right)^2-1\right\} & 2I_i\zeta_i\left(\frac{\omega_i}{\Omega}\right) \\
\hline
0 & -2I_i\zeta_i\left(\frac{\omega_i}{\Omega}\right) & I_i\left\{\left(\frac{\omega_i}{\Omega}\right)^2-1\right\}
\end{array}\right]
$$

$$
+\left[\begin{array}{c|c|c}
C_{ij\xi} & 0 & 0 \\
\hline
0 & C_{ij\eta} & S_{ij\dot{\eta}} \\
\hline
0 & -S_{ij\dot{\eta}} & C_{ij\eta}
\end{array}\right]
+\left[\begin{array}{c|c|c}
-A_{ij\dot{\xi}} & \frac{1}{2}A_{ij\dot{\eta}}^{1s}-\frac{1}{2}A_{ij\dot{\eta}}^{1c} & -\frac{1}{2}A_{ij\dot{\xi}}^{1c}-\frac{1}{2}A_{ij\dot{\eta}}^{1s} \\
\hline
-A_{ij\eta}^{1c} & -A_{ij\eta}-\frac{1}{2}A_{ij\eta}^{2c} & -A_{ij\dot{\eta}}-\frac{1}{2}A_{ij\eta}^{2s} \\
\hline
-A_{ij\eta}^{1s} & A_{ij\dot{\eta}}-\frac{1}{2}A_{ij\eta}^{2s} & -A_{ij\eta}+\frac{1}{2}A_{ij\eta}^{2c}
\end{array}\right]
$$

$$
+\sum_{k=1}^{2}
\begin{bmatrix}
\left(E_{kij\bar{z}\bar{z}}-A_{kij\bar{z}\bar{z}}\right)\bar{q}^{0}_{k} \\
+\frac{1}{2}\left(A^{1S}_{kij\dot{z}\bar{z}}-A^{1C}_{kij\bar{z}\bar{z}}\right)\bar{q}^{1C}_{k} \\
-\frac{1}{2}\left(A^{1C}_{kij\dot{z}\dot{z}}+A^{1S}_{kij\bar{z}\bar{z}}\right)\bar{q}^{1S}_{k}
& \frac{1}{2}\left(A^{1S}_{kij\dot{z}\dot{z}}-A^{1C}_{kij\bar{z}\bar{z}}\right)\bar{q}^{0}_{k} \\
& +\frac{1}{2}\left(-E_{kij\dot{z}\ddot{z}}+E_{kij\bar{z}\dot{z}}\right. \\
& +E_{kij\bar{z}\bar{z}}-E_{kij\ddot{z}\bar{z}} \\
& -A_{kij\dot{z}\dot{z}}-A_{kij\bar{z}\bar{z}} \\
& \left.-\frac{1}{2}A^{2C}_{kij\dot{z}\bar{z}}\right)\bar{q}^{1C}_{k} \\
& +\frac{1}{2}\left(-E_{kij\ddot{z}\dot{z}}+E_{kij\dot{z}\bar{z}}\right. \\
& +A_{kij\dot{z}\bar{z}}-A_{kij\bar{z}\dot{z}} \\
& \left.-\frac{1}{2}A^{2S}_{kij\bar{z}\bar{z}}\right)\bar{q}^{1S}_{k}
& -\frac{1}{2}\left(A^{1C}_{kij\dot{z}\bar{z}}+A^{1S}_{kij\dot{z}\bar{z}}\right)\bar{q}^{0}_{k} \\
& +\frac{1}{2}\left(E_{kij\dot{z}\bar{z}}-E_{kij\bar{z}\dot{z}}\right. \\
& -A_{kij\dot{z}\dot{z}}+A_{kij\bar{z}\bar{z}} \\
& \left.-\frac{1}{2}A^{2S}_{kij\dot{z}\bar{z}}\right)\bar{q}^{1C}_{k} \\
& +\frac{1}{2}\left(-E_{kij\ddot{z}\dot{z}}+E_{kij\dot{z}\dot{z}}\right. \\
& -E_{kij\ddot{z}\bar{z}}+E_{kij\dot{z}\bar{z}} \\
& -A_{kij\dot{z}\dot{z}}-A_{kij\bar{z}\bar{z}} \\
& \left.+\frac{1}{2}A^{2C}_{kij\bar{z}\bar{z}}\right)\bar{q}^{1S}_{k} \\
\hline
-A^{1C}_{kij\bar{z}\bar{z}}\,\bar{q}^{0}_{k} \\
+\left(-E_{kij\ddot{z}\bar{z}}+E_{kij\dot{z}\bar{z}}\right. \\
\left.-A_{kij\dot{z}\bar{z}}\right)\bar{q}^{1C}_{k} \\
+\left(E_{kij\dot{z}\bar{z}}-A_{kij\bar{z}\bar{z}}\right. \\
\left.-\frac{1}{2}A^{2S}_{kij\bar{z}\bar{z}}\right)\bar{q}^{1S}_{k}
& \left(-E_{kij\ddot{z}\bar{z}}+E_{kij\dot{z}\bar{z}}\right. \\
& \left.-A_{kij\dot{z}\bar{z}}\right)\bar{q}^{0}_{k} \\
& +\frac{1}{4}\left(A^{1S}_{kij\dot{z}\bar{z}}\right. \\
& \left.-3A^{1C}_{kij\bar{z}\bar{z}}\right)\bar{q}^{1C}_{k} \\
& +\frac{1}{4}\left(A^{1C}_{kij\dot{z}\dot{z}}-A^{1S}_{kij\bar{z}\bar{z}}\right. \\
& \left.-3A^{1C}_{kij\dot{z}\bar{z}}\right)\bar{q}^{1S}_{k}
& \left(E_{kij\bar{z}\dot{z}}-A_{kij\dot{z}\dot{z}}\right. \\
& \left.-\frac{1}{2}A^{2S}_{kij\bar{z}\bar{z}}\right)\bar{q}^{0}_{k} \\
& +\frac{1}{4}\left(A^{1C}_{kij\dot{z}\dot{z}}+A^{1C}_{kij\bar{z}\bar{z}}\right. \\
& \left.+A^{1S}_{kij\dot{z}\bar{z}}\right)\bar{q}^{1C}_{k} \\
& -\frac{1}{4}\left(A^{1S}_{kij\dot{z}\dot{z}}\right. \\
& \left.+A^{1C}_{kij\bar{z}\bar{z}}\right)\bar{q}^{1S}_{k} \\
\hline
-A^{1S}_{kij\bar{z}\bar{z}}\,\bar{q}^{0}_{k} \\
-\left(E_{kij\dot{z}\bar{z}}-A_{kij\dot{z}\bar{z}}\right)\bar{q}^{1C}_{k} \\
+\left(-E_{kij\ddot{z}\bar{z}}+E_{kij\dot{z}\bar{z}}\right. \\
\left.-A_{kij\dot{z}\bar{z}}-\frac{1}{2}A^{2S}_{kij\bar{z}\bar{z}}\right)\bar{q}^{1S}_{k}
& -\left(E_{kij\dot{z}\bar{z}}-A_{kij\bar{z}\dot{z}}\right. \\
& \left.+\frac{1}{2}A^{2S}_{kij\bar{z}\bar{z}}\right)\bar{q}^{0}_{k} \\
& +\frac{1}{4}\left(A^{1C}_{kij\dot{z}\dot{z}}+A^{1C}_{kij\bar{z}\bar{z}}\right. \\
& \left.-A^{1S}_{kij\dot{z}\bar{z}}\right)\bar{q}^{1C}_{k} \\
& +\frac{1}{4}\left(3A^{1S}_{kij\bar{z}\bar{z}}\right. \\
& \left.-A^{1S}_{kij\dot{z}\dot{z}}\right)\bar{q}^{1S}_{k}
& \left(-E_{kij\bar{z}\ddot{z}}+E_{kij\bar{z}\dot{z}}\right. \\
& \left.-A_{kij\bar{z}\dot{z}}\right)\bar{q}^{0}_{k} \\
& +\frac{3}{4}A^{1S}_{kij\dot{z}\dot{z}}\,\bar{q}^{1C}_{k} \\
& -\frac{1}{4}\left(A^{1C}_{kij\dot{z}\dot{z}}+A^{1C}_{kij\bar{z}\bar{z}}\right. \\
& \left.+3A^{1S}_{kij\bar{z}\bar{z}}\right)\bar{q}^{1S}_{k}
\end{bmatrix}
\tag{117c}
$$

$$
[f_i] = \begin{bmatrix} G_i + G_i^{2C} \\ G_i^{1C} \\ G_i^{1S} \end{bmatrix} + \mathring{\imath} \begin{bmatrix} \frac{1}{2} G_{i\mu}^{C^2} \\ G_{i\mu}^{C} + \frac{1}{4} G_{i\mu}^{S^2C} \\ \frac{1}{2} G_{i\mu}^{2SC} \end{bmatrix}
$$

$$
+ \sum_{k=1}^{2} \begin{bmatrix} (G_{ki\bar{q}} + G_{ki\bar{q}}^{2C}) \bar{q}_k^0 + (\frac{1}{2} G_{ki\bar{q}}^{1C} - \frac{1}{2} G_{ki\dot{\bar{q}}}^{1S}) \bar{q}_k^{1C} + \frac{1}{2} G_{ki\bar{q}}^{1S} \bar{q}_k^{1S} \\ G_{ki\bar{q}}^{1C} \bar{q}_k^0 + (G_{ki\dot{\bar{q}}} + \frac{1}{4} G_{ki\bar{q}}^{2C}) \bar{q}_k^{1C} + (G_{ki\dot{\bar{q}}} + \frac{1}{2} G_{ki\bar{q}}^{2S}) \bar{q}_k^{1S} \\ G_{ki\bar{q}}^{1S} \bar{q}_k^0 + (-G_{ki\dot{\bar{q}}} + \frac{1}{2} G_{ki\bar{q}}^{2S}) \bar{q}_k^{1C} + (G_{ki\bar{q}} + \frac{3}{4} G_{ki\bar{q}}^{2C}) \bar{q}_k^{1S} \end{bmatrix}
$$

$$
+ \sum_{k=1}^{2} \mathring{\imath} \begin{bmatrix} \frac{1}{2} G_{ki\bar{q}\mu}^{C^2} \bar{q}_k^0 + (\frac{1}{8} G_{ki\bar{q}\mu}^{S^2C} + \frac{1}{2} G_{ki\bar{q}\mu}^{C}) \bar{q}_k^{1C} + (\frac{1}{2} G_{ki\dot{\bar{q}}\mu}^{C} + \frac{1}{4} G_{ki\bar{q}\mu}^{2SC}) \bar{q}_k^{1S} \\ (\frac{1}{4} G_{ki\bar{q}\mu}^{S^2C} + G_{ki\bar{q}\mu}^{C}) \bar{q}_k^0 + (\frac{3}{4} G_{ki\bar{q}\mu}^{C^2} - \frac{1}{4} G_{ki\dot{\bar{q}}\mu}^{SC}) \bar{q}_k^{1C} + \frac{1}{4} G_{ki\bar{q}\mu} \bar{q}_k^{1S} \\ \frac{1}{2} G_{ki\bar{q}\mu}^{2SC} \bar{q}_k^0 + \frac{1}{4} G_{ki\bar{q}\mu}^{SC} \bar{q}_k^{1C} + (\frac{1}{4} G_{ki\bar{q}\mu}^{C^2} + \frac{1}{4} G_{ki\dot{\bar{q}}\mu}^{SC}) \bar{q}_k^{1S} \end{bmatrix}
$$

(117d)

where δ_{ij} is the Kronecker delta and $\mathring{\imath}$ is $\sqrt{-1}$.

6.4 Mathematical Methods for Determining System Characteristics

In this subsection, the methods used to determine the system characteristics are briefly described. These methods are the eigenvalue analysis and the frequency response analysis for the vertical gust input. The eigenvalue analysis is performed before the frequency response analysis to confirm the system stability.

The eigenvalue problem is constructed according to Meirovitch (Ref. 45). The set of 3N second-order ordinary differential equations in Eq. 114 can be converted into an equivalent set of 6N first-order ordinary differential equations:

$$\{\dot{X}\} = [A]\{X\} + [B]\,\bar{w}_G \tag{118}$$

where

$$\{X\} = \begin{Bmatrix} \dot{Y} \\ Y \end{Bmatrix} \; ; \; [A] = \begin{bmatrix} -[M]^{-1}[C] & -[M]^{-1}[K] \\ [I] & [O] \end{bmatrix}$$

$$[B] = \begin{bmatrix} [M]^{-1}[F] \\ [O] \end{bmatrix} \tag{119}$$

Hence, the general eigenvalue problem is defined as

$$\{\dot{X}\} = [A]\{X\} \tag{120}$$

where [A] is a 6Nx6N nonsymmetrical matrix. This real general matrix eigenvalue problem is solved by the QR algorithm described in Ref. 46 and eigenvalues and associated eigenvectors are obtained.

The frequency response problem is formulated next. Substituting the unit sinusoidal vertical gust input $\bar{w}_G = e^{i\omega t}$ into Eq. 114 and assuming the system response with the same frequency of the input to obtain the particular solutions of Eq. 114 yield the complex simultaneous equations

$$[H]\{Y\} = [F] \tag{121}$$

where [H] is a (3N)x(3N) complex square matrix:

$$[H] = -[M]\left(\frac{\omega}{\Omega}\right)^2 + i\,[C]\left(\frac{\omega}{\Omega}\right) + [K] \tag{122}$$

Using the Gauss-Jordan reduction, the complex solution of {Y} can be obtained, and the absolute value and the argument of the complex number gives the amplitude and phase angle of the response.

SECTION 3

EXPERIMENTAL PROGRAM

3.1 General Description of Model

An overall view of the model rotor and mount is given in Fig. 10. The model rotor consists of three blades with an offset flapping hinge at 0.176R spanwise location. This flapping hinge configuration was adopted to obtain the desired flap, lag and torsion natural frequencies with the flexure system explained in detail in a later subsection. The rotor diameter is approximately 5 feet and the blade chord is 2 inches. The blades have 8 degree linear geometrical twist. The model rotor is an approximate Froude-scaled dynamic model of a typical soft-inplane hingeless rotor. The model rotor solidity is 0.0704, which is roughly equal to the solidity of most existing full-scale rotors in operation today. However, the Lock number is 2.27, which is very low comparing to full size rotors. Additionally, because of the orientation of the gust generator the rotor disc is located vertically in order to use the lateral gust as the vertical gust in the helicopter sense. Blade characteristics used in the experiment are listed in Table 1 and Fig. 11. Detailed descriptions of the design considerations and the resulting model may be found in Ref. 48.

3.2 Rotor Blades

In the present experiment existing rotor blades are used, which have a NACA 0012 airfoil section and 8-degree linear spanwise geometrical twist.

To achieve the desired rotating natural frequencies of the blade lag and torsional motions the flexure is placed between the blade and hub as shown in Fig. 12. The offset flap hinge at 0.176R spanwise station produces the equivalent hub moment to that of the hingeless rotor. The chordwise bending and torsional stiffness of the flexure determines the rotating lag and torsional natural frequencies and the spanwise location of the hinge gives the appropriate flapping frequency. The cross-sectional dimensions (width and height) of the flexure, which was made of 17-7 PH stainless steel, were chosen to obtain the desired stiffness. In order to evaluate the

rotating blade natural frequencies from the given stiffness of the flexure and blade, the computer program based on the analysis of the previous section was used.

The physical properties of the model rotor such as mass distribution, stiffness and so forth were measured and are shown in Table 1 and Fig. 11.

Lead-lag dampers are uesed to overcome the lag resonance encountered in the preliminary experimental stage. The gravity force excited the one-per-revolution lag motion when the rotor rotational speed was at the lag natural frequency since the rotor was mounted vertically, and the structural and aerodynamic lag damping of the blade was very small. It was found that the lag structural damping was 0.2% of critical without the lead-lag damper, and with the damper it increased to 7.0% of critical.

3.3 Model Hub and Support

The rotor blade is rigidly attached to the rigid rotor hub with no pre-cone or droop. The blade collective pitch can be changed at the hub location, however, no cyclic pitch control is incorporated.

The rotor hub is rigidly mounted to the rotor shaft which runs across the tunnel horizontally as shown in Fig. 10. This is because the rotor disc was located vertically to obtain the vertical gust effect from the existing gust generator at the M.I.T. Wright Brothers Wind Tunnel. The rotor shaft is mounted 3 feet above the tunnel floor to place the rotor in the center of the 7 x 10 foot elliptic cross-section of the wind tunnel. The rotor shaft is supported by two trunnions which are connected to the wind tunnel balance system. Rotor shaft tilting is also possible to simulate the helicopter forward flight cruising configuration. The shaft can be tilted up to 30 degrees forward.

The rotor is driven by a hydraulic motor mounted outside the tunnel and a flow control valve in the hydraulic system is used to vary the rotational speed between zero and approximately 1200 rpm.

3.4 Instrumentation

Each blade flexure was instrumented with strain gages in order to detect lag and torsion motion. The lag bending strain gage was located at 0.128R

spanwise station (1.1 inch from the cantilevered flexure root which is 2.4 inches long) and the torsion gage was at 0.15R spanwise location (1.7 inches from the cantilevered flexure root).

In order to detect the flapping motion a small .007-inch-thick leaf spring was placed between the blade and the flapping pin at the hinge location. The flapping hinge pin, fixed to the flexure, is extended slightly and slotted to provide a built-in mount for the root end of the cantilevered leaf spring. The outboard end of the leaf spring has a sliding fit in a blade-mounted fitting. The leaf spring provides a negligible elastic restraint to the blade flapping motion. This leaf spring was also instrumented with strain gages for the measuring of blade flapping motion in terms of leaf spring bending strain. The instrumentation for flap, lag and torsion motion can be seen in Fig. 12.

In addition to the blade deflection signals, the rotor RPM and blade azimuth angle signal are available on one of the slip rings. Once each revolution the circuit on the slip ring is closed and provides the signal for the RPM frequency counter, while in the recorded time history the location where the circuit is closed gives the blade azimuth angle. The rotation of the shaft of the gust generator was measured as the gust frequency. The gust magnitude was measured separately from the rotor gust response. A hot wire was placed at the rotor hub location and the gust frequencies were set to the same frequencies as those where the rotor gust response was to be measured. Thus, the gust magnitude signal was recorded.

3.5 Rotor Blade with Chordwise Center-of-Gravity Shift Configuration

The purpose of the wind tunnel tests is to validate the theory developed in the previous section concerning the reduction of blade bending motion due to a vertical gust utilizing blade chordwise mass unbalance as a passive control measure. One means of accomplishing the testing of the blades with different center-of-gravity locations would be to design and build rotor blades which actually had different center-of-gravity locations. This method, however, would have proved too costly and time consuming. Therefore, it was decided that through the addition of a variable weight, placed at the blade tip, the designed center-of-gravity shift would be accomplished.

AD-A061 134 MASSACHUSETTS INST OF TECH CAMBRIDGE AEROELASTIC AND--ETC F/G 1/3
GUST RESPONSE AND ITS ALLEVIATION FOR A HINGELESS HELICOPTER RO--ETC(U)
SEP 78 M YASUE N00019-76-C-0278
UNCLASSIFIED ASRL-TR-189-1 NL

2 OF 2
AD
A061134

END
DATE
FILMED
1-79
DDC

The scheme used to apply the tip weight to the model blade is shown in Fig. 13. A stainless steel sleeve/tube is attached to the blade tip. A tungsten slug, weighing 40 grams, is slipped inside the tube. By securing the slug at any location in the tube, an appropriate shift of the chordwise center-of-gravity either fore and aft was achieved.

The slug location allows for effective chordwise C.G. variation (C.G. location averaged in the spanwise direction) ranging from 35% chord from the leading edge (most aft position) to 18% chord (most forward position).

In order that no more than one blade of the model be subjected to the modification for shifting the chordwise C.G. mentioned above, two dummy blades were used in addition to the actual blade having variable chordwise C.G., as shown in Fig. 13.

3.6 Experimental Procedure

Having finished the rotor static balance prior to the wind tunnel test, the rotor blade track check was performed with the rotor spinning at 400 RPM. Rotor blades were set to 0 degree at 75% radius. The rotor stability check and the structural integrity check of the model rotor were also conducted. The blade pitch angle was increased to 4 degrees and finally to 8 degrees. The rotor rotational speed was then increased to 955 RPM without tunnel velocity. The blade pitch angle 8 degrees and the rotor rotational speed 955 RPM are the configuration for the actual test.

In the next step the rotor shaft angle was changed from 0 degree to 10 degrees. The tunnel velocity was increased to 30 MPH and then to 60 MPH, which corresponded to an advance ratio (μ) of 0.192 and 0.384 respectively. Having again confirmed the rotor stability, the sinusoidal vertical gust was applied to the rotor to measure the frequency response of the rotor to the vertical gust. The preliminary testing showed that the rotor response was difficult to distinguish from noise at a gust frequency greater than 500 CPM because of the strong gust dissipation at these higher frequencies. However, the low frequency gust responses are of most interest. Thus, the wind tunnel test was conducted at the gust frequency 500 CPM and below.

The sequence of the testing in which data were taken will be described next. The summarized table of test conditions is shown below.

WIND TUNNEL EXPERIMENT CONDITIONS

TUNNEL VELOCITY			0 MPH (μ=0, HOVER)	30 MPH (μ=0.192)	60 MPH (μ=0.384)
THREE-BLADED ROTOR WITH STIFF BLADE TORSION AND WITHOUT TIP WEIGHT			NO GUST	0,100,200 300,400,500 CPM GUST FREQUENCY APPLIED	0,100,200, 300,400,500 CPM GUST FREQUENCY APPLIED
SINGLE BLADED ROTOR WITH TIP WEIGHT	"STIFF TORSION" BLADE	18% $\bar{c}$ C.G. from L.E.	NO GUST	0,100,150,200 250,300,400, 500,CPM GUST FREQUENCY APPLIED	0,100,150,200 250,300,400,500 CPM GUST FREQUENCY APPLIED
		25% $\bar{c}$ C.G. from L.E.	"	"	"
		35% $\bar{c}$ C.G. from L.E.	"	"	"
	"SOFT TORSION" BLADE	18% $\bar{c}$ C.G. from L.E.	"	"	"
		25% $\bar{c}$ C.G. from L.E.	"	"	"
		35% $\bar{c}$ C.G. from L.E.	"	"	"

NOTE: Ω = 955 RPM, θ_o = 8 deg, α_s (SHAFT ANGLE) = 10 deg.

The first test was conducted on the three-bladed rotor shown in Fig. 10. The shaft forward tilt angle was 10 degrees and the collective pitch was set to 8 degrees at 75% radius location. The rotor rotational speed was 955 RPM (100 rad/sec). First, the hovering condition was achieved when the wind tunnel had no velocity. In this configuration no vertical gust can be applied. The next step involved increasing the wind tunnel velocity to 30 MPH. At this point no gusts were applied in order to define the steady-state rotor motion. Then the vertical gust was applied to the rotor and the responses of the rotor were

measured at gust frequencies of 100, 200, 300, 400, and 500 CPM. Having completed the 30 MPH sequence of the tests, the tunnel velocity was increased to 60 MPH and the same test sequence was followed as for 30 MPH.

The next portion of the test was with the single-bladed rotor with the tip weight shown in Fig. 13. The tungsten slug was positioned in the sleeve of the blade tip to place the chordwise center-of-gravity at 25% chord from the blade leading edge. It should be noted this C.G. location is the averaged one over the span. In this case the "stiff torsion" blade was used (the torsional natural frequency is 5.12/rev). The rotor had 8 degrees of collective pitch, the rotational speed was 955 RPM and the shaft tilt angle was 10 degrees. The same test sequence was followed as that of the three-bladed rotor, to measure the frequency response of the rotor to vertical gusts at advance ratios 0.192 and 0.384.

The tungsten slug was moved forward to place the chordwise C.G. location at 18% chord from the leading edge, and the gust frequency responses were measured. The slug was then moved backwards to obtain the chordwise C.G. location 35% chord from the leading edge, and the frequency responses were again measured. In the above cases the "stiff torsion" blade were used. The rotor blade remained stable in any C.G. location.

The final part of the test used the "soft torsion" blade (the torsional natural frequency is 2.38/rev with 25% chord chordwise C.G. location from the leading edge) with variable C.G. location. The wind tunnel velocity was set to 30 MPH and 60 MPH. The chordwise C.G. location was varied 18%, 25% and 35% chord from the leading edge at both tunnel velocities, and the vertical gust was applied to the rotor.

SECTION 4

RESULTS AND DISCUSSIONS

4.1 Introduction

Using the theory derived in a previous section, the blade chordwise center-of-gravity shift as a gust alleviation method is evaluated and the theory is compared with the experimental results. Rotor blade characteristics employed in this analysis are based on the wind tunnel model described in the previous section and detailed characteristics are listed in Table 1 and Fig. 11. In addition to the chordwise center-of-gravity shift as a principal parameter, the parameters examined in this analysis include cruising flight at advance ratios of 0.192 and 0.384, and blade torsional stiffness.

4.2 Natural Frequencies and Mode Shapes

Based on the mass and stiffness distribution of the wind tunnel model blade as shown in Fig. 11, rotating blade natural frequencies and associated mode shapes are obtained from the theory developed in the previous section. Mode shapes of the blade with "stiff" torsional stiffness and C.G. at 25% chord from the leading edge are shown in Fig. 14. Since existing stiff blades were used in the experiment, bending in the flexure at the root determined the appropriate natural frequencies.

Non-rotating natural frequencies for lag and torsion were determined experimentally with cantilevered hub restraint and compared to the calculated values. These are listed below. The non-rotating flap frequency was zero due to the blade flap hinge. Rotating blade natural frequencies were not obtained in the experiment.

WIND TUNNEL MODEL BLADE

NON-ROTATING NATURAL FREQUENCIES (Hz)

		LAG FREQUENCY		TORSIONAL FREQUENCY	
		EXPERIMENT	THEORY	EXPERIMENT	THEORY
THREE-BLADED		9.1	9.15	109	113
SINGLE-BLADED WITH 25% $\bar{c}$ C.G. FROM L.E.	STIFF TORSION	7.5	7.7	83	81.9
	SOFT TORSION	6.6	6.9	38	39.4

4.3 Trim Conditions and Steady-State Deflections

The no-trim steady-state condition for the three-bladed wind tunnel model rotor described in Table 1 is shown in Fig. 15. Experimental steady-state deflections for flapping and lagging are also shown.

The theoretical thrust coefficient has a maximum point around $\mu = 0.1$ and then decreases. This is due to the inflow ratio decrease around $\mu = 0.1$, which results in an effective angle of attack increase. Large collective lagging deflection was produced by the centrifugal forces, on the lead-lag damper. The damper was not scaled in the size and weight. Therefore, relatively large centrifugal forces were exerted to the damper which was located off the blade elastic axis. Thus, the large collective lagging deflection does not simulate the actual collective lagging deflection.

4.4 Frequency Response to the Vertical Gust

4.4.1 Experimental Data Reduction

The output of the strain gage signals for the blade flap, lag and torsional motions were recorded on magnetic tape using a Hewlett Packard 4 channel model 3960 tape recorder. These recorded data were fed to an analog-

to-digital converter (Digital Equipment Corp. computer PDP-11/40) and 512 digital data points were sampled with a 6 msec sampling rate. This corresponds to 10.5 data points per rotor revolution. After sampling, data were digitally analyzed by Fast Fourier Transform (Ref. 49) with the same machine to obtain the frequency spectrum of the signal.

Sample analog data from the flap and torsion strain gages are shown in Fig. 17. The configuration is the three-bladed rotor with tunnel velocity 30 MPH and vertical gust frequency 200 CPM. From this analog data the frequency spectrum shown in Fig. 18 is obtained by the method mentioned above. The blade motion response to vertical gusts can be expressed in terms of the three frequency modulated motions ω, $(\Omega-\omega)$ and $(\Omega+\omega)$, where Ω is the rotational speed of the rotor and ω is the gust frequency. With reference to the blade flap frequency spectrum of Fig. 18, the first peak from the left is the response to the gust frequency ω, called the collective flapping response. The peak at the nondimensional frequency $\frac{\omega}{\Omega} = 0.791$ corresponds to the $(\Omega-\omega)$ cyclic flapping response. The big peak at $\frac{\omega}{\Omega} = 1.0$ has Ω frequency and comes from the steady state blade flapping motion due to forward flight. From the present linear theory 1Ω steady-state cyclic flapping motion is not affected by the vertical gust, and this is confirmed by the experimental results. The peak to the right of the Ω frequency response is the $(\Omega+\omega)$ cyclic flapping response. The low frequency gust response is of interest in this study and the amplitude of higher frequency responses such as $(2\Omega-\omega)$ and $(2\Omega+\omega)$ are relatively small. Therefore, the gust responses up to $(\Omega+\omega)$ frequency are considered.

The experimental results are compared to the theory in terms of the peak values of the blade motion frequency spectrum at frequencies ω, $(\Omega-\omega)$ and $(\Omega+\omega)$. For important responses such as blade flapping motion the frequency spectrum analysis was conducted several times on different portions of the magnetic tape on which analog signals from strain gages had been recorded for three minutes. This is a kind of averaging process because the total time required for sampling is 3.07 seconds out of 3 minutes data. During the experiment the gust magnitude and the rotor rotation speed are fluctuating. Therefore, the rotor $(\Omega+\omega)$ response amplitudes showed large

variation when the summed frequency of the gust frequency and the rotor rotational speed is close to the blade flap natural frequency, as shown in Fig. 20.

It is obvious from the theoretical analysis in Section 2 how to obtain the three frequency-modulated responses ω, $(\Omega-\omega)$ and $(\Omega+\omega)$. However, it would be helpful to explain the method briefly here. Using the rigid mode for flap motion, the simplified blade flapping equation with vertical gust excitation may be written:

$$\ddot{\beta} + \left\{\frac{\gamma}{8} + \mu\frac{\gamma}{6}\sin(\Omega t)\right\}\dot{\beta} + \left\{\left(\frac{\omega_\beta}{\Omega}\right)^2 + \mu\frac{\gamma}{6}\cos(\Omega t) + \mu^2\frac{\gamma}{8}\sin(\Omega t)\right\}\beta = \frac{\gamma}{2}\int_0^1 x^2 w_G\, dx + \frac{\gamma}{2}\mu\sin(\Omega t)\int_0^1 x\, w_G\, dx \tag{123}$$

where

x = nondimensional radial coordinate

γ = Lock number

μ = Advance ratio

ω_β = Rotating flapping natural frequency

Ω = Rotor rotational speed

t = Time

w_G = Vertical gust velocity nondimensionalized by blade tip speed (ΩR) at the radial coordinate x

and if the vertical gust w_G is the one-dimensional sinusoidal gust in the flight direction it is expressed as

$$w_G = \bar{w}_G \sin(\omega t) - \left(\frac{\omega}{\Omega}\right)\frac{x}{\mu}\bar{w}_G\cos(\omega t)\cos(\Omega t) \tag{124}$$

The first term in Eq. 124 represents the uniform component of the gust velocity over the rotor disc, and the second term represents the gust velocity gradient due to nonuniformity over the rotor disc. The symbol $\bar{w}_G$ expresses the nondimensional gust amplitude at the rotor shaft location. Substituting Eq. 124 into the right-hand side of Eq. 123 yields:

[Left-hand side of Eq. 123]

$$= \frac{\gamma}{6}\,\overline{w_G}\sin\omega t + \frac{1}{2}\left\{\mu\frac{\gamma}{4} + \frac{1}{\mu}\frac{\gamma}{8}\left(\frac{\omega}{\Omega}\right)\right\}\overline{w_G}\cos(\Omega+\omega)t$$

$$+ \frac{1}{2}\left\{\mu\frac{\gamma}{4} - \frac{1}{\mu}\frac{\gamma}{8}\left(\frac{\omega}{\Omega}\right)\right\}\overline{w_G}\cos(\Omega-\omega)t \quad + \text{Higher Order Terms} \quad (125)$$

Therefore, due to the vertical gust with frequency ω, the flapping motions ω, $(\Omega-\omega)$ and $(\Omega+\omega)$ will be excited.

It should be noted that all gust responses in Figs. 20 through 23 are not normalized by the gust magnitude. The gust magnitude can be found in Fig. 19.

4.4.2 Three-Bladed Rotor Gust Response

The three-bladed rotor case provided basic information regarding the overall response of the rotor model to a vertical gust and also validated that there were no major differences between the three-bladed rotor and the single-bladed rotor in terms of the vertical gust frequency response. The three-bladed rotor gust response of the experiment is shown in Fig. 20 for the case of 30 MPH (μ = 0.192) and 60 MPH (μ = 0.384).

The $(\Omega+\omega)$ cyclic flapping response has a peak at a nondimensionalized frequency of $(\frac{\omega}{\Omega})$ = 0.2 in Fig. 20 (a) and (b) since the exciting frequency $(\Omega+\omega)$ becomes 1.2/rev and the frequency $(\Omega+\omega)$ becomes close to the blade flapping natural frequency, which is 1.13/rev in a vacuum, and becomes 1.2/rev in air due to the aerodynamic stiffness caused by pitch-flap coupling due to steady-state flap and lag deflection.

The theoretical predictions of the ω collective flapping response at both 30 MPH (μ = 0.192) and 60 MPH (μ = 0.384) are higher than the experimental results. The collective motions are excited by the uniform component of the vertical gust and in the theoretical prediction this component is assumed to be the same over the rotor disc as the magnitude at the center of the rotor. However, in the wind tunnel the vertical sinusoidal gust is not constant in the Y-direction shown in Fig. 9. At a distance of 2 feet from the center in the Y-direction the gust magnitude falls off to 50% of that of

at the center. This gust profile reduces the blade ω flapping response. However, in this analysis further mathematical modeling of the wind tunnel vertical gust profile has not been conducted. This effect is not significant for the single-bladed rotor blade with tip weight because of the low Lock number.

The $(\Omega-\omega)$ cyclic lag response in Fig. 20(a) and (b) are higher around $(\frac{\omega}{\Omega}) = 0.2$ because the exciting frequency $(\Omega-\omega)$ is 0.8/rev and close to the lag natural frequency.

The $(\Omega+\omega)$ cyclic torsion motion is coupled with the $(\Omega+\omega)$ cyclic flap motion through pitch-flap coupling due to the steady-state flap and lag deflection.

The effect of the inclusion of the gust velocity gradient due to the gust nonuniformity is shown in Fig. 21. Flap response levels are compared with and without the gust velocity gradient. It should be noted that the gust velocity gradient has a significant effect on the cyclic flapping motion even if the ratio of the wave length to the rotor radius is 11.1 in which the advance ratio is 0.192 and the gust frequency ω/Ω is 0.1.

4.4.3 Single-Bladed Rotor Gust Response with Chordwise Center-of-Gravity Shift

While the initial wind tunnel tests dealt with the gust response of the three-bladed rotor, the most important portion of the experiment involved the single-bladed rotor configuration with chordwise center-of-gravity shift. An objective of the test program was to evaluate the effectiveness of torsional stiffness variation in conjunction with chordwise center-of-gravity shifts in alleviating the gust response of a hingeless rotor. The comparison of the theoretical rotor responses with the experimental responses from the wind tunnel test will be discussed.

4.4.3.1 30 MPH (μ = 0.192) Configuration

The gust responses for flap and torsion motions of the "stiff" and "soft" torsion blade in 30 MPH are shown in Fig. 22.

The flap motion response with "stiff torsion" blade are shown in Fig. 22 (a). The $(\Omega+\omega)$ cyclic flapping response has a peak at the frequency

0.15/rev. This is because the $(\Omega+\omega)$ cyclic flap motion is close to the blade rotating natural frequency as explained in Subsection 4.4.2. As expected, the flap response differences resulting from the chordwise center-of-gravity shift are very small, because the torsional motion produced by the C.G. shift was small due to the blade stiff torsional characteristics. In addition to the blade stiff trosional characteristics, the Lock number for this single-bladed rotor is very low at a value of 0.951. This is roughly one-tenth that of a full-scale helicopter and therefore the aerodynamic forces on this blade are one-tenth as effective in comparison with the aerodynamic forces on the full-scale helicopter. Therefore, the small angle of attack change due to the torsional motion did not produce effective aerodynamic forces to suppress or excite the flap motion.

The torsional motion corresponding to the flap response in Fig. 22 (a) is shown in Fig. 22 (b). Since only small variations are obtained in the theoretical predictions, the theoretical results of only the 25% chord center-of-gravity location from the leading edge are shown in Fig. 22 (a) and 22 (b).

When the "soft torsion" blade is utilized, larger flap response level differences due to chordwise C.G. shift at 30 MPH can be observed in Fig. 22 (c). For the $(\Omega+\omega)$ cyclic and ω collective flap response it is clear that the experimental response of 18% chord C.G. location is lowest, that of 25% is in the middle and that of 35% is the highest. This tendency is the same as that of the theoretical prediction shown in Fig. 22 (c). However, predicted response levels for a given C.G. location are higher than the experimental results of corresponding C.G. location in the $(\Omega+\omega)$ cyclic and ω collective flapping responses. It is difficult to describe the vibration response reduction quantatively from these experimental results. Corresponding to the flap response with "soft torsion" blade at 30 MPH, are the torsional responses shown in Fig. 22 (d), and good agreement is obtained between the theoretical prediction and experimental observation.

Lag motion responses of 30 MPH configuration are shown in Fig. 22 (e) and (f); they are very small.

4.4.3.2 60 MPH (μ = 0.384) Configuration

The gust responses at 60 MPH are shown in Fig. 23. As with the 30 MPH configuration, chordwise center-of-gravity shifts for the "stiff torsion" blade did not produce distinctive flapping response reductions. Therefore, the theoretically predicted 25% chordwise center-of-gravity responses for the "stiff" blade are plotted to use as a comparison with the experimental results. Overall agreement between theoretical predictions and experimental results is good. The torsional responses of the "stiff torsion" blade of 60 MPH is shown in Fig. 23 (b).

The flap responses with "soft torsion" blade in 60 MPH are shown in Fig. 23 (c). While there is good agreement regarding the tendencies for the $(\Omega+\omega)$, ω, $(\Omega-\omega)$ flapping responses, the experimental magnitudes are slightly higher than those predicted, particularly the $(\Omega+\omega)$ and ω flap responses of 25 and 35% chordwise center-of-gravity cases. For the $(\Omega+\omega)$ cyclic flap response at the frequency ω/Ω = 0.105 the C.G. shift from 35% from the leading edge to 25% chord did increase the response level slightly in the experiment and no reduction can be seen in the theoretical prediction. At the same frequency the $(\Omega+\omega)$ cyclic flap response is reduced by 25% experimentally after shifting the C.G. forward from 25% $\bar{c}$ to 18% $\bar{c}$ chordwise station, when the response level of 25% $\bar{c}$ C.G. location is taken as 100%. In the theoretical prediction this reduction is 20%. From the theory, response reduction of the $(\Omega+\omega)$ cyclic flap response can be expected below the frequency ω/Ω = 0.105 shown in Fig. 23 (c). This is an important point. A von Karman gust power spectral density in Ref. 26 and 35 is given by:

$$(PSD)_{w_G} = \frac{\sigma_w^2 L}{2\pi V} \frac{1+\frac{8}{3}\left[1.339\left(\omega L/V\right)\right]^2}{\left\{1+\left[1.339\left(\omega L/V\right)\right]^2\right\}^{11/6}} \qquad (126)$$

where ω is the frequency; L the gust characteristic length; σ_w the rms value of the gust velocity; and V is the aircraft speed. Here L is approximately 5000 ft for high altitude and from 400 to 500 ft for low altitude of the full-scale aircraft. This power spectral density scaled down to the present

wind tunnel rotor model is shown in Fig. 24 where the L used is 40 ft, V is 60 MPH and the model scaling factor is one-tenth. As is shown in Fig. 24 the gust power spectrum has a peak at the frequency $\frac{\omega}{\Omega} = 0.01$ and above $\frac{\omega}{\Omega} = 0.01$ it decays very rapidly. Therefore, the frequency response below a frequency ω/Ω of 0.1 is important.

Above the frequency $\frac{\omega}{\Omega} = 0.157$ the $(\Omega+\omega)$ cyclic flap response reduction can be observed clearly in shifting from the 35% C.G. to 25% C.G., however, there is slight reduction from 25% $\bar{c}$ C.G. to 18% $\bar{c}$ C.G. in the experimental results. Experimental reductions of the ω collective flapping response is shown in Fig. 23 (c).

Torsional responses are shown in Fig. 23 (d) and good agreement between the theoretical predictions and the experimental results is obtained.

Lag responses are shown in Fig. 23 (e) and (f). The theory predicts a lag resonance at the lag natural frequency and in the experiment it was not seen. It is not clear why this discrepancy exists. It, however, seems this is a limitation due to experimental accuracy because the lag response level is very low.

4.4.4 Summary of the Vertical Gust Response Analysis

When the rotor gust response is considered, the gust velocity gradient due to the gust nonuniformity over the rotor disc has an important role in the blade cyclic motion responses unless the gust frequency is extremely low and the gust uniformity assumption is reasonable.

The frequency response of blade motion to a vertical gust with frequency ω is described in terms of three frequency-modulated motions at ω, $(\Omega-\omega)$ and $(\Omega+\omega)$, where Ω is the rotational speed. The responses $(\Omega-\omega)$ and $(\Omega+\omega)$ are related to the blade cyclic motions. Therefore, even if the gust frequency ω is low, the response close to 1/rev will be excited as $(\Omega+\omega)$ and $(\Omega-\omega)$ responses.

As is expected, the "soft torsion" blade is more effective in conjunction with the forward chordwise center-of-gravity shift in alleviating the gust response of a hingeless rotor than the "stiff torsion" blade.

With the "soft torsion" blade the $(\Omega+\omega)$ flap response is reduced by 30% in 30 MPH and 25% in 60 MPH at the frequency $\frac{\omega}{\Omega} = 0.105$ when the chordwise

center-of-gravity is shifted from 25% chord from the leading edge to 18% chord from the leading edge. This reduction is based on the experimental results, where the response level of 25% $\bar{c}$ C.G. location is regarded as 100%. Theoretical reduction is much smaller at the frequency $\frac{\omega}{\Omega} = 0.105$ than that of the experiments, but the theoretical prediction also show the tendency to reduce the $(\Omega+\omega)$ cyclic flapping below the frequency $\frac{\omega}{\Omega} = 0.1$. Referring to the von Karman gust power spectral density in Fig. 24, which is scaled down to the present wind tunnel model and has a strong gust excitation below the frequency $\frac{\omega}{\Omega} = 0.1$, the forward chordwise center-of-gravity shift in conjunction with the "soft torsion" blade will be a good gust alleviation system for the blade $(\Omega+\omega)$ cyclic flap vibration. Response reduction of the ω collective flap motion due to the chordwise C.G. shift was observed experimentally except at the frequency $\frac{\omega}{\Omega} = 0.105$.

It should be noted that greater effectiveness of the chordwise center-of-gravity shift would be expected in the full scale rotor since the present wind tunnel model rotor has very low Lock number (see Appendix D).

It should be mentioned that rotor rotational speed fluctuations were not considered in the analysis. However, these were found experimentally to be less than plus or minus three percent.

SECTION 5

CONCLUSIONS AND COMMENTS

5.1 Conclusions

This study has been devoted to the development of a theoretical model of hingeless rotor response to a vertical gust, and to the theoretical and experimental evaluation of the effect of shift of blade chordwise center-of-gravity as a gust alleviation method, particularly to reduce the blade flap motion.

Based upon the theoretical and experimental results in this study, the following conclusions may be stated.

(a) Chordwise center-of-gravity shift is an effective and simple method to alleviate hingeless rotor gust response. In the wind tunnel model blade with Lock number 0.951 and gust frequency 0.105/rev at $\mu = 0.394$, it is experimentally confirmed that the $(\Omega+\omega)$ cyclic flap response is reduced by 25% when the chordwise center-of-gravity is shifted by 7% chord toward the leading edge from 25% chord and the "soft torsion" blade is employed, if the response level of 25% chord center-of-gravity location is regarded as 100%. The theoretical reduction is 20% at this gust frequency. Theoretical prediction also shows the tendency to reduce $(\Omega+\omega)$ cyclic flapping below the frequency $\omega/\Omega = 0.1$ and the response due to atmospheric turbulence will be reduced by chordwise center-of-gravity shift toward the leading edge. Above the gust frequency $\omega/\Omega = 0.2$ at advance ratio of 0.394 it is shown experimentally and theoretically that $(\Omega+\omega)$ cyclic flapping is reduced by forward chordwise center-of-gravity shift. It will therefore reduce the response due to the discrete gust which has higher frequency content than random turbulence.

The reduction of ω collective flapping by the chordwise center-of-gravity shift is also confirmed experimentally and theoretically. $(\Omega-\omega)$ cyclic flapping response is a very low level and is not significant.

The full size blade with higher Lock number of order 10 shows

even larger reductions of flapping response because of greater aerodynamic effectiveness. (See Appendix D.)

(b) The "soft torsion" blade is more effective in conjunction with the forward chordwise center-of-gravity shift in alleviating the gust response than the "stiff torsion" blade.

(c) The agreement between the experimental gust response of the hingeless rotor and the theoretical predictions is good, particularly in the important parameters of flapping and torsion.

(d) The frequency response of blade motion to a vertical gust with gust frequency ω is described in terms of three frequency-modulated motions at the frequencies ω, $(\Omega-\omega)$ and $(\Omega+\omega)$, where Ω is the rotor rotational speed. The responses at the frequency $(\Omega-\omega)$ and $(\Omega+\omega)$ are related to the blade cyclic motions and will be excited even if the gust frequency ω is low.

(e) The gust velocity gradient due to the gust nonuniformity over the rotor disc has a significant effect on the blade cyclic motion responses unless the wave length of the gust is extremely large with respect to the rotor diameter.

5.2 Suggestions for Future Research

Recommendations for the future work before applying the chordwise center-of-gravity shift to the full size rotor will be related to two aspects: the theoretical analysis and the wind tunnel experiments.

In the theoretical analysis, the effectiveness of the chordwise center-of-gravity to the full-scale rotor with Lock number 10 should be studied

further, and it should be confirmed that the center-of-gravity shift does not produce any adverse effect.

In the wind tunnel tests, the response of the rotor with center-of-gravity shift should be tested in the very low gust frequency range below $\omega/\Omega = 0.1$. For this purpose a new device to produce the low frequency turbulence and a more refined signal processing system for the gust input signal and the response output signal will be necessary to distinguish signal and noise.

The present wind tunnel rotor model might be improved by the addition of cyclic pitch control. This could be accomplished fairly easily by incorporating a swash-plate into the model design, and the necessary feathering bearings for this motion in the rotor hub.

REFERENCES

1. Hohenemser, K.H., "Hingeless Rotorcraft Flight Dynamics". AGARD-AG-197, Sept. 1974.

2. Houbolt, J.C. and Brooks, G.W., "Differential Equations of Motion for Combined Flapwise Bending, Chordwise Bending, and Torsion of Twisted, Nonuniform Rotor Blades". NACA Report 1346, 1958.

3. Hodges, D.H. and Dowell, E.H., "Nonlinear Equations of Motion for the Elastic Bending and Torsion of Twisted Nonuniform Rotor Blades". NASA TN D-7818, 1974.

4. Young, M.I., "A Theory of Rotor Blade Motion Stability in Powered Flight". Journal of American Helicopter Society, Vol. 9, No. 3, July 1964, pp 12-25.

5. Hohenemser, K.H. and Heaton, P.W., Jr., "Aeroelastic Instability of Torsionally Rigid Helicopter Blades". Journal of American Helicopter Society, Vol. 12, No. 2, April 1972, pp 2-14.

6. Ormiston, R.A. and Hodges, D.H., "Linear Flap-Lag Dynamics of Hingeless Helicopter Rotor Blades in Hover". Journal of American Helicopter Society, Vol. 17, No. 2, April 1972, pp 2-14.

7. Tong, P., "Nonlinear Instability of Rotor Blades",Massachisetts Institute of Technology, Aeroelastic and Structures Research Laboratory, ASRL TR 166-1, 1972.

8. Tong, P., The Nonlinear Instability in Flap-Lag of Rotor Blades in Forward Flight". Massachusetts Institute of Technology, Aeroelastic and Structures Research Laboratory, ASRL TR 166-2, 1972.

9. Friedmann, P. and Tong, P., "Dynamic Nonlinear Elastic Stability of Helicopter Rotor Blades in Hover and in Forward Flight", Massachusetts Institute of Technology, Aeroelastic and Structures Research Laboratory, TR 166-3.

10. Friedmann, P. and Tong, P., "Nonlinear Flap-Lag Dynamics of Hingeless Helicopter Blades in Hover and in Forward Flight". Journal of Sound

and Vibration, Vol. 30, No. 1, Sept. 1973, pp 9-31.

11. Friedmann, P. and Silverthom, L.J., "Aeroelastic Stability of Coupled Flap-Lag Motion of Hingeless Helicopter Blades at Arbitrary Advance Ratios". Journal of Sound and Vibration, Vol. 39, No. 4, 1975, pp 409-428.

12. Friedmann, P. and Samie, J., "Aeroelastic Stability of Trimmed Helicopter Blades in Forward Flight". Paper presented at the First European Rotorcraft and Powered Lift Aircraft Forum, Southampton, Sept. 1975.

13. Peters, D.A., "Flap-Lag Stability of Helicopter Rotor Blades in Forward Flight". Journal of American Helicopter Society, Vol. 20, No. 4, Oct. 1975, pp 2-13.

14. Miller, R.H. and Ellis, C.W., "Helicopter Blade Vibration and Flutter". Journal of American Helicopter Society, Vol. 1, No. 3, July 1956, pp 19-38.

15. Friedmann, P., "Influence of Structural Damping, Preconing, Offset and Large Deflections on the Flap-Lag-Torsional Stability of a Cantilevered

16. Hodges, D.H. and Ormiston, R.A., "Stability of Elastic Bending and Torsion of Uniform Cantilever Rotor Blades in Hover with Variable Structural Coupling". NASA TN D-8192, April 1976.

17. Hodges, D.H. and Ormiston, R.A., "Stability of Hingeless Rotor Blades in Hover with Pitch-Link Flexibility". Proceedings of AIAA/ASME/SAE 17th Structures, Structural Dynamics and Material Conference, May 1976, pp 412-420.

18. Weiland, E., "Development and Test of the BO 105 Rigid Rotor Helicopter". 24th Annual National Forum Proceedings of the American Helicopter Society, No. 200, May 1968.

19. Reichert, G. and Oelker, P., "Handling Qualities with the Bolkow Rigid Rotor System". 24th Annual National Forum Proceedings of the American Helicopter Society, No. 218, May 1968.

20. Reichert, G., "Basic Dynamics of Rotors Control and Stability of

Rotary Wing Aircraft Aerodynamics and Dynamics of Advanced Rotary-Wing Configurations". AGARD-LS-63, March 1973, pp 3.1-3.50.

21. Huber, H., "Parametric Trends and Optimization - Preliminary Selection of Configuration - Prototype Design and Manufacture". AGARD-LS-63, March 1973, pp 8.1 - 8.55.

22. Woitsh, W. and Weiss, H., "Dynamic Behavior of a Hingeless Fiberglas Rotor". AIAA Paper No. 69-204, Feb. 1969.

23. Huber, H., "Some Objectives in Applying Hingeless Rotors to Helicopters and V/STOL Aircraft". AGARD-CP-111, Sept. 1972, pp 20.1 - 20.16.

24. Reichert, G. and Huber, H., "Influence of Elastic Coupling Effects on the Handling Qualities of a Hingeless Rotor Helicopter". AGARD-CP-121, Feb. 1973, pp 8.1 - 8.15.

25. Hansford, R.E. and Simons, I.A., "Torsion-Flap-Lag Coupling on Helicopter Rotor Blades". Journal of American Helicopter Society, Vol. 18, No. 4, Oct. 1973, pp 2-12.

26. Gaonker, G.H. and Hohenemser, K.H., "Stochastic Properties of Turbulence Excited Rotor Blade Vibrations". AIAA Journal, Vol. 9, No. 3, March 1971, pp 419-424.

27. Gaonker, G.H., Hohenemser, K.H. and Yin, S.K., "Random Gust Response Statistics for Coupled Torsion-Flapping Rotor Blade Vibrations". J. Aircraft, Vol. 9, No. 10, Oct. 1972, pp 726-729.

28. Wan, F.Y.M. and Lakshmikantham, C., "Rotor Blade Response to Random Loading: Direct Time Domain Approach". AIAA Journal, Vol. 11, No. 1, Jan. 1973, pp 24-28.

29. Wan, F.Y.M. and Lakshmikantham, C., "The Special Correlation Method and a Time Varying Flexible Structure". AIAA Paper 73-406, March 1973.

30. Gaonker, G.H. and Hohenemser, K.H., "An Advanced Stochastic Model for Threshold Crossing Studies of Rotor Blade Vibrations". AIAA Journal, Vol. 10, No. 8, August 1972, pp 1100-1111.

31. Arcidiacono, P.J., Bergquist, R.R. and Alexander, W.T., Jr., "Helicopter Gust Response Characteristics Including Unsteady Aerodynamic Stall Effects". Proceedings of Specialists Meeting on Rotorcraft Dynamics, AHS/NASA-Ames Research Center, Paper 9, Feb. 1974.

32. Johnson, W., "Dynamics of Tilting Proprotor Aircraft in Cruise Flight". NASA TN D-7677, May 1974.

33. Yasue, M., "A Study of Gust Response for a Rotor-Propeller in Cruising Flight". Massachusetts Institute of Technology, Aeroelastic and Structures Research Laboratory, ASRL TR 174-1, also NASA CR-137537, August 1974.

34. Johnson, W., "Analytical Model for Tilting Proprotor Aircraft Dynamics, Including Blade Torsion and Coupled Bending Modes, and Conversion Mode Operation". NASA TM X-62369, August 1974.

35. Frick, J.K. and Johnson, W., "Optimal Control Theory Investigation of Proprotor/Wing Response to Vertical Gust". NASA TM X62384, Sept. 1974.

36. Ham, N.D., Bauer, P.H., Lawrence, T.H. and Yasue, M., "A Study of Gust and Control Response of Model Rotor-Propellers in a Wind Tunnel Airstream". Massachusetts Institute of Technology, Aeroelastic and Structures Research Laboratory, ASRL TR 174-4, and also NASA CR-137756, August 1975.

37. Whitaker, H.P. and Cheng, Y., "Use of Active Control Systems to Improve Wing Bending and Rotor Flapping Responses of a Tilt Rotor VTOL Airplane". Massachusetts Institute of Technology, Aeroelastic and Structures Research Laboratory, ASRL TR 183-1, Oct. 1975.

38. Cheng, Y., "Application of Active Control Technology to Gust Alleviation System for Tilt Rotor Aircraft". Massachusetts Institute of Technology, Aeroelastic and Structures Research Laboratory, ASRL TR 174-5, and also NASA CR-137958, Nov. 1976.

39. Miller, R.H., "A Method for Improving the Inherent Stability and Control Characteristics of Helicopters". Journal of the Aeronautical Sciences, Vol. 17, No. 6, June 1950, pp 363-374.

40. Biggers, J.C., "Some Approximations to the Flapping Stability of Helicopter Rotors". Journal of the American Helicopter Society, Vol. 19, No. 4, Oct. 1974.

41. Mil', M.L., et al., "Helicopters: Calculations and Design, Vol. I, Aerodynamics". NASA TT F-494, Sept.1967.

42. Pian, T.H.H. and Tong, P., "Finite Element Methods in Continuum Mechanics". Advances in Applied Mechanics, Vol. 12, Academic Press, Inc., 1972, pp. 1-58.

43. Bathe, K.J., "Solution Methods for Large Generalized Eigenvalue Problems in Structural Engineering". UCSESM 71-20, Structural Engineering Laboratory, University of California, Berkeley, Nov. 1971 and also PB 208853 National Technical Information Service.

44. Mau, S.T. and Pian, T.H.H., "Linear Dynamic Analyses of Laminated Plates and Shells by the Hybrid-Stress Finite-Element Method". M.I.T., ASRL TR 172-2 and also AMMRC CTR 73-40, Army Materials and Mechanics Research Center, Oct. 1973.

45. Bisplinghoff, R.L., Ashley, H. and Halfman, R.L., "Aeroelasticity". Addison-Wesley Pub. Co., 1955.

46. Klema, V.K., Garbow, B.S. and Moler, C.B., "EISPACK, User's Information", Argonne National Laboratory, Applied Mathematics Division, June 1973.

47. Hirsh, H., Hutton, R.E. and Rasumoff, A., "Effect of Spanwise and Chordwise Mass Distribution on Rotor Blade Cyclic Stresses", Journal of American Helicopter Society, Vol. 1, No. 2, April 1956.

48. Vehlow, C.A., "Experimental Investigation of Gust Response of Hingeless Helicopter Rotors", M.S. Thesis, Dept. of Aeronautics and Astronautics, Massachusetts Institute of Technology, May 1977.

49. Rabiner, L.R. and Gold, B., "Theory and Application of Digital Signal Processing", Prentice-Hall, 1975.

TABLE 1

DESCRIPTION OF THE ROTOR BLADE

USED IN THE WIND TUNNEL TEST

	THREE-BLADED ROTOR	SINGLE-BLADED ROTOR WITH TIP WEIGHT AND 25% CHORD C.G. LOCATION FROM LEADING EDGE
Number of blades	3	1
Radius, R	2.26 ft	2.26 ft
Chord, C	2 in	2 in
Lock number, γ (basic configuration)	2.27	0.954
Solidity, σ	0.0704	0.0235
Collective pitch, θ_o	8 deg	8 deg
Shaft tilt angle in crusing flight	10 deg forward	10 deg. forward
Lift-curve slope, a	5.7	5.7
Drag coefficient, Cd_o	0.012	0.012
Rotational speed, Ω	100 rad/sec	100 rad/sec
Built-in blade angle of twist, θ_{TW}	8 deg (linear)	6 deg (linear)
Elastic axis	25% chord	25% chord
Aerodynamic center	25% chord	25% chord
Precone, β_p	0 deg	0 deg
Droop, δ_D	0 deg	0 deg
Torque offset, e_o	0 in	0 in
Control linkage flexibility	rigid	rigid
Basic Natural Frequencies		
Lag	0.823/rev	0.57/rev
Flap	1.13/rev	1.13/rev
Torsion	6.85/rev	5.21/rev (stiff)
		2.38/rev (soft)

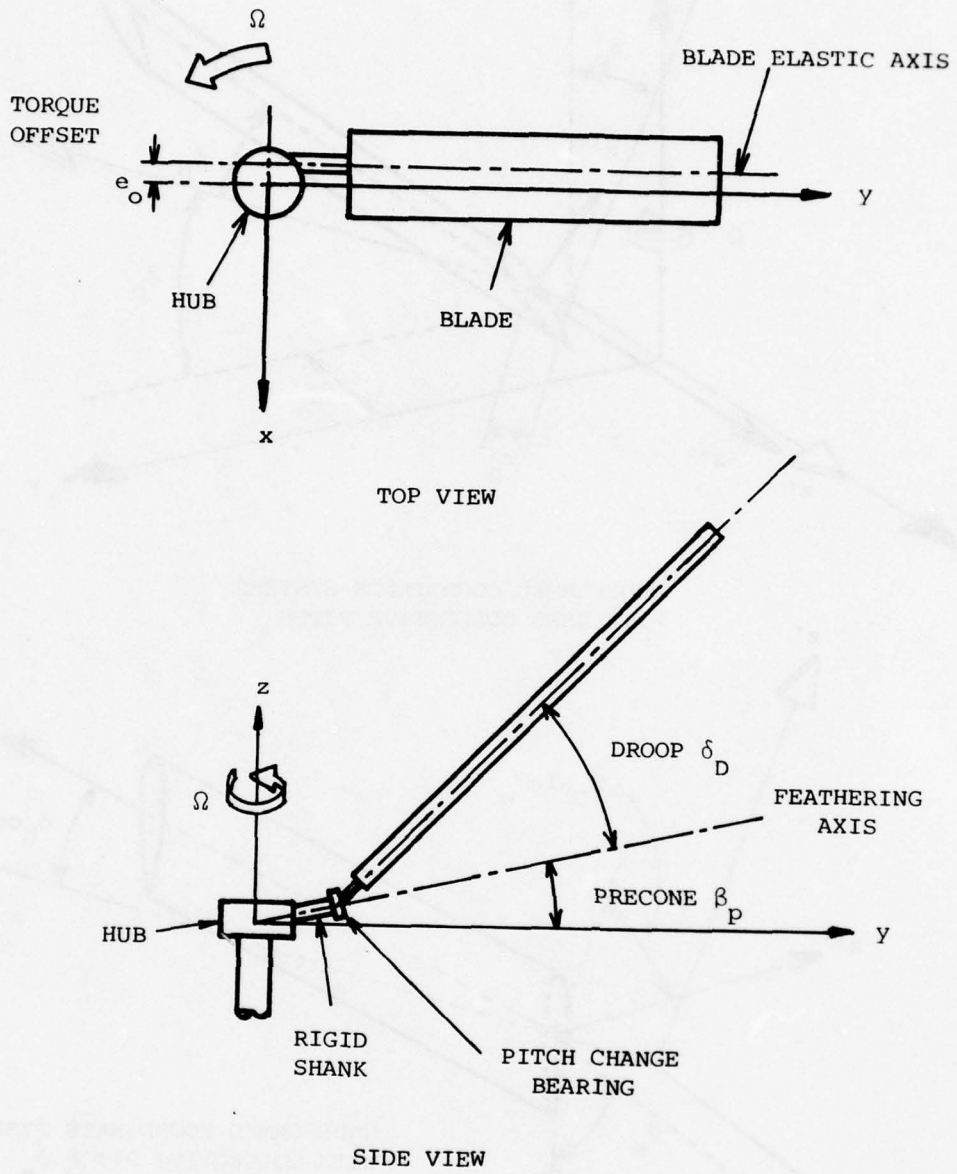

FIG. 1 ROTOR BLADE CONFIGURATION

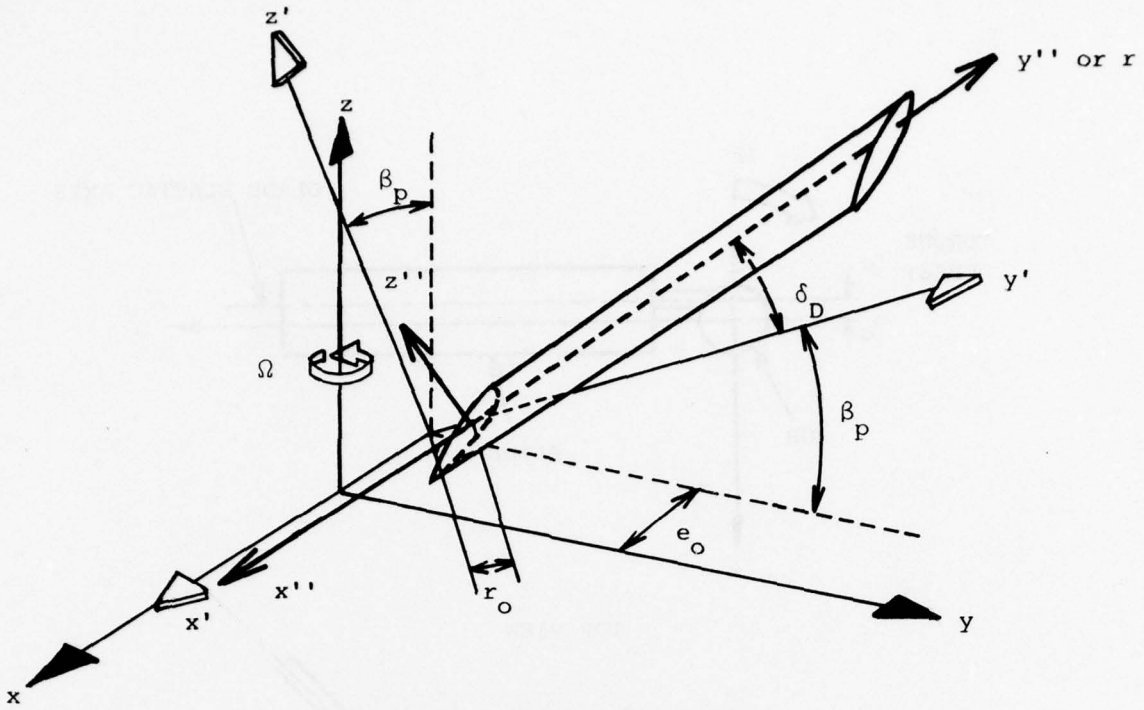

UNDEFORMED COORDINATE SYSTEMS
WITH ZERO COLLECTIVE PITCH

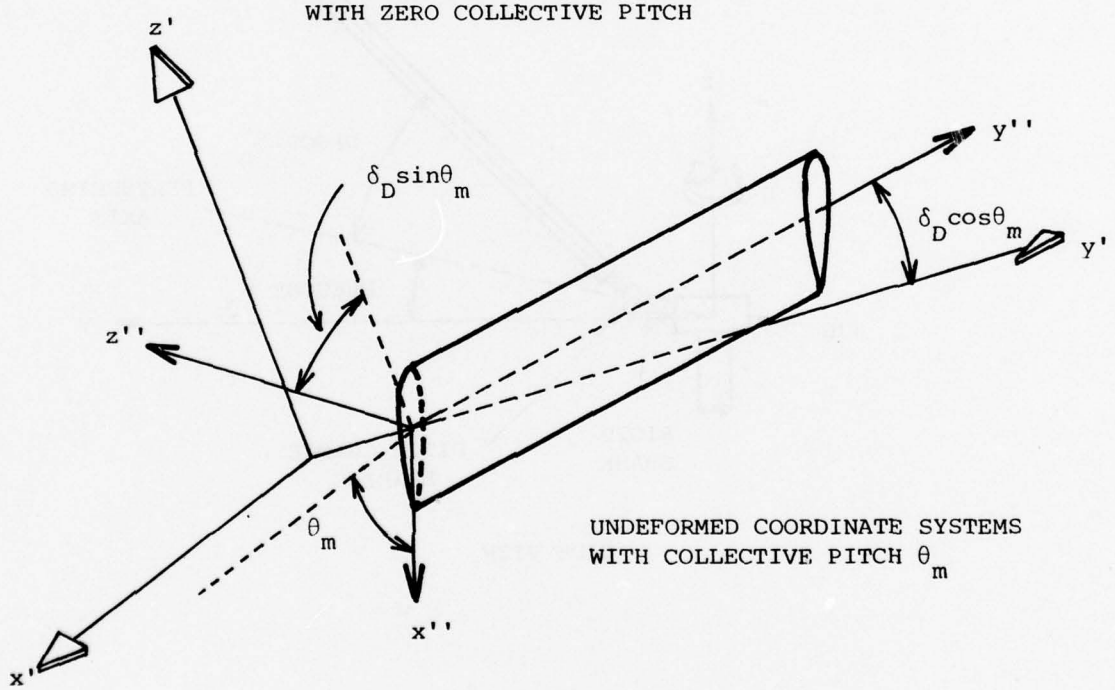

UNDEFORMED COORDINATE SYSTEMS
WITH COLLECTIVE PITCH θ_m

FIG. 2 COORDINATE SYSTEMS

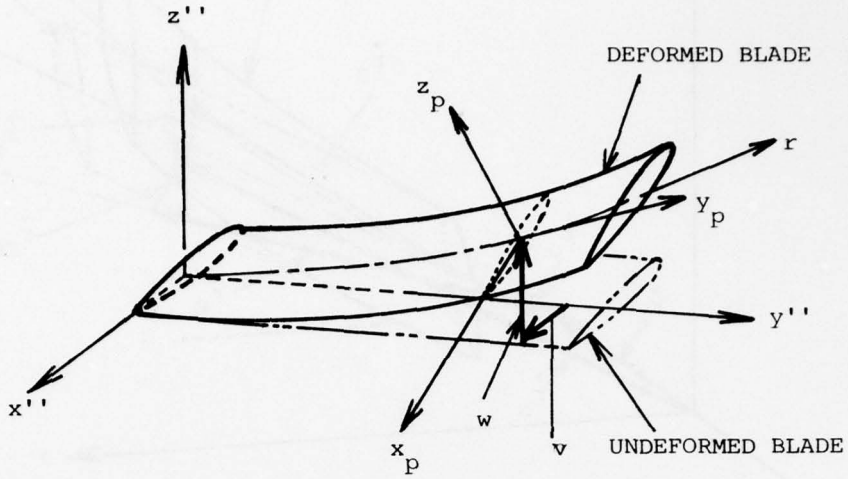

(a) Blade Displacements

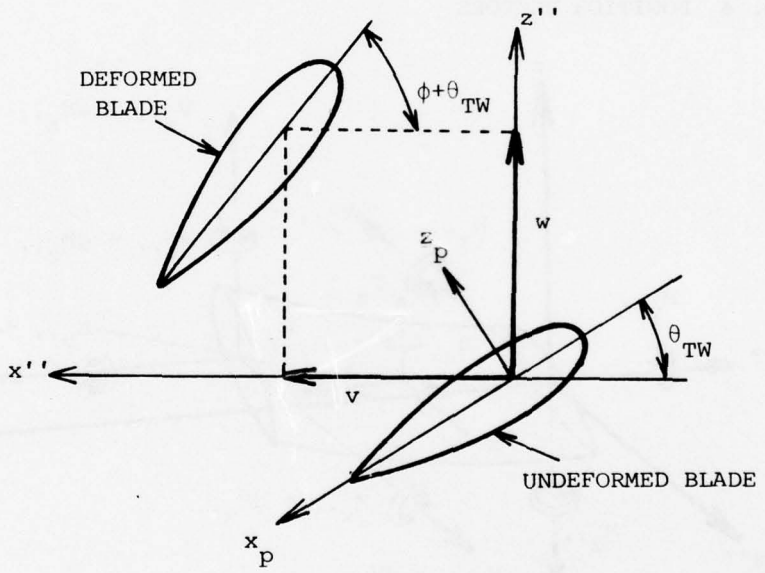

(b) Cross Section Coordinate Systems and Deformations

FIG. 3 BLADE DISPLACEMENTS

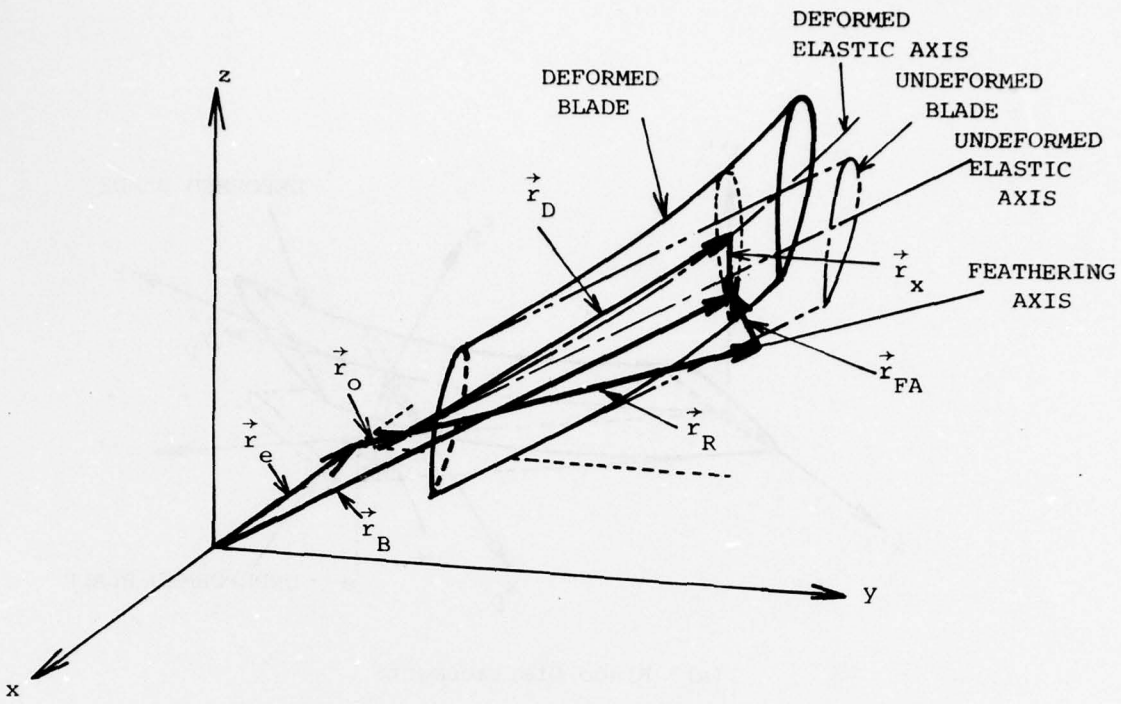

FIG. 4 POSITION VECTORS

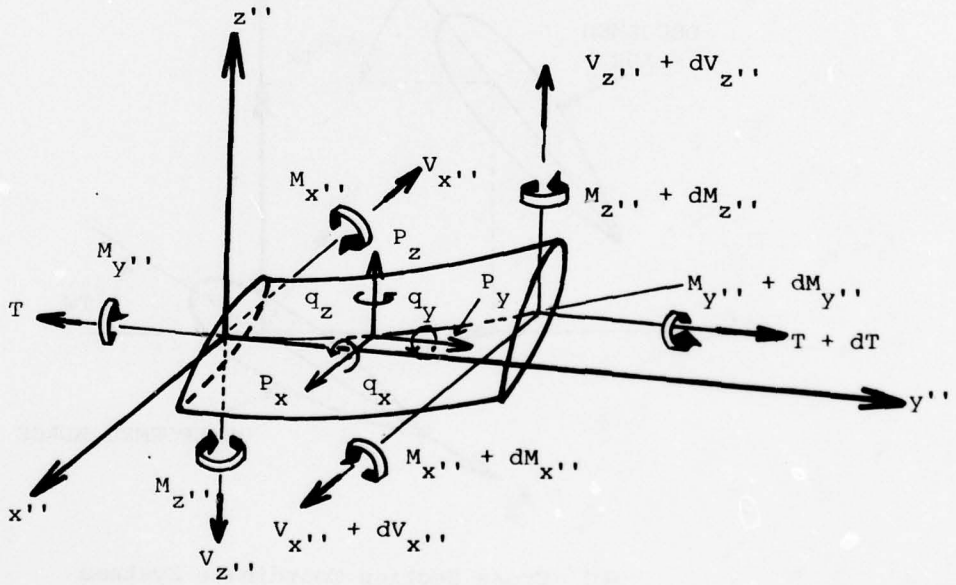

FIG. 5 EQUILIBRIUM OF FORCES AND MOMENTS

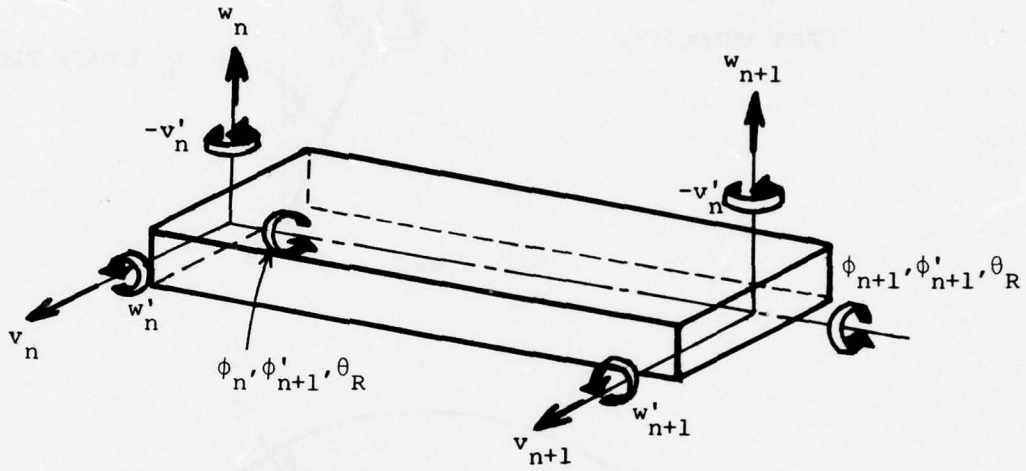

nth Element

FIG. 6 DIRECTION OF POSITIVE DISPLACEMENTS AND ROTATIONS AT NODES OF THE BEAM ELEMENT IN THE FINITE ELEMENT METHOD

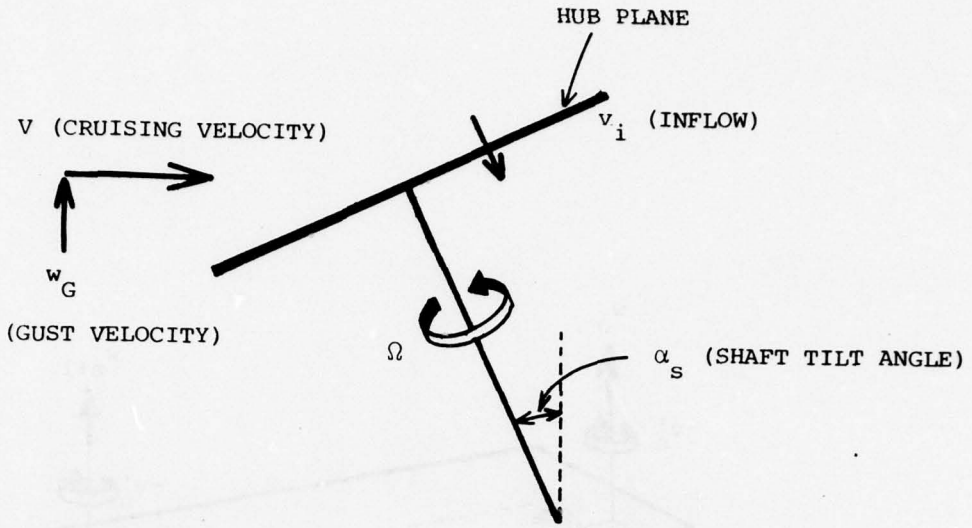

Side View

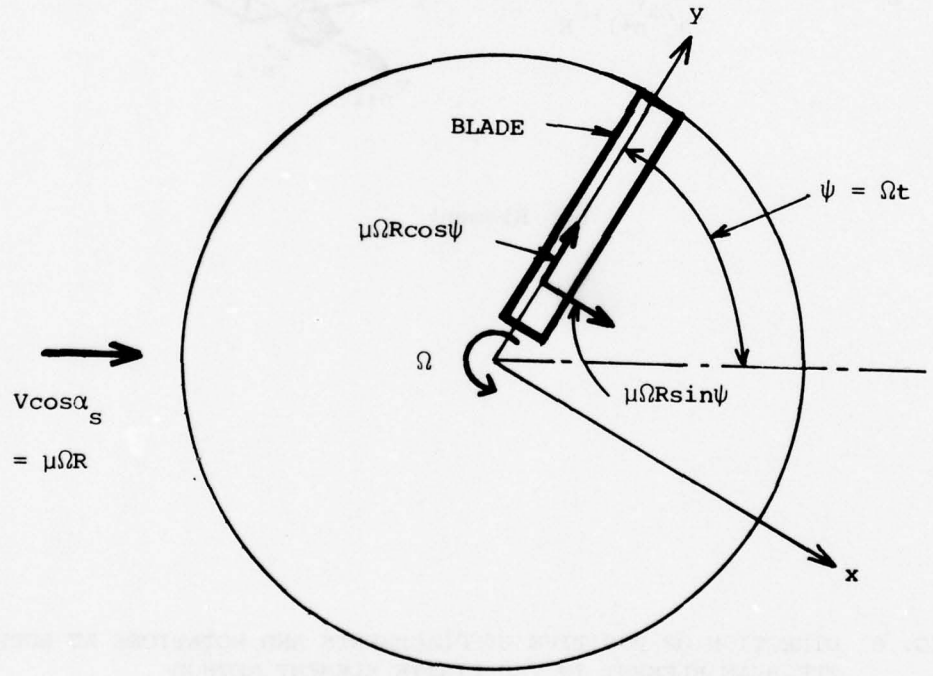

Top View of the Rotor Disk

FIG. 7 ORIENTATION OF CRUISING VELOCITY, INFLOW AND GUST VELOCITY

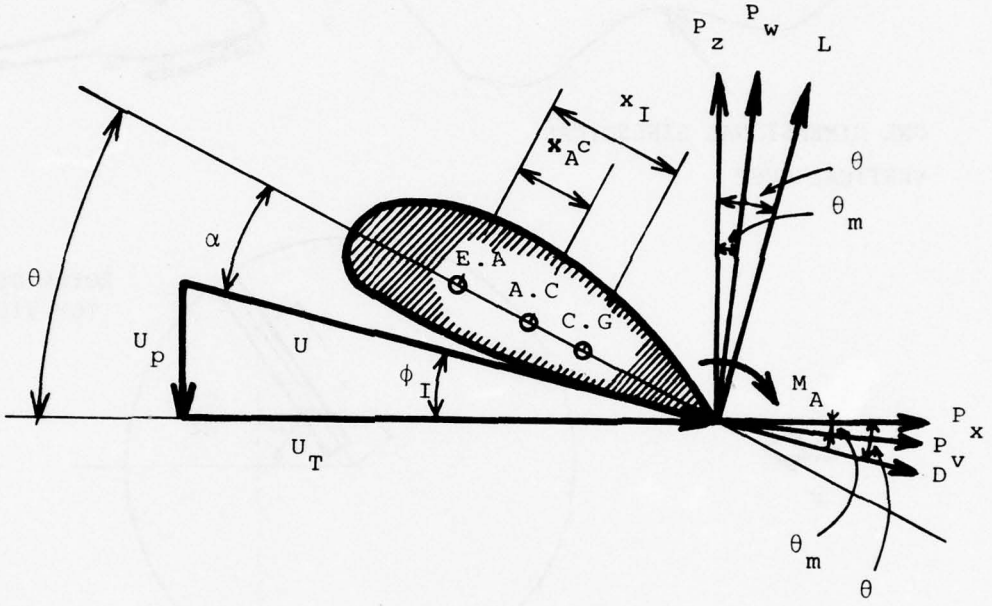

FIG. 8 ROTOR BLADE SECTION AERODYNAMICS

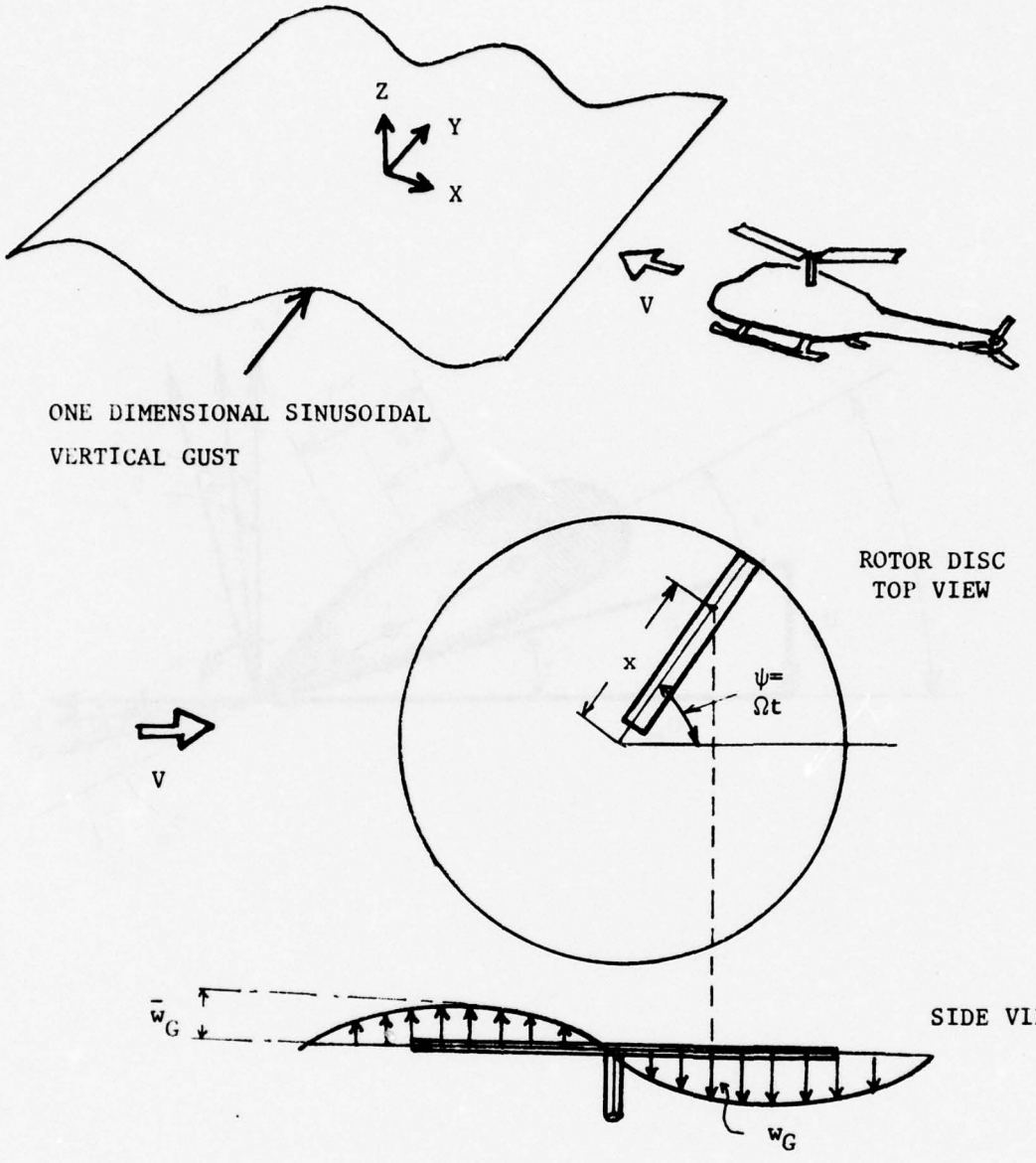

FIG. 9 GUST VELOCITY GRADIENT DUE TO GUST NONUNIFORMITY OVER THE ROTOR DISC

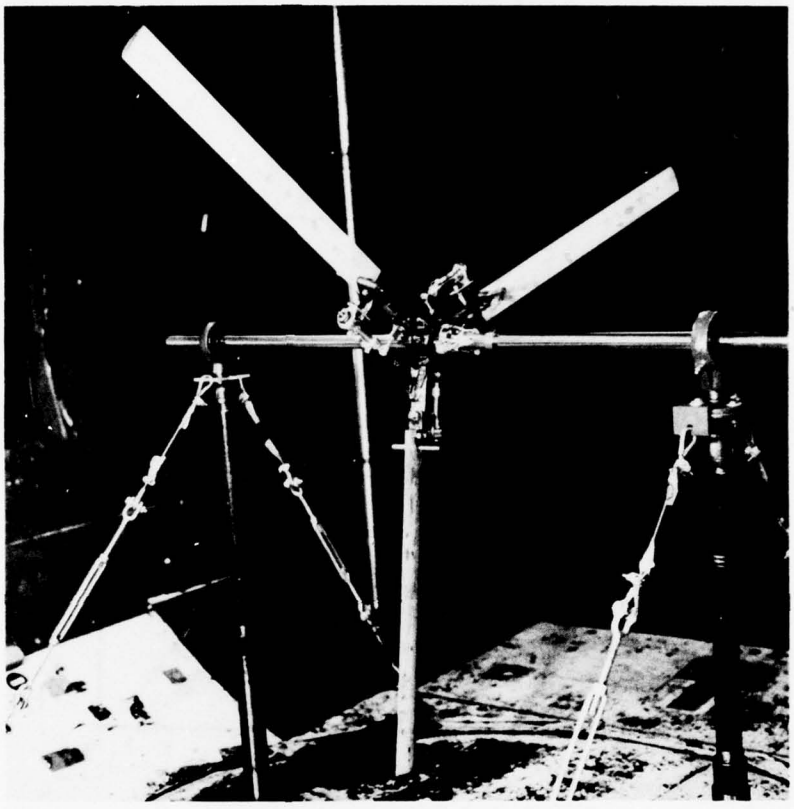

FIG. 1 THREE-BLADED ROTOR

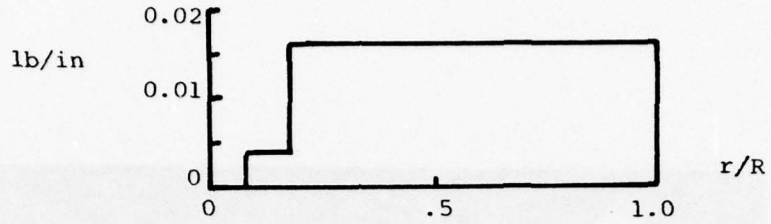

(a) Mass Distribution

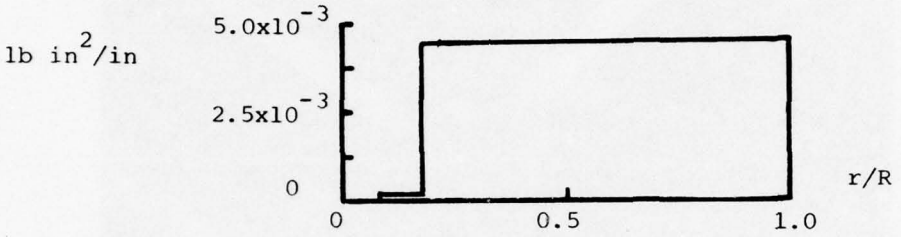

(b) Cross-Sectional Moment of Inertia

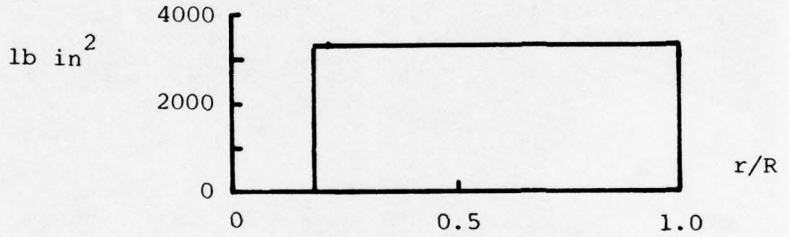

(c) Flapwise Stiffness

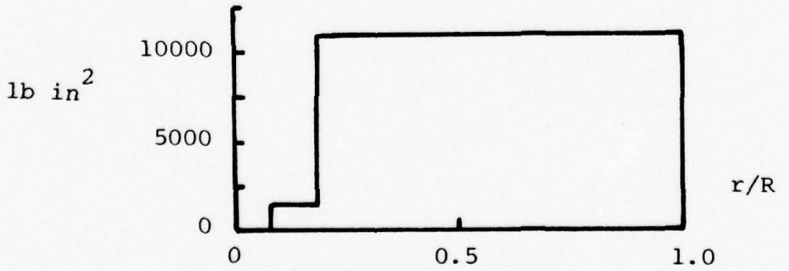

(d) Chordwise Stiffness

FIG. 11 STRUCTURAL CHARACTERISTICS OF WIND TUNNEL MODEL BLADE (STATION 0. TO 0.087R IS A RIGID PORTION OF THE ROTOR AND FLAP HINGE IS LOCATED AT 0.176R)

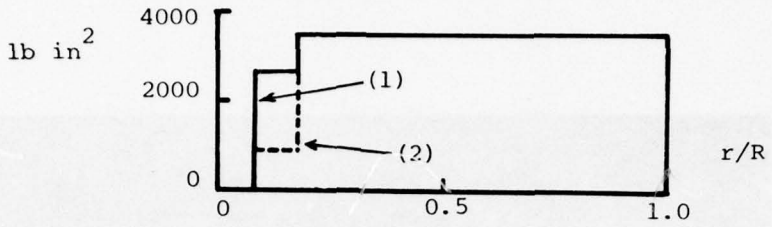

(e) Torsional Rigidity

(1) **Stiff Torsional Stiffness**

(2) Soft Torsional Stiffness

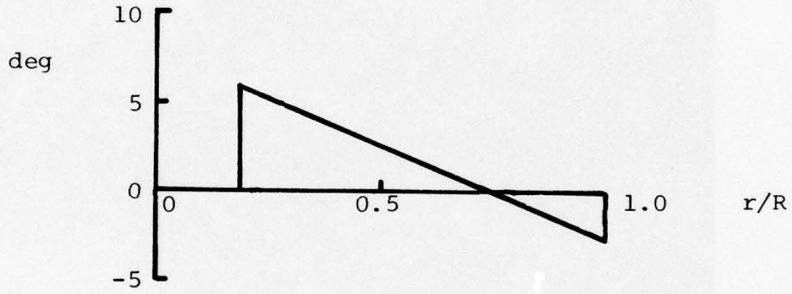

(f) Angle of Twist

FIG. 11 CONCLUDED

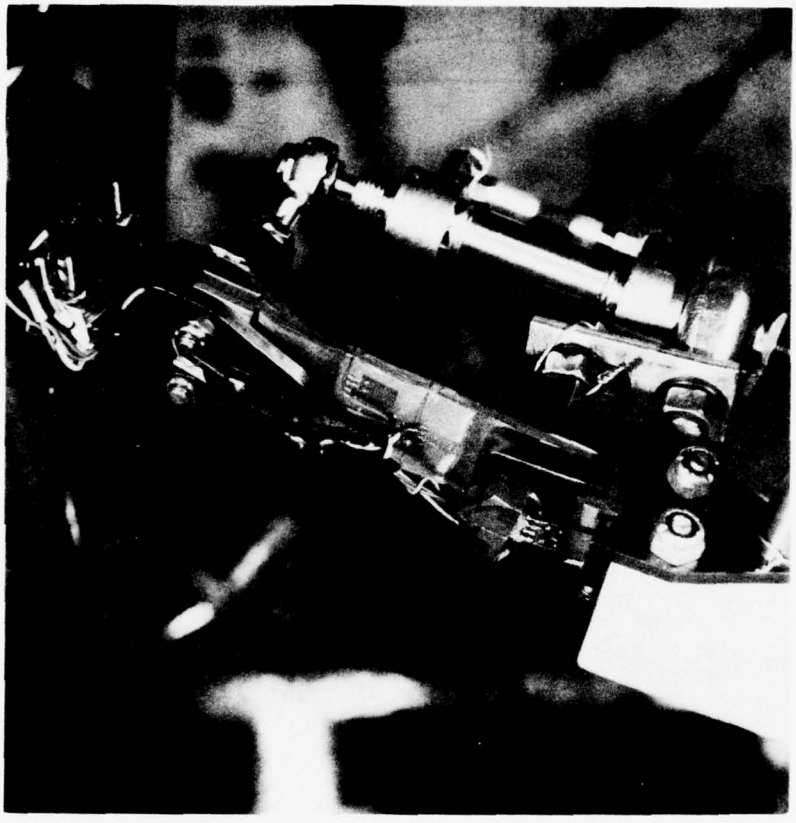

FIG. 2 ROTOR BLADE FLEXURE, STRAIN GAGES,

AND LEAD-LAG DAMPER

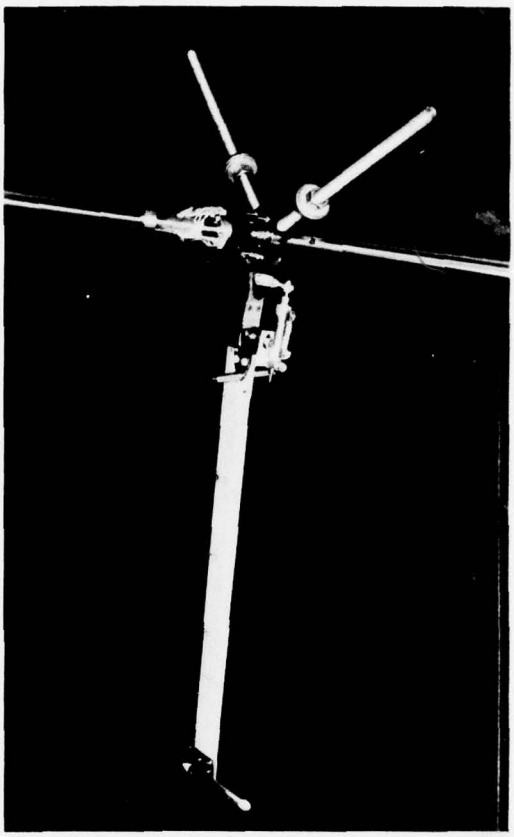

FIG. 3 SINGLE-BLADED ROTOR WITH TIP WEIGHT

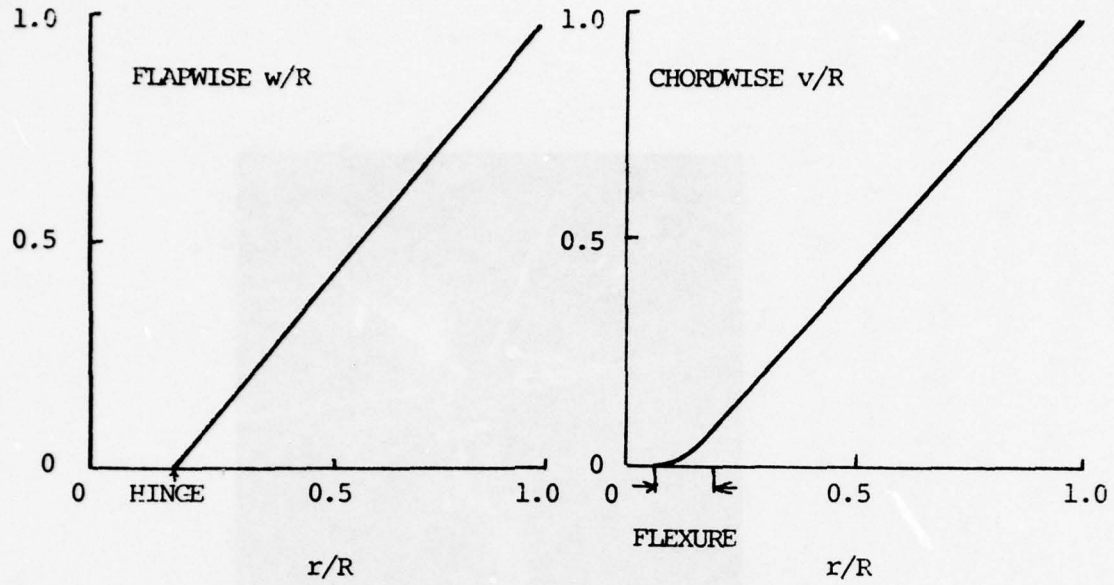

NATURAL FREQUENCY 1.13/rev

NATURAL FREQUENCY 0.82/rev

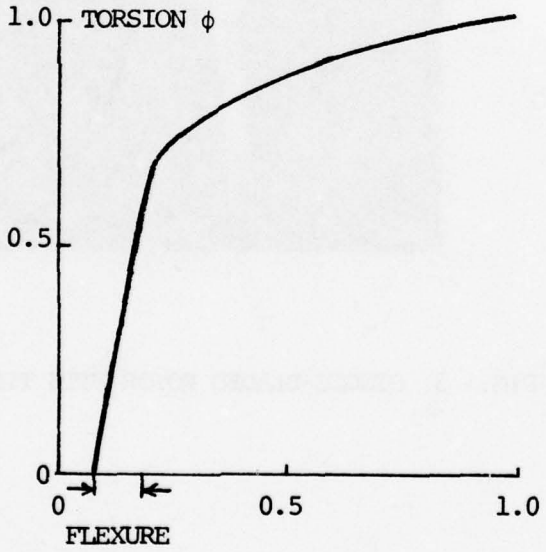

NATURAL FREQUENCY 6.85/rev

FIG. 14 MODE SHAPES OF THE WIND TUNNEL MODEL BLADE (THREE-BLADED ROTOR)

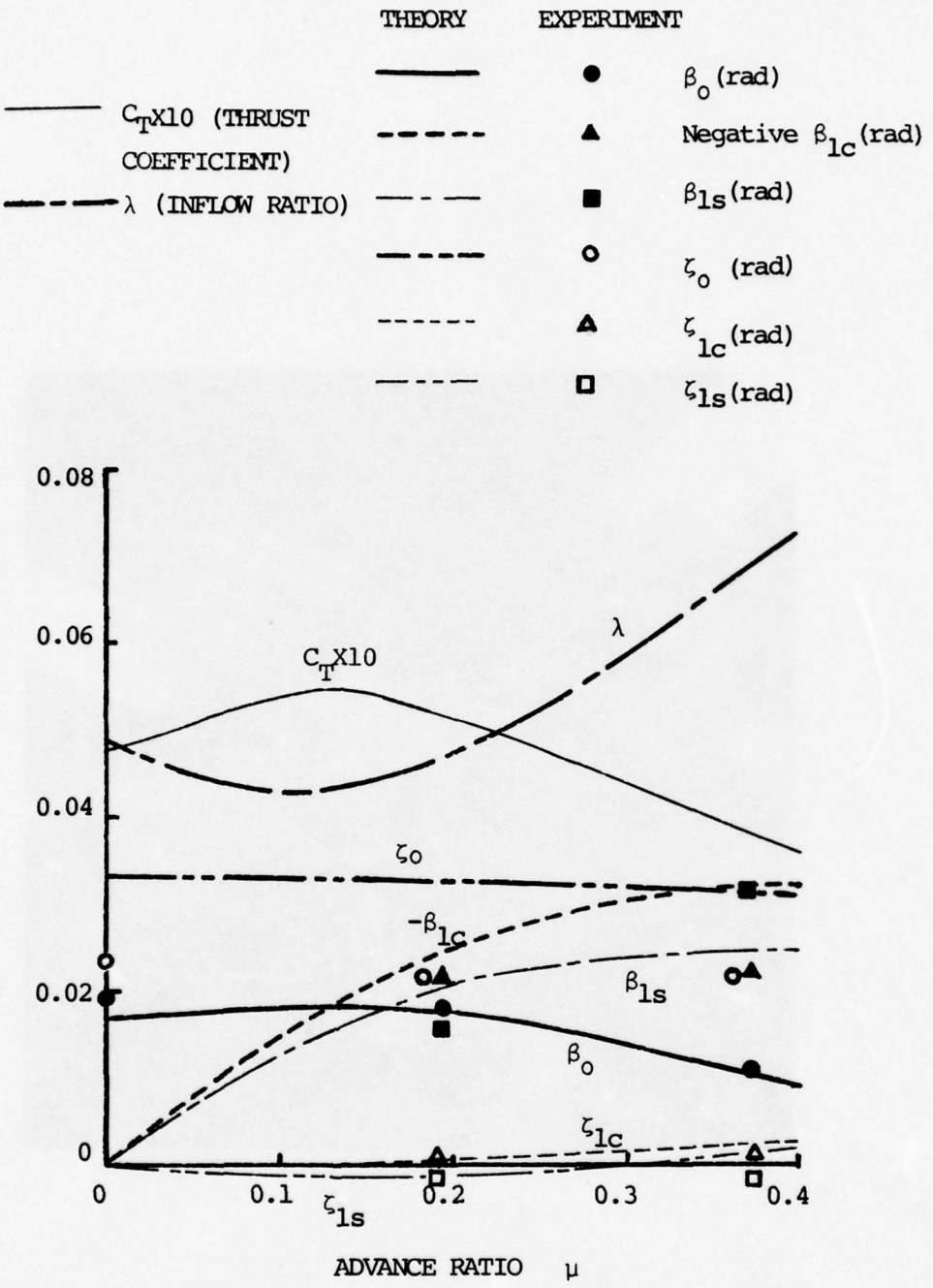

FIG.15 STEADY-STATE CONDITIONS IN NO-TRIM OPERATION FOR THE WIND TUNNEL THREE-BLADED ROTOR MODEL: $\gamma=2.27, \theta_{3/4R}=8$ deg., $\alpha_s=10$ deg., $(-\frac{\omega}{\Omega}\beta)=1.13$/rev, $(-\frac{\omega}{\Omega}\zeta)=0.82$/rev

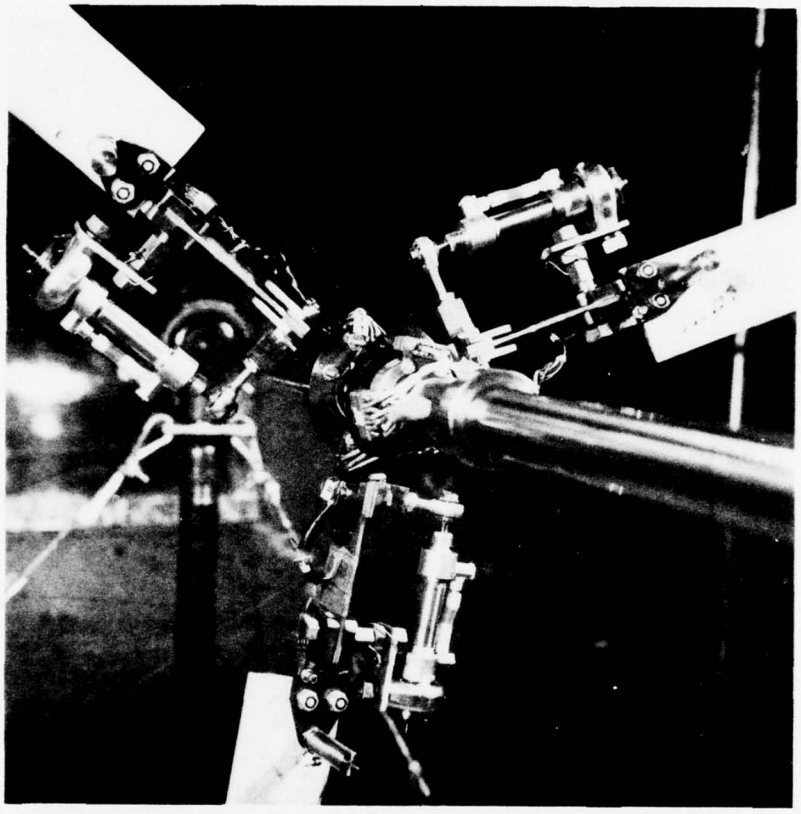

FIGURE 16 ROTOR HUB DETAILS

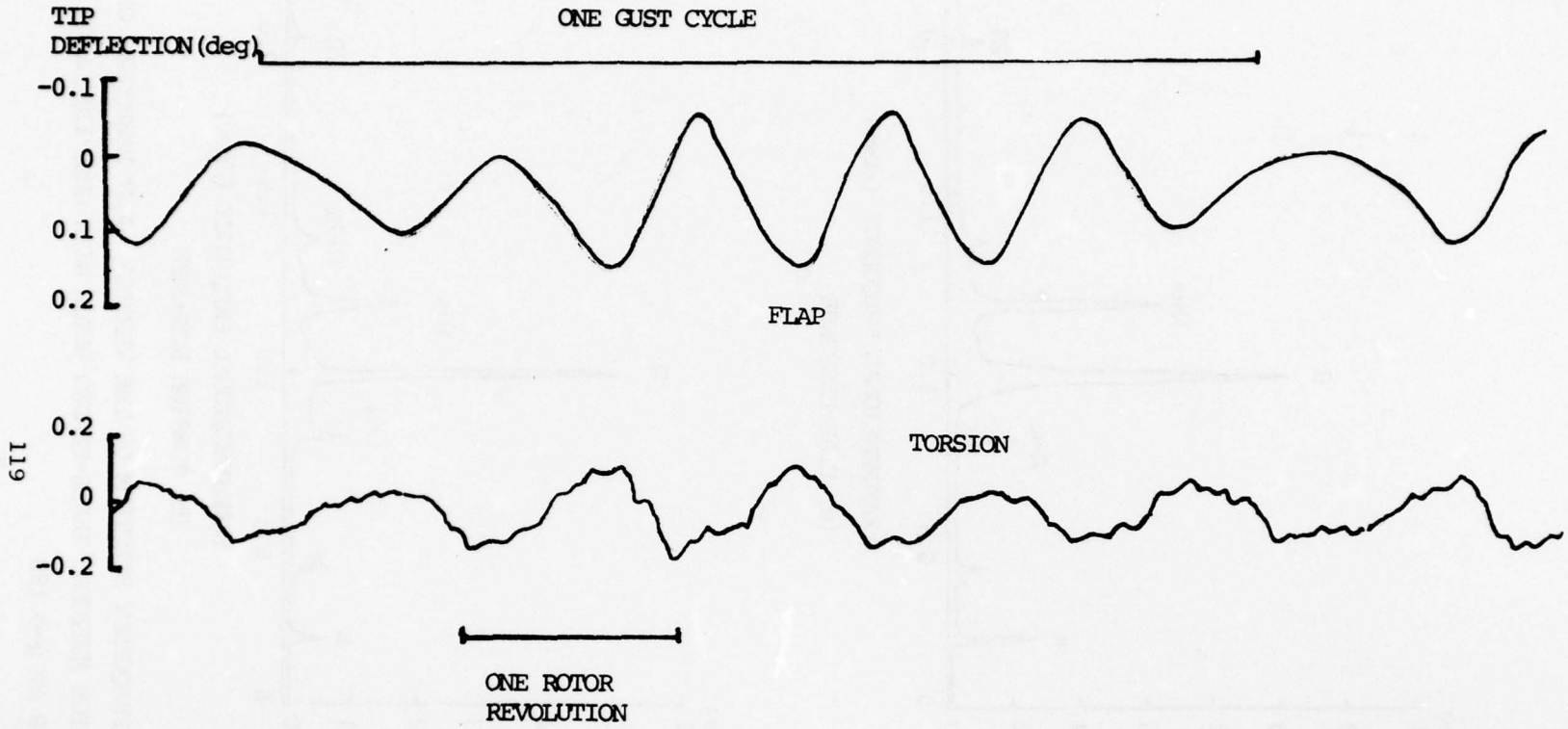

FIG. 17 TYPICAL TIME HISTORY OF THE VERTICAL GUST RESPONSES OF FLAP AND TORSION MOTIONS: THREE-BLADED ROTOR, μ=0.192 AND NONDIMENSIONAL GUST FREQUENCY ω/Ω=0.209

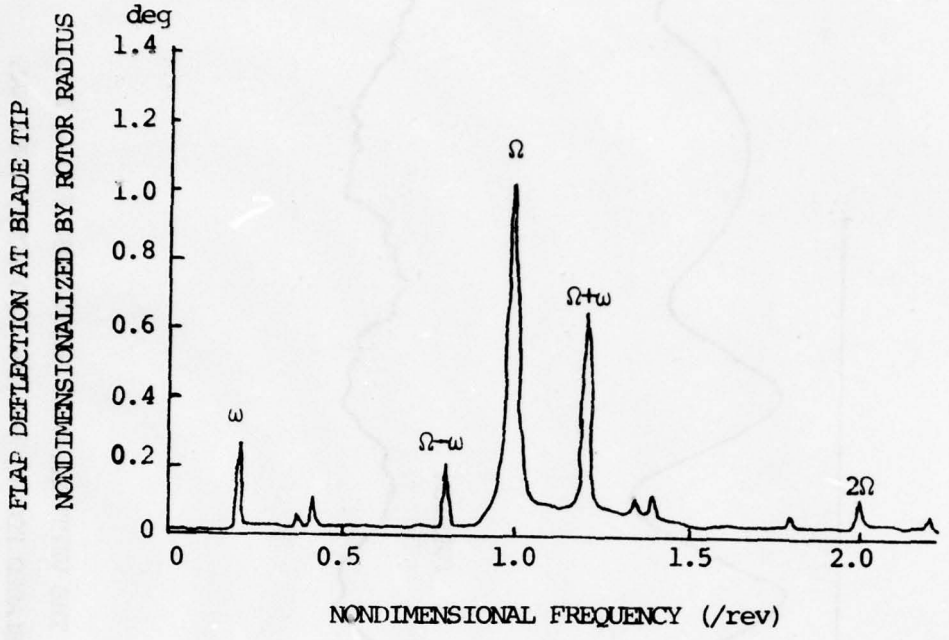

(a) FLAP RESPONSE

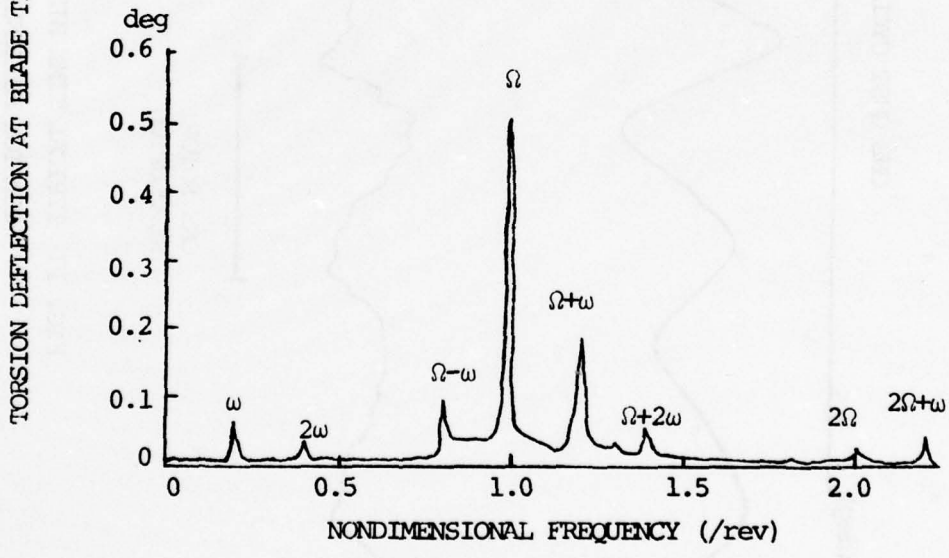

(b) TORSION RESPONSE

FIG.18 TYPICAL FREQUENCY SPECTRUM OF THE VERTICAL GUST RESPONSES OF FLAP AND TORSION MOTIONS: THREE-BLADED ROTOR WITH GUST FREQUENCY $\omega/\Omega=0.209$ AT $\mu=0.192$

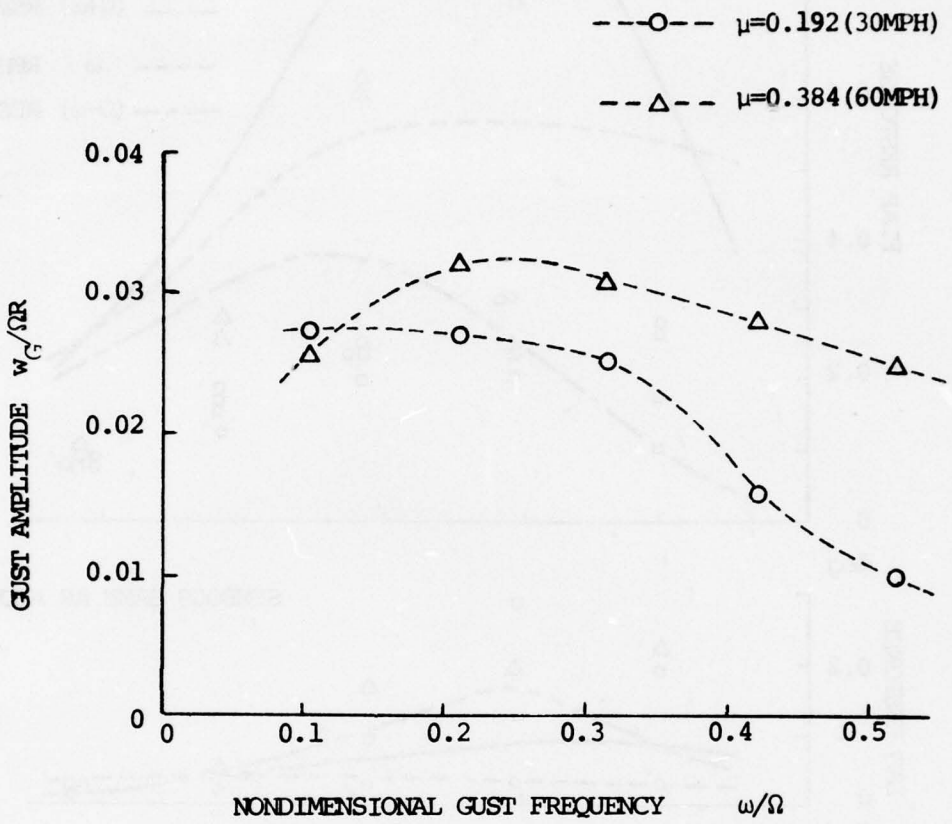

FIG.19 VERTICAL GUST AMPLITUDE AT THE CENTER OF THE ROTOR DISC

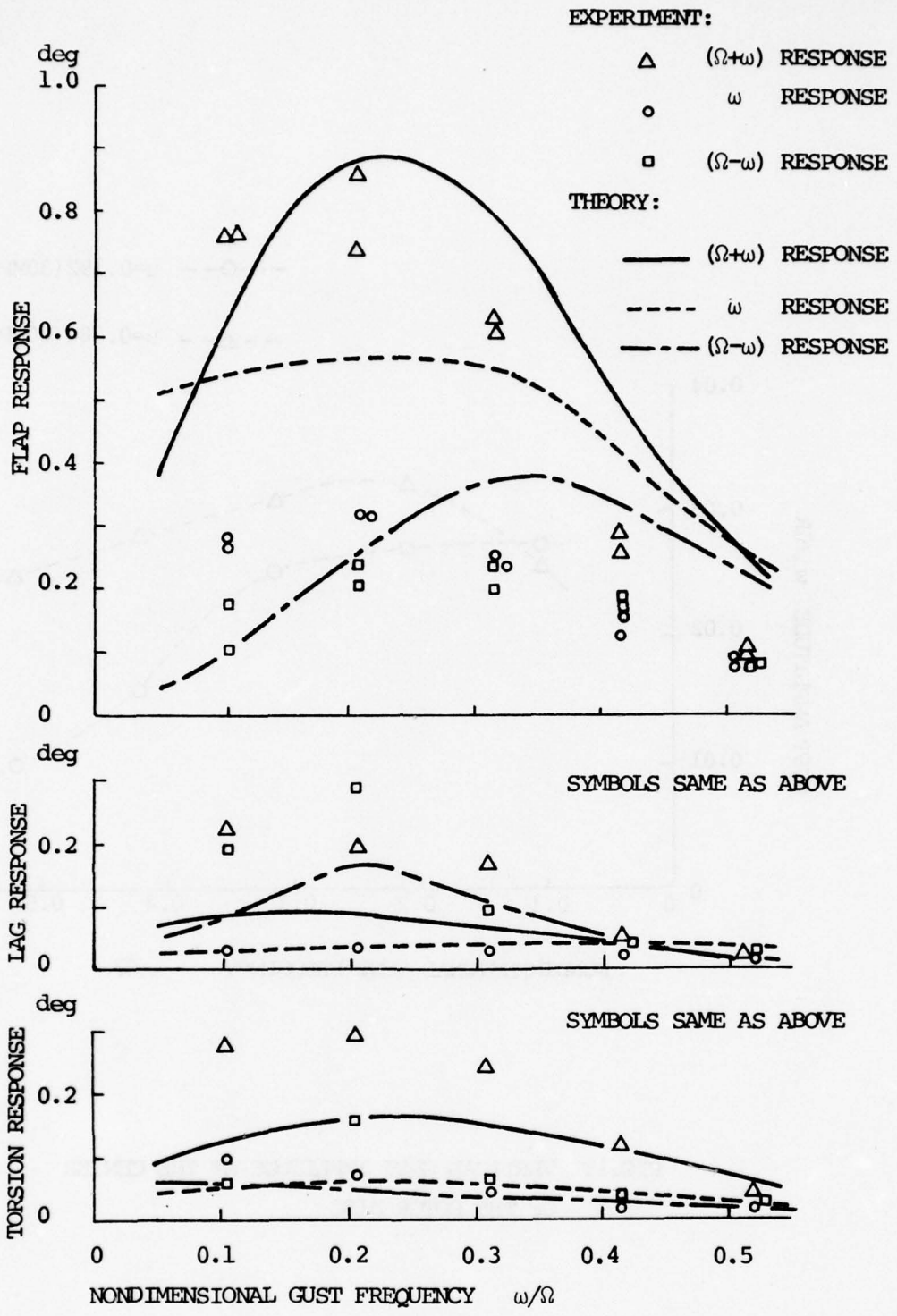

(a) ADVANCE RATIO 0.192 (30 MPH)

FIG. 20 THREE BLADED ROTOR EXPERIMENTAL VERTICAL GUST RESPONSE

NOTE: FLAP AND LAG RESPONSES ARE EXPRESSED IN TERMS OF TIP DEFLECTION NONDIMENSIONALIZED BY RADIUS. TORSION IN TERMS OF TIP DEFLECTION.

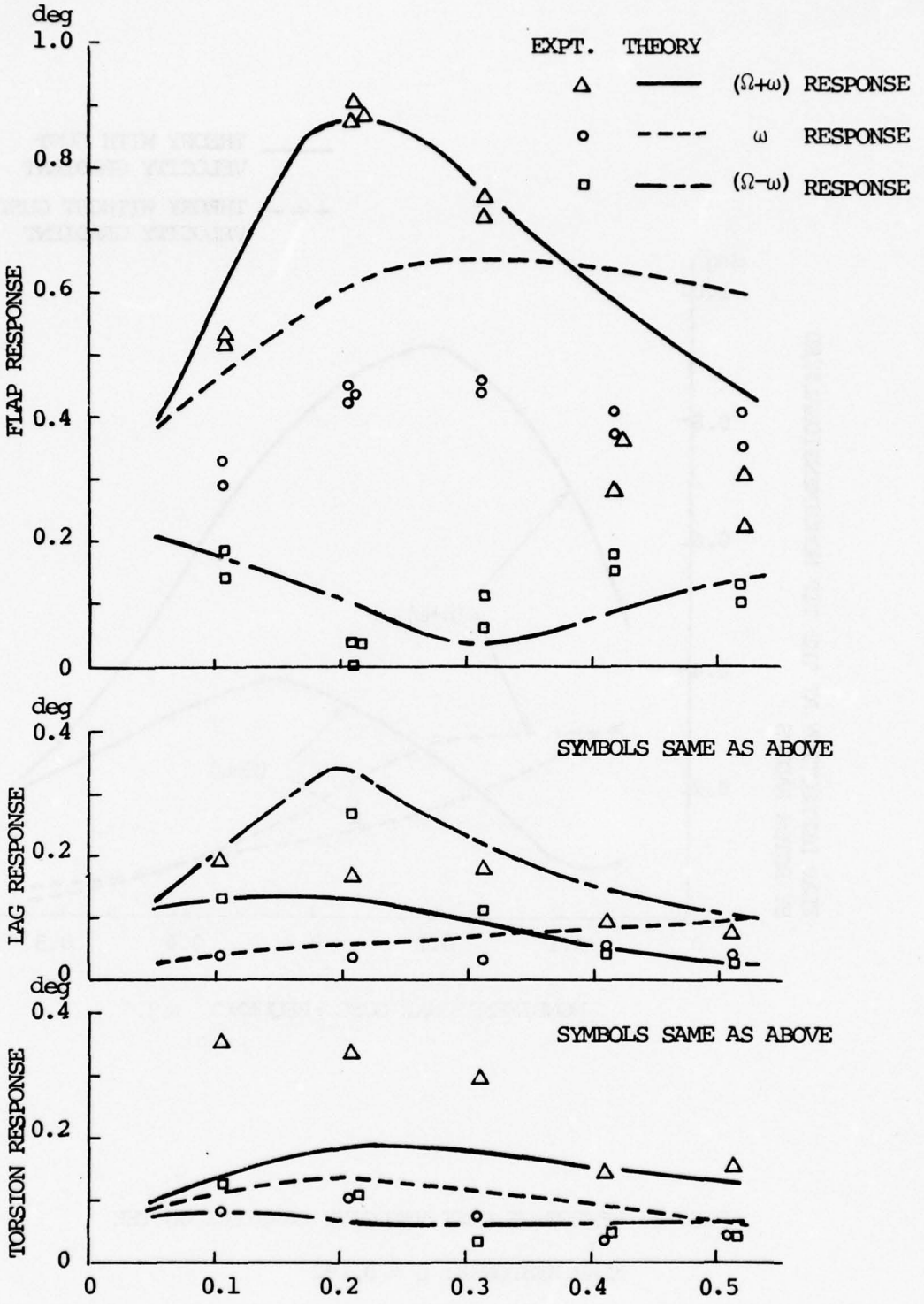

(b) ADVANCE RATIO 0.384 (60 MPH)

FIG. 20 CONCLUDED

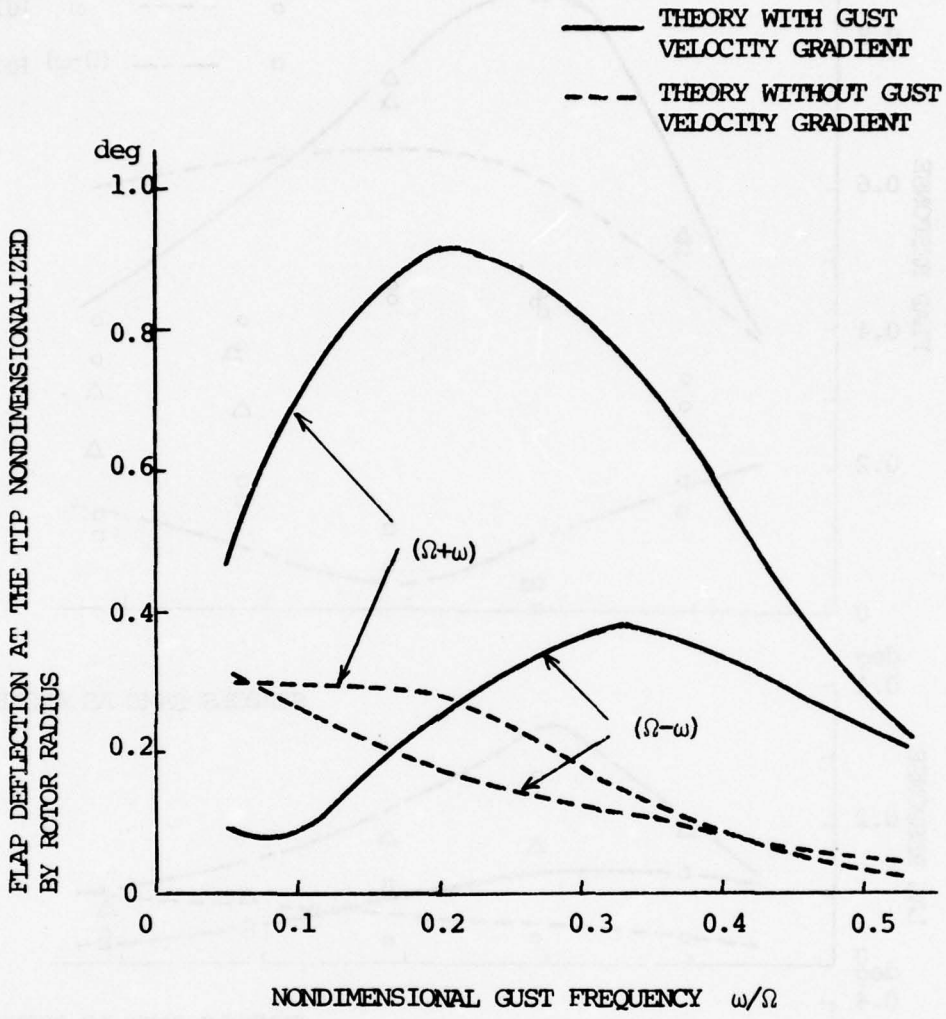

FIG. 21 EFFECT OF GUST VELOCITY GRADIENT ON THE FLAP RESPONSE: $\mu = 0.192$

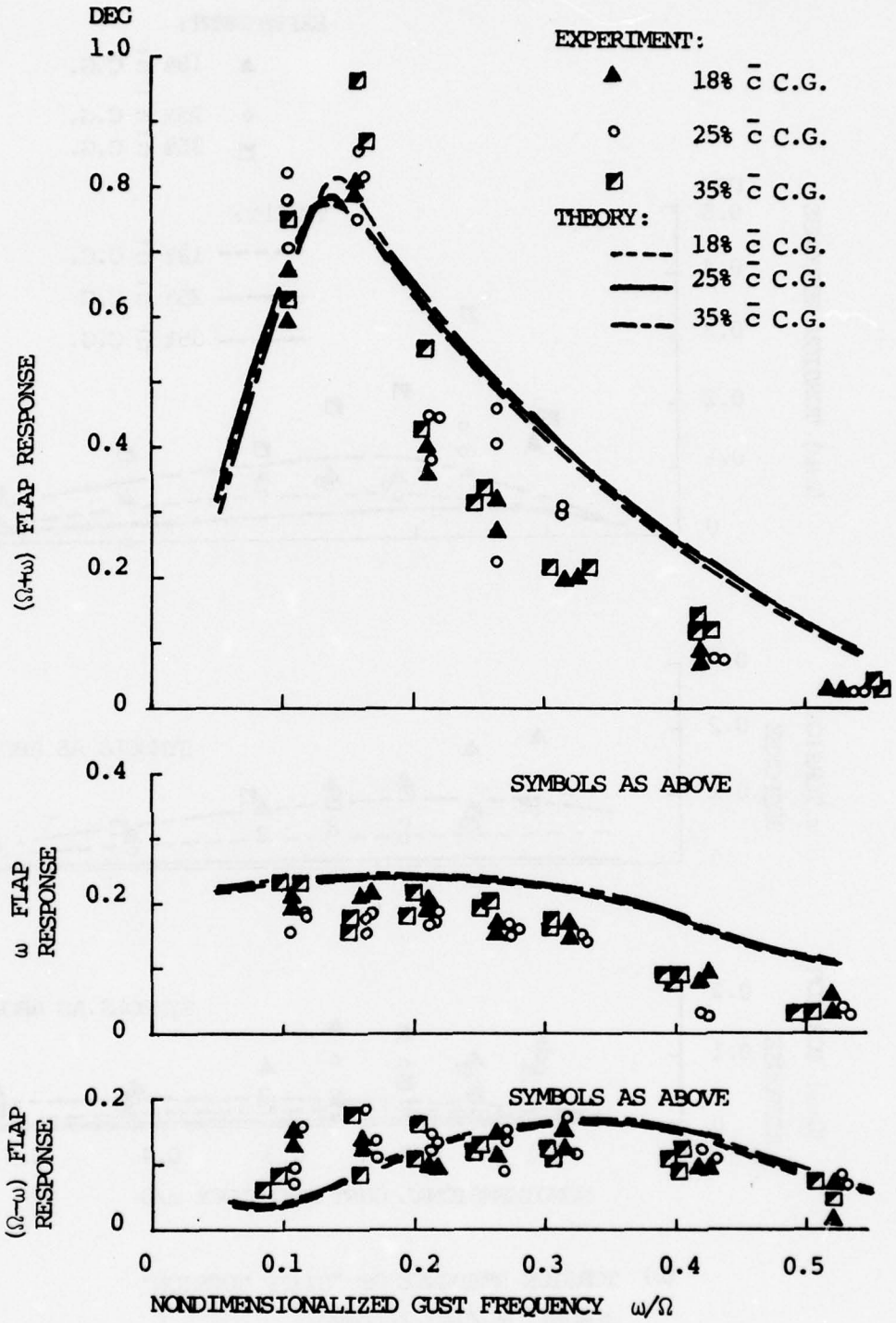

(a) FLAP RESPONSE OF "STIFF TORSION" BLADE: $^{\omega}\phi/\Omega = 5.21$ / rev

FIG. 22 SINGLE-BLADED ROTOR VERTICAL GUST RESPONSE IN ADVANCE RATIO 0.192 WITH CHORDWISE C.G. SHIFT. NOTE: FLAP AND LAG RESPONSES ARE EXPRESSED IN TERMS OF TIP DEFLECTION NONDIMENSIONALIZED BY RADIUS. TORSION IN TERMS OF TIP DEFLECTION

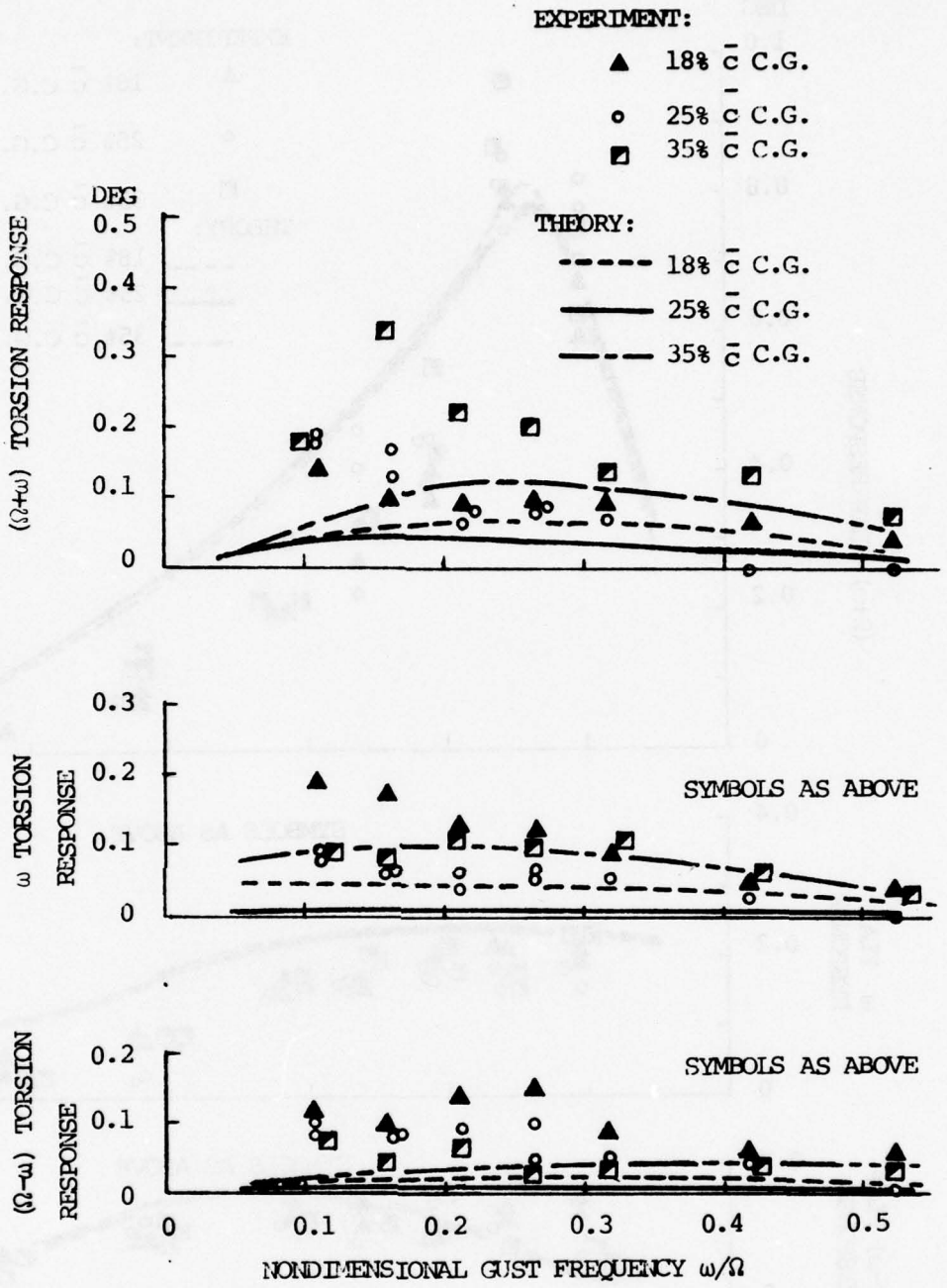

(b) TORSION RESPONSE OF "STIFF TORSION" BLADE: $\omega_\phi/\Omega=5.21/\text{rev}$

FIG. 22 CONTINUED

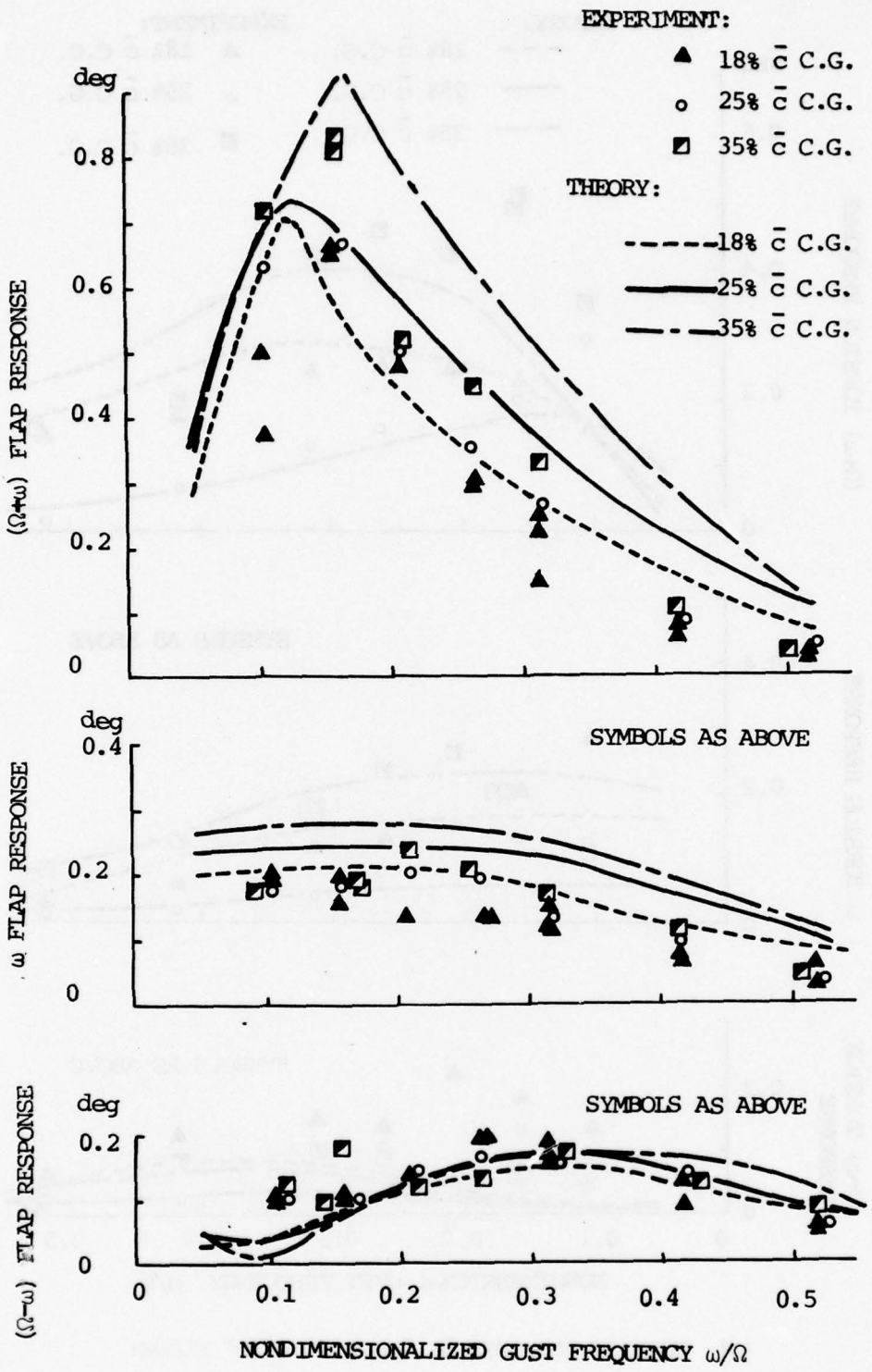

(c) FLAP RESPONSE OF " SOFT TORSION " BLADE: $\omega_\phi / \Omega = 2.38$ / rev

FIG. 22 CONTINUED

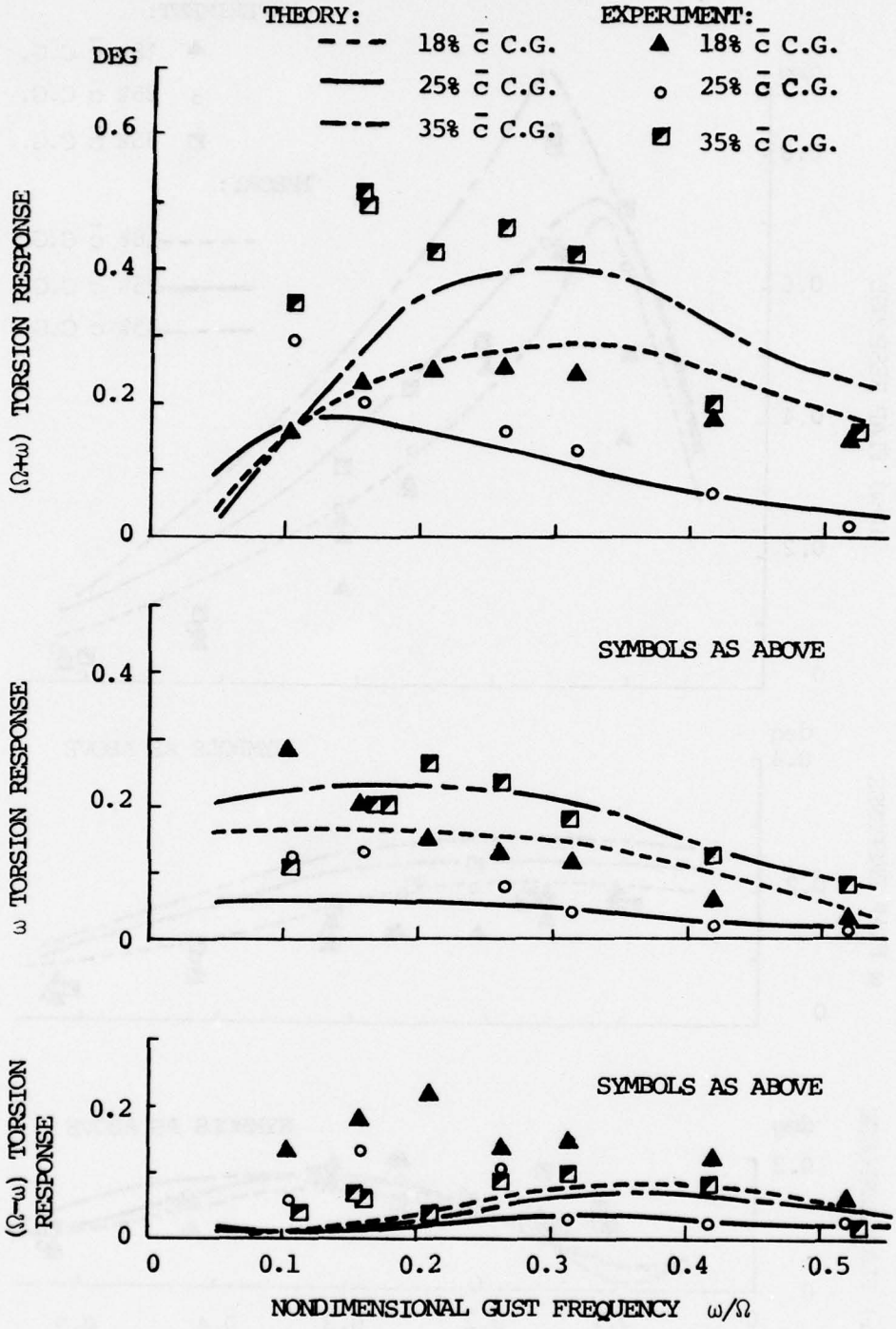

(d) TORSION RESPONSE OF "SOFT TORSION" BLADE:
ω_ϕ/Ω=2.38/rev

FIG. 22 CONTINUED

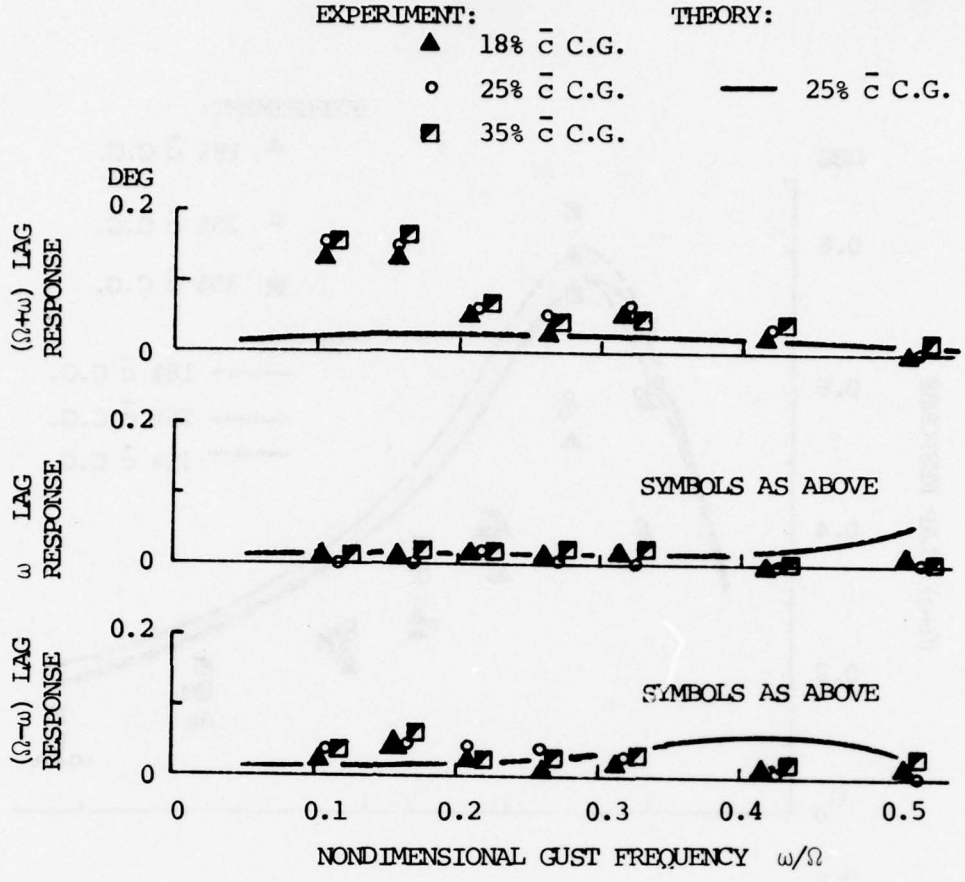

(e) LAG RESPONSE OF "STIFF TORSION" BLADE: ω_ϕ/Ω =5.21/rev

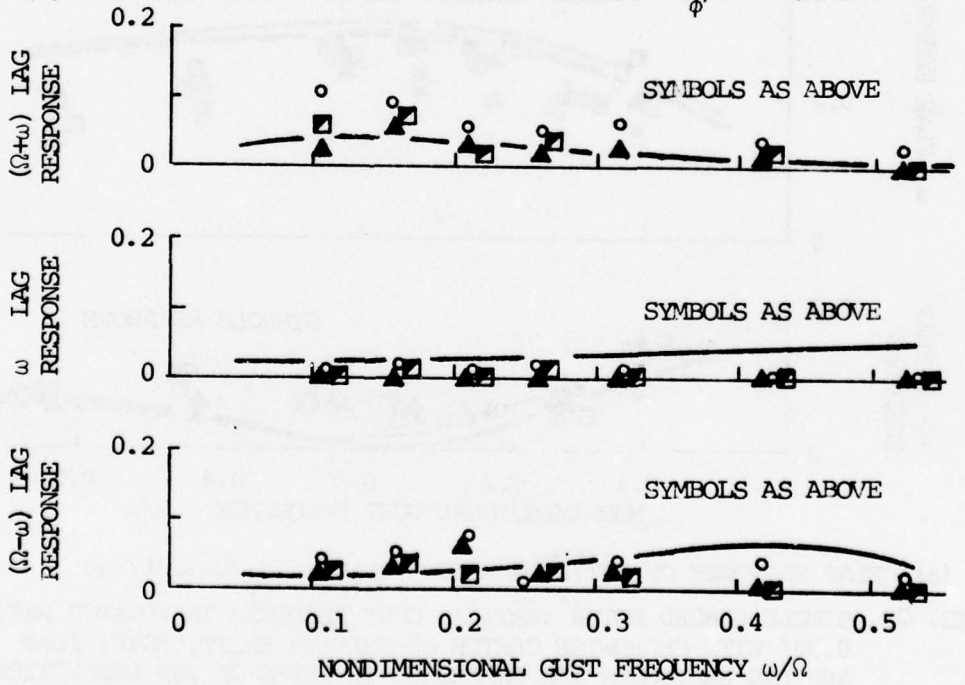

(f) LAG RESPONSE OF "SOFT TORSION" BLADE: ω_ϕ/Ω=2.38/rev

FIG. 22 CONCLUDED

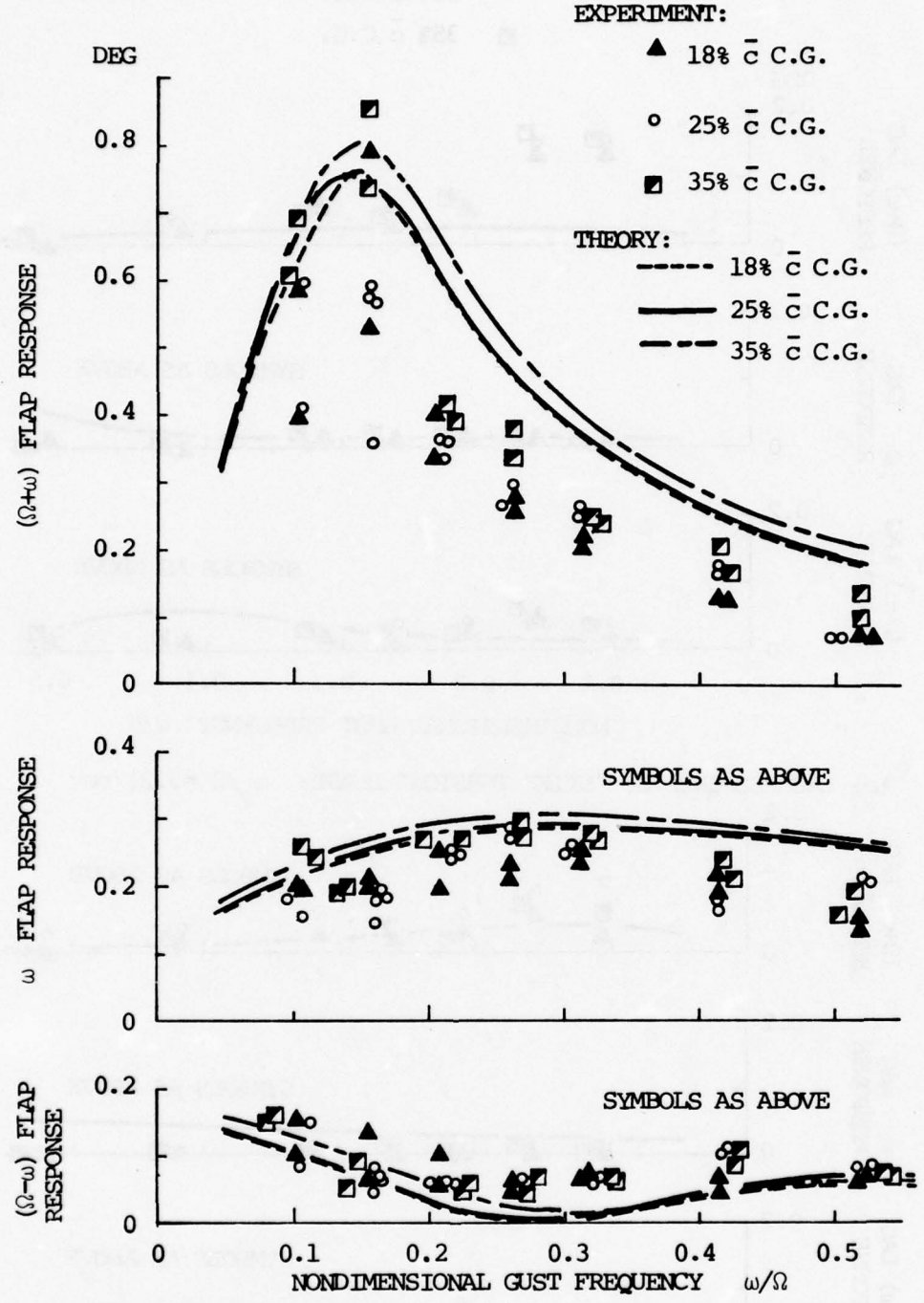

(a) FLAP RESPONSE OF "STIFF TORSION" BLADE: ω_ϕ/Ω=5.21/rev

FIG. 23 SINGLE-BLADED ROTOR VERTICAL GUST RESPONSE IN ADVANCE RATIO 0.384 WITH CHORDWISE CENTER-OF-GRAVITY SHIFT. NOTE: FLAP AND LAG RESPONSES ARE EXPRESSED IN TERMS OF TIP DEFLECTION NONDIMENSIONALIZED BY RADIUS. TORSION IN TERMS OF TIP DEFLECTION.

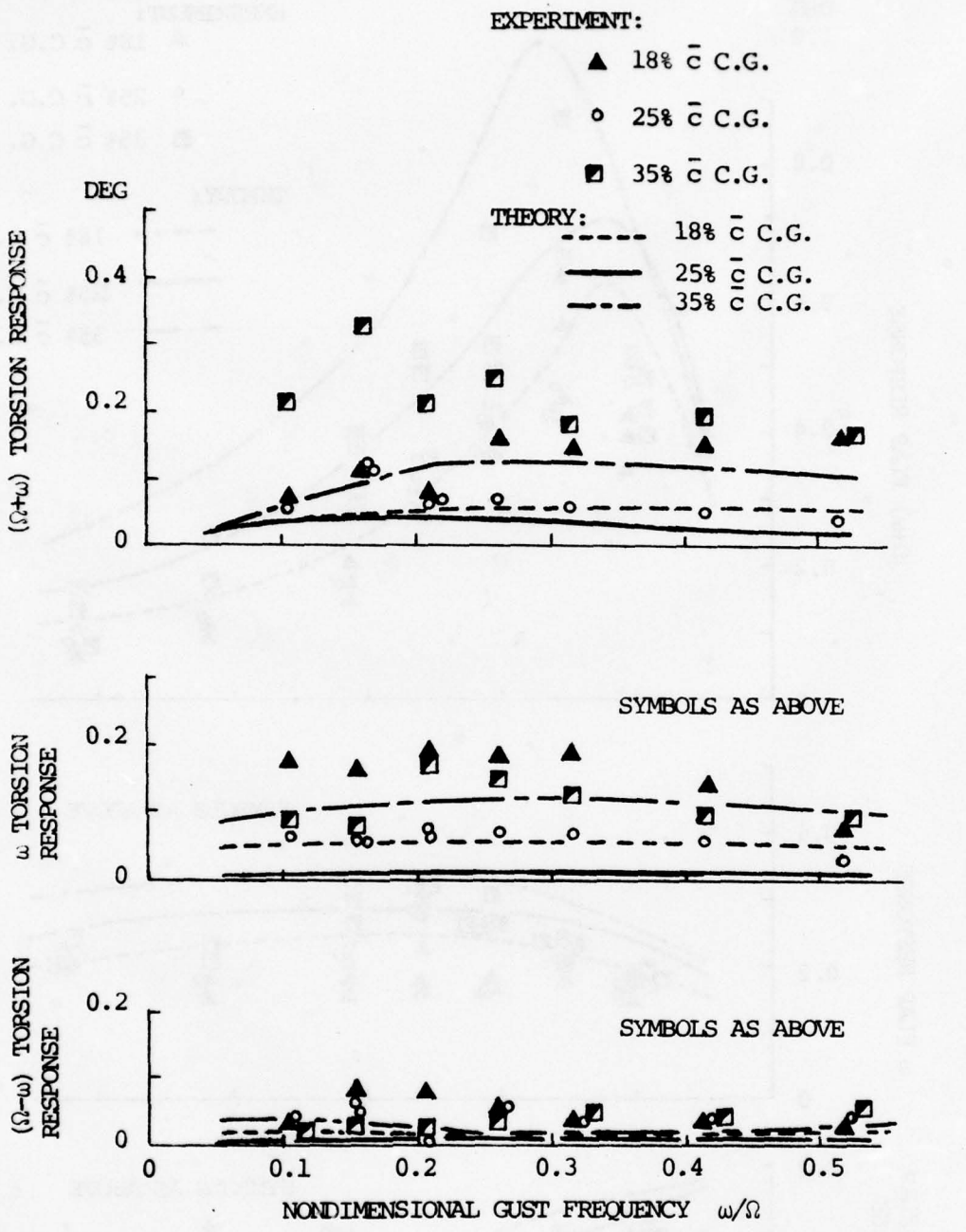

(b) TORSION RESPONSE OF "STIFF TORSION" BLADE: ω_ϕ/Ω=5.21/rev

FIG. 23 CONTINUED

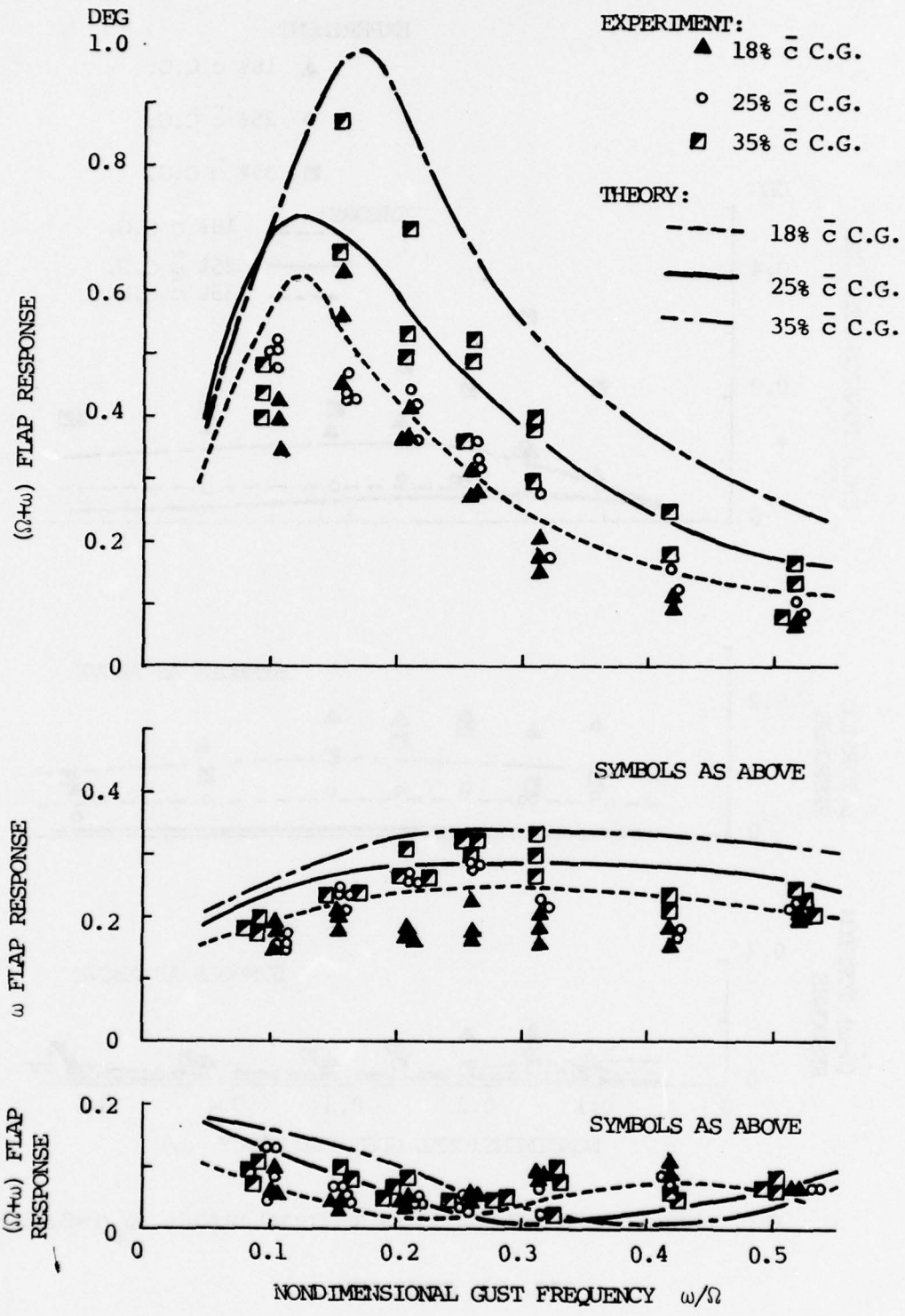

(c) FLAP RESPONSE OF "SOFT TORSION" BLADE: ω_ϕ/Ω=2.38/rev

FIG. 23 CONTINUED

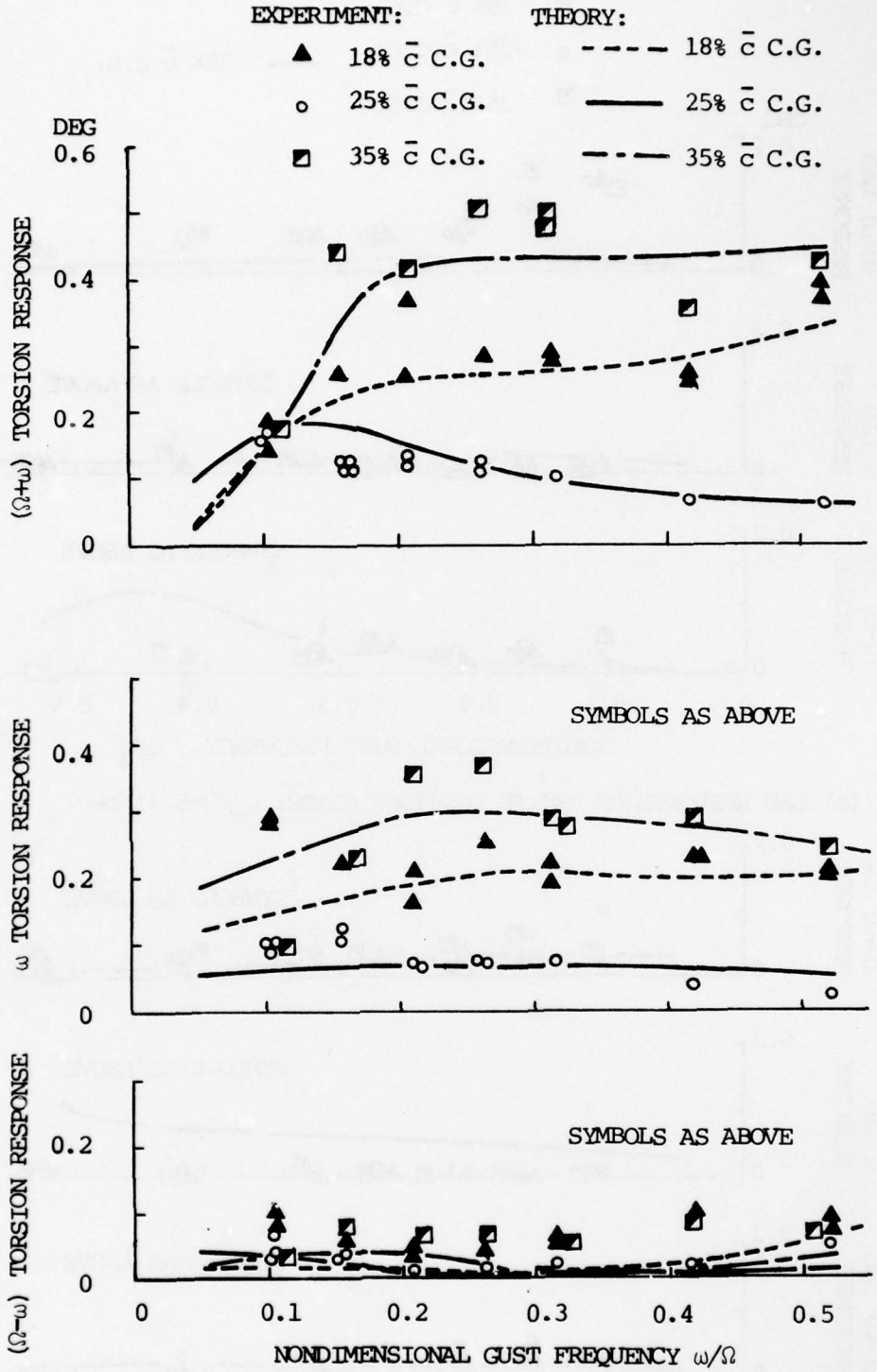

(d) TORSION RESPONSE OF "SOFT TORSION" BLADE: ω_ϕ/Ω=2.38/rev

FIG. 23 CONTINUED

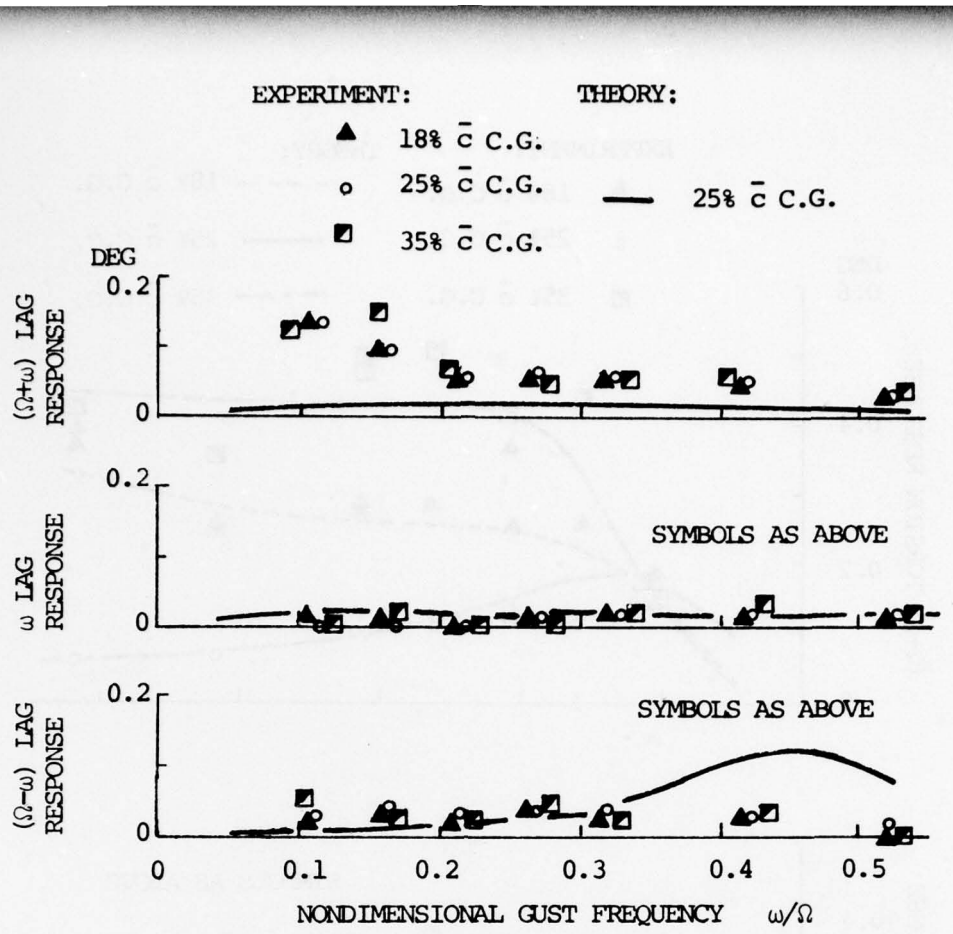

(e) LAG RESPONSE OF "STIFF TORSION" BLADE: ω_ϕ/Ω=5.21/rev

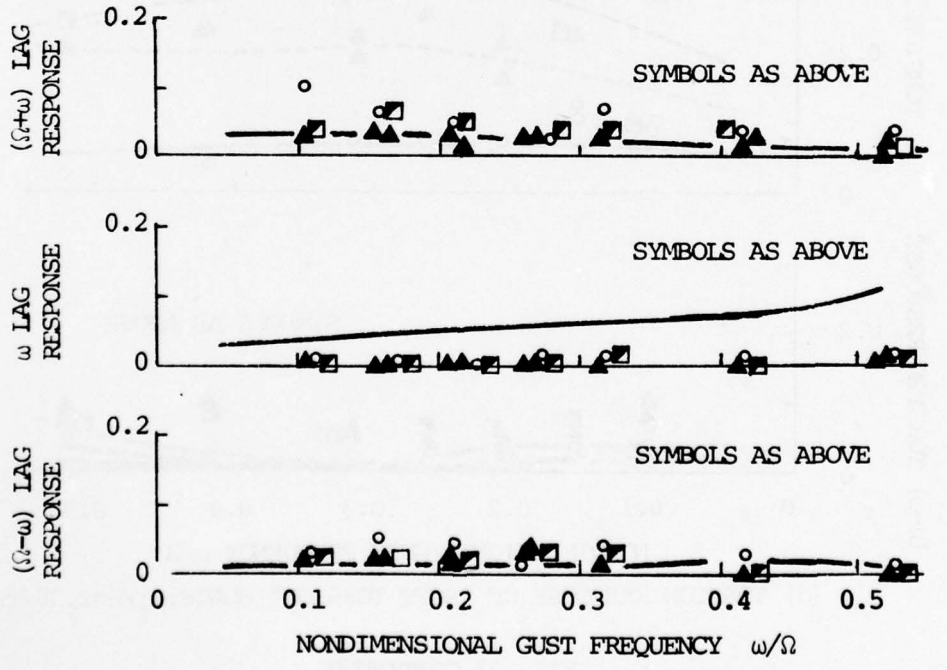

(f) LAG RESPONSE OF "SOFT TORSION" BLADE: ω_ϕ/Ω=2.38/rev

FIG. 23 CONTINUED

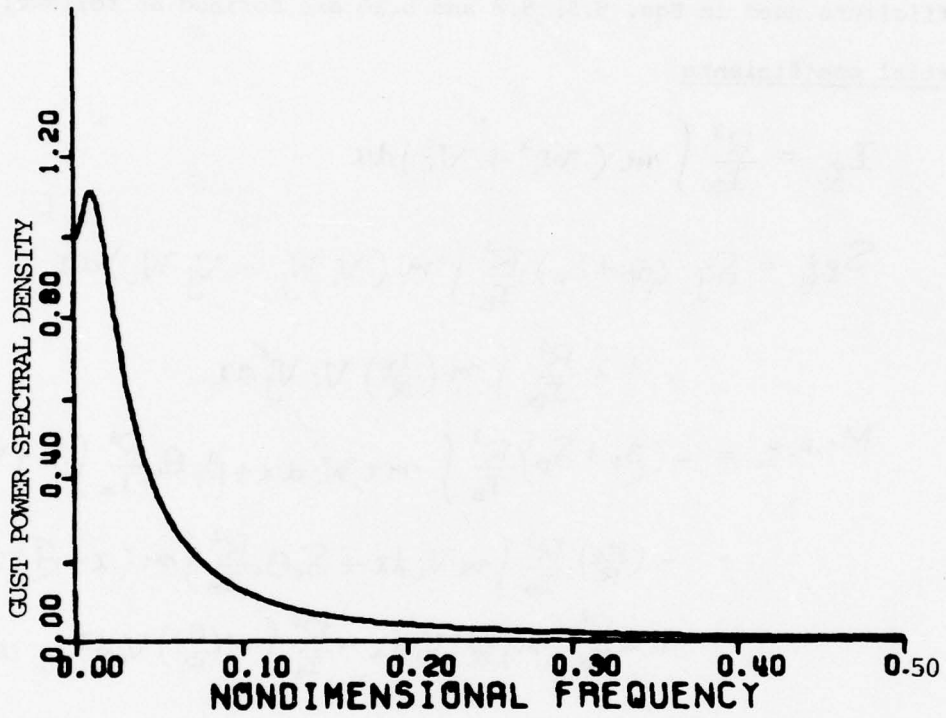

FIG. 24 VON KARMAN GUST POWER SPETRAL DENSITY SCALED TO WIND TUNNEL MODEL BLADE.

$$(PSD) = \frac{1 + 8/3\ [\ 1.339(\omega L/V)\ ]^2}{\{1 + [1.339(\omega L/V)]^2\}^{11/6}}$$

WHERE, L= 40 FT., V= 60 MPH., Ω= 955 RPM

APPENDIX A

EXPRESSIONS ASSOCIATED WITH STEADY-STATE EQUATIONS

Coefficients used in Eqs. 5.5, 5.8 and 5.10 are defined as follows:

Inertial coefficients

$$I_{q_i} = \frac{R^3}{I_B}\int m\,(W_i^2 + V_i^2)\,dx$$

$$S_{q_i\dot{q}_j} = \delta_{ij}\,(\beta_p+\delta_D)\frac{R^3}{I_B}\int m\,(V_i W_j - V_j W_i)\,dx + 2\,\frac{R^3}{I_B}\int m\left(\frac{x_I}{R}\right) V_i V_j'\,dx$$

$$M_{c.F.q_i} = -(\beta_p+\delta_D)\frac{R^3}{I_B}\int m x W_i\,dx + \beta_p\theta_o\frac{R^3}{I_B}\int m x V_i\,dx - \left(\frac{e_o}{R}\right)\frac{R^3}{I_B}\int m V_i\,dx + \delta_D\theta_o\frac{R^3}{I_B}\int m\left(x-\frac{r_o}{R}\right)V_i\,dx + 2\frac{R^3}{I_B}\int m\left(\frac{x_I}{R}\right)V_i\,dx - \frac{R^3}{I_B}\int m\left(\frac{e_N}{R}\right)V_i\,dx \qquad (A.1)$$

Aerodynamic coefficients

$$M_{q_i\dot{q}_j} = M^{o}_{q_i\dot{q}_j} + M^{s}_{q_i\dot{q}_j}\sin\psi$$

$$M_{q_iq_j} = M^{c}_{q_iq_j}\cos\psi + M^{2s}_{q_iq_j}\sin(2\psi)$$

$$M_{q_i} = M^{o}_{q_i} + M^{s}_{q_i}\sin\psi \qquad (A.2)$$

$$M_{q_i\theta} = M^{o}_{q_i\theta} + M^{s}_{q_i\theta}\sin\psi + M^{2c}_{q_i\theta}\cos(2\psi)$$

where

$$M^{o}_{q_i\dot{q}_j} = \frac{1}{2}\gamma\left[2G^{(x)}_{\theta ij} - \left(1-2\frac{c_{do}}{a}\right)\lambda G^{(0)}_{ij} + \left(1+\frac{c_{do}}{a}\right)F^{(x)}_{ij}\right.$$

$$+\lambda L^{(0)}_{\theta ij} + 2\frac{C_{do}}{a} L^{(I)}_{ij} - G^{(I)}_{\theta ji} + (2-\frac{C_{do}}{a})\lambda G^{(0)}_{ji} + 2\theta_0 L^{(I)}_{\theta ij} - \theta_0 G^{(I)}_{ji} \Big]$$

$$M^{S}_{\dot{\xi}_i \dot{\xi}_j} = \tfrac{1}{2}\gamma \Big[2\mu G^{(0)}_{\theta ij} + (1+\frac{C_{do}}{a})\mu F^{(0)}_{ij} - \mu G^{(0)}_{\theta ji} - 2\mu\theta_0 L^{(0)}_{\theta ij} - \mu\theta_0 G^{(0)}_{ji} \Big]$$

$$M^{C}_{\dot{\xi}_i \xi_j} = \tfrac{1}{2}\gamma \Big[2\mu D^{(I)}_{\theta ji} + \mu A^{(I)}_{ij} - \mu C^{(I)}_{\theta ij} \Big]$$

$$M^{2S}_{\dot{\xi}_i \xi_j} = \tfrac{1}{4}\gamma\mu^2 A^{(0)}_{ij} \qquad \text{(A.4)}$$

$$M^{0}_{\xi_i} = \tfrac{1}{2}\gamma \Big[W^{(II)}_{\theta i} - (1+\frac{C_{do}}{a})\lambda W^{(I)}_{i} + \lambda V^{(I)}_{\theta i} + \frac{C_{do}}{a} V^{(II)}_{i} - \lambda^2 V^{(0)}_{i} + \tfrac{1}{2}\mu^2 W^{(0)}_{\theta i} - \theta_0 V^{(II)}_{\theta i} - \tfrac{1}{2}\mu^2 V^{(0)}_{\theta i} + \lambda\theta_0 V^{(0)}_{i} \Big]$$

$$M^{S}_{\xi_i} = \tfrac{1}{2}\gamma \Big[2\mu W^{(I)}_{\theta i} - \lambda\mu W^{(0)}_{i} - 2\mu\theta_0 V^{(I)}_{\theta i} + \lambda\mu\theta_0 V^{(0)}_{i} \Big]$$

$$M^{0}_{\xi_i \theta} = \tfrac{1}{2}\gamma \Big[W^{(II)}_{i} + \tfrac{1}{2}\mu^2 W^{(0)}_{i} + 2\lambda V^{(I)}_{i} - V^{(II)}_{\theta i} - \tfrac{1}{2}\mu^2 V^{(0)}_{\theta i} - \theta_0 V^{(II)}_{i} - \tfrac{1}{2}\mu^2\theta_0 V^{(0)}_{i} \Big]$$

$$M^{S}_{\xi_i \theta} = \tfrac{1}{2}\gamma \Big[2\mu W^{(I)}_{i} - 2\mu V^{(I)}_{\theta i} - 2\mu\theta_0 V^{(I)}_{i} + 2\lambda\mu V^{(0)}_{i} \Big]$$

$$M^{2C}_{\xi_i \theta} = \tfrac{1}{2}\gamma \Big[-\tfrac{1}{2}\mu^2 W^{(0)}_{i} - \tfrac{1}{2}\mu^2 V^{(0)}_{\theta i} + \tfrac{1}{2}\mu^2\theta_0 V^{(0)}_{i} \Big]$$

and

$$G^{(K)}_{\theta ij} = \int \theta_s x^{(K)} W_i V_j \, dx \,, \quad G^{(K)}_{ij} = \int x^{(K)} W_i V_j \, dx$$

$$F^{(K)}_{\theta ij} = \int \theta_s x^{(K)} W_i W_j \, dx \,, \quad F^{(K)}_{ij} = \int x^{(K)} W_i W_j \, dx \qquad \text{(A.5)}$$

$$L^{(K)}_{\theta ij} = \int \theta_s x^{(K)} V_i V_j \, dx \,, \quad L^{(K)}_{ij} = \int x^{(K)} V_i V_j \, dx$$

$$W^{(K)}_{\theta i} = \int \theta_s x^{(K)} W_i \, dx \,, \quad W^{(K)}_{i} = \int x^{(K)} W_i \, dx$$

$$V^{(K)}_{\theta i} = \int \theta_s x^{(K)} V_i \, dx \,, \quad V^{(K)}_{i} = \int x^{(K)} V_i \, dx$$

$$A_{ij}^{(k)} = \int \chi^{(k)} W_i W_j' dx \quad , \quad C_{\theta ij}^{(k)} = \int \theta_s \chi^{(k)} V_i W_j' dx$$

$$D_{\theta ij}^{(k)} = \int \theta_s \chi^{(k)} V_i' W_j dx$$

It should be noted i and j take 1 or 2.

APPENDIX B

EXPRESSIONS ASSOCIATED WITH MODAL EQUATIONS

Coefficients used in Eq. 6.4 are defined as follows:

Inertial Coefficients

$$I_i = \frac{R^3}{I_B}\int\Big[m W_i^2 + m V_i^2 + I_o\bar{\Phi}_i^2 + (I_o + m x^2\delta_D^2$$

$$- 2m\frac{\chi_I}{R} x\delta_D \sin\theta_{TW})\Theta_i^2 + 2(m x\delta_D - m\frac{\chi_I}{R}\sin\theta_{TW})V_i\Theta_i$$

$$- 2(m\frac{\chi_I}{R}\cos\theta_{TW})W_i\Theta_i - 2(m\frac{\chi_I}{R}\sin\theta_{TW})V_i\bar{\Phi}_i$$

$$- 2(m\frac{\chi_I}{R}\cos\theta_{TW})W_i\bar{\Phi}_i + 2(I_o - m\frac{\chi_I}{R}x\delta_D\sin\theta_{TW})\bar{\Phi}_i\Theta_i\Big]dx$$

$$S_{ij\dot{\beta}} = \frac{R^3}{I_B}(\beta_p + \delta_D\cos\theta_o)\int 2m(V_i W_j - W_i V_j)dx$$

$$+ \frac{R^3}{I_B}\int\Big\{-4m\left(\frac{\chi_I}{R}\right)\sin\theta_o\sin\theta_{TW}W_i W_j'$$

$$+ 2m\left(\frac{\chi_I}{R}\right)\sin(\theta_o - \theta_{TW})W_i V_j'$$

$$+ 2m\left(\frac{\chi_I}{R}\right)\sin(\theta_o - \theta_{TW})V_i W_j' + 4m\left(\frac{\chi_I}{R}\right)\cos\theta_o\cos\theta_{TW}V_i V_j'\Big\}dx$$

$$C_{ij\zeta} = \frac{R^3}{I_B}\int m\left(\frac{\chi_I}{R}\right)\Big\{(W_i\cos\theta_{TW} + V_i\sin\theta_{TW})(x\bar{\Phi}_j' + \bar{\Phi}_j)$$

$$- \bar{\Phi}_i(x W_j' + x V_j')\Big\}dx + \frac{R^3}{I_B}\int m\left(\frac{e_w}{R}\right)\Big\{(W_i\cos\theta_{TW}$$

$$+ V_i\sin\theta_{TW})(-\bar{\Phi}_j - x\bar{\Phi}_j' + T_o\bar{\Phi}_j'')$$

$$- \bar{\Phi}_i(W_j''\cos\theta_{TW} + V_j''\sin\theta_{TW})\Big\}dx \qquad (B.1)$$

where

$$T_o = \int_x' m x dx \qquad (B.2)$$

Steady-State Deflection Coefficients

$$E_{kij\ddot{\beta}\ddot{\zeta}} = \frac{R^3}{I_B}\int\Big[m\Theta_i(W_k V_j - V_k W_j)$$

$$+ m\Theta_j(W_k V_i - V_k W_i)\Big]dx$$

$$E_{\alpha ij\dot{\beta}\dot{\beta}} = \frac{R^3}{I_B}\int\left[2m\left(W_\alpha V_i - V_\alpha W_i\right)\textcircled{H}_j\right]dx$$

$$E_{\alpha ij\bar{\beta}\dot{\beta}} = \frac{R^3}{I_B}\int 2m\left[\left\{V_i\int_0^x\left(W'_\alpha W'_j + V'_\alpha V'_j\right)dx_0\right\} - W'_\alpha W_i V_j - V'_\alpha V_i V_j\right]dx$$

$$E_{\alpha ij\ddot{\beta}\beta} = \frac{R^3}{I_B}\int m\,\textcircled{H}_i\left(V_\alpha W_j - W_\alpha V_j\right)dx \qquad \text{(B.3)}$$

$$E_{\alpha ij\dot{\beta}\beta} = \frac{R^3}{I_B}\int 2m\Big[-V_\alpha W_i W'_j - V_\alpha V_i V'_j + V_i\int_0^x\left(W'_\alpha W'_j + V'_\alpha V'_j\right)dx_0 - W_i W''_j\int_x^1 W_\alpha dx_0 + V_i V''_j\int_x^1 V_\alpha dx_0\Big]dx$$

$$E_{\alpha ij\beta\beta} = \frac{R^3}{I_B}\int\Big[m\Big\{-V_\alpha W_i\textcircled{H}_j - W_\alpha V_i\textcircled{H}_j - V_\alpha W_j\textcircled{H}_i\cos(2\theta_0) - W_\alpha V_j\textcircled{H}_i\cos(2\theta_0)\Big\} - \left(\frac{EI_F}{\Omega^2R^4} - \frac{EI_C}{\Omega^2R^4}\right)\Phi_i\Big\{V''_\alpha W''_j\cos(2\theta_0) - W''_\alpha W''_j\sin(2\theta_0) + V''_\alpha V''_j\sin(2\theta_0) + W''_\alpha V''_j\cos(2\theta_0)\Big\}\Big]dx$$

Aerodynamic Coefficients

$$\begin{aligned}A_{ij\dot{\beta}} = \frac{1}{2}\gamma\Big[&-2G^{(I)}_{\theta ij} + \lambda G^{(0)}_{ij} - F^{(I)}_{ij} - \lambda L^{(0)}_{\theta ij} - 2\frac{c_{d_0}}{a}L_{ij} - 2\theta_0 L^{(I)}_{\theta ij}\\ &+ G^{(I)}_{\theta ji} - 2\lambda G^{(0)}_{ji} + \theta_0 G^{(I)}_{ji} - \left(\frac{c}{R}\right)A^{(I)}_{\phi i v_j} + \lambda\left(\frac{c}{R}\right)B^{(0)}_{\phi i v_j} + \lambda\left(\frac{c}{R}\right)A^{(0)}_{\phi i w_j}\\ &+ \left(\frac{c}{R}\right)B^{(I)}_{\phi i w_j} + \left(\frac{c}{R}\right)^2 C^{(I)}_{\phi i\phi_j} + \left(\frac{c}{R}\right)^2 C^{(I)}_{\phi i}\textcircled{H}_j - \left(\frac{c}{R}\right)A^{(I)}_{v_j}\textcircled{H}_i\\ &+ \lambda\left(\frac{c}{R}\right)B^{(0)}_{v_j}\textcircled{H}_i + \lambda\left(\frac{c}{R}\right)A^{(0)}_{w_j}\textcircled{H}_i + \left(\frac{c}{R}\right)B^{(I)}_{w_j}\textcircled{H}_i + \left(\frac{c}{R}\right)^2 C^{(I)}_{\phi_j}\textcircled{H}_i\\ &+ \left(\frac{c}{R}\right)^2 C^{(I)}\textcircled{H}_i\textcircled{H}_j - \lambda\delta_D V^{(I)}_{\theta j}\textcircled{H}_i - 2\frac{c_{d_0}}{a}\delta_D V^{(II)}_j\textcircled{H}_i\\ &+ \delta_D W^{(II)}_{\theta j}\textcircled{H}_i - 2\lambda\delta_D W^{(I)}_j\textcircled{H}_i - 2\delta_D W^{(II)}_{\theta i}\textcircled{H}_j + \left(\frac{c}{R}\right)D^{(I)}_{v_i}\textcircled{H}_j\\ &+ \left(\frac{c}{R}\right)D^{(I)}_{w_i\phi_j} + \left(\frac{c}{R}\right)\lambda D^{(0)}_{v_i}\textcircled{H}_j + \left(\frac{c}{R}\right)\lambda D^{(0)}_{v_i\phi_j}\Big]\end{aligned}$$

$$A^{1S}_{ij\dot\beta\dot\beta} = \tfrac{1}{2}\gamma\Big[-2\mu G^{(0)}_{\theta ij} - \mu F^{(0)}_{ij} - 2\mu\theta_0 L^{(0)}_{\theta ij} + \mu G^{(0)}_{\theta ji} + \mu\theta_0 G^{(0)}_{ji}$$
$$- \mu\left(\tfrac{c}{R}\right) A^{(0)}_{\phi i v_j} + \mu\left(\tfrac{c}{R}\right) B^{(0)}_{\phi i w_j} + \mu\left(\tfrac{c}{R}\right)^2 C^{(0)}_{\phi i \phi_j} + \mu\left(\tfrac{c}{R}\right)^2 C^{(0)}_{\phi_i}\textcircled{H}_j$$
$$- \mu\left(\tfrac{c}{R}\right) A^{(0)}_{v_j}\textcircled{H}_i + \mu\left(\tfrac{c}{R}\right) B^{(0)}_{w_j}\textcircled{H}_i + \mu\left(\tfrac{c}{R}\right)^2 C_{\phi_j}\textcircled{H}_i + \mu\left(\tfrac{c}{R}\right)^2 C^{(0)}\textcircled{H}_i\textcircled{H}_j$$
$$+ \mu\delta_D W^{(I)}_{\theta j}\textcircled{H}_i - 2\mu\delta_D W^{(I)}_{\theta i}\textcircled{H}_j + \mu\left(\tfrac{c}{R}\right) D^{(0)}_{w_i}\textcircled{H}_j + \mu\left(\tfrac{c}{R}\right) D^{(0)}_{w_i\phi_j}\Big]$$

$$A^{1C}_{\underset{k}{}ij\dot\beta\dot\beta} = \tfrac{1}{2}\gamma\Big[\mu_{w_k} G^{(0)}_{ij} - \mu_{v_k} F^{(0)}_{ij} - \mu_{w_k} L^{(0)}_{\theta ij}\Big]$$

$$A^{1C}_{ij\,\dot\beta} = \tfrac{1}{2}\gamma\Big[\mu(\beta_P+\delta_D)\left(G^{(0)}_{ij} - L^{(0)}_{\theta ij} - 2G^{(0)}_{ji}\right)\Big]$$

$$A_{\underset{k}{}ij\dot\beta\dot\beta} = \tfrac{1}{2}\gamma\Big[{}_{w_k}G^{(0)}_{ij} + {}_{v_k}F^{(0)}_{ij} - {}_{w_k}L^{(0)}_{\theta ij} - 2\,{}_{w_k}G^{(0)}_{ji} + \left(\tfrac{c}{R}\right){}_{v_k}A^{(0)}_{\phi i v_j}$$
$$+ \left(\tfrac{c}{R}\right){}_{w_k}B^{(0)}_{\phi i v_j} + \left(\tfrac{c}{R}\right){}_{w_k}A^{(0)}_{\phi i w_j} - \left(\tfrac{c}{R}\right){}_{v_k}B^{(0)}_{\phi i w_j} - \left(\tfrac{c}{R}\right)^2{}_{v_k}C^{(0)}_{\phi i \phi_j}$$
$$- \left(\tfrac{c}{R}\right)^2{}_{v_k}C^{(0)}_{\phi_i}\textcircled{H}_j + \left(\tfrac{c}{R}\right){}_{v_k}A^{(0)}_{v_j}\textcircled{H}_i + \left(\tfrac{c}{R}\right)B^{(0)}_{v_j}\textcircled{H}_i + \left(\tfrac{c}{R}\right){}_{w_k}A^{(0)}_{w_j}\textcircled{H}_i$$
$$- \left(\tfrac{c}{R}\right){}_{v_k}B_{w_j}\textcircled{H}_i - \left(\tfrac{c}{R}\right)^2{}_{v_k}C_{\phi_j}\textcircled{H}_i - \left(\tfrac{c}{R}\right)^2{}_{v_k}C^{(0)}\textcircled{H}_i\textcircled{H}_j$$
$$- 2\delta_D\,{}_{w_k}W^{(I)}_j\textcircled{H}_i - \delta_D\,{}_{w_k}V^{(I)}_{\theta j}\textcircled{H}_i\Big]$$

$$A_{\underset{k}{}ij\dot\beta\dot\beta} = \tfrac{1}{2}\gamma\Big[-\lambda\,{}_{w_k}V^{(0)}_{\theta j}\textcircled{H}_i - 2\tfrac{c_0}{a}\,{}_{w_k}V^{(I)}_j\textcircled{H}_i + {}_{w_k}V^{(I)}_{\theta j}\textcircled{H}_i - 2\lambda\,{}_{w_k}W^{(0)}_j\textcircled{H}_i$$
$$- 2\,{}_{w_k}W^{(0)}_{\theta i}\textcircled{H}_j + \lambda\,{}_{w_k}W^{(0)}_i\textcircled{H}_j + {}_{v_k}W^{(I)}_{\theta i}\textcircled{H}_j + \mu\,{}_{v_k}W^{(0)}_i\textcircled{H}_j - 2\,{}_{v_k}V^{(0)}_{\theta j}\textcircled{H}_i$$
$$- \lambda\,{}_{v_k}V^{(0)}_j\textcircled{H}_i + {}_{v_k}W^{(I)}_j\textcircled{H}_i - \lambda\,{}_{w_k}V^{(0)}_{\theta i}\textcircled{H}_j - 2\tfrac{c_0}{a}\,{}_{w_k}V^{(I)}_i\textcircled{H}_j$$
$$- {}_{v_k}V^{(I)}_{\theta i}\textcircled{H}_j - \mu\,{}_{v_k}V^{(0)}_{\theta i}\textcircled{H}_j + 2\lambda\,{}_{v_k}V^{(0)}_i\textcircled{H}_j\Big]$$

$$A_{ij\,\beta} = \tfrac{1}{2}\gamma\Big[W^{(II)}_i\textcircled{H}_j + \tfrac{1}{2}\mu^2 W^{(0)}_i\textcircled{H}_j + F^{(II)}_{v_i\phi_j} + \tfrac{1}{2}\mu^2 F^{(0)}_{v_i\phi_j}$$
$$+ 2\lambda V^{(I)}_i\textcircled{H}_j + 2\lambda L^{(I)}_{v_i\phi_j} - L^{(II)}_{v_i\phi_j} - V^{(II)}_{\theta i}\textcircled{H}_j - \theta_0 L^{(II)}_{v_i\phi_j}$$
$$- \theta_0 V^{(II)}_i\textcircled{H}_j - \tfrac{1}{2}\mu^2\theta_0 L^{(0)}_{v_i\phi_j} - \tfrac{1}{2}\mu^2\theta_0 V^{(0)}_i\textcircled{H}_j$$
$$- \left(\tfrac{c}{R}\right)B^{(I)}_{\phi_i\phi_j} - \tfrac{1}{2}\mu^2\left(\tfrac{c}{R}\right)B^{(0)}_{\phi_i\phi_j} - \left(\tfrac{c}{R}\right)B^{(II)}_{\phi_i}\textcircled{H}_j - \tfrac{1}{2}\mu^2\left(\tfrac{c}{R}\right)B^{(0)}_{\phi_i}\textcircled{H}_j$$
$$- \left(\tfrac{c}{R}\right)B^{(II)}_{\phi_j}\textcircled{H}_i - \tfrac{1}{2}\mu^2\left(\tfrac{c}{R}\right)B^{(0)}_{\phi_j}\textcircled{H}_i - \left(\tfrac{c}{R}\right)B^{(II)}\textcircled{H}_i\textcircled{H}_j$$

$$-\tfrac{1}{2}\mu^2\left(\tfrac{c}{R}\right)B^{(0)}\Theta_i\Theta_j + \lambda W_{\theta j}^{(I)}\Theta_i - \lambda^2 W_j^{(I)}\Theta_i + \tfrac{c_{a_0}}{a} W_j^{(II)}\Theta_i$$
$$- V_{\theta j}^{(II)}\Theta_i - \lambda V_j^{(I)}\Theta_i + \lambda\delta_D \Phi_j^{(II)}\Theta_i + \tfrac{1}{3}\lambda\delta_D \Theta_i\Theta_j$$
$$+ \tfrac{1}{2}\mu^2(\beta_p+\delta_D) H_{w_i v_j'} - \tfrac{1}{2}\mu^2(\beta_p+\delta_D) L_{\theta v_i v_j'}$$
$$-\mu^2(\beta_p+\delta_D) H_{v_i w_j'}]$$

$$A^{1S}_{\alpha ij\beta\delta} = \tfrac{1}{2}\gamma\left[\mu_{w_\alpha} W_{\theta j}^{(0)}\Theta_i + 2\mu_{v_\alpha} V_{\theta j}^{(0)}\Theta_i + \mu_{v_\alpha} W_j^{(0)}\Theta_i - 2\mu_{w_\alpha} W_{\theta i}^{(0)}\Theta_j\right]$$

$$A^{1C}_{ij\beta} = \tfrac{1}{2}\gamma\left[-2\mu H_{\theta w_i v_j'}^{(I)} + \lambda\mu H_{w_i v_j'}^{(0)} - \mu F_{w_i w_j'}^{(I)} - \lambda\mu L_{\theta v_i v_j'}^{(0)}\right.$$
$$- 2\tfrac{c_{a_0}}{a}\mu L_{v_i v_j'}^{(I)} + \mu H_{\theta v_i w_j'}^{(I)} - 2\lambda\mu H_{v_i w_j'}^{(I)} + (\beta_p+\delta_D)\mu V_i^{(I)}\Theta_j$$
$$+(\beta_p+\delta_D)\mu L_{v_i\phi_j}^{(I)} - \mu\left(\tfrac{c}{R}\right) A_{\phi_i v_j'} + \mu\left(\tfrac{c}{R}\right) B_{\phi_i w_j'}^{(I)}$$
$$\left.-\mu\left(\tfrac{c}{R}\right) A_{v_j}^{(I)}\Theta_i + \left(\tfrac{c}{R}\right)\mu B_{w_j}^{(I)}\Theta_i\right]$$

$$A^{1S}_{ij\beta} = \tfrac{1}{2}\gamma\left[2\mu W_i^{(I)}\Theta_j + 2\mu L_{w_i\phi_j}^{(I)} - 2\mu\left(\tfrac{c}{R}\right) B_{\phi_i\phi_j}^{(I)}\right.$$
$$-2\mu\left(\tfrac{c}{R}\right) B_{\phi_i}^{(I)}\Theta_j - 2\mu\left(\tfrac{c}{R}\right) B_{\phi_j}^{(I)}\Theta_i - 2\mu\left(\tfrac{c}{R}\right) B^{(I)}\Theta_i\Theta_j$$
$$-2\mu V_{\theta j}^{(I)}\Theta_i + \lambda\mu V_j^{(0)}\Theta_i - 2\mu V_{\theta i}^{(I)}\Theta_j + 2\lambda\mu V_i^{(0)}\Theta_j$$
$$\left.+2\lambda\mu L_{v_i\phi_j}^{(0)} - 2\theta_0\mu V_i^{(I)}\Theta_j - 2\theta_0\mu L_{v_i\phi_j}^{(I)}\right]$$

$$A^{2S}_{ij\beta} = \tfrac{1}{2}\gamma\left[-\mu^2 H_{\theta w_i v_j'}^{(0)} - \tfrac{1}{2}\mu^2 F_{w_i w_j'}^{(0)} + \tfrac{1}{2}\mu^2 H_{\theta v_i w_j'}^{(0)}\right.$$
$$+\tfrac{1}{2}\mu^2(\beta_p+\delta_D) V_i^{(0)}\Theta_j + \tfrac{1}{2}\mu^2(\beta_p+\delta_D) L_{v_i\phi_j}^{(0)}$$
$$-\tfrac{1}{2}\mu^2\left(\tfrac{c}{R}\right) A_{\phi_i w_j'}^{(0)} + \left(\tfrac{c}{R}\right)\mu^2 B_{\phi_i w_j'}^{(0)} - \tfrac{1}{2}\left(\tfrac{c}{R}\right)\mu^2 A_{ii'}^{(0)}\Theta_i$$
$$\left.+\tfrac{1}{2}\mu^2\left(\tfrac{c}{R}\right) B_{w_j'}^{(0)}\Theta_i\right]$$

$$A^{2C}_{ij\beta} = \tfrac{1}{2}\gamma\left[-\tfrac{1}{2}\mu^2 W_i^{(0)}\Theta_j - \tfrac{1}{2}\mu^2 F_{v_i\phi_j}^{(0)} + \tfrac{1}{2}\mu^2\left(\tfrac{c}{R}\right)^2 B_{\phi_i\phi_j}^{(0)}\right.$$
$$+\tfrac{1}{2}\mu^2\left(\tfrac{c}{R}\right) B_{\phi_i}^{(0)}\Theta_j + \tfrac{1}{2}\mu^2\left(\tfrac{c}{R}\right) B_{\phi_j}^{(0)}\Theta_i + \tfrac{1}{2}\mu^2\left(\tfrac{c}{R}\right) B^{(0)}\Theta_i\Theta_j$$
$$\left.-\tfrac{1}{2}\mu^2(\beta_p+\delta_D) H_{w_i v_j'}^{(0)} - \tfrac{1}{2}\mu^2(\beta_p+\delta_D) L_{\theta v_i v_j'}^{(0)}\right.$$

$$- \mu^2(\beta_p+\delta_0)\, H_{v_i w_j'} + \tfrac{1}{2}\mu^2\theta_0\, L^{(0)}_{v_i\phi_j} - \tfrac{1}{2}\mu^2 V^{(0)}_{\theta_i}\textcircled{H}_j$$
$$+ \tfrac{1}{2}\mu^2\theta_0\, V_i^{(0)}\textcircled{H}_j\Big]$$

$$A_{kij\,\text{ggg}} = \tfrac{1}{2}\gamma\Big[-2_{v_k}W_i^{(I)}\textcircled{H}_j - 2_{v_k}F^{(I)}_{\omega_i\phi_j} + 2_{w_k}V_i^{(I)}\textcircled{H}_j + \theta_0{}_{v_k}V_i^{(I)}\textcircled{H}_j$$
$$+ \theta_0{}_{v_k}L^{(I)}_{v_i\phi_j} + 2\left(\tfrac{c}{R}\right)_{v_k}B^{(0)}_{\phi_i\phi_j} + 2\left(\tfrac{c}{R}\right)_{v_k}B^{(0)}_{\theta_i}\textcircled{H}_j + 2\left(\tfrac{c}{R}\right)_{v_k}B^{(0)}_{\phi_j}\textcircled{H}_i$$
$$+ 2\left(\tfrac{c}{R}\right)_{v_k}B^{(0)}\textcircled{H}_i\textcircled{H}_j - \lambda\,{}_{v_k}W^{(0)}_{\theta_j}\textcircled{H}_i - 2\tfrac{C_{d_0}}{a}\,{}_{v_k}W_j^{(I)}\textcircled{H}_i + {}_{w_k}W^{(I)}_{\theta_j}\textcircled{H}_i$$
$$- 2\lambda_{w_k}W_j^{(0)}\textcircled{H}_i + 2\,{}_{v_k}V^{(I)}_{\theta_j}\textcircled{H}_i - \lambda\,{}_{v_k}V_j^{(0)}\textcircled{H}_i + {}_{w_k}V_j^{(I)}\textcircled{H}_i + \delta_0{}_{w_k}\Phi_j^{(I)}\textcircled{H}_i$$
$$+ \delta_0\, W_k^{(II)}\textcircled{H}_i\textcircled{H}_j\Big]$$

$$A_{kij\,\text{ggg}} = \tfrac{1}{2}\gamma\Big[-{}_{v_k}\Phi_j^{(II)}\textcircled{H}_i - \tfrac{1}{2}\mu^2\,{}_{v_k}\Phi_j^{(0)}\textcircled{H}_i - V_k^{(II)}\textcircled{H}_i\textcircled{H}_j - \tfrac{1}{2}\mu^2 V_k^{(0)}\textcircled{H}_i\textcircled{H}_j$$
$$+ \lambda\,{}_{w_k}\Phi_j^{(I)}\textcircled{H}_i + \lambda\, W_k^{(I)}\textcircled{H}_i\textcircled{H}_j - \lambda\, V_\theta^{(I)}\textcircled{H}_i\textcircled{H}_j + \lambda^2 V_k^{(0)}\textcircled{H}_i\textcircled{H}_j$$
$$+ \tfrac{C_{d_0}}{a}\,V_k^{(II)}\textcircled{H}_i\textcircled{H}_j - {}_\theta W_k^{(II)}\textcircled{H}_i\textcircled{H}_j + \lambda W_k^{(I)}\textcircled{H}_i\textcircled{H}_j + \tfrac{1}{2}\mu^2\,{}_{w_k}W^{(0)}_{\omega_i v_j'}$$
$$- \tfrac{1}{2}\mu^2\,{}_{v_k}F^{(0)}_{\omega_i w_j'} - \tfrac{1}{2}\mu^2\,{}_{w_k}L_{v_i v_j'} - \mu^2\,{}_{w_k}V_{v_i w_j'}\Big]$$

$$A^{1S}_{kij\,\text{ggg}} = \tfrac{1}{2}\gamma\Big[\mu_{w_k}W^{(0)}_{\theta_j}\textcircled{H}_i + 2\mu\,{}_{v_k}V^{(0)}_{\theta_j}\textcircled{H}_i - \mu\,{}_{w_k}V_j^{(0)}\textcircled{H}_i - 2\mu\,{}_{v_k}F^{(0)}_{\omega_i\phi_j}$$
$$- 2\mu_{v_k}W_i^{(0)}\textcircled{H}_j + \mu_{w_k}V_i\textcircled{H}_j + \mu_{w_k}V_j^{(0)}\textcircled{H}_i - 2\mu_{v_k}F^{(0)}_{\omega_i\phi_j} - 2\mu_{v_k}W_i^{(0)}\textcircled{\theta}_j$$
$$+ \mu_{w_k}V_i\textcircled{H}_j + \mu_{w_k}L_{v_i\phi_j} + 2\mu\theta_0{}_{v_k}L^{(0)}_{v_i\phi_j} + 2\mu\theta_0{}_{v_k}V_i^{(0)}\textcircled{H}_j\Big]$$

$$A^{1C}_{kij\,\text{ggg}} = \tfrac{1}{2}\gamma\Big[\mu_{w_k}H^{(0)}_{\omega_i v_j'} + \mu_{v_k}F^{(0)}_{\omega_i\omega_j'} - \mu_{w_k}L^{(0)}_{\theta v_i v_j'} - 2\mu_{w_k}V^{(0)}_{v_i\omega_j'}\Big]$$

$$A^{1S}_{kij\,\text{ggg}} = \tfrac{1}{2}\gamma\Big[-2\mu\,{}_{v_k}\Phi_j^{(I)} - 2\mu V_k^{(II)}\textcircled{H}_i\textcircled{H}_j - 2\mu_\theta W_k^{(I)}\textcircled{H}_i\textcircled{H}_j$$
$$+ \lambda\mu W_k^{(0)}\textcircled{H}_i\textcircled{H}_j\Big]$$

$$A^{2S}_{kij\,\text{ggg}} = \tfrac{1}{2}\gamma\Big[\tfrac{1}{2}\mu^2\,{}_{w_k}W^{(0)}_{\theta_j}\textcircled{H}_i + \mu^2\,{}_{v_k}V^{(0)}_{\theta_j} + \tfrac{1}{2}\mu^2\,{}_{w_k}V_j^{(0)}\textcircled{H}_i + \tfrac{1}{2}\mu^2 V_k^{(0)}\textcircled{H}_i\textcircled{H}_j$$
$$+ \tfrac{1}{2}\mu^2\,{}_{w_k}V_i\textcircled{H}_j + \tfrac{1}{2}\mu^2\,{}_{w_k}L_{v_i\phi_j}\Big]$$

$$A^{1c}_{kij\bar{g}\bar{g}} = \tfrac{1}{2}\gamma\Big[\tfrac{1}{2}\mu^2_{v_k}\bar{\Phi}^{(0)}_j \Theta_i + \tfrac{1}{2}\mu^2_{w_k} H^{(0)}_{w_i v_j} - \tfrac{1}{2}\mu^2_{v_k} F^{(0)}_{w_i w_j}$$
$$- \tfrac{1}{2}\mu^2_{w_k} L^{(0)}_{v_i v_j} - \mu^2_{w_k} H^{(0)}_{v_i w_j} - 2\theta_0 \mu_{v_k} L^{(I)}_{v_i \phi_j} - 2\theta_0 \mu_{v_k} V^{(I)}_i \Theta_j$$
$$+ 2\mu_{v_k} F^{(I)}_{w_i \phi_j} + 2\mu_{v_k} W^{(I)}_i \Theta_j - 2\mu_{w_k} G^{(0)}_{ji} + \mu_{w_k} V^{(I)}_i \Theta_j$$
$$+ \mu_{w_k} L^{(I)}_{v_i \phi_j}\Big]$$

$$A^{2c}_{kij\bar{g}\bar{g}} = \tfrac{1}{2}\gamma\Big[\tfrac{1}{2}\mu^2_{v_k}\bar{\Phi}^{(0)}_j \Theta_i + \tfrac{1}{2}\mu^2_{w_k} H^{(0)}_{v_i v_j} - \tfrac{1}{2}\mu^2_{v_k} F^{(0)}_{w_i w_j}$$
$$- \tfrac{1}{2}\mu^2_{w_k} L^{(0)}_{v_i v_j} - \mu^2_{w_k} H^{(0)}_{j w_i}\Big]$$

$$G_i = \tfrac{1}{2}\gamma\Big[W^{(I)}_i - V^{(I)}_{\theta i} + 2\lambda V^{(0)}_i - \theta_0 V^{(I)}_i - \lambda\left(\tfrac{c}{R}\right) A^{(0)}_{\phi i}$$
$$- \left(\tfrac{c}{R}\right) B^{(I)}_{\phi i} - \lambda\left(\tfrac{c}{R}\right) A^{(0)} \Theta_i - \left(\tfrac{c}{R}\right) B^{(I)} \Theta_i - \delta_D \theta^{(II)} \Theta_i$$
$$+ \lambda\delta_D \Theta_i\Big] \cos\alpha_s$$
$$+ \tfrac{1}{2}\gamma\Big[\mu W^{(0)}_{\theta i} + \tfrac{1}{2}\mu\left(\tfrac{c}{R}\right) A^{(0)}_{\phi i} + \tfrac{1}{2}\mu A^{(0)} \Theta_i - \theta_0 \mu V^{(0)}_{\theta i}\Big]$$
$$\times \sin\alpha_s$$

$$G_{ki\bar{g}} = \tfrac{1}{2}\gamma\Big[-{}_{v_k} W^{(0)}_i + 2_{w_k} V_i - \left(\tfrac{c}{R}\right)_{w_k} A^{(0)}_{\phi i} + \left(\tfrac{c}{R}\right)_{v_k} B^{(0)}_{\phi i}$$
$$- \left(\tfrac{c}{R}\right)_{w_k} A^{(0)} \Theta_i + \left(\tfrac{c}{R}\right)_{v_k} B^{(0)} + V^{(0)}_k \Theta_i$$
$$+ 2\delta_D W^{(I)}_k \Theta_i\Big] \cos\alpha_s$$

$$G^{1c}_i = \tfrac{1}{2}\gamma\Big[2\mu(\beta_p + \delta_D) V_i\Big] \cos\alpha_s$$

$$G^{1c}_{ki\bar{g}} = \tfrac{1}{2}\gamma\Big[2\mu_{w_k} V_i + \mu_{v_k} W_i\Big] \cos\alpha_s$$

$$G^{1s}_i = \tfrac{1}{2}\gamma\Big[2 W^{(I)}_{\theta i} - \lambda W^{(0)}_i + \lambda V_{\theta i} + 2\tfrac{C_{d_0}}{a} V^{(I)}_i$$
$$- 2\theta_0 V^{(I)}_{\theta i} + \left(\tfrac{c}{R}\right) A_{\phi i} - \lambda\left(\tfrac{c}{R}\right) B^{(0)}_{\phi i} + \left(\tfrac{c}{R}\right) A^{(I)} \Theta_i$$
$$- \lambda\left(\tfrac{c}{R}\right) B^{(0)} \Theta_i + \lambda\delta_D \theta^{(I)} \Theta_i + \tfrac{2}{3}\tfrac{C_{d_0}}{a}\delta_D \Theta_i\Big] \sin\alpha_s$$
$$+ \tfrac{1}{2}\gamma\Big[\mu W^{(0)}_i - \mu V^{(0)}_{\theta i} + \theta_0 \mu V^{(0)}_i - \mu\left(\tfrac{c}{R}\right) B^{(0)}_{\phi i}$$

$$- \mu \left(\frac{c}{R}\right) B^{(0)} \textcircled{H}_i - \mu \delta_D \theta^{(I)} \textcircled{H}_i \Big] \cos\alpha_s$$

$$G_i^{2S} = \tfrac{1}{2}\gamma \left[-\mu(\delta_D + \beta_p) W_i + \mu(\beta_p + \delta_D) V_{\theta i} \right] \sin\alpha_s$$

$$G_{ki\bar{\xi}}^{1S} = \tfrac{1}{2}\gamma \Big[-2 {}_{\theta}V_k^{(I)} \textcircled{H}_i + \lambda V_k^{(0)} \textcircled{H}_i + \lambda {}_{\theta}W_k^{(0)} \textcircled{H}_i + 2 \frac{C_{d_0}}{a} W_k^{(I)} \textcircled{H}_i \Big] \sin\alpha_s + \tfrac{1}{2}\gamma \Big[-\mu V_k^{(0)} \textcircled{H}_i - \mu {}_{\theta}W_k^{(I)} \textcircled{H}_i \Big] \cos\alpha_s$$

$$G_{ki\bar{\xi}}^{2C} = \tfrac{1}{2}\gamma \Big[-\mu {}_{\theta}V_k^{(0)} \textcircled{H}_i \Big] \sin\alpha_s$$

$$G_{ki\bar{\xi}}^{2S} = \tfrac{1}{2}\gamma \Big[-\mu_{W_k} W_i + \mu_{V_k} V_i \Big] \sin\alpha_s$$

$$G_{ki\bar{\xi}}^{1S} = \tfrac{1}{2}\gamma \Big[-{}_{W_k}W_i^{(0)} + {}_{W_k}V_{\theta i} - \left(\frac{c}{R}\right)_{V_k} A_{\Phi i}^{(0)} - \left(\frac{c}{R}\right)_{W_k} B_{\Phi i}^{(0)} - \left(\frac{c}{R}\right)_{V_k} A^{(0)} \textcircled{H}_i - \left(\frac{c}{R}\right)_{W_k} B^{(0)} \textcircled{H}_i + \delta_D {}_{\theta}W_k^{(I)} \textcircled{H}_i \Big] \sin\alpha_s$$

$$G_{ki\bar{\xi}} = \tfrac{1}{2}\gamma \Big[-{}_{\theta}W_k^{(I)} \textcircled{H}_i + 2\lambda W_k^{(0)} \textcircled{H}_i - V_k^{(I)} \textcircled{H}_i \Big] \cos\alpha_s$$

$$G_i^{2C} = \tfrac{1}{2}\gamma \Big[-\mu W_{\theta i}^{(0)} - \tfrac{1}{2}\mu \left(\frac{c}{R}\right) A_{\Phi i}^{(0)} - \tfrac{1}{2}\mu \left(\frac{c}{R}\right) A^{(0)} \textcircled{H}_i + \theta_0 \mu V_{\theta i}^{(0)} \Big] \sin\alpha_s \qquad \text{(B.4)}$$

where

$$A_{\Phi_i V_j}^{(K)} = \int A_M \chi^{(K)} \bar{\Phi}_i V_j \, dx \quad , \quad A_{\Phi_i W_j}^{(K)} = \int A_M \chi^{(K)} \bar{\Phi}_i \bar{W}_j dx \quad , \quad A_{\Phi_i}^{(K)} = \int A_M \chi^{(K)} \bar{\Phi}_i dx$$

$$A_{V_i}^{(K)} = \int A_M \chi^{(K)} V_i dx \quad , \quad A_{W_i}^{(K)} = \int A_M \chi^{(K)} \bar{W}_i \, dx \quad , \quad {}_{V_k}A_{\Phi_i V_j}^{(K)} = \int A_M \chi^{(K)} V_k \bar{\Phi}_i V_j dx$$

$${}_{W_k}A_{\Phi_i V_j}^{(K)} = \int A_M \chi^{(K)} V_k \bar{\Phi}_i V_j dx \quad , \quad {}_{V_k}A_{V_j}^{(K)} = \int A_M \chi^{(K)} V_k V_j dx \quad , \quad {}_{W_k}A_{W_j}^{(K)} = \int A_M \chi^{(K)} W_k W_j dx$$

$$A_{\Phi_i V_j'}^{(K)} = \int A_M \chi^{(K)} \bar{\Phi}_i V_j' dx \quad , \quad A_{V_j'}^{(K)} = \int A_M \chi^{(K)} V_j' dx \quad , \quad {}_{V_k}A_{\Phi_j}^{(K)} = \int A_M \chi^{(K)} V_k \Phi_j dx$$

$${}_{V_k}A^{(0)} = \int A_M \chi^{(K)} V_k dx$$

$$B^{(k)}_{\Phi_i V_j} = \int B_M x^{(k)} \overline{\Phi}_i V_j \, dx \,, \quad B^{(k)}_{\Phi_i W_j} = \int B_M x^{(k)} \Phi_i W_j \, dx \,, \quad B^{(k)}_{V_i} = \int B_M x^{(k)} V_i \, dx$$

$$B^{(k)}_{W_i} = \int B_M x^{(k)} V_i \, dx \,, \quad {}_{W_k}B^{(k)}_{\Phi_i V_j} = \int B_M x^{(k)} W_k \overline{\Phi}_i V_j \, dx \,, \quad {}_{V_k}B^{(k)}_{\Phi_i W_j} = \int B_M x^{(k)} V_k \overline{\Phi}_i W_j \, dx$$

$${}_{V_k}B^{(k)}_{W_i} = \int B_M x^{(k)} W_k V_j \, dx \,, \quad {}_{W_k}B^{(k)}_{W_i} = \int B_M x^{(k)} W_k W_i \, dx \,, \quad B^{(k)}_{\Phi_i \Phi_j} = \int B_M x^{(k)} \overline{\Phi}_i \overline{\Phi}_j \, dx$$

$$B^{(k)}_{\Phi_i} = \int B_M x^{(k)} \overline{\Phi}_i \, dx \,, \quad B^{(k)} = \int B_M x^{(k)} \, dx \,, \quad B^{(k)}_{\Phi_i V_j'} = \int B_M x^{(k)} \overline{\Phi}_i V_j' \, dx$$

$$B^{(k)}_{W_j'} = \int B_M x^{(k)} W_j' \, dx \,, \quad {}_{V_k}B^{(k)}_{\Phi_i \Phi_j} = \int B_M x^{(k)} V_k \overline{\Phi}_i \overline{\Phi}_j \, dx \,, \quad {}_{V_k}B^{(k)}_{\Phi_i} = \int B_M x^{(k)} V_k \overline{\Phi}_i \, dx$$

$${}_{V_k}B^{(k)} = \int B_M x^{(k)} V_k \, dx \,, \quad {}_{W_k}B^{(k)}_{\Phi_i} = \int B_M x^{(k)} W_k \overline{\Phi}_i \, dx \,, \quad {}_{W_k}B^{(k)} = \int B_M x^{(k)} W_k \, dx$$

$$C^{(k)}_{\Phi_i \Phi_j} = \int C_M x^{(k)} \overline{\Phi}_i \overline{\Phi}_j \, dx \,, \quad C^{(k)}_{\Phi_i} = \int C_M x^{(k)} \overline{\Phi}_i \, dx \,, \quad C^{(k)} = \int C_M x^{(k)} \, dx$$

$${}_{V_k}C^{(k)}_{\Phi_i \Phi_j} = \int C_M x^{(k)} V_k \overline{\Phi}_i \overline{\Phi}_j \, dx \,, \quad {}_{V_k}C^{(k)}_{\Phi_i} = \int C_M x^{(k)} V_k \overline{\Phi}_i \, dx \,, \quad {}_{V_k}C^{(0)} = \int C_M x^{(k)} V_k \, dx$$

$$D^{(k)}_{W_i \Phi_j} = \int D_M x^{(k)} W_i \overline{\Phi}_j \, dx \,, \quad D^{(k)}_{W_i} = \int D_M x^{(k)} W_i \, dx \,, \quad D^{(k)}_{V_i \Phi_j} = \int D_M x^{(k)} V_i \overline{\Phi}_j \, dx$$

$$D^{(k)}_{V_i} = \int D_M x^{(k)} V_i \, dx$$

$$F^{(k)}_{\theta_{ij}} = \int \theta_s x^{(k)} W_i W_j \, dx \,, \quad F^{(k)}_{ij} = \int x^{(k)} W_i W_j \, dx \,, \quad {}_{W_k}F^{(k)}_{ij} = \int x^{(k)} V_k' W_i W_j \, dx$$

$${}_{V_k}F^{(k)}_{ij} = \int x^{(k)} V_k W_i W_j \, dx \,, \quad F^{(k)}_{W_i \Phi_j} = \int x^{(k)} W_i \overline{\Phi}_j \, dx \,, \quad F^{(k)}_{W_i W_j'} = \int x^{(k)} W_i W_j' \, dx$$

$${}_{V_k}F^{(k)}_{W_i \Phi_j} = \int x^{(k)} V_k W_i \overline{\Phi}_j \, dx \,, \quad {}_{W_k}F^{(k)}_{W_i W_j'} = \int x^{(k)} V_k' W_i W_j' \, dx$$

$${}_{V_k'}F^{(k)}_{W_i \Phi_j} = \int x^{(k)} V_k' W_i \overline{\Phi}_j \, dx \,,$$

$$G_{\theta_{ij}}^{(k)} = \int x^{(k)} \theta_s W_i V_j \, dx \,, \quad G^{(k)}_{ij} = \int x^{(k)} W_i V_j \, dx \,, \quad {}_{W_k}G^{(k)}_{ij} = \int x^{(k)} W_k' W_i V_j \, dx$$

$${}_{W_k}G^{(k)}_{ij} = \int x^{(k)} W_k W_i V_j \, dx$$

$$H^{(k)}_{w_i v_j'} = \int x^{(k)} W_i V_j' dx, \quad H^{(k)}_{v_i w_j'} = \int x^{(k)} V_i W_j' dx, \quad H^{(k)}_{\theta w_i v_j'} = \int \theta_s x^{(k)} W_i V_j' dx$$

$$H^{(k)}_{\theta v_i w_j'} = \int \theta_s x^{(k)} V_i W_j' dx, \quad {}_{w_k'}H^{(k)}_{w_i v_j'} = \int x^{(k)} W_k' W_i V_j' dx,$$

$${}_{w_k'}H^{(k)}_{v_i w_j'} = \int x^{(k)} W_k' V_i W_j' dx, \quad {}_{w_k}H^{(k)}_{w v_j'} = \int x^{(k)} W_k W_i V_j' dx$$

$${}_{w_k}H^{(k)}_{v_i w_j'} = \int x^{(k)} W_k V_i W_j' dx, \quad {}_{w_k'}H^{(k)}_{v_i v_j'} = \int x^{(k)} W_k' V_i W_j dx$$

$$L^{(k)}_{\theta ij} = \int x^{(k)} \theta_s V_i V_j dx, \quad L^{(k)}_{ij} = \int x^{(k)} V_i V_j dx, \quad {}_{w_k'}L^{(k)}_{\theta ij} = \int \theta_s x^{(k)} W_k' V_i V_j dx$$

$${}_{w_k}L^{(k)}_{\theta ij} = \int \theta_s x^{(k)} V_i V_j dx, \quad L^{(k)}_{v_i \phi_j} = \int x^{(k)} V_i \Phi_j dx, \quad L^{(k)}_{\theta v_i v_j'} = \int \theta_s x^{(k)} V_i V_j' dx$$

$$L^{(k)}_{v_i v_j'} = \int x^{(k)} V_i V_j' dx, \quad {}_{v_k}L^{(k)}_{v_i \phi_j} = \int x^{(k)} V_k V_i \Phi_j dx, \quad {}_{w_k'}L^{(k)}_{v_i v_j'} = \int x^{(k)} W_k' V_i V_j' dx$$

$${}_{w_k}L^{(k)}_{v_i \phi_j} = \int x^{(k)} W_k V_i \Phi_j dx, \quad {}_{w_k}L^{(k)}_{v_i \phi_j} = \int x^{(k)} W_k V_i \Phi_j dx, \quad {}_{w_k}L^{(k)}_{\theta v_i v_j'} = \int \theta_s x^{(k)} V_i V_j' dx$$

$${}_{w_k'}L^{(k)}_{v_i v_j} = \int x^{(k)} W_k' V_i V_j dx, \quad {}_{v_k'}L^{(k)}_{v_i \phi_j} = \int x^{(k)} V_k' V_i \Phi_j dx$$

$${}_{w_k'}L^{(k)}_{v_i \phi_j} = \int x^{(k)} W_k' V_i \Phi_j dx$$

$$V^{(k)}_{\theta i} = \int \theta_s x^{(k)} V_i dx, \quad V^{(k)}_i = \int x^{(k)} V_i dx, \quad {}_{w_k}V^{(k)}_j = \int x^{(k)} W_k V_j dx$$

$${}_{w_k}V^{(k)}_{\theta j} = \int \theta_s x^{(k)} W_k V_j dx, \quad {}_{v_k}V_{\theta i} = \int \theta_s x^{(k)} V_k V_i dx, \quad {}_{v_k}V_i = \int x^{(k)} V_k V_i dx$$

$$V^{(k)}_k = \int x^{(k)} V_k dx, \quad {}_{\theta}V^{(k)}_k = \int \theta_s x^{(k)} V_k dx, \quad {}_{v_k}V^{(k)}_{\theta j} = \int \theta_s x^{(k)} V_k' V_j dx$$

$${}_{w_k'}V^{(k)}_j = \int x^{(k)} W_k' V_j dx, \quad {}_{v_k'}V^{(k)}_i = \int x^{(k)} V_k' V_i dx$$

$$W^{(k)}_{\theta i} = \int \theta_s x^{(k)} W_i dx, \quad W^{(k)}_i = \int x^{(k)} W_i dx, \quad {}_{w_k}W^{(k)}_i = \int x^{(k)} W_k W_i dx$$

$${}_{w_k}W^{(k)}_{\theta j} = \int \theta_s x^{(k)} W_k W_j dx, \quad {}_{v_k}W^{(k)}_{\theta i} = \int \theta_s x^{(k)} V_k W_i dx, \quad {}_{v_k}W^{(k)}_i = \int x^{(k)} V_k W_i dx$$

$$W^{(k)}_k = \int x^{(k)} W_k dx, \quad {}_{\theta}W^{(k)}_k = \int \theta_s x^{(k)} W_k dx, \quad {}_{w_k'}W^{(k)}_{\theta i} = \int x^{(k)} \theta_s W_k' W_i dx$$

$${}_{v_k'}W^{(k)}_i = \int x^{(k)} V_k' W_i dx, \quad {}_{w_k'}W^{(k)}_i = \int x^{(k)} W_k' W_i dx$$

$$
{}_{W_a}\bar{\Phi}_j^{(k)} = \int x^{(k)} W_a \bar{\Phi}_j \, dx \;,\; {}_{V_k}\bar{\Phi}_j^{(k)} = \int x^{(k)} V_k \bar{\Phi}_j \, dx \;,\; {}_{V_k}\bar{\Phi}_i^{(k)} = \int x^{(k)} V_k \bar{\Phi}_i \, dx
$$

$$
\bar{\Phi}_i^{(k)} = \int x^{(k)} \bar{\Phi}_i \, dx
$$

$$
\Theta^{(k)} = \int \Theta_s x^{(k)} dx \qquad \text{(B.5)}
$$

and

$$
\begin{aligned}
A_M &= -2x_A\Theta_0 + 2\frac{C_{M_0}}{a} + 2\frac{C_{M_\alpha}}{a}\Theta_0 \\
B_M &= x_A - \frac{C_{M_q}}{a} \qquad \text{(B.6)} \\
C_M &= -\left(\frac{1}{8} + \frac{3}{4}x_A + x_A^2\right) \\
D_M &= \frac{3}{4} + x_A
\end{aligned}
$$

In addition, the gust velocity gradient terms are expressed by

$$
\begin{aligned}
G_{i\mu}^{c} &= -\frac{1}{\mu}\left(\frac{\omega}{\Omega}\right) x G_i \\
G_{ki\bar{\bar{\eta}}\mu}^{c} &= -\frac{1}{\mu}\left(\frac{\omega}{\Omega}\right) x G_{ki\bar{\bar{\eta}}} \\
G_{i\mu}^{c^2} &= -\frac{1}{\mu}\left(\frac{\omega}{\Omega}\right) x G_i^{1c} \\
G_{i\mu}^{2sc} &= -\frac{1}{\mu}\left(\frac{\omega}{\Omega}\right) x G_i^{2s} \\
G_{i\mu}^{s^2c} &= -\frac{1}{\mu}\left(\frac{\omega}{\Omega}\right) x G_i^{2c} \qquad \text{(B.7)} \\
G_{ki\bar{\eta}\mu}^{c^2} &= -\frac{1}{\mu}\left(\frac{\omega}{\Omega}\right) x G_{ki\bar{\eta}}^{1c} \\
G_{ki\bar{\eta}\mu}^{sc} &= -\frac{1}{\mu}\left(\frac{\omega}{\Omega}\right) x G_{ki\bar{\eta}}^{1s} \\
G_{ki\bar{\eta}\mu}^{s^2c} &= -\frac{1}{\mu}\left(\frac{\omega}{\Omega}\right) x G_{ki\bar{\eta}}^{2c} \\
G_{ki\bar{\eta}\mu}^{2sc} &= -\frac{1}{\mu}\left(\frac{\omega}{\Omega}\right) x G_{ki\bar{\eta}}^{2s} \\
G_{ki\bar{\bar{\eta}}\mu}^{sc} &= -\frac{1}{\mu}\left(\frac{\omega}{\Omega}\right) x G_{ki\bar{\bar{\eta}}}^{1s}
\end{aligned}
$$

It should be noted that the radial coordinate x in Eq. B.7 should be integrated in the integrand of the expressions G_i, G_i^{1c} and so forth.

APPENDIX C

OUTLINE OF EQUATIONS OF MOTION WHEN CYCLIC PITCH CONTROL IS APPLIED

When cyclic pitch control is applied to the rotor blade, this pitch control consists of the trim cyclic pitch, and perturbation pitch control for the evaluation as the gust alleviation system.

The trim pitch $\bar{\theta}$ is defined in Eq. 5.7, and if it is applied in moment trim operation, the term θ_s in Eq. 4.18 should include this effect. Therefore, θ_s in Eq. 4.19 will be rewritten as

$$\theta_S = \bar{\theta}_0 + \bar{\theta}_{1C} \cos\psi + \bar{\theta}_{1S} \sin\psi + \theta_{TW} \tag{C.1}$$

and the coefficients in Appendix B should be slightly modified.

As for the perturbation pitch control, a few considerations are required. If the rigid pitch motion is included and the control linkage is flexible, rigid pitch motion as one degree of freedom is described as

$$I_\theta \ddot{\theta}_R + K_\theta \theta_R = K_\theta \theta_c \tag{C.2}$$

where θ_c is the perturbation pitch control. Therefore, if the control linkage is flexible, the excitation input for the perturbation pitch control is only the pitch control expression in the rigid pitch equation: for example, in Eq. 6.1d, $K_\theta \theta_R$ should be replaced by $K_\theta(\theta_R - \theta_c)$. Aerodynamic loadings due to perturbation pitch control are expressed by aerodynamic loadings due to rigid pitch motion in Eqs. 6.1 a, b, c, and d. The final modal equations of motion may be written, modifying Eq. 6.6

$$[M]\{\ddot{Y}\} + [C]\{\dot{Y}\} + [K]\{Y\} = [F]\bar{w}_G + [P]\begin{Bmatrix}\theta_0\\ \theta_{1C}\\ \theta_{1S}\end{Bmatrix} \tag{C.3}$$

where

$$[P] = \begin{bmatrix} [P_1] \\ [P_2] \\ \vdots \\ [P_N] \end{bmatrix} \quad , \quad [P_i] = \frac{K_\theta \Phi_i}{I_\theta \Omega^2} \begin{bmatrix} 1 & 1 & 1 \end{bmatrix} \qquad \text{(C.4)}$$

If one wishes the equations for the rigid control linkage, the rigid pitch motions for the inertial loading in Eqs. 6.1 a, b, and c should be dropped and aerodynamic loadings due to the rigid pitch motion in these equations should be retained to express the aerodynamic loadings due to perturbation pitch control.

APPENDIX D

GUST RESPONSE OF THE FULL-SIZE ROTOR

The preliminary results of the gust response of the hingeless rotor with Lock number of 10 are shown in Fig. D.1. The structural characteristics of the rotor blade are the same as those of the single-bladed rotor with tip mass used in the wind tunnel. The "soft torsion" blade, $^{\omega}\phi/\Omega$ = 2.38/rev, is employed. Blade density is reduced to obtain a typical full-size blade Lock number. The chordwise center-of-gravity is varied over 18%, 25% and 35% chord from the blade leading edge. For the 35% chord C.G. location the classical flap-torsion flutter occurred. Therefore, the results are not shown here. The gust magnitude in Fig. 19 is used.

It is shown in Fig. D.1(a) that the center-of-gravity shift is a very effective method to reduce the flapping response due to the greater aerodynamic forces. It is interesting that the peak at 0.2/rev in the $(\Omega+\omega)$ flap response disappeared because of the large aerodynamic damping in the flapping motion. The ω flap response is higher than the cyclic flapping responses since the gust effectiveness has increased through the Lock number. In the $(\Omega-\omega)$ flap response the response of the 25% chord C.G. is less than that of the 18% chord C.G. at the gust frequency 0.4 because the phase of the torsional motion is not such as to reduce the flapping motion.

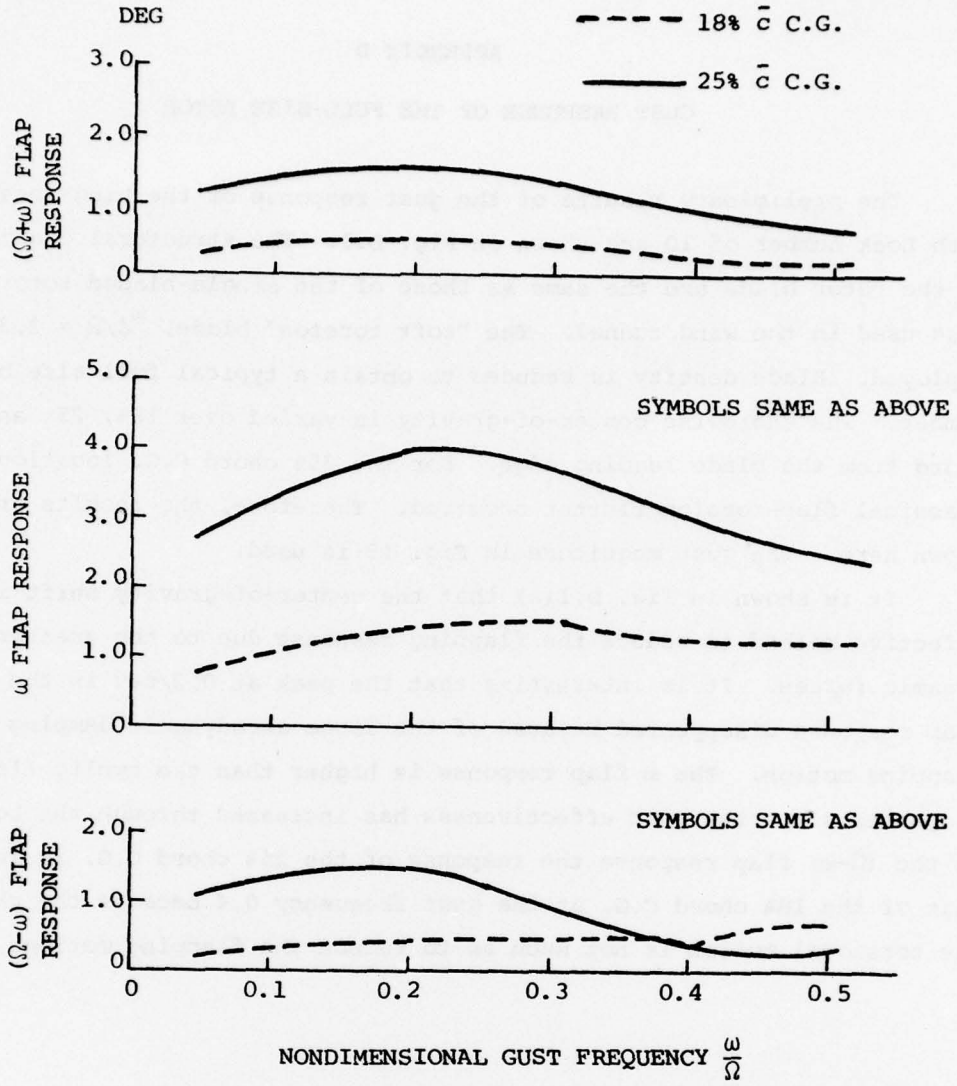

(a) Flap Response

FIG. D.1 VERTICAL GUST RESPONSE OF HINGELESS ROTOR WITH LOCK NUMBER OF 10; $(\omega_\phi/\Omega) = 2.32$

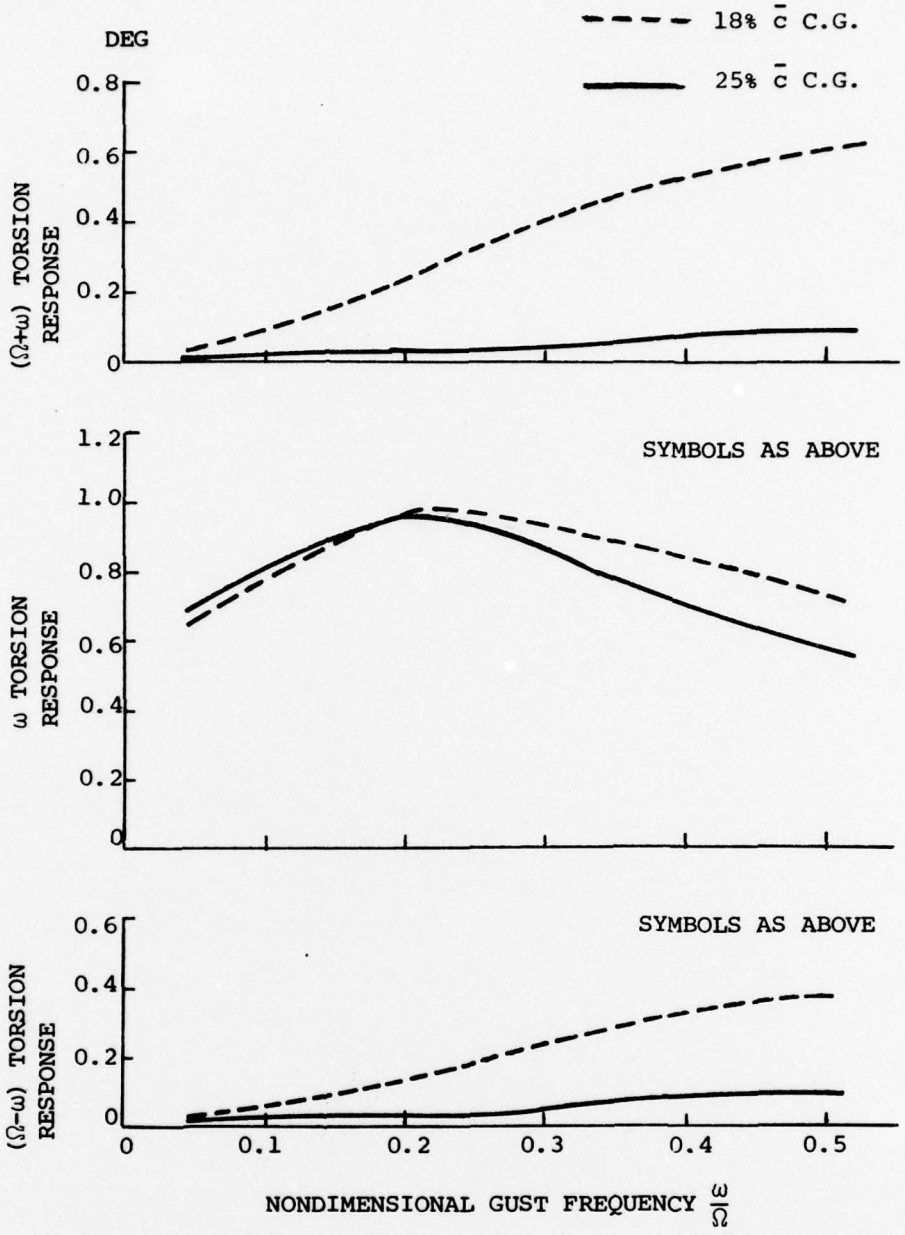

(b) Torsional Response

FIG. D.1 CONCLUDED

APPENDIX E

ADEQUACY OF HARMONIC BALANCE METHOD

In this appendix the adequacy of the harmonic balance method used in this report is examined. The one-degree-of-freedom flap equation is employed for this purpose. This equation is obtained from Eq. 123 as follows:

$$\begin{aligned}
&\ddot{\beta} + \left\{\frac{\gamma}{8} + \mu\frac{\gamma}{6}\sin(\Omega t)\right\}\dot{\beta} + \left\{\left(\frac{\omega_\beta}{\Omega}\right)^2 + \mu\frac{\gamma}{6}\cos(\Omega t) + \mu^2\frac{\gamma}{8}\sin(2\Omega t)\right\}\beta \\
&= \frac{\gamma}{6}\bar{w}_G\sin(\omega t) + \mu\frac{\gamma}{4}\bar{w}_G\sin(\omega t)\sin(\Omega t) \\
&\quad - \frac{\gamma}{8}\frac{1}{\mu}\left(\frac{\omega}{\Omega}\right)\bar{w}_G\cos(\omega t)\cos(\Omega t) \\
&\quad - \frac{\gamma}{6}\left(\frac{\omega}{\Omega}\right)\bar{w}_G\cos(\omega t)\sin(\Omega t)\cos(\Omega t)
\end{aligned} \tag{E.1}$$

To compare with the results of the harmonic balance method, the numerical integration (the predictor-corrector method) is adopted to solve the differential equation of E.1. The initial conditions are $\beta=0$ and $\dot{\beta}=0$ at $t=0$. The results show the transient motion decay and the forced oscillations due to the gust.

After applying the harmonic balance method to Eq. E.1, the expressions may be written:

$$\begin{aligned}
&\begin{bmatrix} 1 & 0 & 0 \\ 0 & 1 & 0 \\ 0 & 0 & 1 \end{bmatrix}\begin{Bmatrix} \ddot{\beta}_0 \\ \ddot{\beta}_{1c} \\ \ddot{\beta}_{1s} \end{Bmatrix} + \begin{bmatrix} \frac{\gamma}{8} & 0 & \mu\frac{\gamma}{12} \\ 0 & \frac{\gamma}{8} & 2 \\ \mu\frac{\gamma}{6} & -2 & \frac{\gamma}{8} \end{bmatrix}\begin{Bmatrix} \dot{\beta}_0 \\ \dot{\beta}_{1c} \\ \dot{\beta}_{1s} \end{Bmatrix} \\
&+ \begin{bmatrix} \left(\frac{\omega_\beta}{\Omega}\right)^2 & 0 & 0 \\ \mu\frac{\gamma}{6} & \left(\frac{\omega_\beta}{\Omega}\right)^2 - 1 & \frac{\gamma}{8}\left(1+\frac{1}{2}\mu^2\right) \\ 0 & -\frac{\gamma}{8}\left(1-\frac{1}{2}\mu^2\right) & \left(\frac{\omega_\beta}{\Omega}\right)^2 - 1 \end{bmatrix}\begin{Bmatrix} \beta_0 \\ \beta_{1c} \\ \beta_{1s} \end{Bmatrix} \\
&= \begin{bmatrix} \frac{\gamma}{6} \\ 0 \\ \mu\frac{\gamma}{4} \end{bmatrix}\bar{w}_G\sin(\omega t) - \begin{bmatrix} 0 \\ \frac{\gamma}{8}\frac{1}{\mu}\left(\frac{\omega}{\Omega}\right) \\ 0 \end{bmatrix}\bar{w}_G\cos(\omega t)
\end{aligned} \tag{E.2}$$

These equations are solved by the same predictor-corrector method with the initial conditions $\beta_o=\beta_{1c}=\beta_{1s}=0$ and $\dot{\beta}_o=\dot{\beta}_{1c}=\dot{\beta}_{1s}=0$ at t=0. Obtaining the responses of β_o, β_{1c} and β_{1s} at time t, the flap response β is calculated as follows.

$$\beta(t) = \beta_o(t) + \beta_{1c}(t)\cos(\Omega t) + \beta_{1s}(t)\sin(\Omega t) \qquad \text{(E.3)}$$

It should be noted that in Eq. E.1 the periodic coefficients higher than one per revolution such as $\sin(2\Omega t)$ and $\cos(3\Omega t)$ are included. However, in Eq. E.2 they are neglected.

The results are shown in Fig. E.1 to E.4. In Fig. E.1 the gust response with nondimensional gust frequency 0.2/rev are shown. Lock numbers were chosen as 10 and 0.954. The latter corresponds to the value which was used in the present experiment. The flapping frequency is 1.127/rev in both cases. The results from the numerical integration and the harmonic balance method revealed very small difference.

In Fig. E.2 the flapping natural frequency is fictitiously set to 3/rev to see the adequacy of the expansion of the harmonic balance method written in Eq. E.3 which neglects harmonics higher than 1/rev. The results show good agreement between the numerical integration and the harmonic balance method when the gust frequency is of the order of 0.2/rev.

The only discrepancy can be seen in Fig. E.3 between the numerical integration and the harmonic balance method when the gust frequency is chosen as 3/rev which is much higher than normal. The 3/rev gust magnified the motion in the results for the numerical integration method through the 3/rev harmonics which are retained in this method. In the harmonic balance method these terms are discarded. Thus, the response of the harmonic balance method is smaller than that of the numerical integration method for this case.

The final figure E.4 shows the results when the flapping natural frequency of 3/rev and the gust frequency of 3/rev are chosen. In this case the stiffness terms become dominant due to the high natural frequency and the aerodynamic terms of 3/rev become less effective. Therefore, the results show very little difference between the numerical integration and the harmonic balance method.

It is concluded that the harmonic balance method used in this study is adequate for the present rotor configuration. However, there are two restrictions when the harmonic balance method is applied to general rotor dynamics. The first is that the exciting gust frequency should not be near the same frequency as those harmonics which are neglected in the method. The second restriction is that the eigenvalues of the system should be far from 0.5/rev, 1.5/rev and so on, for certain values of Lock number and advance ratio (see Ref. E.1). Higher natural frequencies such as 3/rev cause little difference in the response obtained by the numerical integration and the harmonic balance methods because of the increased stiffness.

Reference.

E.1 Biggers, J.C., "Some Approximations to the Flapping Stability of Helicopter Rotors", Journal of the American Helicopter Society, Vol. 19, No. 4, Oct. 1974.

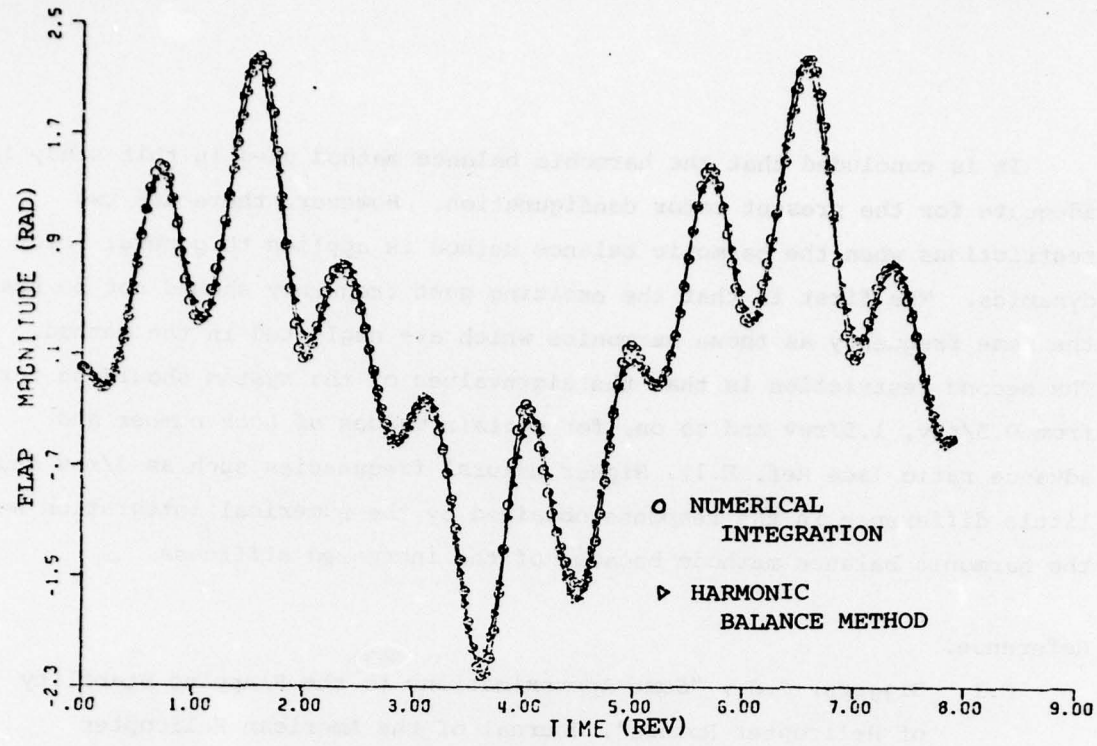

(a) Lock Number 10

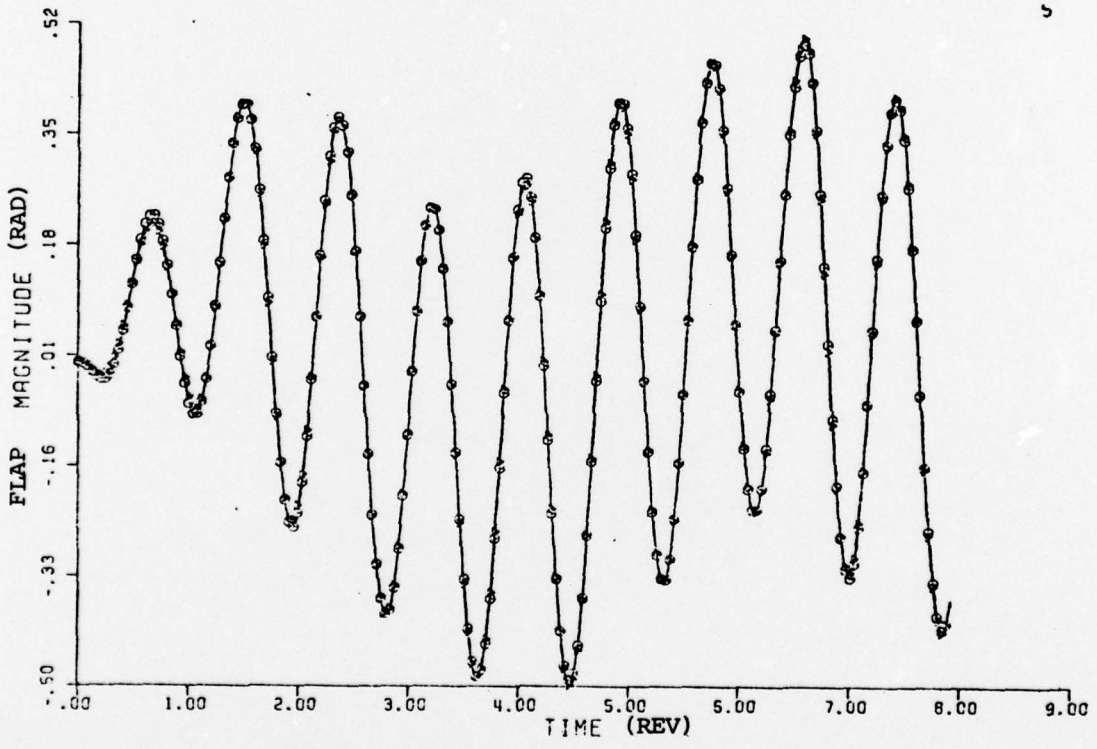

(b) Lock Number 0.954

FIG. E.1 TIME HISTORY OF ROTOR GUST RESPONSE: μ=0.4, $(\frac{\omega_\beta}{\Omega})$ = 1.13, GUST FREQUENCY $(\frac{\omega}{\Omega})$ = 0.2

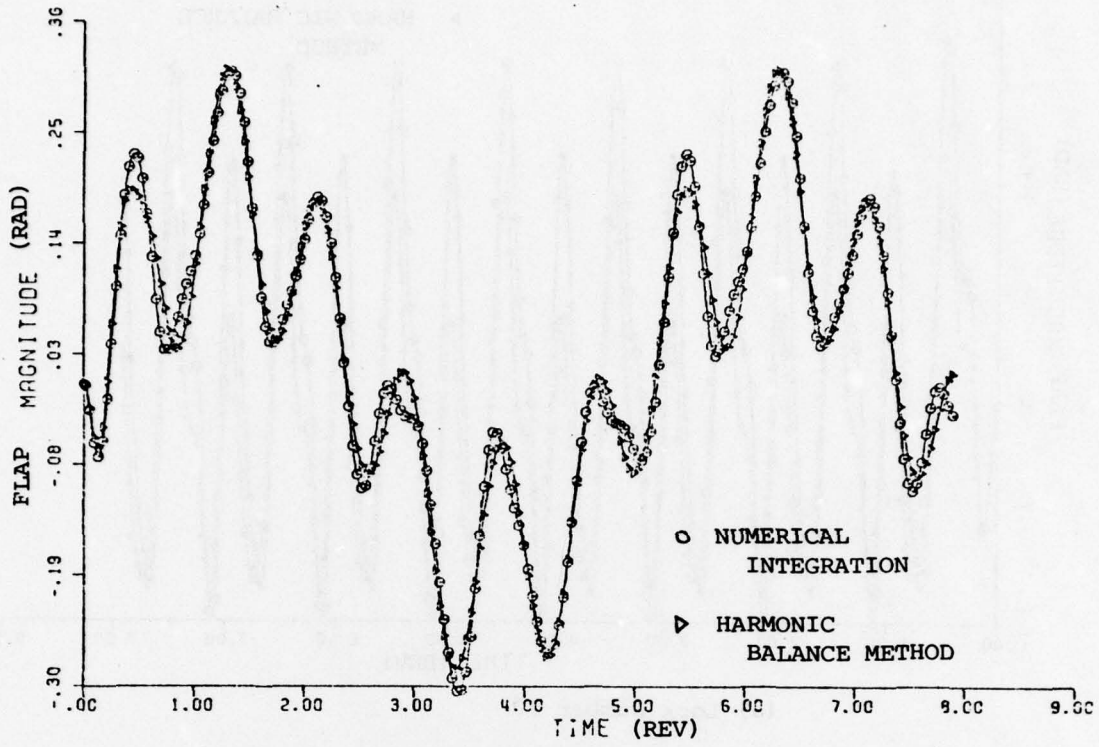

(a) Lock Number 10

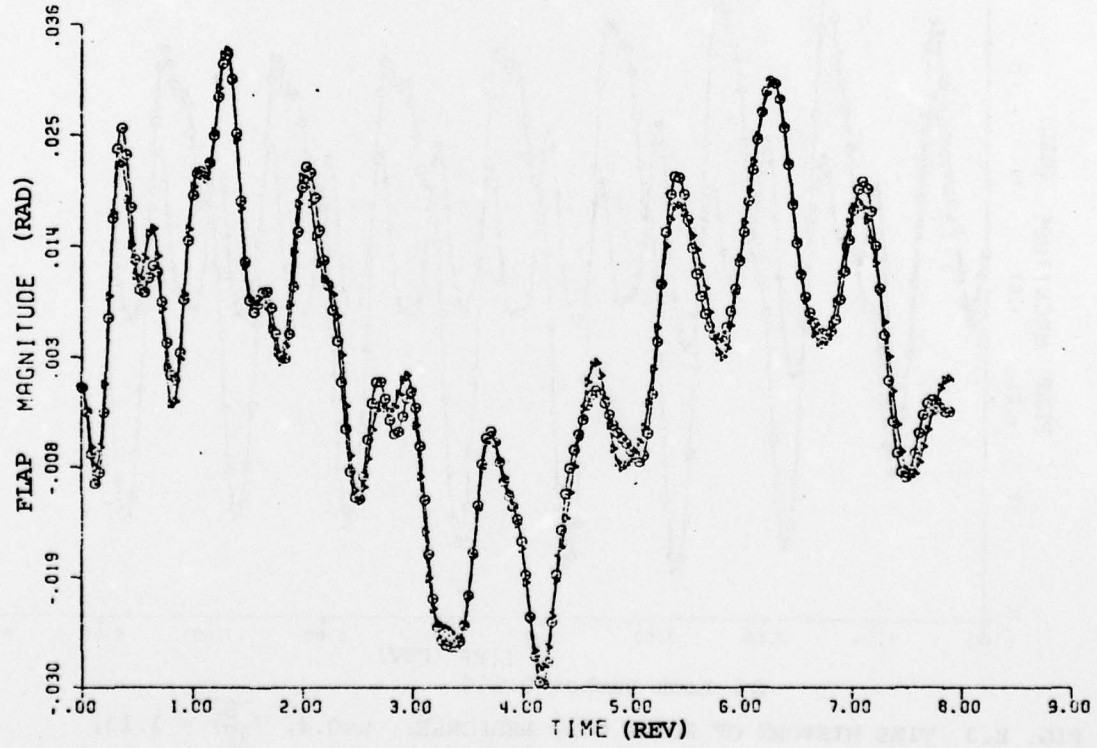

(b) Lock Number 0.954

FIG. E.2 TIME HISTORY OF ROTOR GUST RESPONSE: μ=0.4, $(\frac{\omega_\beta}{\Omega})$ = 3, GUST FREQUENCY $(\frac{\omega}{\Omega})$ = 0.2

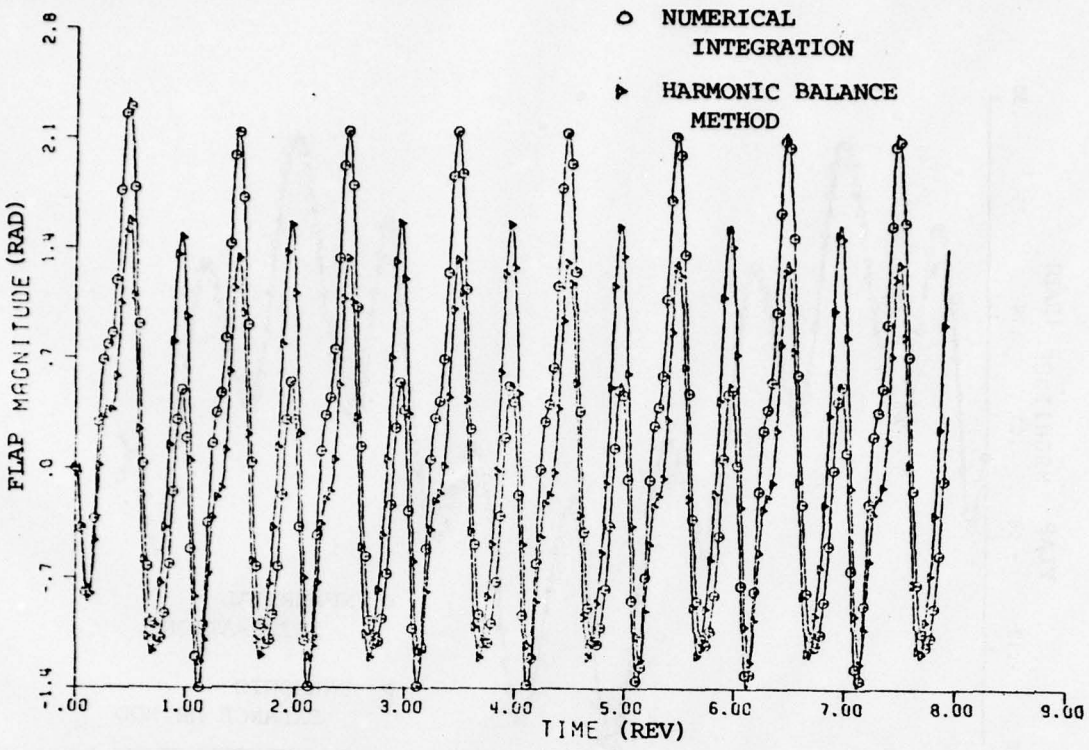

(a) Lock Number 10

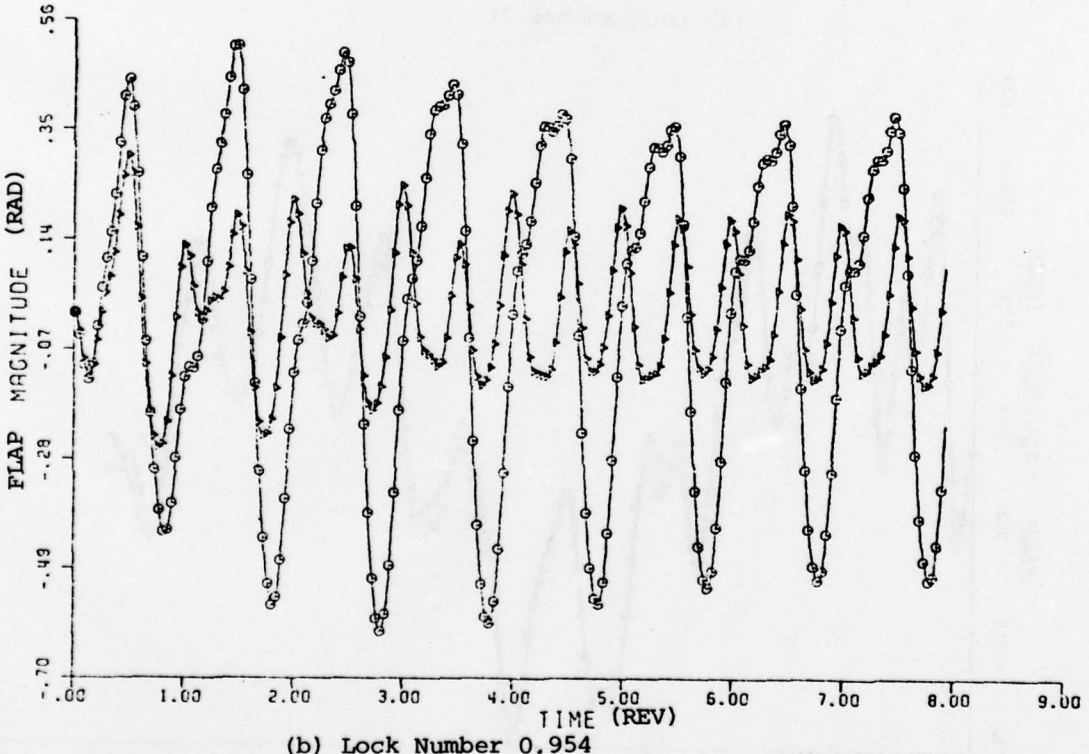

(b) Lock Number 0.954

FIG. E.3 TIME HISTORY OF ROTOR GUST RESPONSE: μ=0.4, $(\frac{\omega_\beta}{\Omega})$ = 1.13, GUST FREQUENCY $(\frac{\omega}{\Omega})$ = 3

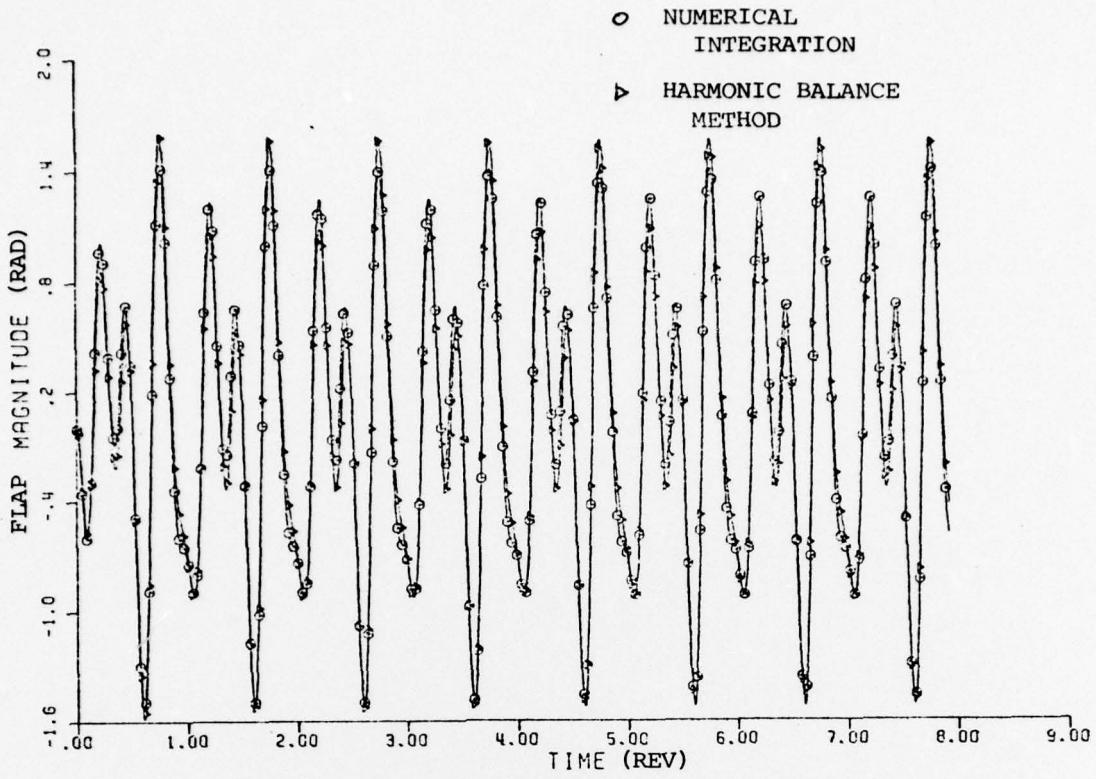

(a) Lock Number 10

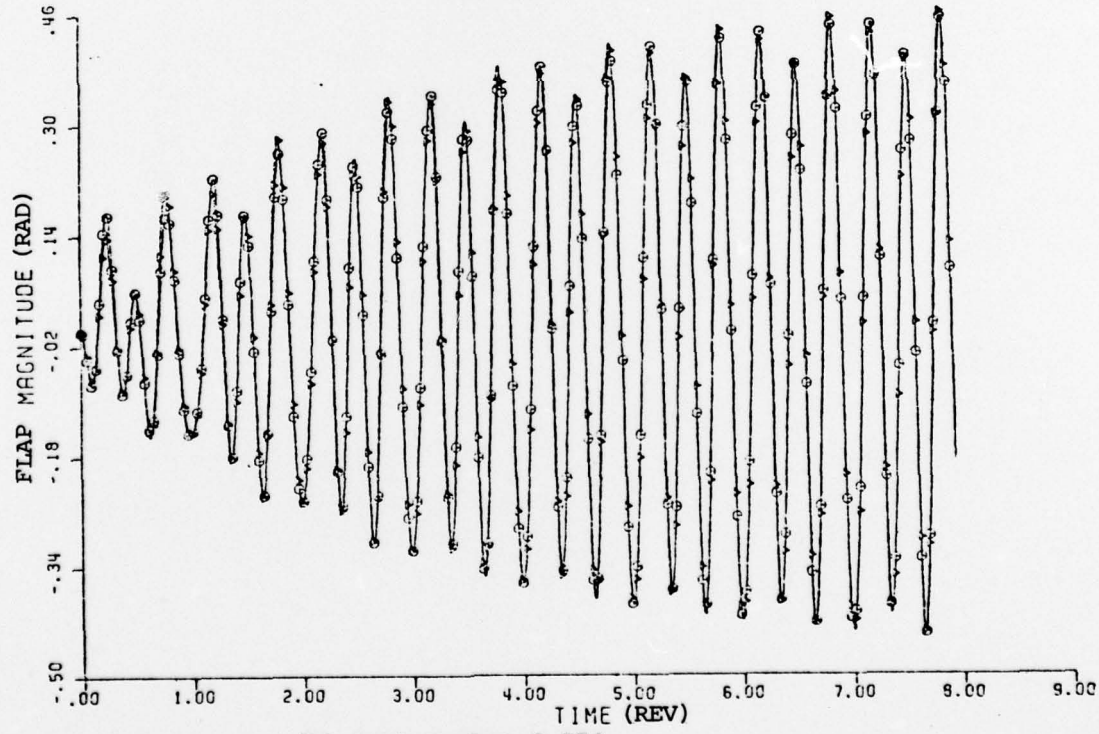

(b) Lock Number 0.954

FIG. E.4 TIME HISTORY OF ROTOR GUST RESPONSE: μ=0.4, $(\frac{\omega_\beta}{\Omega})$ = 3, GUST FREQUENCY $(\frac{\omega}{\Omega})$ = 3

APPENDIX F

CORRELATION OF HUB SHEARS WITH BLADE FLAPPING RESPONSE

In this report the blade flapping response was chosen as a measure of the effectiveness of the gust alleviation system. Therefore, the appropriateness of the flapping response as a measure is examined by evaluating the vertical shear force at the blade root, and also the blade root bending moment.

The vertical shear force at the root is obtained by integrating the aerodynamic and inertial forces on the blade:

$$S = \int_0^R (P_z - m\ddot{z})\, dr \tag{F.1}$$

using the force summation method, the vibratory shear force is expressed as

$$S = \int_0^R \left[\left(\frac{\partial P_z}{\partial u_T}\right)_0 \delta u_T + \left(\frac{\partial P_z}{\partial u_P}\right)_0 \delta u_P + \left(\frac{\partial P_z}{\partial \theta}\right)_0 (\delta\theta + \delta\phi) + \left(\frac{\partial P_z}{\partial \dot{\theta}}\right)_0 (\delta\dot{\theta} + \delta\dot{\phi}) \right] dr - \int_0^R m\ddot{z}\, dr \tag{F.2}$$

To evaluate the coefficients of Eq. F.2 the expressions in Appendix B are used, and subscript i is taken as unity. Mode shapes for i=1 are specified as $W_i = W_1 = 1.0$ and $V_i = V_1 = \Phi_i = \Phi_1 = \Theta_i = \Theta_1 = 0$ for convenience in calculating the shear force. Subscripts j are repeated from 1 to 4, which includes first mode lagging, first mode flapping, second mode flapping, and first mode torsion.

The harmonic balance method was applied to Eq. F.2 to eliminate the periodic coefficients, and the shear force is expressed in terms of ω, $(\Omega-\omega)$ and $(\Omega+\omega)$ vibratory shear forces.

The results shown in Fig. F.1 are the calculated shear forces due to gusts of the single-bladed model rotor with the "soft torsion" blade at advance ratio 0.394 with chordwise center-of-gravity shift. Note that the shear force components at frequencies ω, $(\Omega-\omega)$, and $(\Omega+\omega)$ are reduced by shifting the chordwise center-of-gravity forward. The flapping responses corresponding to these shear forces are shown in Fig. 22(c) and it is

obvious that the flapping may be taken as a measure of the effectiveness of the gust alleviation system in reducing hub shears. In the present wind tunnel model, the hub moment is expressed in terms of the product of the vertical shear force and the flap hinge offset. Therefore, the hub moment is proportional to the shear force and further evaluation of the hub moment is not required.

The second mode flapping response is shown in Fig. F.2. It is negligible compared to the first mode flapping response when the gust frequencies are as low as in the present case. It should be noted that the shear force calculation in Fig. F.1 included both the first and second mode flapping motions.

As an example of the effect of higher harmonic loading, the hub shears due to airloads at frequencies up to 5/rev. are presented in Fig. F.3 for a hovering rotor of Lock number 10. As an expression of the shear force the nondimensional form $S/[\rho A(\Omega R)^2]$ is used where S is the shear force, ρ the air density, and A is disk area. Below the gust frequency of 1/rev the center-of-gravity shift forward works very well as a gust alleviation system. The peak around 4/rev is due to the second mode flapping response, and again the center-of-gravity shift reduces the response and there seems no adverse effect from the center-of-gravity shift.

It can be concluded that the first mode flapping motion may be chosen as an indicator of the effectiveness of the gust alleviation system.

It should be noted that careful choice of blade mass balance spanwise location and blade torsional frequency are necessary to avoid possible amplification of hub shears due to higher harmonic airloads, as discussed in Reference F.1.

Reference.

F.1 Miller, R.H. and Ellis, C.W., "Helicopter Blade Vibration and Flutter", Journal of the American Helicopter Society, Vol. 1, No. 3, July 1956, pp. 19-38.

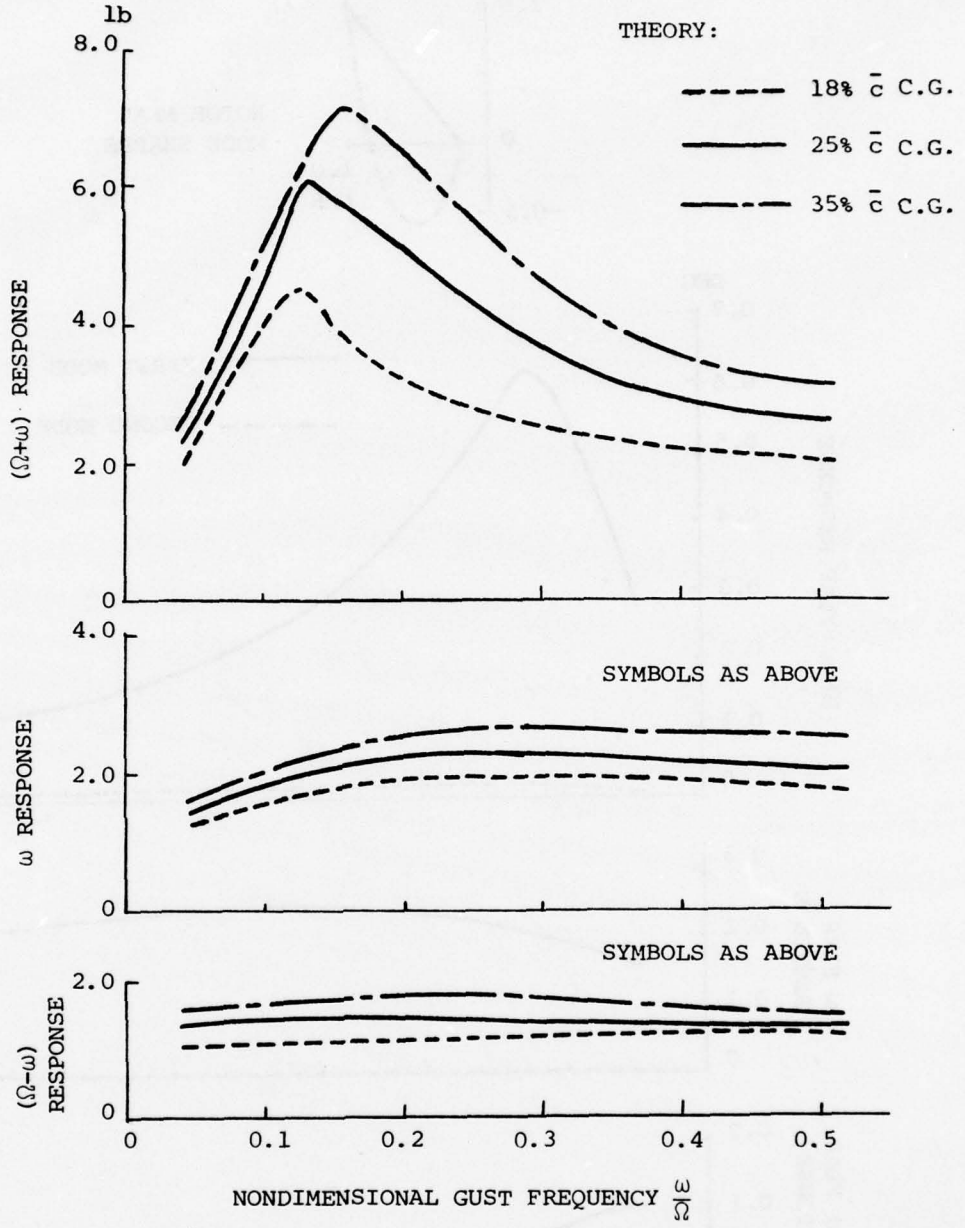

FIG. F.1 VERTICAL SHEAR FORCE RESPONSE OF THE SINGLE-BLADED ROTOR TO THE VERTICAL GUST IN ADVANCE RATIO 0.384: "SOFT TORSION" BLADE $(\frac{\omega_\phi}{\Omega})$ = 2.38/REV WITH CHORDWISE C.G. SHIFT

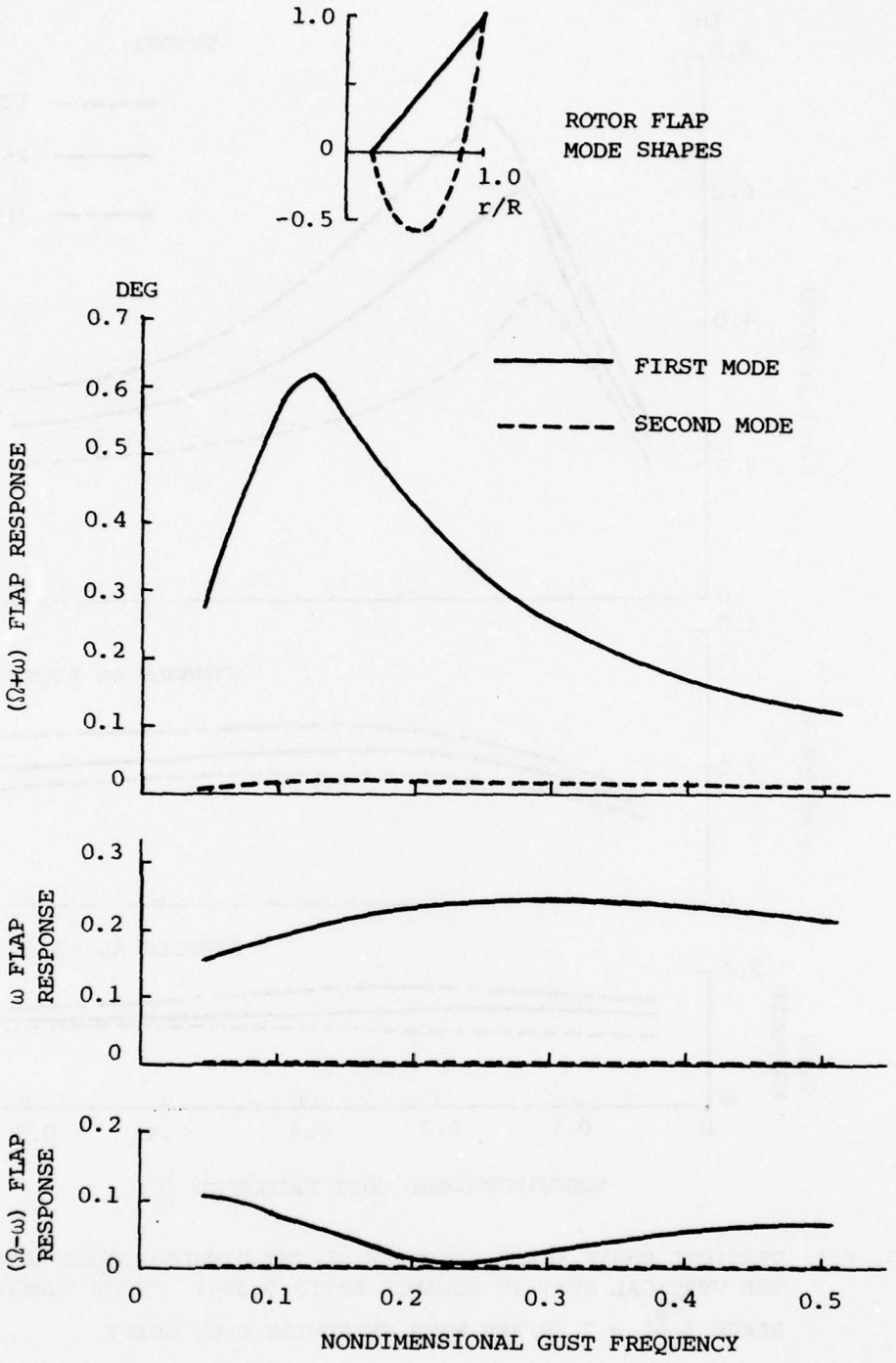

FIG. F.2 FIRST AND SECOND FLAP MODE VERTICAL GUST RESPONSE OF THE "SOFT TORSION" BLADE WITH 18% $\bar{c}$ C.G. IN ADVANCE RATIO 0.384: FLAP RESPONSES ARE EXPRESSED IN TERMS OF TIP DEFLECTION NONDIMENSIONALIZED BY RADIUS

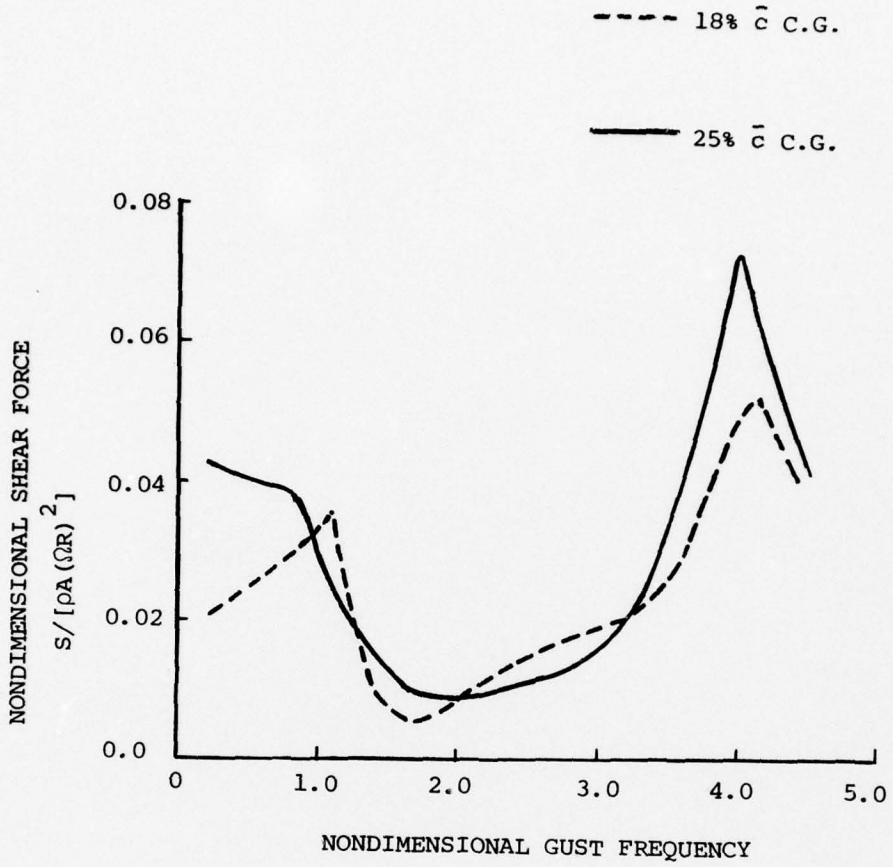

FIG. F.3 HUB SHEAR FORCE OF THE ROTOR OF LOCK NUMBER 10 AND WITH CENTER-OF-GRAVITY SHIFT IN HOVER